IMPULSIVE OVERTOPPING OF VERTICAL SEAWALLS UNDER OBLIQUE WAVE CONDITIONS

BY

NICOLAS NAPP

DOCTOR OF PHILOSOPHY

THE UNIVERSITY OF EDINBURGH

2004

ABSTRACT

Seawalls and breakwaters seldom align perfectly with incoming waves, but many prediction methods for wave overtopping are only valid for shore-normal wave attack. In particular, there is no guidance available for either mean or wave-by-wave overtopping discharges over vertical seawalls subject to oblique and impulsive wave attack. Impulsive wave attack (i.e. waves break onto the structure) may lead to substantially higher overtopping volumes than pulsating wave attack and can arise at relatively low water levels.

Mean and wave-by-wave overtopping discharges represent important quantities in the design of coastal structures. They not only affect the structural safety and determine the capacity of the drainage system behind the structure, but also pose a hazard to communications, buildings, and members of the public. Previous work has shown that impulsive overtopping can substantially increase overtopping volumes and velocities, thus underlining the importance of robust prediction tools.

This PhD thesis describes experiments and analysis to provide design guidance in wave overtopping of vertical seawalls under oblique and impulsive wave attack. The guidance extends existing design tools for wave overtopping which cover both wave conditions (reflecting and impulsive) under shore-normal wave attack, but only reflecting conditions under oblique wave attack.

Special attention is given to the transition from impulsive to reflecting wave conditions, which goes along with a significant reduction in overtopping towards higher obliquities. For moderate obliquities (15° and 30°) a new intermediate wave condition is defined as the "impact-like" condition, which – in terms of overtopping – has still to be treated as impulsive. Contrary to a few previous investigations on sloping walls, no increase in overtopping could be found at small obliquities (15°). Spatial variability, however, could be measured along the seawall and has been considered in the design guidance offered in this thesis.

DECLARATION

This thesis has been composed by myself and, except where stated, the work contained is my own. Furthermore, the work contained has not been submitted for any other degree or professional qualification.

.....

Nicolas Napp

December, 2004

CONTENTS

1 INTRODUCTION

1.1 General

Seawalls and breakwaters shelter coastlines and harbours from the direct impact of high water levels and waves typically generated by severe storms. Although sea level rise is predicted and the number and severity of storm surges appears to be increasing rapidly, more and more people settle in coastal regions, further increasing the economic value protected by seawalls. While this demands more and perhaps higher seawalls, construction is not only expensive but high seawalls also decrease the social value of the seaside, e.g. by blocking the view towards the sea. Thus, there is a trade off between cost (financially and socially) and benefit (safety). The accurate assessment of the performance of seawalls is therefore crucial in order to ensure an optimum design. This in turn requires reliable and well validated prediction methods.

Figure 1: Oblique and Impulsive overtopping event at a plain vertical seawall (Hartlepool, courtesy George Motyka, HR Wallingford)

A seawall is designed with two important basic measures of performance in mind: the mean overtopping discharge and the wave-by-wave overtopping volumes. The first quantity, the mean overtopping discharge, is mostly important when designing the drainage system behind a seawall in order to avoid flooding. There are also models linking the structural safety of the seawall itself to the mean discharge. Furthermore, current guidance for the evaluation of hazards to communications, infrastructure and people is also based on the mean discharge.

The other basic quantity, the wave-by-wave overtopping, also plays an important role. As there is no continuous flow of water over the seawall, but individual overtopping volumes, it is actually the individual waves which cause the structural damage to the seawall or present a hazard. It has also been found that it is the large individual overtopping events that cause most of the problems. Despite some effort no simple link between mean and peak individual discharges has been found. There is even some evidence that ratios of mean to peak discharges can vary by more than two orders of magnitude.

This underlines that peak individual discharges are truly a different quantity from the mean discharge and they both have to be treated separately. Research is underway (CLASH workshop) to link overtopping hazards not only to mean, but also to peak discharges, which should result in a more accurate assessment.

1.2 Outline of the thesis

The hydraulic performance of a vertical seawall or breakwater depends strongly on the mode of wave attack. The two most important modes can be classified as pulsating and impacting wave attack (see chapter 4). In the case of pulsating wave attack the incoming waves simply run up and reflect from the seawall back to the sea. Wave overtopping occurs when the run-up exceeds the crest height of the seawall. In the case of impacting wave attack, however, the wave breaks onto the seawall entrapping a pocket of air which is then compressed leading to a subsequent sudden "explosive" release of the pressure. This may result in water being thrown up several times the incident wave height.

Few (2D) prediction methods for wave overtopping distinguish between pulsating and impacting wave attack on a vertical seawall. This distinction, however, is very important as the underlying physics are quite different resulting in overtopping volumes which are up to several orders of magnitude higher when the waves are in impacting mode. Once the mode

of the waves (i.e. reflecting or impacting) has been established, the appropriate formulae can be chosen in order to assess the overtopping performance of a vertical seawall.

When waves attack a vertical seawall perpendicularly then guidance for mean and wave-by-wave overtopping is available for waves in both predominantly impacting and reflecting mode. However, when the seawall is subject to oblique wave attack then guidance is only available when the waves are in reflecting mode. For impacts, which can give very much larger discharges than pulsating methods would predict, there is no guidance on the effect of oblique wave overtopping. There are, however, some indications that the percentage of impacts reduces at increasing obliquities.

This PhD thesis provides a literature review which highlights this gap (chapter 2) and describes a model study (chapter 3) and analysis (chapters 4 to 8) to provide design guidance in wave overtopping of vertical seawalls under oblique wave attack with a focus on impulsive wave conditions (chapter 9). The guidance offered extends existing design tools for wave overtopping which cover both wave conditions (reflecting and impulsive) under shore-normal wave attack, but only reflecting conditions under oblique wave attack.

The underlying physical model study is described in chapter 3, while the main analysis is summarised in chapters 4 to 8. As a first step in chapter 4 wave impacts are defined for 2D perpendicular wave attack. Subsequently, the gradual change of the physics of wave impacts is described on a visual basis and illustrated by series of pictures for increasing angles of wave attack. As wave impacts have a great influence on overtopping volumes a closer look at the percentage of wave impacts and its gradual change towards higher obliquities is taken in chapter 5.

The effect of increasing obliquities on the mean overtopping discharge is investigated in chapter 6. This chapter clarifies up to which obliquities a modified 2D impacting formula can still be applied. It also investigates at what angles the waves swap entirely to reflecting conditions and whether the existing prediction tools for reflecting wave conditions can then be used.

The final two chapters (7 and 8) of the analysis deal with the prediction of wave-by-wave discharges. First the existing guidance for impulsive 2D wave attack is validated. In an attempt to improve the prediction method all input parameters will be further analysed and

different quantities such as V_{max}, $V_{x\%}$, and $V_{1/m}$ will be discussed. Finally, the existing 2D method will be extended to oblique wave attack. Additionally, throughout chapters 4 to 8, two other issues are investigated as well: the existence of a small increase in overtopping at small angles of wave attack and the occurrence of spatial variability.

The results are summarised and the implications for design are discussed in chapter 9. Chapter 10 finally summarises the key conclusions and gives recommendations for future research.

2 RESEARCH CONTEXT

2.1 Introduction

In this chapter the previous work on mean and wave-by-wave overtopping discharge is discussed. This includes the effect of angled wave attack and methods to predict the likelihood of waves breaking onto a vertical seawall. A section on admissible overtopping discharges is included to show that not only the mean but also the individual discharge is an important parameter when designing plain vertical seawalls. Although the focus of this review is on empirical models a brief overview of the status of other methods including neural networks and numerical models is also given. Finally, a section on scale effects discusses briefly the issue of scale and model effects on the results of this study.

First of all a section on the prediction of the incidence of wave breaking onto a vertical seawall is given (section 2.2), because the mode of the waves, i.e. either reflecting or impacting, has a substantial influence on the overtopping.

The discussion on mean overtopping discharge (section 2.3) will then start with a review of some of the early studies on simply sloped, impermeable, and smooth structures and will then lead to a focus on vertical seawalls. The effect of oblique wave attack is then discussed for all types of seawalls including permeable structures under long crested and short crested wave attack. Although all types of structures are discussed it will be shown in particular that no guidance is available for the prediction of mean discharge over plain vertical seawalls under oblique and impulsive wave attack. The main purpose of this thesis is to close this gap and derive prediction tools for this case. The second issue to be discussed in this section is whether as reported in some previous studies, small angles of wave attack can lead to an increase in overtopping.

Section 2.4 presents methods for the prediction of maximum overtopping discharges at plain vertical seawalls. These methods are all based on the Weibull probability function. As the Weibull function requires a prediction of the proportion of overtopping waves (N_{ow}/N_w) prediction methods for this quantity are given as well. Similar to the mean discharge it will

be shown that no guidance is available when waves are in impacting mode and attack obliquely.

Section 2.5 focuses on admissible overtopping with an emphasis on personal hazards. The definition of tolerable limits for overtopping proves to be difficult as many different factors – and not only technical ones – have to be taken into account.

Finally, after a brief discussion of possible scale effects (section 2.6), methods other than empirical formulae for the prediction of overtopping are presented (section 2.7). This includes neural networks and numerical models.

The usual notations and symbols are used in this thesis and can be reviewed in the Appendix (Table 1).

2.2 Wave Breaking onto Vertical Seawalls

The way waves interact with a vertical seawall, i.e. whether they are predominantly in reflecting or in impacting mode, has a great influence on the overtopping behaviour (see sub-section 2.3.3). Allsop et al. (1995) and the EA manual (1999) suggest the h* parameter to distinguish between the two modes. The h* parameter is a function of the local water depth at the toe of the structure h (m), the local significant wave height H_s (m), and the local mean wave period T_m (s):

$$h^* = \frac{h}{H_s} \frac{2\pi h}{g T_m^2} \tag{1}$$

When $h^* > 0.3$ then reflecting waves predominate; when $h^* \leq 0.3$ then impacting waves predominate.

The equation for h* (equation (1)) can be interpreted in the following way:

$$h^* = \frac{h}{H_s} \frac{h}{L_{om}} \tag{2}$$

where h/H_s and h/L_{om} are the relative water depth in relation to the significant wave height and offshore mean wave period, respectively. When waves are small compared to water depth ($h^* > 0.3$), the waves impinging on a vertical / composite wall are generally reflected back. When waves are large relative to water depth ($h^* < 0.3$), then they can break onto the structure.

The h* parameter does not include the influence of the approach beach. Waves, however, may break more than once travelling up a relatively shallow approach beach of e.g. 1:100. On relatively steep approach beaches (e.g. 1:10) on the other hand waves may break only once and then straight onto the structure leading to high impact loads and much more violent wave overtopping. This shows that the slope angle of the approach beach should have an influence on the h* parameter.

An alternative method to predict wave breaking has been suggested by Allsop et al. (1996a) and Allsop et al. (1996b) which has also been recommended by the PROVERBS workshop (Oumeraci et al., 2001). A parameter map has been developed, which in the case of a plain vertical wall uses the local water depth h and the local significant wave height H_s only to distinguish between the two modes (Figure 2).

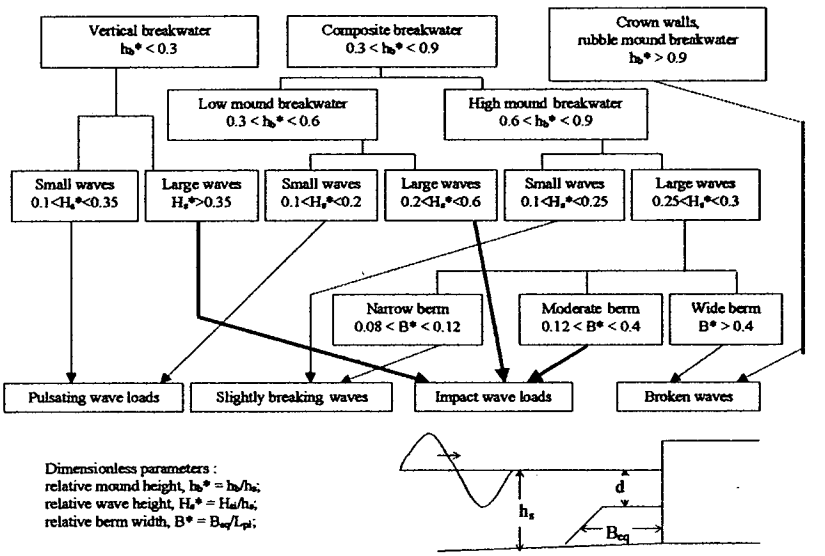

Figure 2: PROVERBS parameter map (Oumeraci et al., 2001)

In the case of a plain vertical seawall "large" waves predominate, when the ratio of local significant wave height H_{si} to local water depth h_s is larger than 0.35 ($H_{si}/h_s > 0.35$). "Large" waves give impact loads onto the seawall and "small waves ($H_{si}/h_s < 0.35$) pulsating wave loads.

One criticism of the PROVERBS parameter map and also of the h* parameter approach is that they imply a switch between reflecting and impacting conditions and do not describe the actual transition between both modes. On top of that both methods ignore the influence of the steepness of the foreshore on wave breaking.

The PROVERBS workshop (Oumeraci et al., 2001) also gives a procedure developed by Calabrese (1998 and 1999) to estimate the proportion of impacts onto the vertical seawall. This is done in two steps: first the proportion of breaking waves is determined. This includes not only the waves actually breaking onto the structure but also the waves breaking clear of the structure, i.e. broken waves. In the second step the proportion of broken waves is estimated and subtracted from the previous result of step 1. This yields an estimation of the proportion of impacting waves.

In the case of plain vertical seawalls the procedure starts with the calculation of the peak period wave length L_{pi} in the local water depth h:

$$L_{pi} = \frac{gT_p^2}{2\pi} \tanh \frac{2\pi h}{L_{pi}} \tag{3}$$

The breaking wave height H_{bc} is calculated as follows:

$$H_{bc} = 0.1025 L_{pi} \tanh \frac{2\pi h}{L_{pi}} \tag{4}$$

The incident wave height H_{si} is then compared to the breaking wave height H_{bc}:

$H_{si} / H_{bc} \leq 0.6$	No evident breaking occurs and wave load is non-breaking
$0.6 < H_{si} / H_{bc} < 1.2$	Wave breaking occurs and waves may give impacts
$H_{si} / H_{bc} \geq 1.2$	Heavy breaking or waves may give broken loads

The proportion of waves breaking either in front of the structure (broken waves) or straight onto the structure (impacting waves) can then be estimated by:

$$P_b = \exp\left[-2\left(\frac{H_{bc}}{H_{si}}\right)^2\right] \tag{5}$$

The predicted value of P_b can be considered an upper limit for the proportion of impacting waves because it includes both the proportion of broken and impacting waves. Equation (5) is valid for $0.08 \leq h_s/L_{pi} \leq 0.2$ and $H_{si}/d \leq 1.3$.

The maximum wave height which describes the transition from impacting to broken mode can be estimated as follows:

$$H_{bs} = 0.1242 L_{pi} \tanh \frac{2\pi h}{L_{pi}} \tag{6}$$

Thus, the proportion of waves which actually break onto the structure P_i can be estimated as follows:

$$P_i = \exp\left[-2\left(\frac{H_{bc}}{H_{si}}\right)^2\right] - \exp\left[-2\left(\frac{H_{bs}}{H_{si}}\right)^2\right] \tag{7}$$

One disadvantage of this method is that the steepness of the approach beach has been neglected although waves may break more than once on a long and shallow slope, whereas on a short and steep slope waves may break only once and are much more likely to actually break straight onto the seawall.

2.3 Mean Overtopping Discharge

2.3.1 Introduction

In this section previous work on mean overtopping discharge over coastal structures is discussed. First an overview of key methods for simply sloped, impermeable, and smooth structures is given. Subsequently, prediction methods for plain vertical seawalls are presented. Finally, the effect of obliquity is discussed for all types of seawalls including permeable structures under long crested and short crested wave attack.

Sub-section 2.3.2 gives a general overview of prediction methods for simply sloped, impermeable, and smooth structures, which were historically the starting point for research in wave overtopping. They are to some extent related to those of plain vertical seawalls and give a basis of knowledge on the physical dependencies of the overtopping discharge.

In sub-section 2.3.3 plain vertical seawalls are discussed. This includes methods which distinguish explicitly or implicitly between waves in impacting or reflecting mode. Some methods, however, are only valid in deepwater under reflecting conditions.

The final sub-section 2.3.4 covers the effect of oblique wave attack. It will be shown that guidance for the prediction of mean discharge over vertical seawalls under oblique wave attack is only available for waves in deep water and reflecting mode. When waves are predominantly in impacting mode then no guidance is available under oblique wave attack.

The main purpose of this thesis is to close this gap and derive prediction tools for this case. The second issue to be discussed in this sub-section is whether small angles of wave attack can lead to an increase in overtopping.

2.3.2 Simply sloped, impermeable, and smooth structures

This sub-section covers simply sloped, impermeable, and smooth structures giving a general overview of key prediction methods. Some of the overtopping models are very similar to models developed subsequently for plain vertical walls.

Owen (1980) completed a comprehensive study on simply sloped and bermed seawalls (see Figure 3) under irregular wave attack. He proposed the following general design formula for the mean overtopping discharge:

$$Q^* = A\exp(-BR^*) \tag{8}$$

Q* and R* are the dimensionless discharge and the dimensionless freeboard, respectively. They are defined as follows:

$$Q^* = \frac{Q}{T_m g H_s} \tag{9}$$

$$R^* = \frac{R_c}{T_m \sqrt{g H_s}} \tag{10}$$

where Q is the mean overtopping discharge rate per metre run of seawall. A and B are empirical coefficients which depend on the profile of the seawall. He offers values of A and B for simply sloped seawalls ranging in slope angle from 1:1 to 1:5. They were derived either from own model tests or by interpolations based on published run-up data.

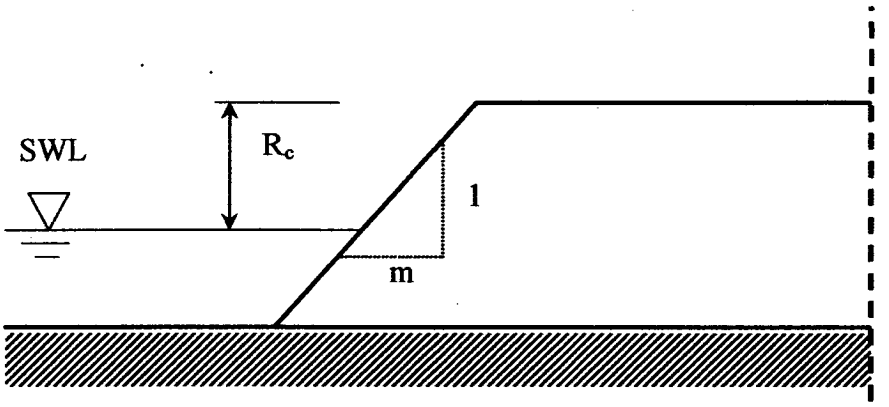

Figure 3: Simply sloped seawall investigated by Owen (1980)

De Waal and van der Meer (1992) proposed an alternative set of equations to determine the mean overtopping over simply sloped and bermed seawalls. The starting point is a formula for the $R_{u2\%}$ run-up on the slope. The $R_{u2\%}$ run-up above SWL is exceeded by 2% of the incident waves only.

$$\frac{R_{u2\%}}{H_s} = 1.5\xi_{op} \tag{11}$$

where $R_{u2\%}/H_s$ has a maximum of 3.0. H_s is the significant wave height (m) and ξ_{op} the Iribarren number or "surf similarity" parameter defined as:

$$\xi_{op} = \frac{\tan\alpha}{\sqrt{s_{op}}} \tag{12}$$

tan α is the slope of the approach sea bed and s_{op} the offshore wave steepness based upon the peak period. Influence factors for roughness of the slope (γ_f), shallow water (γ_h), and oblique wave attack (γ_β) can be added to equation (11):

$$\frac{R_{u2\%}}{H_s} = 1.5\,\gamma_f\,\gamma_h\,\gamma_\beta\,\xi_{op} \tag{13}$$

Equation (13) then feeds into the overtopping formula which is given by:

$$\frac{Q}{\sqrt{gH_s^3}} = 8.10^{-5}\exp\left(3.1\frac{R_{u2\%}-R_c}{H_s}\right) \tag{14}$$

where Q is again the mean overtopping rate per metre run of seawall ($m^3/m/s$) and $R_{u2\%}$ the 2% run-up as defined above (m). The term

$$\frac{R_{u2\%} - R_c}{H_s} \tag{15}$$

is strictly speaking not a dimensionless freeboard but the dimensionless excess of the crest level above the 2% run-up level.

Hedges and Reis (1998) developed a model which assumes that no overtopping (apart from wind blown spray) occurs if the seawall freeboard exceeds the maximum wave run-up on the face of the structure. They based their method on a re-analysis of Owen's (1980) data covering uniform seaward slopes of 1:1, 1:2, and 1:4, subject to random waves approaching normal to the slope. They suggest an equation of the following form:

For $0 \leq R_* < 1$:

$$Q_* = A(1 - R_*)^B \tag{16}$$

and for $R_* \geq 1$:

$$Q_* = 0 \tag{17}$$

where:

$$Q_* = \frac{Q}{\sqrt{gR_{max}^3}} \tag{18}$$

and:

$$R_* = \frac{R_c}{R_{max}} \tag{19}$$

A and B are regression coefficients which depend on the slope angle and the regression model. R_{max} is the maximum run-up (m) induced by the random incident waves. Unless R_{max} exceeds the freeboard R_c there is no overtopping.

Van der Meer (2002) recommends an exponential relationship between dimensionless discharge Q* and freeboard R*:

$$Q^* = A\exp(-BR^*) \tag{20}$$

The coefficients A and B are functions of wave height, slope angle, breaker parameter, and influence factors. The following formulae represent average values for the mean

overtopping discharge. The actual overtopping formula is dependent on the breaker parameter ξ. For $\xi < 2$ the following formula is given:

$$\frac{Q}{\sqrt{gH_{mo}^3}} = \frac{0.06}{\sqrt{\tan\alpha}} \gamma_b \xi_o \exp\left(-4.7 \frac{R_c}{H_{mo}} \frac{1}{\xi_o} \frac{1}{\gamma_b \gamma_f \gamma_\beta \gamma_v}\right) \tag{21}$$

H_{m0} is the significant spectral wave height at the toe of the dike (m), ξ_0 the breaker parameter (-) and the γ values represent influence factors for the influence of berm, roughness of slope, angle of wave attack, and vertical wall, respectively.

For $2 < \xi < 5$ the following formula is given:

$$\frac{Q}{\sqrt{gH_{mo}^3}} = 0.2 \exp\left(-2.3 \frac{R_c}{H_{mo}} \frac{1}{\gamma_f \gamma_\beta}\right) \tag{22}$$

In order to account for shallow and very shallow foreshores yet another formula is given for $\xi > 7$:

$$\frac{Q}{\sqrt{gH_{mo}^3}} = 0.12 \exp\left(-\frac{R_c}{H_{mo}} \frac{1}{(0.33 + 0.022\xi_o)} \frac{1}{\gamma_f \gamma_\beta}\right) \tag{23}$$

In the range of $5 < \xi < 7$ the logarithm of q can be interpolated between the formulae for $\xi = 5$ and $\xi = 7$.

It is interesting to note that there is no dependency of the mean discharge on the wave period in equations (21) to (23). This is in line with current guidance for models on vertical seawalls if the waves are predominantly in reflecting mode (see sub-section 2.3.3).

These key prediction methods for the mean overtopping discharge over simply sloped, impermeable, and smooth seawalls are summarised in Table 1. The first column gives the appropriate reference. The second and third columns give the definition of the dimensionless discharge Q* and dimensionless freeboard R*, respectively. The last column specifies the proposed overtopping model.

Table 1: Examples of formulae for simply sloped, impermeable, and smooth structures

Reference	Dimensionless discharge Q_*	Dimensionless freeboard R_*	Overtopping model
Owen (1980)	$\frac{Q}{T_m g H_s}$	$\frac{R_c}{T_m \sqrt{g H_s}}$	$Q^* = A\exp(-BR^*)$
de Waal and van der Meer (1992)	$\frac{Q}{\sqrt{g H_s^3}}$	$\frac{R_c - R_{u2\%}}{H_s}$	$Q^* = A\exp(-BR^*)$
Hedges and Reis (1998)	$\frac{Q}{\sqrt{g R_{\max}^3}}$	$\frac{R_c}{R_{\max}}$	$Q_* = A(1-R_*)^B$ $Q_* = 0$ ($R_* \geq 1$)
van der Meer (2002)			$Q^* = A\exp(-BR^*)$
$\xi_p < 2$:	$\frac{Q}{\sqrt{g H_{mo}^3}} \frac{\sqrt{\tan\alpha}}{\xi_o}$	$\frac{R_c}{H_{mo}} \frac{1}{\xi_o}$	
$2 < \xi_p < 5$:	$\frac{Q}{\sqrt{g H_{mo}^3}}$	$\frac{R_c}{H_{mo}}$	
$5 < \xi_p < 7$:	interpolation	interpolation	
$\xi_p > 7$:	$\frac{Q}{\sqrt{g H_{mo}^3}}$	$\frac{R_c}{H_{mo}} \frac{1}{(0.33 + 0.022\xi_o)}$	

2.3.3 Plain Vertical Seawall

Tsuruta and Goda (1968) were the first researchers to conduct experiments on wave overtopping over vertical seawalls with irregular waves. They derived design diagrams for two types of seawalls: one for a plain vertical wall with a 1:20 approach bathymetry and one for a simply sloped seawall covered with concrete blocks.

Other design diagrams have been added at a later stage (Goda (1971), Goda et al. (1975), and Goda (2000)). In the case of vertical seawalls additional sets of diagrams for 1:10 and 1:30 approach beaches were derived. The discharge has been non-dimensionalised by

$$Q^* = \frac{Q}{\sqrt{2g(H_o')^3}} \tag{24}$$

where H_o' is the equivalent deepwater wave height (m), which has been adjusted for refraction and diffraction.

Goda's equivalent deepwater wave height H_0' is a hypothetical wave devised for the purpose of adjusting the heights of waves which may have undergone refraction and diffraction, so that the estimation of wave transformation, such as shoaling and breaking, can be carried out more easily when dealing with complex topographies. H_0' corresponds to the statistical significant wave height, i.e. the average of the highest one third of all wave heights.

Three other input parameters for the design diagrams are required: the relative water depth h/H_o', the relative freeboard R_c/H_o', and the wave steepness H_o'/L_o.

Each diagram was derived for a particular wave steepness and three wave steepnesses are offered for each structure configuration covering H_o'/L_o = 0.012, 0.017, and 0.036. An example is shown in Figure 4. It should be noted that Goda used the symbol "q" and not "Q" for the mean discharge per unit length of structure (q = Q).

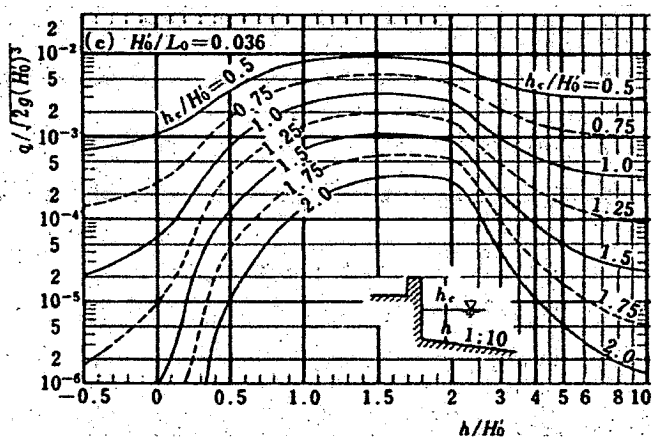

Figure 4: Example design diagram (Goda, 2000)

Although not explicitly stated by Goda, the design diagrams can be divided into different sections along the relative water depths h/H_s, which can be classified as reflecting, impacting and broken waves (Figure 5) with impacting waves giving the highest overtopping. The transition from reflecting to impacting waves is characterised by a high gradient in the design diagram, i.e. a steep increase in overtopping towards lower relative water depths. The transition zone, which marks the transition between impacting and reflecting mode, is about in line with the PROVERBS parameter map (H_{si}/h_s=0.35) (Oumeraci et al., 2001, see section 2.2). It should be noted, however, that "H_{si}/h_s=0.35" is inshore, whereas Goda uses the offshore wave height ("equivalent deepwater wave height"). Thus, in order to compare H_0' and H_{si}, H_0' needs to be adjusted for the shallow water effects wave shoaling and breaking.

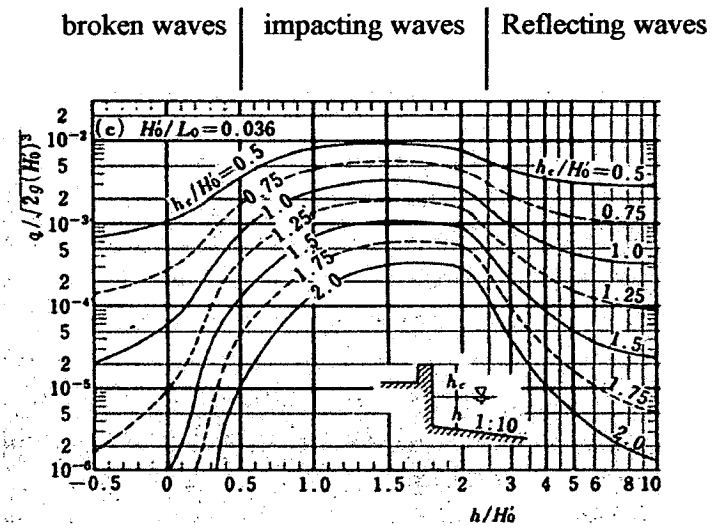

Figure 5: Approximate distinction of broken, impacting, and reflecting waves

The prediction methods by Goda cover a wide range of test conditions. The offshore wave steepness, however, is limited to H_o'/L_o = 0.036, which can easily be exceeded in the North Sea. Another limitation is the relatively low relative freeboard of $R_c/H_o' \leq 2.0$, which is exceeded in many sites around the UK.

Ahrens and Heimbaugh (1988) conducted laboratory tests with irregular waves for a number of seawall and seawall / revetment configurations including a plain vertical seawall. The tests were carried out in deepwater. They found an exponential relationship between the dimensionless discharge Q* and the dimensionless freeboard R*:

$$Q^* = A\exp(-BR^*) \tag{25}$$

where

$$Q^* = \frac{Q}{\sqrt{gH_{mo}^3}} \tag{26}$$

and

$$R^* = \frac{R_c}{\left(H_{mo}^2 L_p\right)^{1/3}} \tag{27}$$

H_{mo} is the energy based zero-moment wave height at the toe of the seawall (m). This approach was also confirmed by Schüttrumpf et al. (1999), who conducted model tests on different structures including a vertical seawall.

Mizuguchi (1993) derived a set of equations for the wave overtopping rate over a vertical wall and the resulting wave reflection coefficient using regular waves. The formulae were derived analytically on the basis of the wave energy flux concept and no experimental constants were needed. The results have been confirmed by a series of model tests. However, as the approach is based on regular waves and the author has no knowledge of any subsequent extension to irregular seas, the equations are not presented in this thesis.

Franco et al. (1994) conducted a series of 2-d model tests on the overtopping response of various caisson breakwaters. The basic reference structure was a plain vertical wall. They measured mean and wave-by-wave discharges under deepwater non-breaking wave conditions. The following formulae have been derived for mean overtopping discharge:

$$Q^* = \frac{Q}{\sqrt{gH_s^3}} \tag{28}$$

$$Q^* = 0.2 \exp\left(-4.3 \frac{R_c}{H_s}\right) \tag{29}$$

It should be noted that the structure of equation (29) including the dimensionless discharge and freeboard is the same as the one offered by the EA manual (1999) for reflecting conditions. Only the coefficients differ, but the actual predictions over the valid range of wave conditions are almost identical. Both formulae give the mean discharge as functions of the freeboard R_c and the significant wave height H_s and do not include the wave period. Franco's approach could also be confirmed by Schüttrumpf et al. (1998).

Results of Allsop et al. (1995) indicated that the overtopping performance of vertical walls is dependent on the "mode" which the waves are in when they interact with the structure. In deep water waves generally do not break and are reflected from the structure. The waves are then in reflecting mode. However, if the water depth at the toe of the structure is sufficiently shallow then the waves start breaking onto the structure, causing a change in the overtopping performance.

The results by Allsop et al. (1995) and their design guidance have been summarised by the EA manual (1999) (UK Environment Agency manual for "Overtopping of Seawalls"). They suggest the h* parameter to distinguish between waves predominantly in reflecting and impacting mode:

$$h^* = \frac{h}{H_s}\frac{2\pi h}{g T_m^2} \tag{30}$$

When $h^* > 0.3$ then reflecting waves predominate; when $h^* \leq 0.3$ then impacting waves predominate. In the case of impacting waves new dimensionless parameters were derived and overtopping equations were presented for both modes of wave action.

When reflecting waves predominate ($h^* > 0.3$) then the following equation applies:

$$Q\# = 0.05 \exp\left(-2.78 \frac{R_c}{H_s}\right) \tag{31}$$

where Q# is the dimensionless discharge, given by

$$Q\# = \frac{Q}{\sqrt{g H_s^3}} \tag{32}$$

Equation (31) is valid for $0.3 < R_c/H_s < 3.2$. It has the same structure as equation (29) which was also derived for reflecting conditions by Franco et al. (1994), but uses different coefficients (see also Table 2). A comparison between the methods offered by the EA manual (1999) and Franco et al. (1994) is given in Figure 6:

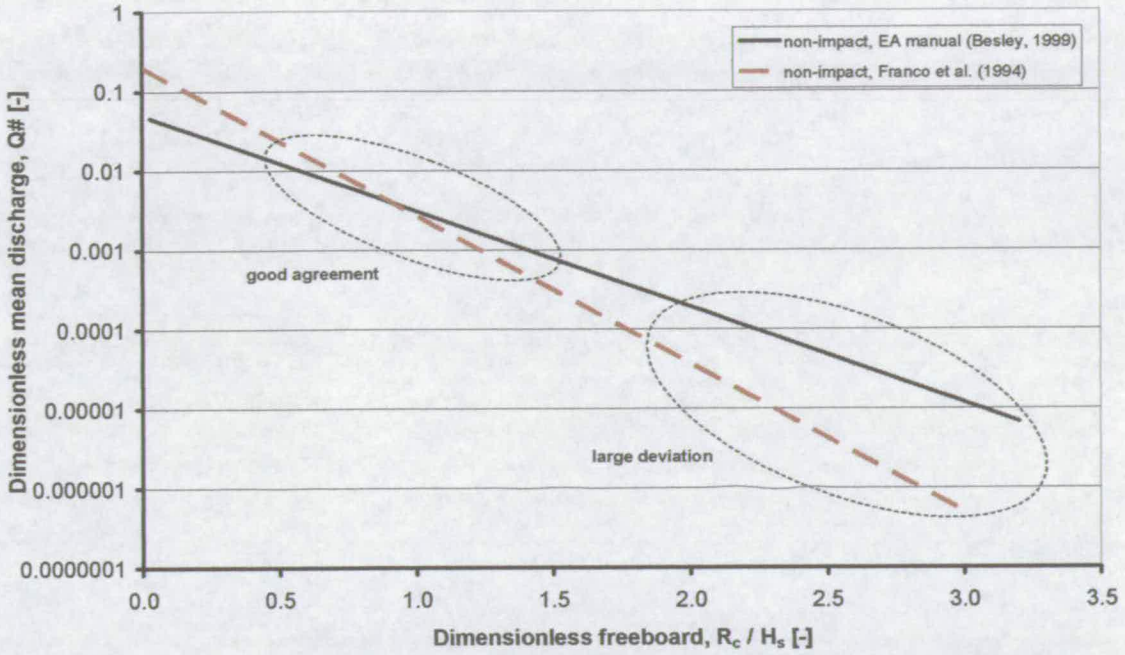

Figure 6: Comparison: prediction methods for reflecting conditions after EA manual (1999) and Franco (1994)

For dimensionless freeboards of about $0.5 < R_c/H_s < 1.5$ both formulae give good agreement. Towards higher dimensionless freeboards of about $2.0 < R_c/H_s$ and above up to the end of the valid range, however, the non-impact formula by Franco et al. (1994) predicts up to more than an order of magnitude less overtopping.

When impacting waves predominate ($h^* \leq 0.3$) then the EA manual (1999) suggests a power law type equation:

$$Q_h = 0.000137 R_h^{-3.24} \tag{33}$$

where Q_h is the dimensionless discharge given by:

$$Q_h = \frac{Q}{h^{*2}\sqrt{gh^3}} \tag{34}$$

and R_h is the dimensionless crest freeboard given by:

$$R_h = \frac{R_c}{H_s} h^* \tag{35}$$

Equation (33) is valid for $0.05 < R_h < 1.00$. This approach could be confirmed by Bruce et al. (2001) and Pearson et al. (2002). Pearson et al. (2002) conducted tests at small and large scale also showing that within experimental limitations there was no significant difference between Q_h measured in small- and large-scale studies.

It should be noted that the overtopping equation for reflecting conditions, equation (31), is driven by only two parameters: the freeboard R_c and the significant wave height H_s. In the case of impacting conditions, however, the mean wave period T_m and the local water depth h are included as well (equation (33)).

The key prediction methods for wave overtopping over plain vertical seawalls are summarised in Table 2. The table gives the reference and the overtopping model including the dimensionless discharge and freeboard.

Table 2: Examples for design formulae for vertical seawalls

Reference	Dimensionless discharge Q*	Dimensionless freeboard R*	Overtopping model	wave mode*
Tsuruta and Goda (1968)	$\frac{Q}{\sqrt{2g(H_o')^3}}$	$f = \frac{R_c}{H_0'}, \frac{h}{H_0'}, \frac{H_0'}{L_o}, \frac{1}{m}$	design diagrams	refl + imp
Ahrens and Heimbaugh (1988)	$\frac{Q}{\sqrt{gH_{mo}^3}}$	$\frac{R_c}{\left(H_{mo}^2 L_p\right)^{1/3}}$	$Q^* = A\exp(-BR^*)$	refl
Franco et al. (1994)	$\frac{Q}{\sqrt{gH_s^3}}$	$\frac{R_c}{H_s}$	$Q^* = A\exp(-BR^*)$	refl
Allsop et al. (1995) refl. mode: ($h^* > 0.3$)	$\frac{Q}{\sqrt{gH_s^3}}$	$\frac{R_c}{H_s}$	$Q^* = A\exp(-BR^*)$	refl
Allsop et al. (1995) impacts: ($h^* \leq 0.3$)	$\frac{Q}{\sqrt{gh^3}\left(\frac{h}{H_s}\frac{2\pi h}{gT_m^2}\right)^2}$	$\frac{R_c}{H_s}\frac{h}{H_s}\frac{2\pi h}{gT_m^2}$	$Q_h = AR_h^{-B}$	imp

* "refl." / "imp" = formula valid for waves predominantly in reflecting or impacting mode, respectively

2.3.4 Effect of Obliquity (sloped and vertical structures)

This sub-section covers the effect of oblique wave attack. Although all types of structures are discussed it shows in particular that no guidance is available for the prediction of mean discharge over plain vertical seawalls under oblique and impulsive wave attack. The main purpose of this thesis is to close this gap and derive prediction tools for this case. The second issue to be discussed in this sub-section is whether small angles of wave attack can lead to an increase in overtopping.

Tautenhain et al. (1982) investigated the influence of oblique wave attack on wave run-up and overtopping over a simply sloped smooth structure. The slope was set to 1:6 and obliquities of up to 60° were analysed. They found a decrease in wave run-up for angles of wave attack larger than 35°. In the range of $0 < \beta \leq 35°$, however, they found an increase of up to 10% in wave run-up.

De Waal and van der Meer (1992) also conducted model tests on simply sloped smooth structures under oblique wave attack. The approach angle was varied between 0° and 80°. The slope angles covered 1:1.5 to 1:8 and long as well as short crested waves were investigated.

They found that short crested perpendicular wave attack gave similar results in overtopping as long crested perpendicular wave attack. However, under oblique wave attack the results differed. At up to about 30° obliquity long crested exceeded short crested overtopping and from then on short crested overtopping was more significant. In both cases they could not confirm an increase in overtopping for small angles of wave attack as reported by Tautenhain et al. (1982).

Moriya and Mizuguchi (1996) extended the overtopping model by Mizuguchi (1993), which predicts the wave overtopping over plain vertical seawalls under regular wave attack. They ran model tests with oblique and regular waves. Results of their numerical calculations showed a slight decrease in the wave overtopping rate with increasing angle of wave attack. This could be confirmed by model tests in a multidirectional wave basin.

Juhl and Sloth (1994) studied the effect of oblique wave attack on wave overtopping over a rubble mound breakwater without superstructure and with an armour layer slope of 1:2. They varied the angle of wave attack between 0° and 50° in steps of 10° and ran long crested irregular waves.

They introduced a reduction factor defined as the ratio of overtopping for oblique versus perpendicular waves. The reduction factor appeared to be dependent on the three different freeboards tested. In the case of the smallest tested freeboard the average of all tests showed an increase in mean overtopping at 10° obliquity. At 20° and 30° obliquity a pronounced decrease has been measured and at 50° the reduction factor reduced to 0.1, i.e. the overtopping was 90% lower than at perpendicular wave attack. This reduction is significantly higher than the reduction measured by de Waal and van der Meer (1992), which was only 40%.

For the other (higher) freeboards only a few tests showed an increase at 10% obliquity and on average a decrease was found. In general, Juhl and Sloth (1994) found a higher decrease in overtopping at 10° and 20° obliquity for higher freeboards than for lower ones. The reduction for the highest tested freeboard, for example, at 20° obliquity was about 80%, whereas the reduction for the lowest tested freeboard at 20° was only about 40%.

Galland (1994) also investigated the effect of long crested oblique wave attack on rubble mound breakwaters. He tested four different types of armouring units (quarry stone, Antifer cube, tetrapod and Accropode) under six angles of waves attack (0°, 15°, 30°, 45°, 60°, and 75°). He found no reduction in overtopping for 15° obliquity and from then on the overtopping decreased continuously until the overtopping was reduced to nearly zero at 60°.

Banyard and Herbert (1995) investigated the effect of oblique wave attack on simply sloped and bermed seawalls. They found a slight increase in wave overtopping at small angles of wave attack under only a few conditions, but overtopping was generally found to decrease with increased angle of attack. The reduction was smaller for short crested seas than for long crested seas. They developed equations to determine the ratio Q_r which is defined as the ratio of overtopping at a given angle of wave attack to that predicted under normal wave attack:

For simply sloping seawalls:

$$Q_r = 1 - 0.000152\beta^2 \tag{36}$$

and for bermed seawalls:

$$Q_r = 1.99 - 1.93(1.0 - ((\beta - 60)/69.8)^2)^{0.5} \tag{37}$$

In this approach Q_r is a function of the angle of wave attack β only. While this might be the case for simply sloped and bermed seawalls, it is rather unlikely for vertical structures under impulsive wave attack as investigated in this thesis. The overtopping is strongly driven by wave impacts which, as will be shown later, diminish at increasing angles of wave attack. The extent at which wave impacts reduce, however, depends on the wave conditions as well. High wave conditions are less affected then low wave conditions. Thus, for vertical structures Q_r will not only be a function of β but would be expected to be a function of the wave conditions as well.

Sakakiyama and Kajima (1996) studied the effect of wave obliquity and multidirectional waves on wave overtopping along a simply sloped armoured seawall. They concluded that oblique waves gave less overtopping than multidirectional waves, which in turn gave less overtopping than waves which reach the structure perpendicularly.

Franco et al. (1994) developed a method to predict wave overtopping over a plain vertical seawall under perpendicular, deepwater (i.e. reflecting) wave attack. Franco et al. (1995), Franco (1996), and Franco and Franco (1999) extended this method to oblique wave attack. The influence of geometrical changes, wave obliquity, and multi directionality has been described by reduction factors referring to the case of a simple vertical structure under long crested head-on wave attack (i.e. equation (29), sub-section 2.3.3). As before all tests were conducted in deep water with non-breaking (i.e. reflecting) waves.

In order to properly detect 3d effects in overtopping equation (29) has first been modified by re-doing the regression analysis choosing only the most consistent test data. This led to the following equation, which was then used as the 2d reference case:

$$Q^* = 0.082 \exp\left(-3.0 \frac{R_c}{H_s}\right) \tag{38}$$

Different wave obliquities and multi directionality were then described by a reduction factor $\gamma_{\beta\sigma}$. The value of $\gamma_{\beta\sigma}$ can be interpreted as the potential reduction of freeboard to accommodate the same overtopping rate under similar incident wave heights in 3d seas.

$$Q^* = 0.082 \exp\left(-\frac{3.0}{\gamma_{\beta\sigma}} \frac{R_c}{H_s}\right) \tag{39}$$

They found that for long crested waves the overtopping discharges over a plain vertical wall reduced noticeably in the range of $\beta = 0°$ to 40° and then remained nearly constant up to $\beta = 60°$. In the case of short crested waves, however, a clear reduction in overtopping was only observed for angles of wave attack larger than 40° ($\beta \geq 40°$), whereas between β = 20-30° even a slight increase has been observed.

Allsop et al. (1995) and the EA manual (1999) suggested a method for the prediction of wave overtopping over a plain vertical wall under perpendicular wave attack (see sub-section 2.3.3). They distinguished between reflecting and impacting wave conditions offering design formulae for each condition. The distinction is based upon the **h*** parameter as given in equation (30) sub-section 2.3.3.

In the case of reflecting wave conditions they suggest a reduction factor when waves approach at an angle. This reduction factor γ is added to equation (31) (see sub-section 2.3.3) in a similar way as Franco and Franco (1999):

$$Q\# = 0.05 \exp\left(-\frac{2.78}{\gamma}\frac{R_c}{H_s}\right) \tag{40}$$

γ is given by:

$$\gamma = 1 - 0.0062\beta \quad \text{for } 0° < \beta \leq 45° \tag{41}$$

$$\gamma = 0.72 \quad \text{for } \beta > 45° \tag{42}$$

where β is the angle of wave attack relative to the normal in degrees. As can be seen from the values of γ the overtopping reduces up to 45° and then remains constant. This is again in line with Franco and Franco (1999). Allsop et al. (1995) and the EA manual (1999) offer no guidance for the effect of angled wave attack when waves are in impacting mode.

Gronbech et al. (1997) studied the effect of wave impacts and obliquity on vertical caisson breakwaters situated in irregular, multidirectional breaking seas. They varied the angle of wave attack from 0° to 50°. The study showed that the 3d formula for wave overtopping by Franco et al. (1995) gave good agreements for both non breaking and breaking waves in deep water. It also showed no significant difference in wave overtopping behaviour between both wave modes (i.e. non breaking and breaking). They explained this rather surprising behaviour with the particular process of wave breaking in deep water, which was

characterised by spilling breakers. Plunging breakers, which occurred in shallow water, had a different physical behaviour.

This thesis is mostly concerned with seawalls under wave attack in shallow water, where heavy wave breaking in the form of plunging breakers predominates. Thus, based upon extensive evidence from 2d studies a considerable difference in overtopping between reflecting and impacting conditions is expected.

Hiraishi and Maruyama (1998) propose a numerical model to estimate the overtopping rate for oblique and multidirectional waves, which has been experimentally verified. They found that the overtopping rate is smaller for multidirectional waves than for unidirectional oblique waves when the angle of wave attack is smaller than 30°. For angles of wave attack larger than 30° they found that multidirectional waves gave higher overtopping.

Daemrich and Mathias (1999) investigated the effect of obliquity on wave overtopping for a vertical wall with a steep 1:1.7 approach revetment and a short 1 m berm. The tests were performed with long crested irregular waves and approach angles of $\beta = 0$, 20 and 40°. The results show an overall reduction in the wave overtopping rate with increasing obliquity.

Ohle et al. (2002) studied wave run-up on a smooth 1:6 sloped seawall under oblique wave attack. The angles of wave attack ranged from 0° to 40° and the directional spreading from 0°, 10°, 20°, and 30°. In contrast to de Waal et al. (1992) they found no significant difference in wave run-up between long and short crested waves under oblique waves of up to 40°. They also found no increase in run-up for small angles of wave attack.

2.3.5 Summary and Conclusions

In this section previous work on mean overtopping discharge over seawalls has been discussed. First an overview of key methods for simply sloped, impermeable, and smooth structures was given. Subsequently, prediction methods for plain vertical seawalls were presented. Finally, the effect of obliquity was discussed for all types of seawalls including permeable structures under long crested and short crested wave attack.

The process of wave overtopping over a plain vertical seawall is strongly influenced by the mode which the waves are in. Waves can either be predominantly in reflecting or in impacting mode – depending essentially on the local water depth, wave height, and wave period. Different design guidance has been offered for either wave mode.

The literature review has revealed that when waves attack at an angle prediction tools are available when the waves are in reflecting mode only. No design guidance is available for the mean wave overtopping discharge when a plain vertical seawall is subject to oblique and violent (i.e. impulsive) wave attack. The main purpose of this thesis is to close this gap and derive prediction tools for this case.

Another issue discussed in this sub-section was whether small angles of wave attack can lead to an increase in overtopping. This has been investigated for all types of coastal structures including sloped and vertical seawalls and rubble mound breakwaters. The evidence in literature is somewhat contradictory: in most cases only reductions in overtopping have been found. Only few authors reported a slight increase (i.e. less than 10%) at small angles of wave attack ($0° < \beta < 20°$).

Finally, no authors reported on any laboratory data or observations of spatial variability along plain vertical seawalls subject to oblique wave attack.

2.4 Individual Overtopping Discharge

In this section the (few) methods to predict the maximum individual overtopping volumes over plain vertical seawalls are presented. These methods are all based on a Weibull probability function. As the Weibull function requires a prediction of the proportion of overtopping waves (N_{ow}/N_w) prediction methods for this quantity are given as well. The Weibull probability function is given as:

$$P(V_i < V) = 1 - \exp(-(V/a)^b) \qquad (43)$$

where $P(V_i < V)$ is the probability of an overtopping event V_i being smaller than a given Volume V, a is the "scale parameter", which can be calculated from Q and N_{ow}, and b is the "shape parameter".

Franco et al. (1994) conducted a series of 2d model tests on the overtopping performance of various caisson breakwaters including one with a plain vertical front face (see sub-section 2.3.3). The tests were carried out in deepwater with waves entirely in reflecting mode. It could be shown that individual overtopping volumes followed a Weibull probability distribution. This led to a set of formulae for the maximum overtopping discharge:

$$V_{max} = a \ln(N_{ow})^{1/b} \qquad (44)$$

where V_{max} is the maximum expected individual overtopping volume (m^3), N_{ow} the number of overtopping waves (-), and b a shape parameter equal to 0.75. a is a scale parameter defined as:

$$a = 0.84\, V_{bar} = 0.84\, \frac{T_m Q}{\left(\frac{N_{ow}}{N_w}\right)} \tag{45}$$

The mean individual overtopping volume V_{bar} (m^3) can be determined from the mean wave period T_m, the mean overtopping discharge Q ($m^3/m/s$) as given also by Franco et al. (1994) (see sub-section 2.3.3, equation (29)), and the proportion of overtopping waves N_{ow}/N_w (-). The proportion of overtopping waves can be calculated as follows:

$$\frac{N_{ow}}{N_w} = \exp\left(-\frac{1}{0.91}\frac{R_c}{H_s}\right)^2 \tag{46}$$

Franco and Franco (1999) extended this method to oblique wave attack. It should be noted that this method is valid for deepwater reflecting waves only. The basic formula for V_{max}, equation (44), remains the same. However, they give new equations for the Weibull scale and shape parameters, a and b, and for the proportion of overtopping waves. They also recommend the use of the formula for Q under oblique wave attack, equation (39), sub-section 2.3.4. The proportion of overtopping waves for the oblique case can be determined by adding a factor γ_{Pow} to equation (46):

$$\frac{N_{ow}}{N_w} = \exp\left(-\frac{1}{0.91\gamma_{Pow}}\frac{R_c}{H_s}\right)^2 \tag{47}$$

Franco and Franco (1999) give the influence factor γ_{Pow} for angles of wave attack of up to 60°. The values for γ_{Pow} differ slightly for long and short crested seas.

The EA manual (1999) also offers methods for the prediction of maximum overtopping events at plain vertical seawalls. As in the case of the mean overtopping discharge he first determines whether the waves are predominantly impacting or reflecting using the h* parameter (see also sub-section 2.3.3):

$$h^* = \frac{h}{H_s}\frac{2\pi h}{g T_m^2} \tag{48}$$

Reflecting waves predominate when $h^* > 0.3$ and impacting waves predominate when $h^* \leq 0.3$.

For both wave modes (i.e. reflecting and impacting) the EA manual (1999) gives the same formula for V_{max}, i.e. individual overtopping volumes follow a Weibull probability distribution. This formula is identical to the one offered by Franco and Franco (1999), equation (44):

$$V_{\max} = a \ln(N_{ow})^{1/b} \tag{49}$$

The input parameters, however, vary slightly from Franco and Franco (1999), whose approach is only valid for waves in reflecting mode.

When waves are predominantly in reflecting mode then the EA manual (1999) suggests the following values for the Weibull a and b parameters:

$a = 0.74\ V_{bar}$, $b = 0.66$ for $s_{op} = 0.02$

$a = 0.90\ V_{bar}$, $b = 0.82$ for $s_{op} = 0.04$

where s_{op} is the offshore wave steepness and V_{bar} the mean individual overtopping discharge, given by:

$$V_{bar} = \frac{QT_m N_w}{N_{ow}} \tag{50}$$

where Q is the mean discharge ($m^3/s/m$), N_{ow} the number of overtopping waves (-), N_w the number of incoming waves (-), and T_m the mean wave period at the toe of the structure (s). Q can be calculated as given by the EA manual (1999) in sub-section 2.3.3. For the proportion of overtopping waves N_{ow}/N_w he gives the same formula as Franco and Franco (1999):

$$\frac{N_{ow}}{N_w} = \exp\left(-\frac{1}{0.91}\frac{R_c}{H_s}\right)^2 \tag{51}$$

When the waves attack at an angle then basic formulae and the Weibull a and b parameters remain the same. Only the mean discharge Q and the proportion of overtopping waves change. Q can be determined after the EA manual (1999) in sub-section 2.3.4. The proportion of overtopping waves can be calculated as follows:

$$\frac{N_{ow}}{N_w} = \exp\left(-\frac{1}{C}\frac{R_c}{H_s}\right)^2 \tag{52}$$

The structure of this formula is nearly identical to equation (47) (Franco and Franco, 1999), but the "C" parameter differs slightly.

When waves are predominantly in impacting mode then the basic equations for V_{max} and V_{bar} (equations (49) and (50), respectively) still hold. The Weibull a and b parameters change to:

$$a = 0.92\ V_{bar}, \quad b = 0.85$$

with no dependency on the wave steepness. The formula for the percentage of overtopping waves changes to:

$$\frac{N_{ow}}{N_w} = 0.031\, R_h^{-0.99} \tag{53}$$

where R_h is the dimensionless freeboard given by:

$$R_h = \frac{R_c}{H_s}\frac{h}{H_s}\frac{2\pi h}{gT_m^2} \tag{54}$$

There is no guidance available for angled wave attack, when the waves are predominantly in impacting mode.

Schüttrumpf et al. (1999) presented a method for the prediction of the proportion of overtopping waves without giving further guidance on how to determine individual overtopping volumes:

$$\frac{N_{ow}}{N_w} = \exp(-4.16R_*) \tag{55}$$

where R_* is the dimensionless freeboard given by:

$$R_* = \frac{R_c}{\left(H_s^2 L\right)^{1/3}} \tag{56}$$

Schüttrumpf et al. (1999), however, do not further specify whether this method is valid for reflecting or impacting conditions.

In this section the (few) methods to predict the maximum individual overtopping volumes over plain vertical seawalls have been presented. These methods are all based on a Weibull probability function. There are two methods available for deepwater when waves are predominantly in reflecting mode. Both methods have the same structure and use only slightly different coefficients. Both methods have been extended to angled wave attack.

When waves are in impacting mode, however, then there is only one method available. This method has not been extended to angled wave attack and, hence, no design guidance for this case could be found in literature.

2.5 Admissible Overtopping

The definition of tolerable limits for overtopping proves to be difficult as many different factors – and not only technical ones – have to be taken into account. The tolerable limits must ensure the structural safety of the seawall and the drainage system must be designed such that it can cope with the amount of overtopping water (Goda (1971), Fukuda et al. (1974) and Goda (1975)). There are, however, also limits given by the safety of members of the public using the seawall.

The structural safety of the breakwater typically demands less restrictive limits of overtopping than the safety of the public (functional safety). Thus, larger overtopping can be allowed during extreme storms if transit on the breakwater is then prohibited (Franco et al., 1994).

This section focuses on the previous work on limits to overtopping which arise from hazards to the public. Fukuda et al. (1974) carried out full-scale measurements on seawall overtopping. Overtopping discharges were measured and filmed simultaneously. The films were then analysed by port and harbour research engineers for their individual assessment of the likely damage or injury to a walking person, an automobile, and a house. The assessment was then linked to the measured mean discharge. The results have also been summarised by Owen (1980).

Franco et al. (1994) summarised the threshold levels of overtopping which cause damage to embankments, promenade seawalls, buildings, vehicles, and pedestrians based on the mean discharge. They also took the results from Fukuda et al. (1974) and Goda (1975) into account. This approach has been updated several times. Figure 7 shows an example chart.

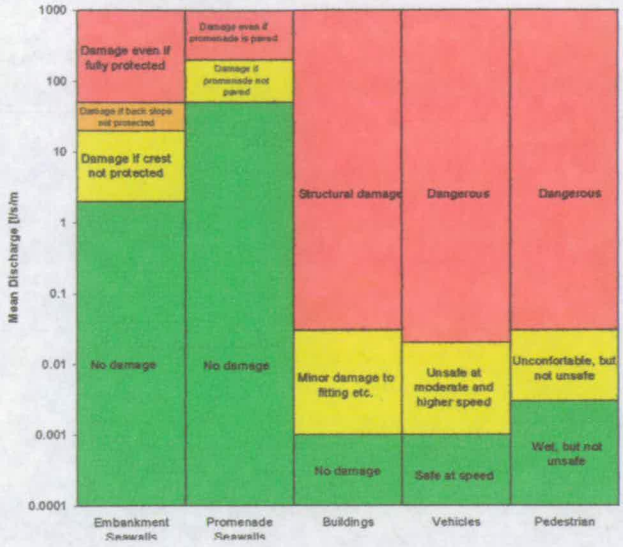

Figure 7: Threshold discharges after Franco et al. (1994), developed from Owen (1980), Fukuda et al. (1974) and Goda (1975)

Franco et al. (1994) also point out that it is the individual overtopping volume by wave – and not the mean discharge – which is actually responsible for the damage to the seawall or to the public. They analysed the stability of model pedestrians subject to single overtopping volumes. Franco et al. (1994) conclude that perhaps the overtopping volume per wave might be a better hydraulic parameter than the mean discharge.

Franco et al. (1994) found that there is no simple relationship between the mean discharge Q and the maximum individual overtopping discharge V_{max}. Ratios of Q/V_{max} (which are not dimensionless) can vary between 100 and 10000.

An ongoing research project "CLASH" (de Rouck et al., 2002) also seeks to give guidance on allowable overtopping based on hazard analysis. The project runs from January 2002 until December 2004 and the final results on this are still awaited.

Other parameters such as the overtopping induced loads on the crown of seawalls (Bruce et al., 2001) or the throw velocities and trajectories (Bruce et al., 2002) have also been suggested as parameters to measure hazards.

2.6 Scale and Model Effects

Scale and model effects are both inherent in any physical model test and compromise the applicability of the results for full scale design. Model effects arise from the basin and model

set-up in the laboratory. Examples are friction along the wave guides or deviations of the actual from the desired wave spectrum due to incorrect wave generation. Scale effects on the other hand arise from the inability of a scale model to reproduce all relevant forces of the prototype (Oumeraci, 2003) by fulfilling the related similarity laws (such as Froude or Reynolds law).

While model effects can be limited by optimising the basin and model set-up scale effects are caused by the smaller size of the model as compared to the prototype and can only be reduced by increasing the scale of the model. The extent of scale effects on run-up or overtopping may depend strongly on the structure to be modelled and can only be determined by a comparison of small scale tests to either large scale model tests or prototype measurements.

The EU project OPTICREST, for example, found that the wave run-up $Ru_{2\%}$ on rubble mound slopes, measured at prototype during full scale storms, was about 20% higher than modelled by selected hydraulic laboratories in small scale facilities (De Rouck et al., 2001; De Rouck et al., 2002). The reduced run-up may also mean a reduction in overtopping.

The BigVOWS project, however, could not find any scale effects in modelling overtopping of plain vertical seawalls (Pearson et al., 2002). The BigVOWS project measured mean and wave-by-wave overtopping at large scale and compared the results to predictions derived from small scale tests. Within experimental limitations (model effects) they found that the results showed no significant difference in small and large scale overtopping.

It should be noted that the physical model tests conducted as part of this thesis model such a vertical seawall. Thus, assuming that there are no significant scale effects introduced by the 3D model set-up the scale effects are assumed to be negligible.

An ongoing major European research project (January 2002 until December 2004), CLASH, is currently investigating the presence of scale effects in physical model tests by full scale measurements at different structures and sites (de Rouck et al., 2002). Final analysis is ongoing with results expected early in 2005.

2.7 Other Methods

2.7.1 Neural Networks

The design and prediction methods presented above have all been derived empirically from field data or data collected in physical model tests. These methods are essentially applicable only to a limited range of structure configurations, such as sea dikes or vertical seawalls. The CLASH project (de Rouck et al., 2002), an ongoing major European research project (January 2002 until December 2004), seeks to produce a generic prediction method for wave overtopping providing a tool for crest height design and assessment of coastal structures.

In a first step the prediction method will be based on a homogenous database where all available overtopping data is screened and gathered. This includes over 6000 tests described by 14 parameters.

Afterwards, a generally applicable design method will be developed with the use of neural methods. A neural network tries to recognise patterns in large data sets with a great number of parameters despite a lack of physical understanding (van Gent and van den Bogaard, 1998, Medina, 1999, and Medina et al., 2002).

2.7.2 Numerical models

Empirical overtopping models as discussed in sections 2.3 and 2.4 are limited to the wave conditions and spectra under which they were developed and tested. The same applies to the structural types, such as the slope angle and the berm type. Numerical models, however, have the potential to provide the means to cost-efficiently predict wave overtopping for different types of spectra (e.g. broad banded or bimodal) and complex structures.

Many numerical models have been developed to predict wave run-up and overtopping, most of which have been based on non linear shallow water equations (e.g. Hibberd and Peregrine, 1979; Kobayashi and Watson, 1987; Kobayashi et al., 1987; Titov and Synolakis, 1995; Kobayashi and Wurjanto, 1989; Dodd, 1998; Hu et al., 2000). The quality of the predictions of numerical models appears to have improved significantly since they were first introduced. Experiments of random wave (uni- and bimodal) overtopping, e.g. by Dodd (1998), indicate that for a particular set of conditions his model performs better than empirical formulae in predicting mean overtopping rates.

Richardson et al. (2002) and Shiach et al (2004) showed that approaches using the non linear shallow water equations give reasonable results under less impulsive conditions, but cannot be used to predict jet velocities and impact pressures. In any event, the underlying assumptions of continuous water surface and negligible vertical acceleration are violated during an overtopping event.

Ingram et al. (2002) and Isobe et al. (2002) suggest using a numerical method which solves for the location of the free surface in some way. Volume of fluid (VoF) schemes, for example, have been successfully applied to overtopping events (Troch, 1997; Isobe, 1999). They require, however, complex reconstruction algorithms to locate the water surface and are commonly formulated with a "numerical vacuum" above the water. Thus, Ingram et al. (2002) prefer the multi-fluid surface capturing approach, which provides an alternate formulation where the location of the water surface is determined by solving a transport equation for the density of the fluid. This has two primary advantages: well mixed spray and highly aerated water can be simulated and no interface reconstruction is required. Ingram et al. (2002) could validate their approach on a simulation of a dam break flow interacting with a vertical wall.

Although the non linear shallow water equations are not suitable for the prediction of violent wave overtopping, Mingham et al. (2002) have used such a model to successfully model refraction and diffraction effects within a wave basin. Their numerical model provides guidance to experimentalists in setting up wave basin experiments to investigate violent wave overtopping. In particular, they were able to optimise the length of the wave guides and to minimise the corruption effects of diffraction and reflection on the incident wave field.

An ongoing major European research project (January 2002 until December 2004), de Rouck et al. (2003) and CLASH (2002), seeks to improve the above mentioned groups of numerical models: firstly, the Volume of Fluid (VoF) approaches and secondly the 2D plan shallow water / long wave codes (non linear shallow water equations).

One of the current disadvantages of numerical models is that most codes require a large amount of computing time, which only allows simulating a very limited number of waves. Probabilistic effects, such as particularly high wave-structure interactions, which occur only once every 100 to 1000 waves, cannot be modelled in many cases.

2.8 Discussion and Conclusion

In this chapter the previous work on mean and wave-by-wave overtopping discharge has been discussed. This included the effect of angled wave attack and methods to predict the likelihood of waves breaking onto a vertical seawall. It could be shown that there is no guidance available for oblique and impulsive wave attack on a vertical seawall. The main purpose of this thesis is to close this gap and offer design guidance for this case.

A section on admissible overtopping discharges has been added to show that not only the mean but also the individual discharge is an important parameter when designing plain vertical seawalls. A short section on scale effects suggests that no substantial scale effects have to be expected when modelling vertical seawalls. Although the focus has been on empirical models a brief overview of other methods including neural networks and numerical models has been given as well.

It could be shown that the process of wave overtopping over a plain vertical seawall is strongly influenced by the mode which the waves are in. Waves can either be predominantly in reflecting or in impacting mode – depending essentially on the local water depth, wave height, and wave period. In literature, different design guidance has been offered for either wave mode.

The literature review has also revealed that when waves attack a plain vertical seawall at an angle prediction tools are available when the waves are in reflecting mode only. No design guidance is available – neither for mean nor maximum discharge – when a plain vertical seawall is subject to oblique and violent (i.e. impulsive) wave attack. As stated above, the main purpose of this thesis is to close this gap and derive prediction tools for this case.

The section on admissible overtopping has confirmed that not only mean but also individual overtopping is an important parameter when designing seawalls. The definition of tolerable limits for overtopping proves to be difficult as many different factors – and not only technical ones – have to be taken into account. The tolerable limits must ensure the structural safety of the seawall and the drainage system must be designed such that it can cope with the amount of overtopping water. There are, however, also limits given by the safety of members of the public using the seawall.

Another critical issue was whether small angles of wave attack can lead to an increase in overtopping. This has been investigated for all types of coastal structures including sloped

and vertical seawalls and rubble mound breakwaters. The evidence in literature is somewhat contradictory: in most cases only reductions in overtopping have been found. Only few authors reported a slight increase (i.e. less than 10%) at small angles of wave attack ($0° < \beta < 20°$).

Finally, no authors reported on any spatial variability along plain vertical seawalls subject to oblique wave attack.

3 PHYSICAL MODEL STUDY

3.1 Introduction

This chapter gives a detailed description of the physical model study conducted in order to derive guidance for mean and wave-by-wave overtopping over plain vertical seawalls subject to violent (impulsive) and oblique wave attack. Detailed sketches of all structure configurations including the position of wave gauges and measurement points can be reviewed in the Appendix. The usual notations and symbols are used throughout this thesis and can be reviewed in the Appendix Table 1.

First an overview of the experimental facility and measurement devices is given (section 3.2) and the design process of the structure, the test conditions, and the 3d structure configurations is outlined. As not all structure configurations could be calibrated a description of the wave calibration procedure and the determination of all relevant wave parameters is given in section 3.3.

Section 3.4 provides information on the analysis procedure and software, which allowed the analysis of the load cell and event detection traces including the influence of the pumps which have been used to drain the overtopping collection containers during test runs. The output of the software is a table of all individual overtopping volumes with the exact timing of each event. This output is then further analysed in chapters 7 and 8. Information on the accuracy of the measurements and the resolution of the load cell and event detector is given as well.

3.2 Measurement Devices, Test Structure, and Target Wave Conditions

3.2.1 Experimental Facility

The experimental facility was located at HR Wallingford, UK, and comprised of a wave basin 22m long by 19m wide, with a multi-element absorbing wave maker (Figure 8). The rim of the basin was 0.8m high allowing for a maximum water depth (SWL) of 0.6m. The

position of the wave paddle remained the same for all test conditions. In order to avoid reflections from the basin walls, an absorbing shingle beach was placed along two walls of the basin. The structure configurations were designed such that reflected wave components were either directed back to the absorbing paddle or into the absorbing shingle beach, which - like the wave paddle - also remained at the same position.[1] In order to minimise the loss of wave energy due to diffraction effects, wave guides were placed on either side of the wave paddle. The wave guides were varied in length according to the actual position and configuration of the structure.

A sketch of the basin is given in Figure 8 showing its dimensions, the position of the wave paddle, the wave guides, and the location of the absorbing shingle beach.

[1] In some special cases, in particular during wave calibration when the structure had been removed, some wave components reached the other side of the wave basin where no absorbing shingle beach was placed by default. For those configurations, extra shingle or absorbing "horse-hair" mattresses were moved to the appropriate positions along the wall to avoid reflections.

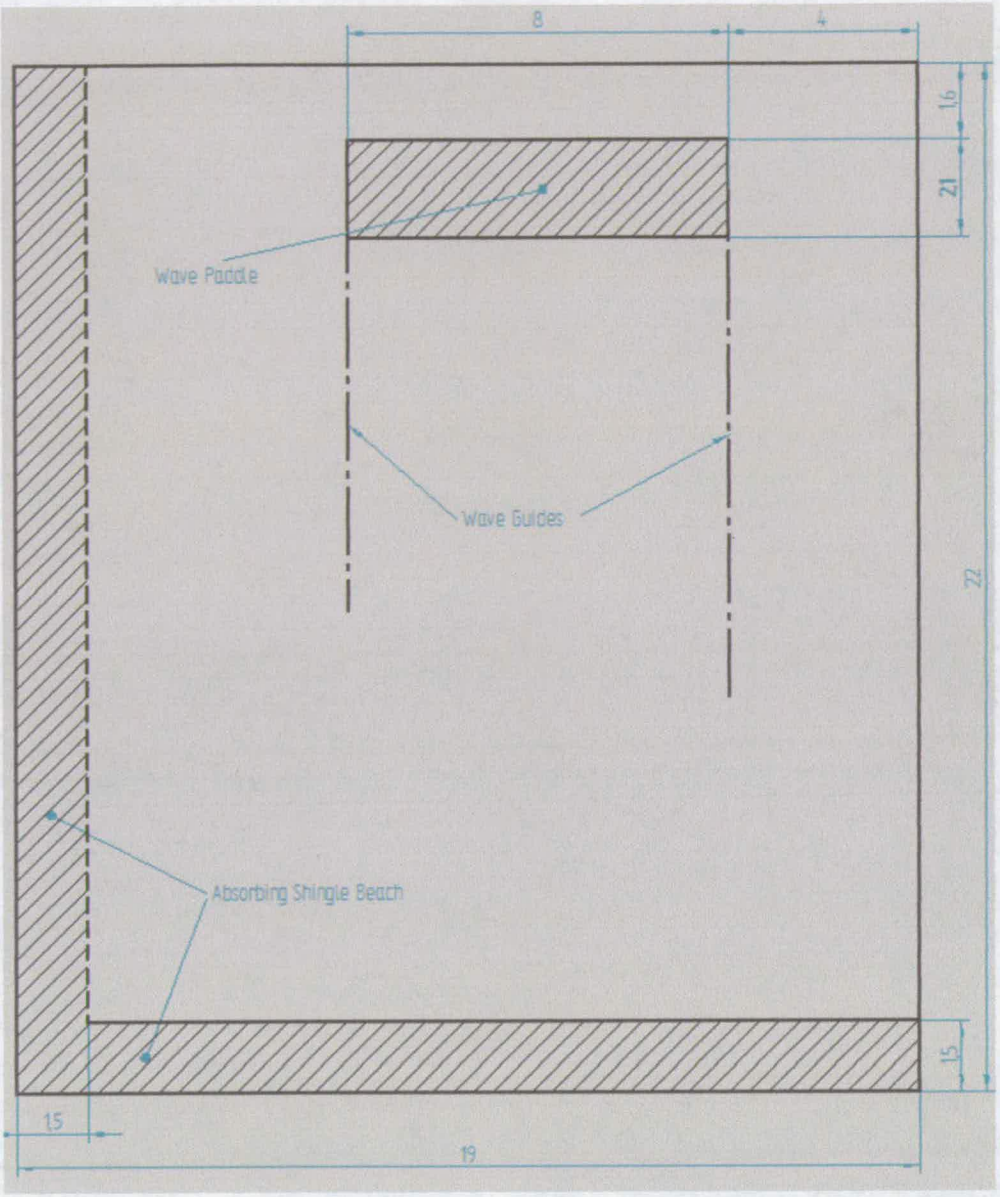

Figure 8: Wave Basin

The wave maker consisted of two banks of multi-element wave paddles (Figure 9). Each bank comprised eight individual paddles which could move independently to one another. The paddles were mounted on linear slide assemblies that were supported by a common framework and moved backwards and forwards horizontally.

The wave maker provided some means to absorb reflected waves. Each paddle had a wave probe fitted to its front, which allowed to compare the expected water level to the actual

water level, and hence to correct the paddle movement in order to absorb reflected waves. According to a classification of 3d wave absorption methods by Schäffer and Klopman (1997) this wave maker could be regarded as a "quasi" 3d system, because each paddle acted independently from its neighbours as a "flume-like" system. There were no means to discriminate between reflected waves from different directions. The absorption was designed to give best results for reflected waves approaching the wave maker perpendicularly. Hence, a best effort was made to design the plan geometries such that waves were reflected either perpendicularly back to the wave maker or out of the test area into the absorbing shingle beach.

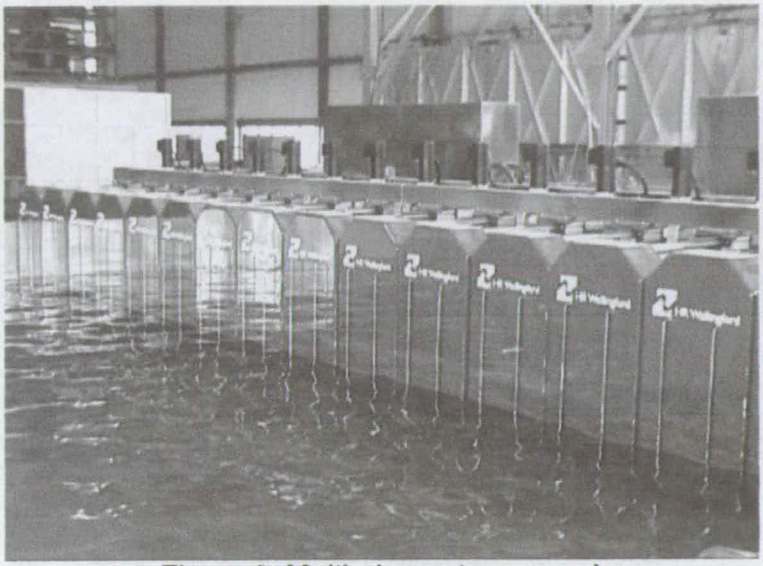

Figure 9: Multi-element wave maker

3.2.2 Measurement Devices

Waves were measured using standard twin wire resistance wave gauges mounted vertically on a tripod and immersed in the water (Figure 10). The wave probes were connected by cable to a wave monitor unit whose output was recorded by a computer data acquisition system. When correctly set-up and calibrated the system had a linear output and could resolve water level changes to 0.2 mm. By default the data was then analysed using the "zero-down-crossing" method.

Figure 10: Twin wire resistance wave gauge mounted on a tripod

The main measurements in this study were of mean and wave-by-wave overtopping discharges. In order to capture any spatial variations four measurement points were deployed along the walls, each using a chute directing water into a container suspended from a load cell (Figure 11a and b). In combination with an overtopping event detector the load cell output could then be analysed to give individual overtopping volumes. Two aluminium strips across the chute formed this "event detector" (see Figure 11a), giving a signal for each flow over it. A more detailed description of the combined measurement system of load cell and event detector is given in section 3.4.

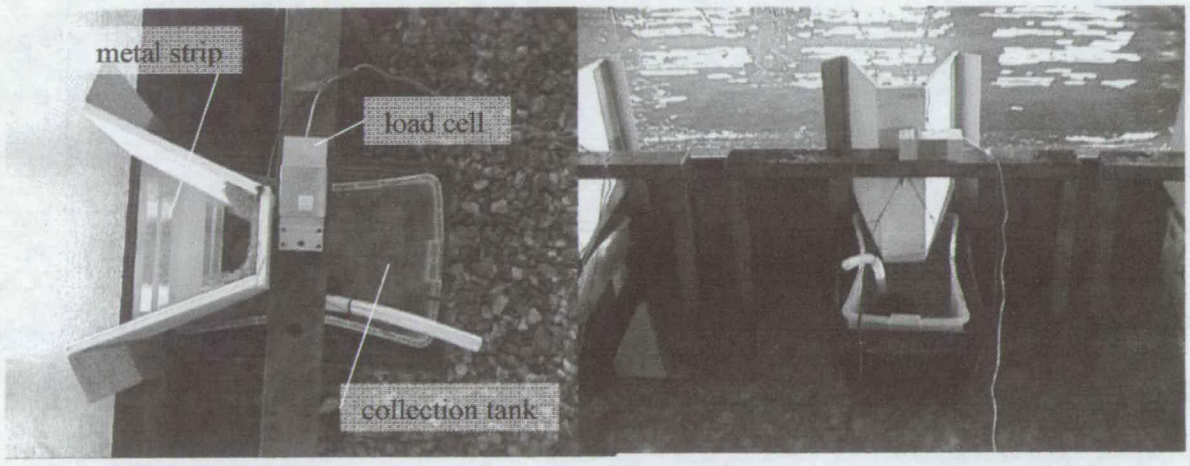

Figure 11: Individual collection station: a) plan view (wave from the left) and b) rear view

Figure 12 shows a generic sketch of an overtopping measurement point. The waves were coming in from the left hand side interacting with the vertical wall. Any overtopping water

was collected by a chute and directed across the event detector (two metal strips) into a tank. The tank was suspended from a load cell.

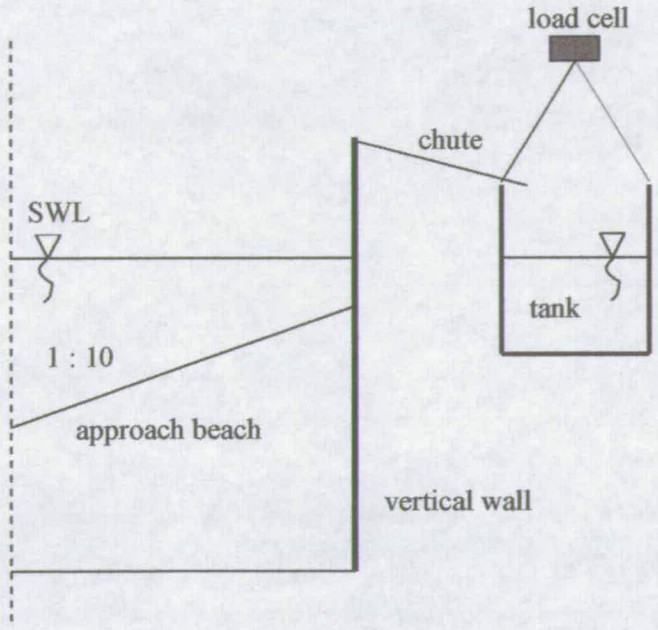

Figure 12: Generic sketch of an overtopping measurement point

In order to catch any spatial variations in overtopping along the seawall four measurement points were deployed. Figure 13 shows a test of 15° obliquity. Although 6 measurement points can be seen only 4 were actually used to measure overtopping. Initially, the model tests were designed for up to 8 measurement points. Due to edge-effects, however, only the 4 measurement points in the middle marked 3-6 were finally analysed. In the following analysis (chapters 4 to 8) the measurement positions will still be marked 3-6 in order to provide a clear and traceable reference to the lab book and the underlying analysis spreadsheets.

Figure 13: Collection stations along the wall

3.2.3 Design of Test Structure and Target Wave Conditions

The design of the structure was based on the 2-d method for mean overtopping discharge reported by the EA manual (1999) (for more details see chapter 2). A comprehensive series of experiments was undertaken by Bruce et al (2001) in a 2d laboratory flume, which showed good agreement with the EA manual (1999). An advantage of this method is the clear distinction between reflecting and impacting wave conditions. This is vital because this study is mostly interested in violent wave conditions (see chapter 1 and 2). In order to fulfil all constraints given by the research project and also by the limitations of the experimental facility, the design process involved several loops. Some of the constraints were formal such as the limited financial resources and testing time, others were technical such as water depth, maximum wave height, and capacity of overtopping collection containers, to name but a few.

The overall goal was to generate a test matrix of sea states, which – in the case of perpendicular wave attack – were designed for predominately impacting conditions. The matrix was required to cover the range from "nearly" impacting conditions, i.e. waves are still just in reflecting mode, up to extremely violent conditions, where overtopping has been shown in 2-d tests to be significantly greater than for pulsating conditions and where no guidance on oblique attack is yet available.

The criterion adopted to ensure significant breaking onto the wall was the h* parameter as defined by the EA manual (1999):

$$h^* \equiv \left(\frac{h}{H_s}\right)\left(\frac{2\pi h}{gT_m^{\,2}}\right) \tag{57}$$

The EA manual (1999) suggests that pulsating / non-breaking waves predominate for $h^* > 0.3$, and that impulsive breaking wave conditions become increasingly prevalent for $h^* < 0.3$. The mean overtopping discharge for pulsating conditions ($h^* > 0.3$) can be described by:

$$\frac{Q}{\sqrt{gH_s^{\,3}}} = 0.05\exp\left(-2.78\frac{R_c}{H_s}\right) \tag{58}$$

where Q is the mean discharge (m^3/s.m). For impacting conditions ($h^* < 0.3$), the suggested relation is:

$$Q_h = 1.37\times10^{-4}\frac{1}{R_h^{\,3.24}} \tag{59}$$

It should be noted that this relation uses different non-dimensional discharge and freeboard, Q_h and R_h defined as

$$Q_h \equiv \frac{Q}{\sqrt{gh_s^{\,3}\times h^{*2}}} \qquad R_h \equiv \left(\frac{R_c}{H_s}\right)h^* \tag{60}$$

The target (or nominal) wave conditions were a result of the iterative design process as described above. They were designed to yield predominantly impacting conditions with h^* parameters between 0.02 and 0.3. The nominal deep water wave steepness fell in the range of 0.015 and 0.060. Figure 14: gives the nominal test matrix for this study. The significant wave height H_s and mean period T_m were derived statistically. Each test was run for approximately 1000 long crested irregular waves with a JONSWAP spectrum ($\gamma = 3.3$) and for two water depths: d=0.450m and d=0.525m (see Table 3). The actual incoming waves at different locations in the basin were later determined by calibration tests with the approach beach in place, but without the (reflecting) vertical seawall (see section 3.3).

Table 3: Tested Water Depths and Freeboards

Water depth d, m	Freeboard Rc , m	Depth at toe of structure hs, , m
0.525	0.200	0.175
0.450	0.275	0.100

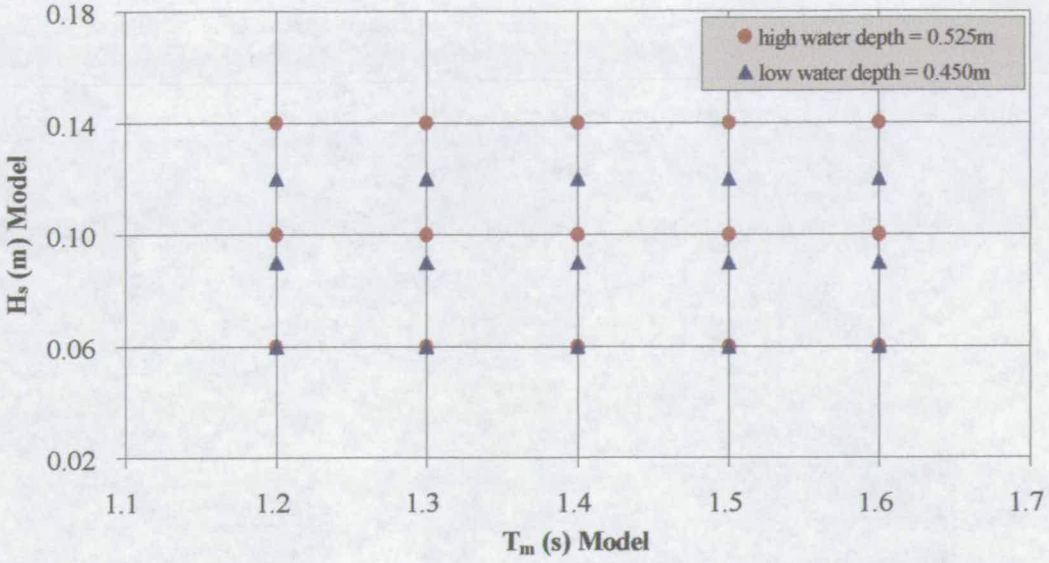

Figure 14: Nominal wave conditions

The iterative design process as described above also yielded the cross section of the structure. Figure 15 shows the cross section giving the definitions of beach height h_{Beach}, water depth at the toe of the structure h_s, the freeboard R_c, and the offshore water depth d. The approach beach retained a constant slope of 1:10 and a constant height at the toe of the seawall (h_{Beach} = 0.350m) for all structure configurations. Also, no berm was deployed.

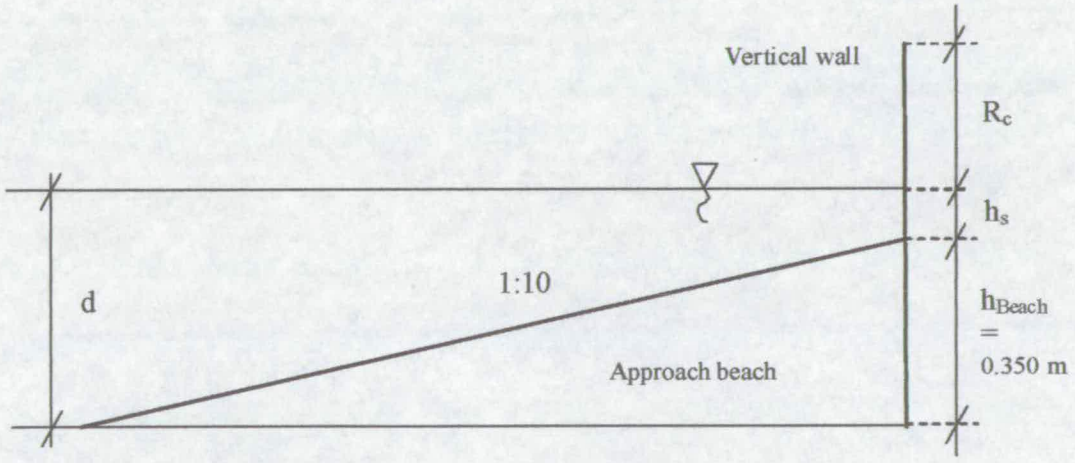

Figure 15: Definition of h_{Beach}, h_s, R_c, and d

The structure was divided into a total of 8 elements in order to facilitate the changeovers for the different configurations. The total length of the seawall was 9.76m. The exact

dimensions of the structure can be reviewed in the Appendix, where also a 3D sketch is presented.

3.2.4 3D Structure Configurations

The same test matrix of sea states was run for all structure configurations, i.e. for a reference configuration ($\beta = 0°$) and 3 different oblique configurations ($\beta = 15°$, 30°, and 60°). Figure 16 shows a picture of a test run ($\beta = 30°$) and a definition sketch of the angle of wave attack β. Detailed sketches giving the exact location of the wave paddle, wave guides, absorbing shingle beaches, structure, approach beaches, wave probes, and overtopping measurement points are presented in the Appendix.

In the case of the reference configuration ($\beta = 0°$) the waves reach the structure perpendicularly. It was assumed that any cross-flume effects would be negligible and hence this set-up was seen as a 2-d flume-like system. It provided a benchmark for all other configurations (see chapters 4 to 8).

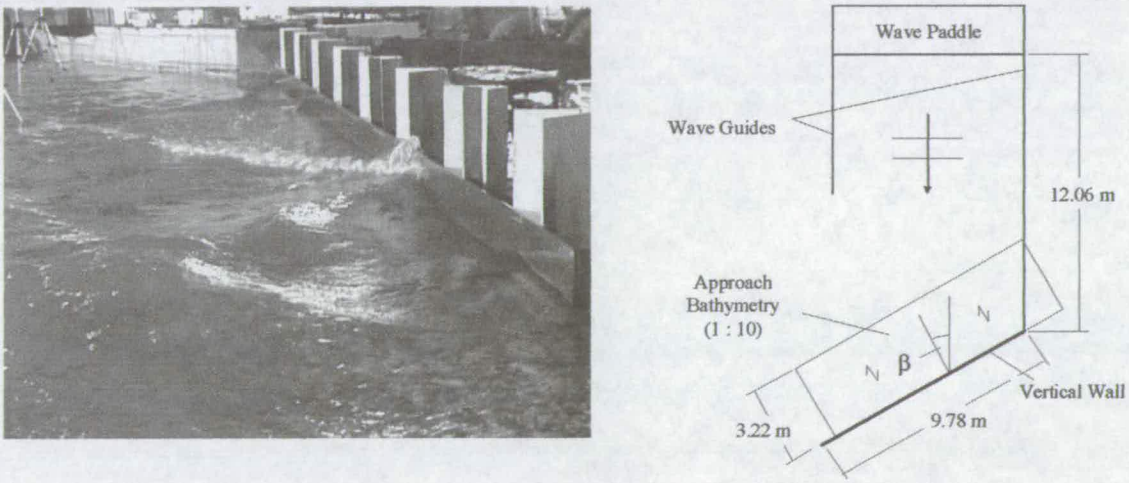

Figure 16: Basin set-up for plain obliquity.

3.3 Wave Calibration

The wave calibration has been done in two steps. Initially, a series of tests has been run to calibrate the wave maker allowing the reproduction of the target (nominal) wave conditions. For this purpose two wave guides on either side of the paddle had been extended to avoid diffraction effects (Figure 17). On the far side of the paddle an absorbing shingle beach had been placed in order to prevent any wave reflections. The wave field was measured by wave

probes in the middle of the generated wave field. The wave probes were then statistically and spectrally analysed. In an iterative process the paddle-settings were adjusted until the target wave conditions were met satisfactorily.

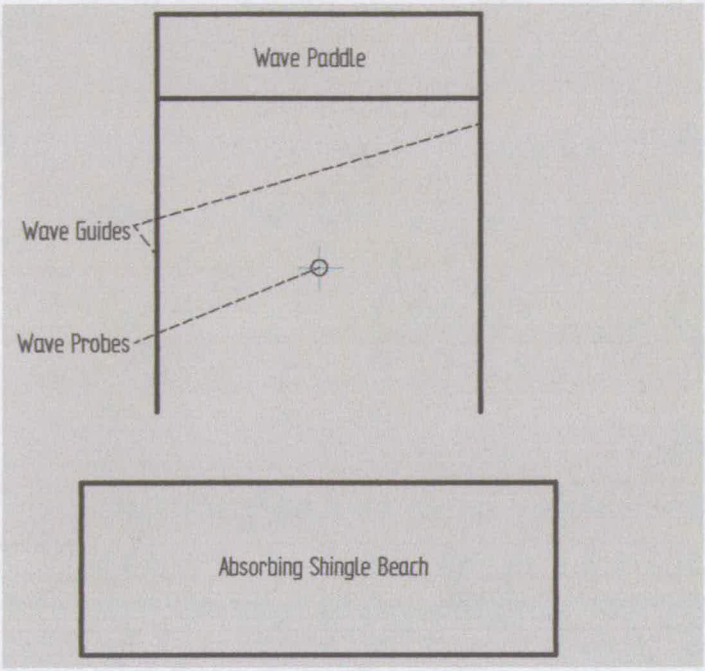

Figure 17: Basin set-up for the calibration of the wave paddle

The main wave calibrations were carried out for the reference configuration ($\beta = 0°$) and for one oblique configuration ($\beta = 30°$). The wave calibrations were undertaken with exactly the same basin set-up as the respective test configuration, but with the structure and overtopping measurement equipment removed. All other components, such as wave guides, approach beaches, etc. remained unchanged. Wave reflections in the basin were avoided by absorbing shingle beaches along the basin walls. The wave field was measured at various points in the basin, in particular at the exact positions of the measurement points atop the approach beaches. Detailed information on the basin set-up and wave probe positions can be found in the Appendix.

Due to limited facility time and resources two oblique configurations ($\beta = 15°$ and $60°$) could not be calibrated in the wave basin, but were determined on the basis of results for 30° obliquity adjusted for shallow water and diffraction effects. This approach could be verified with the two calibrated configurations ($\beta = 0°$ and $30°$) as will be shown below.

Analysing the mean wave period T_m for the two calibrated structure configurations ($\beta = 0°$ and 30°) it turned out that its variation across the basin was typically less than 5% and in all cases less than 10%. Thus, the spatial distribution of T_m was assumed to be constant and the prediction of the wave parameters for structure configurations $\beta = 15°$ and 60° focused on the significant wave height H_s.

The same matrix of wave conditions has been run for all structure configurations (see section 3.2). The wave paddle remained at the same position throughout the whole model study and although the length of the wave guides was varied depending on the individual structure configuration the first 8m on either side of the paddle remained unchanged. Thus, it could be safely assumed that the incoming wave field – without any reflections – was practically identical for all configurations on the first metres after its generation.

As the incoming waves travelled on and transformed, any differences among the structure configurations could only occur due to the varying lengths of the wave guides (diffraction effects) and due to the varying position of the bottom bathymetry (shallow water effects).

In order to determine the wave conditions for 15° and 60° obliquity at key locations (e.g. atop the approach beaches at the position of the measurement points), a reference wave gauge close to the wave paddle has been chosen, where the incoming wave field was assumed to be the same for all structure configurations. The wave conditions measured there were then transformed to the key locations.

As a first step, models for wave shoaling (Shuto's method as described by Goda, 2000) and wave breaking (Allsop and Durand, 1999b) were chosen and validated against the measured data for 0° obliquity. Although the waves were long crested there were small variations in wave heights across the wave basin due to edge effects such as friction along the wave guides and submerged lead weights supporting the wave guides. These variations were very constant for all wave conditions. This was accounted for by factors based on measurements across the wave basin.

In a second step the effects of diffraction and refraction were determined. The oblique configurations 15° and 60° were set up with different lengths of wave guides (diffraction effects) and different positions and angles of the approach beaches (refraction effects). The diffraction coefficients were determined after CEM (2002) and the refraction coefficients after Dean and Dalrymple (1991). The combined results of the shallow water effects (shoaling, breaking, and refraction) and diffraction effects were then validated against the

measured data for 30° obliquity. In a final step the significant wave heights were determined for 15° and 60° obliquity.

3.4 Analysis Procedure and Software

3.4.1 Overview

The overtopping at each collection station was determined using a computer program written by the author of this thesis and specially designed for this project. It is written in FORTRAN and analysed the synchronised signals of the load cell and its corresponding detection trace (for test set-up see sub-section 3.2.2). This introduction gives a brief overview of how this program works, which is then discussed in more depth in the subsequent sub-sections.

The program first evaluates the detection trace and determines the total number of overtopping waves and stores the exact time when each individual event happened. As a second step the load cell trace is calibrated by applying the appropriate calibration factor. Spikes, which can be caused by switching other electrical equipment on, such as pumps, are then removed from the load cell trace by an algorithm.

In case the pumps have been used to empty the containers during a test run the program reconstitutes the load cell trace, in order to compensate for the drop in voltage. In a final step using both the list of individual overtopping times and the reconstituted load cell trace the individual overtopping volumes are calculated. At this point another quality check of the detected overtopping events has been built in. To ensure that the list of individual overtopping events does not contain possible noise from the detection trace, the minimum volume V_{min} has been set to above 0 ml ($V_{min} > 0$). Hence, it is ensured that overtopping volumes can only be positive. This may sound trivial, but given the underlying noise in the load cell signal, this can be the case for a phantom event when no water actually overtopped.

The individual overtopping volumes are then stored in a file giving the time and volume of each individual event. In order to ensure the quality of the data, for each single test run and individual load cell an output sheet has been generated, which shows the raw load cell trace, the reconstituted load cell trace, and the detection trace. Furthermore, each detected overtopping event has been marked by a dot. An example is shown in Figure 18. The detection trace is given in volts, whereas the load cell traces have already been multiplied by the calibration factor. Thus, an increment in the load cell traces reflects a change in volume

(litres). The offset, however, is unknown (and not relevant), so the graph does not give absolute volumes. This output sheet allows a visual quality check. The next sub-sections will give more detailed information on the analysis program.

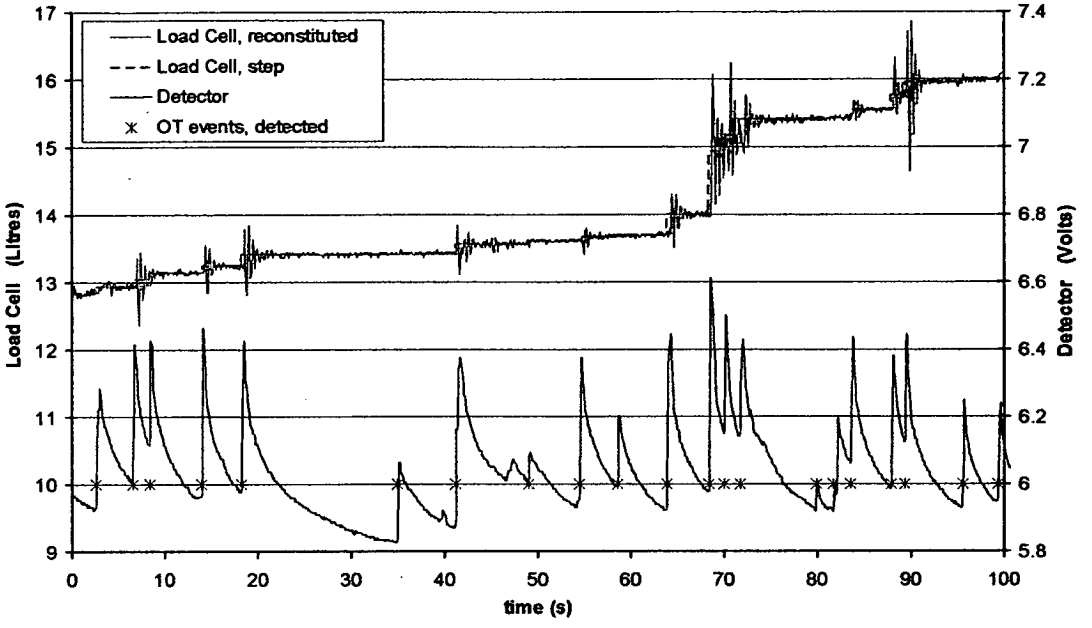

Figure 18:Typical load cell and detector traces (test: VC3033a, LC7)

3.4.2 Overtopping Event Detection

As discussed in previous sub-sections, each measurement point used a chute directing overtopped water into a container suspended from a load cell. Two metal strips across the chute formed an event detector giving a signal in form of a spike for each flow over it. Figure 19 shows a typical detection trace plotted at 10 Hz. Dots were added by the analysis program to indicate detected overtopping events allowing a visual quality check of the analysis.

The signal of the overtopping detector was in the range of 0 – 10V logged at 100 Hz. The actual analysis was performed at a sample rate of 50 Hz. The program used 3 criteria to identify overtopping events. Analysing the detection trace the program searches for sudden increases in voltage (spikes). If they are above a certain threshold the program identifies an event (1st criterion). In order to smooth the detection trace the gradient is determined for each point by subtracting it from the mean value of the 5 following data points, which is, given the sample rate of 50 Hz, 1/10th of a second.

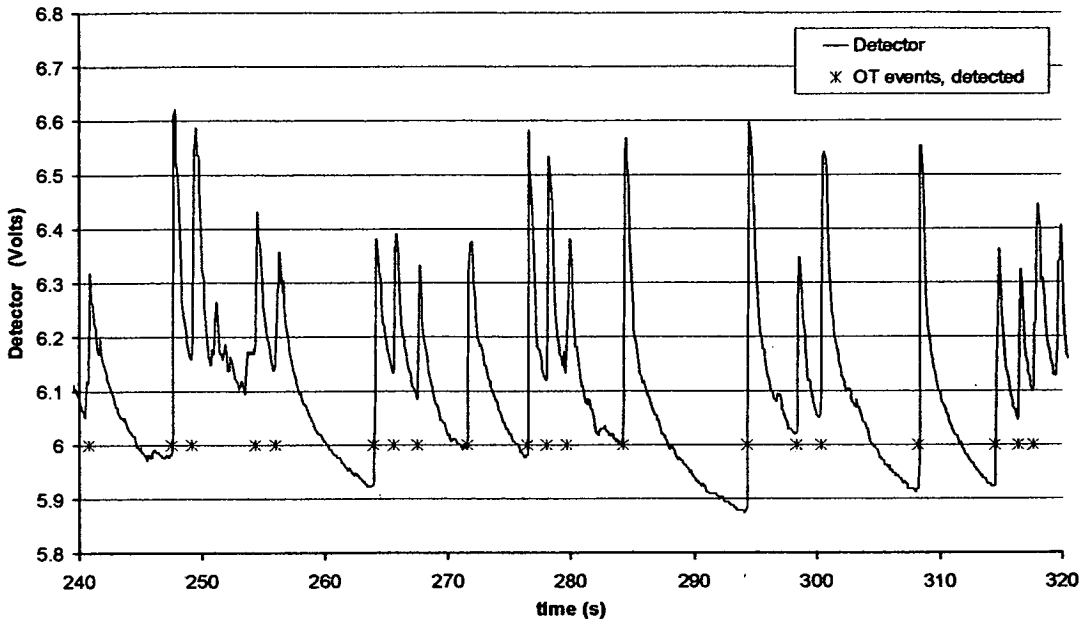

Figure 19:Typical detection trace (test: VC3033a, LC7)

The second criterion is a minimum time interval between consecutive events. Its purpose was to avoid one event to be counted more than once. Due to the high level of noise at the moment of overtopping, especially for large quantities of water, the threshold gradient might be exceeded several times for one overtopping event. However, allowing for dispersion, i.e. waves of different periods travel at different velocities and hence can arrive at the structure shortly after one another, this interval was set to a very low value of less than 1s.

These two parameters, the gradient and the minimum time interval, were set individually for each measurement point. A third parameter has been introduced at a later stage of the program to ensure that each individual overtopping event is larger than "zero". This was necessary to filter out phantom events which were detected because of noise in the detection trace. The next sub-section outlines the video calibration of the overtopping detector and gives an indication on the reliability and accuracy of the results.

3.4.3 Video calibration of Overtopping Detector

In order to calibrate the detection system, a synchronised video signal was analysed for each individual measurement point. The number and time of overtopping events was counted and recorded and subsequently compared to the detection trace. The parameters of the analysis program were then optimised to give the highest possible level of agreement between video and computer analysis.

It could be shown that most overtopping events (i.e. more than 80%) gave clear spikes which were easily detectable. Fine tuning of the parameters increased the performance above 90%. As it appeared the most important parameter is the gradient as described in the previous sub-section. It takes account of the increase in the gradient triggered by an overtopping wave. The minimum time interval between events, influences only about 5% of the cases, but is very useful for fine tuning.

Figure 20 shows a typical section of a detection trace. Two spikes are highlighted. The first and larger one is very clear and belongs to a typical overtopping event shown in Figure 21. The second one is much smaller and demonstrates a very low event which was identified in the video analysis (shown in Figure 22) but not by the analysis program. With a reduction in the minimum gradient even this event could have been detected, but then an increasing number of phantom events would also have been picked up due to the background noise in the detection trace. It should be noted that the smallest detected events were below the measurability of the load cell.

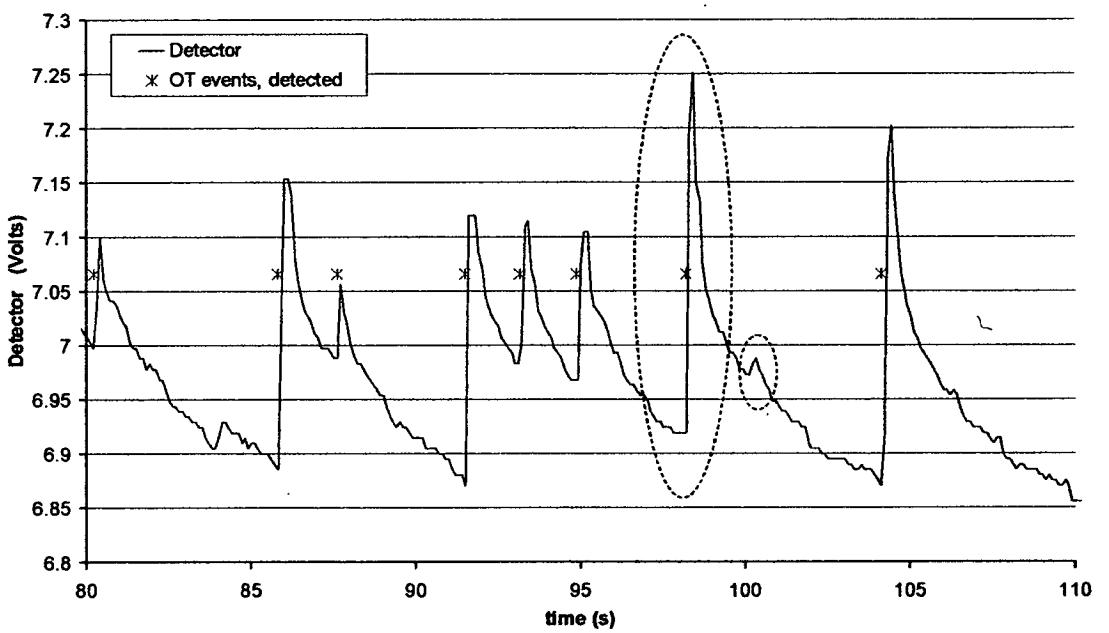

Figure 20: Typical section of detection trace (test: VO0009c, LC4)

Figure 21: Easily detectable overtopping event (1st highlighted spike, Figure 20)

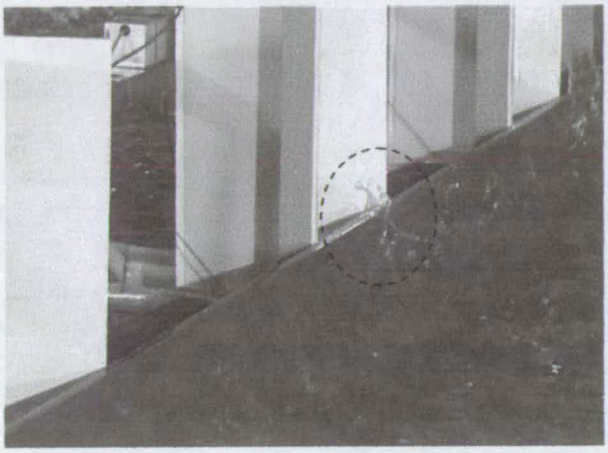

Figure 22: Event on video, but not detected by program (2nd highlighted spike in Figure 20)

A correlation between the size of a spike and the related overtopping volume could not be established. The shape of the signal appears to be more influenced by how the water flows down the chute rather than by how much water overtops. A highly aerated medium event may only give a small signal, whereas a small event may result in a quick rush of water causing a sharp spike.

3.4.4 Reconstitution of Load Cell Trace

When the overtopping volume during a test run exceeds the capacity of a collection container, then it becomes necessary to remove some of the water from the container during a test run. This is done by pumps, which could be operated from outside the wave basin. As

water is being pumped out of a container, its weight is reduced resulting in a drop in the load cell output voltage. The process of compensating for this drop is called "reconstitution of the load cell trace" in this thesis. Care needs to be taken, as the operation of the pumps may take up to a few minutes and overtopping events occur simultaneously.

The pumps were only needed for highly impulsive wave conditions, which gave more than about 30 litres of overtopping. In those cases the load cell trace was reconstituted, in order to compensate for the drop in voltage. This was done by the analysis program in various steps.

The first stage after calibration of the load cell trace was to identify the precise time of the pump intervals. To achieve more reliable results large spikes, caused by other electrical equipment (such as the pump itself), were removed. The trace was further smoothed by undertaking a running average of one second. The program then scanned the trace looking for a drop which exceeds a certain threshold. This threshold is set close to the pump rate. The end of a pump interval is found correspondingly.

Once the pump intervals were established, the gradient in the load cell trace caused by the pump was determined. Any overtopping event reduces this gradient, thus the interval was divided further into subintervals between events. In order to avoid noise in the load cell trace caused by overtopping events only the second half of these subintervals were then used to calculate the gradient by a linear regression analysis. This calculation was based on the calibrated raw load cell trace which had not been smoothed. Some intervals could be very short, i.e. less than a second. In those cases, given the background noise in the signal, very large or positive gradients might have been produced. This was avoided by upper and lower bounds. Once the gradient for each subinterval was known, the trace was reconstituted.

Figure 23 shows an example of a reconstituted load cell trace. It can be seen that even while using the pump to empty the container, overtopping water can still be measured. This allowed test runs with much larger overtopping than the capacity of the collection container. Figure 23 also shows the detection trace and indicates detected overtopping events with a dot. The encircled section has been enlarged in Figure 24. The "step" load cell trace reflects the result of the analysis program: the steps are equal to the individual overtopping events.

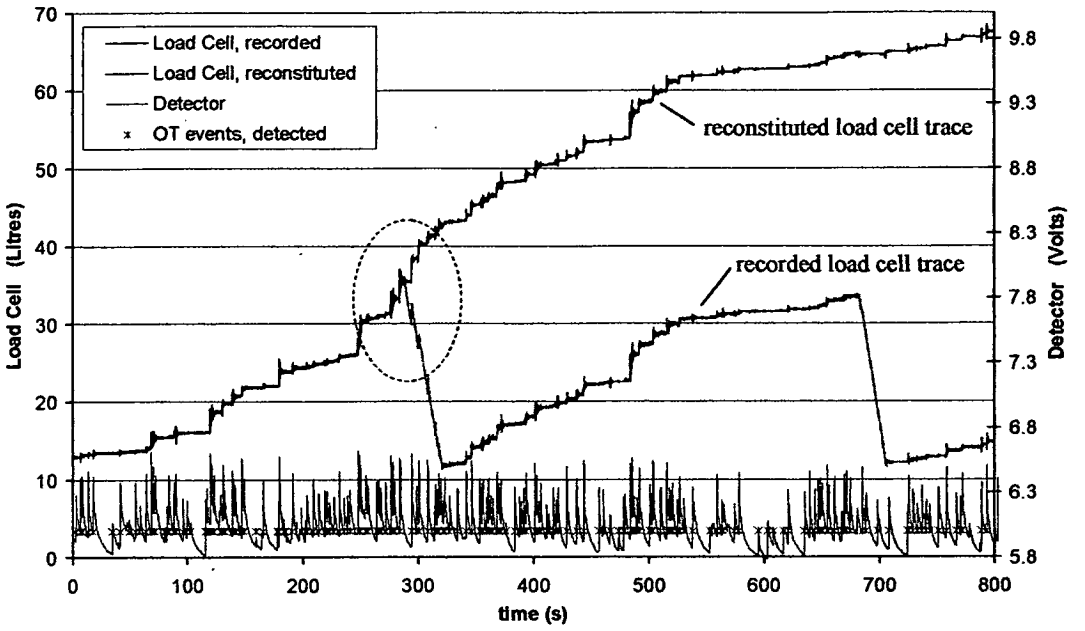

Figure 23: Typical reconstituted load cell trace (test: VC3033a, LC7)

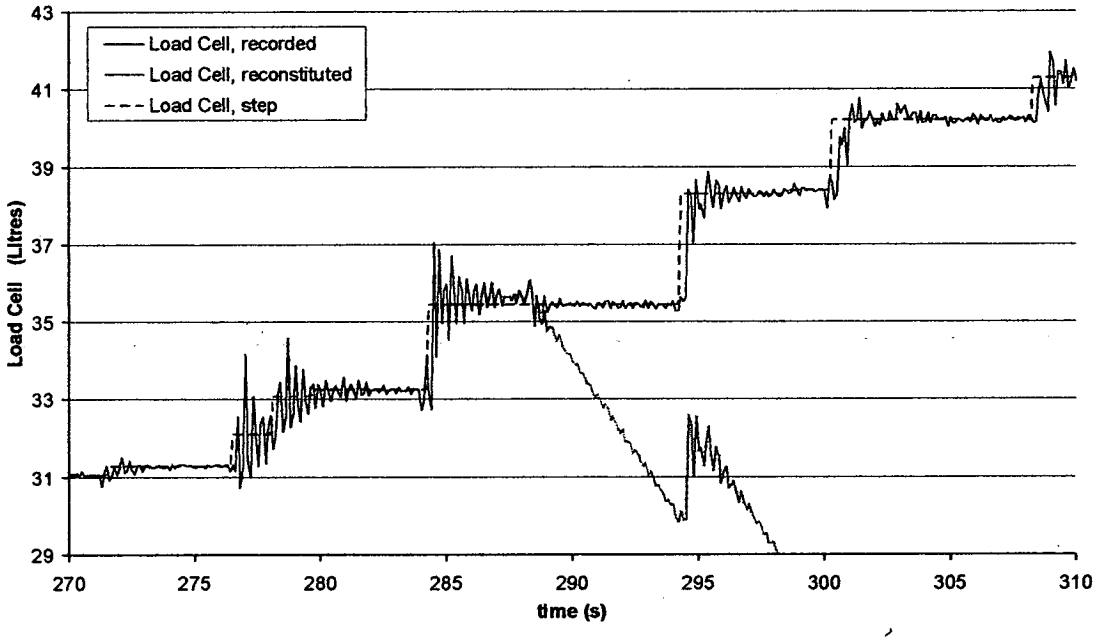

Figure 24: Typical reconstituted load cell trace (detail) (test: VC3033a, LC7)

3.4.5 Individual Volumes and Resolution of Load Cell

The final step of the analysis program was to determine the mean overtopping discharge and the individual "wave-by-wave" overtopping volume. This was done on the basis of the calibrated and reconstituted load cell trace. The program calculated the mean value before and after an overtopping event, the difference being the individual overtopping volume. In order to avoid noise caused by the overtopping water, only the second half of the time interval between events was taken for the calculation. The mean discharge was determined in a similar way by calculating the difference between the mean values at the beginning and at the end of the whole test sequence.

The resolution of the load cell depended on two factors: one was set by the conversion of the analogue signal into a digital signal and the other one was given by the noise in the system. The ADC converted the analog signal into a digital one with 4096 points. This was then converted by the analysis program into a voltage range of ± 10V. Applying a calibration factor of about 5l/V yielded:

$$\frac{20V}{4096} * 5l/V \approx 0.025l \tag{61}$$

The noise in the system was found to be lower than this value. As volumes were always determined by calculating mean values over a number of successive data points, the analysis program also detected volumes of less than 0.025l. All volumes were subject to error bars of:

$$\pm 0.025l/2 = \pm 0.0125l \tag{62}$$

3.5 Summary

This section gave a detailed description of the physical model study conducted to derive guidance for mean and wave-by-wave overtopping over plain vertical seawalls subject to violent (impulsive) and oblique wave attack. Detailed sketches of all structure configurations including the position of wave gauges and measurement points can be reviewed in the Appendix.

The test facility comprised of a 3D wave basin, a multi-element absorbing wave maker, absorbing shingle beaches, and wave guides to avoid diffraction effects. The wave conditions were measured with standard twin wire resistance wave gauges which were placed at key locations throughout the wave basin.

Mean and wave-by-wave overtopping volumes were measured using a combination of a load cell and an event detector. The analysis software was written specifically for this project. It analysed mean and wave-by-wave overtopping volumes even when pumps were used to drain the containers during a test run.

In order to capture any spatial variations in overtopping four measurement points were deployed along the seawall. The model tests had initially been designed for up to 8 measurement points. Due to edge-effects, however, only the 4 measurement points in the middle marked 3-6 were finally analysed. In the following analysis (chapters 4 to 8) the measurement positions will still be marked 3-6 in order to provide a clear and traceable reference to the lab book and the underlying analysis spreadsheets.

The test matrix and the size and dimensions of the vertical seawall and approach beaches were designed in several loops after a method by the EA manual (1999). Two water depths (0.450m and 0.525m) were tested. Each test was run for approximately 1000 long crested irregular waves with a JONSWAP spectrum (γ = 3.3). Four different obliquities were investigated: 0, 15, 30, and 60°.

The wave conditions were calibrated for 0° and 30° obliquity with the structure removed, but all other elements such as wave guides and approach beaches left in place. Shingle beaches were deployed along the basin walls in order to avoid any reflections during the calibration tests. The wave conditions of the other two obliquities (15° and 60°) were determined based on the measurements for 0° and 30° and adjusted for shallow water and diffraction effects.

4 OBSERVATIONS AND DEFINITIONS OF "WAVE – STRUCTURE INTERACTIONS"

4.1 Introduction

An approaching wave can interact with a vertical seawall in three basic ways: it can simply run up and reflect from, break onto, or break before the seawall as a highly aerated body of water. The exact way in which an individual wave interacts with the seawall is generally a function of structural parameters, wave conditions, and water levels. It also depends, however, on its interaction with the other waves close by, particularly with the previous wave and its own interaction with the seawall. Thus, the breaking behaviour of individual waves is very difficult to predict and can only be described in a statistical way.

This thesis is mostly concerned with waves in impacting mode at perpendicular wave attack and the gradual change – transition – to reflecting mode towards higher angles of wave attack. A sea-state is defined as being in "predominantly reflecting mode" when a certain percentage of waves reflect from the structure. Similarly, a sea-state is defined as being in "predominantly impacting mode" when a certain percentage of waves break onto the structure. An exact percentage for either mode has not been defined in literature yet, although attempts have been made to link the "mode" of a sea-state directly to the wave parameters (section 2.2).

The "mode" (i.e. predominantly reflecting or impacting) of the waves at the seawall has a major influence on the amount of overtopping to be expected. The prediction of mean overtopping rates for 0° obliquity lies between almost "zero" and three orders of magnitude higher for "impacting" conditions than for "reflecting" conditions (EA manual, 1999). It will be shown later that a percentage of impacts of even less than 1% has an influence on the overtopping behaviour, i.e. the prediction method for impacting conditions after the EA manual (1999) leads to a better fit to the data (chapter 6).

At higher angles of wave attack an increasing number of waves which would have broken (impacted) onto the wall at perpendicular wave attack start sliding along the wall "throwing up" water. This behaviour is not an impacting event as defined for the 2D case, but in terms of overtopping it leads to similar results (i.e. a power law-type relation similar to equation

(33), sub-section 2.3.3). This phenomenon will be called an "impact-like" event throughout this thesis.

The "impact-like" event is an intermediate step in the transition from impacting to reflecting events due to increasingly oblique wave attack. At 0° obliquity waves only impacted onto, reflected from, or broke before the structure. With an increasing angle of wave attack (i.e. 15° and 30°) impacts started changing to "impact-like" behaviour and then eventually to reflecting behaviour. At 60° neither impacts nor "impact-like" events occurred and all previously (i.e. at 0° obliquity) "impacting" tests were then in reflecting mode.

The term "impulsiveness" in this thesis is used as a synonym for "percentage of impacts", whereby impacts can be "classical" impacts or "impact-like" events. The term "more impulsive" refers to a "higher percentage of impacts". The word "violent" overtopping simply states that "impacts" occur, i.e. the percentage of impacts is larger than "zero".

The next sections illustrate how a "wave impact" and an "impact-like" event are defined in this thesis. This is done for each angle of wave attack by a series of pictures. It should be noted that the definitions in this thesis are based on visual evaluations and not on pressure measurements.

4.2 Obliquity 0° (Reference Configuration)

At 0° obliquity only "standard" impacting events occurred. "Impact-like" events were not recorded. This section defines an "impacting" event at perpendicular (2D) wave attack. Figure 25 shows a series of pictures for illustration taken in the wave flume of the University of Edinburgh (courtesy of Tom Bruce and Jonathan Pearson). In the first picture a wave is breaking just in front of a vertical wall. The wave entraps a pocket of air (1st picture) which is then compressed (2nd picture) leading to a subsequent sudden "explosive" release of the pressure (3rd picture). This may result in water being thrown up several times the incident wave height.

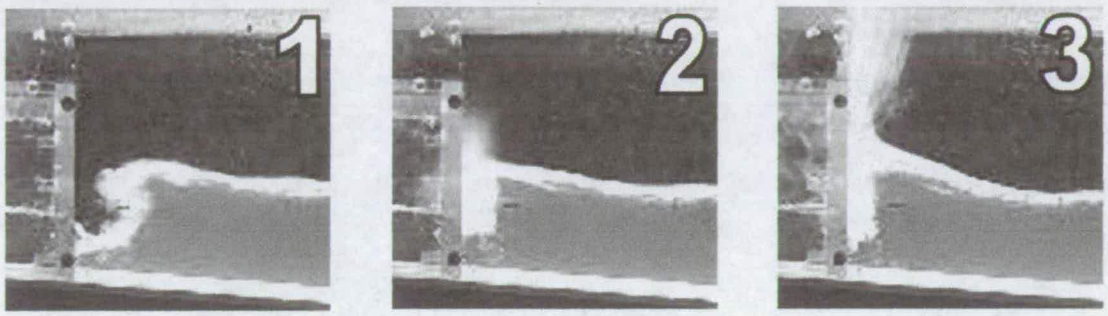

Figure 25: Impacting event at 0° obliquity

Figure 26 shows a typical impacting event as recorded in this study for the reference test ($\beta = 0°$). In picture "1" the wave is just about to break. In picture "2" the wave is in the same stage of breaking (c.f. Figure 25, picture "1"). In Figure 26 picture "3" the wave compresses the entrapped air (c.f. Figure 25 picture "2"). Finally, in Figure 26 picture "4" the compressed air breaks free violently throwing up water.

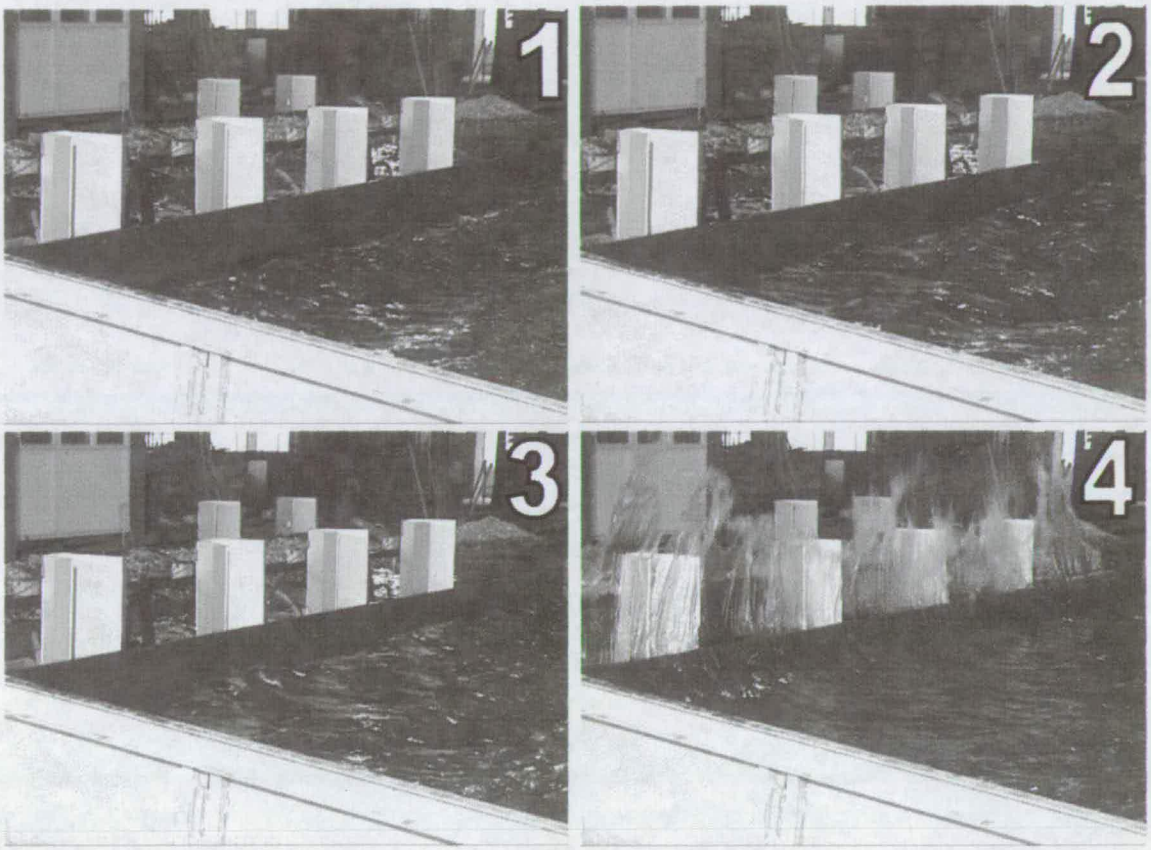

Figure 26: Impacting event at 0° obliquity

4.3 Obliquity 15°

Wave-structure interactions change when waves approach at angles larger than 0°. Especially the process of wave impacts may look quite different. Towards higher angles of wave attack an increasing number of waves which would have broken (impacted) onto the wall at perpendicular wave attack start sliding along the wall "throwing up" water. This behaviour is not an impacting event as defined for the 2D case, but in terms of overtopping it leads to similar results (see chapter 6). In this thesis such an event is called an "impact-like" event. First, two typical "normal" impacting events at 15° are presented in this section (see Figure 27 and Figure 28). A typical "impact-like" event at 15° is then introduced in Figure 29.

In Figure 27 pictures "1" – "3" show how the long crested wave approaches the vertical wall. On the far side of the wall close to the wave guide the wave has nearly reached the structure (Figure 27). In this area the wave is already breaking with the crest of the wave reaching forward. In picture "3" the wave crest connects to the wall entrapping a pocket of air, but still leaving a small gap open to the side. As the wave moves farther on the gap on the side of the air pocket is closed and the entrapped air compressed (picture "4"). In picture "5" the pressure is released suddenly and water is thrown upwards. While the wave is travelling forwards the wave impacts along the wall (pictures "5" and "6").

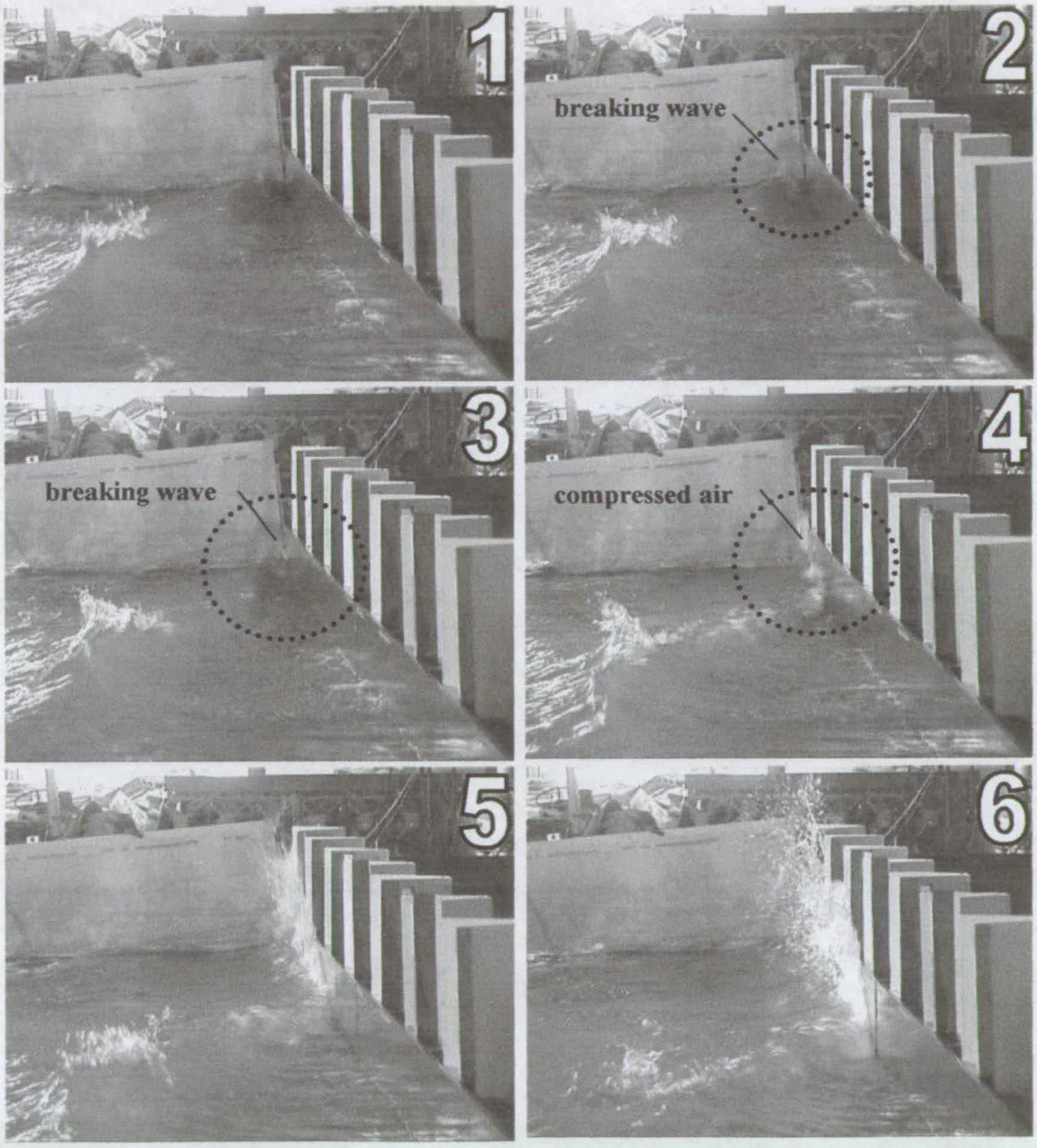

Figure 27: Impacting event at 15° obliquity

Figure 28 shows another impacting event from a different perspective. The process of wave breaking is the same as described in Figure 27.

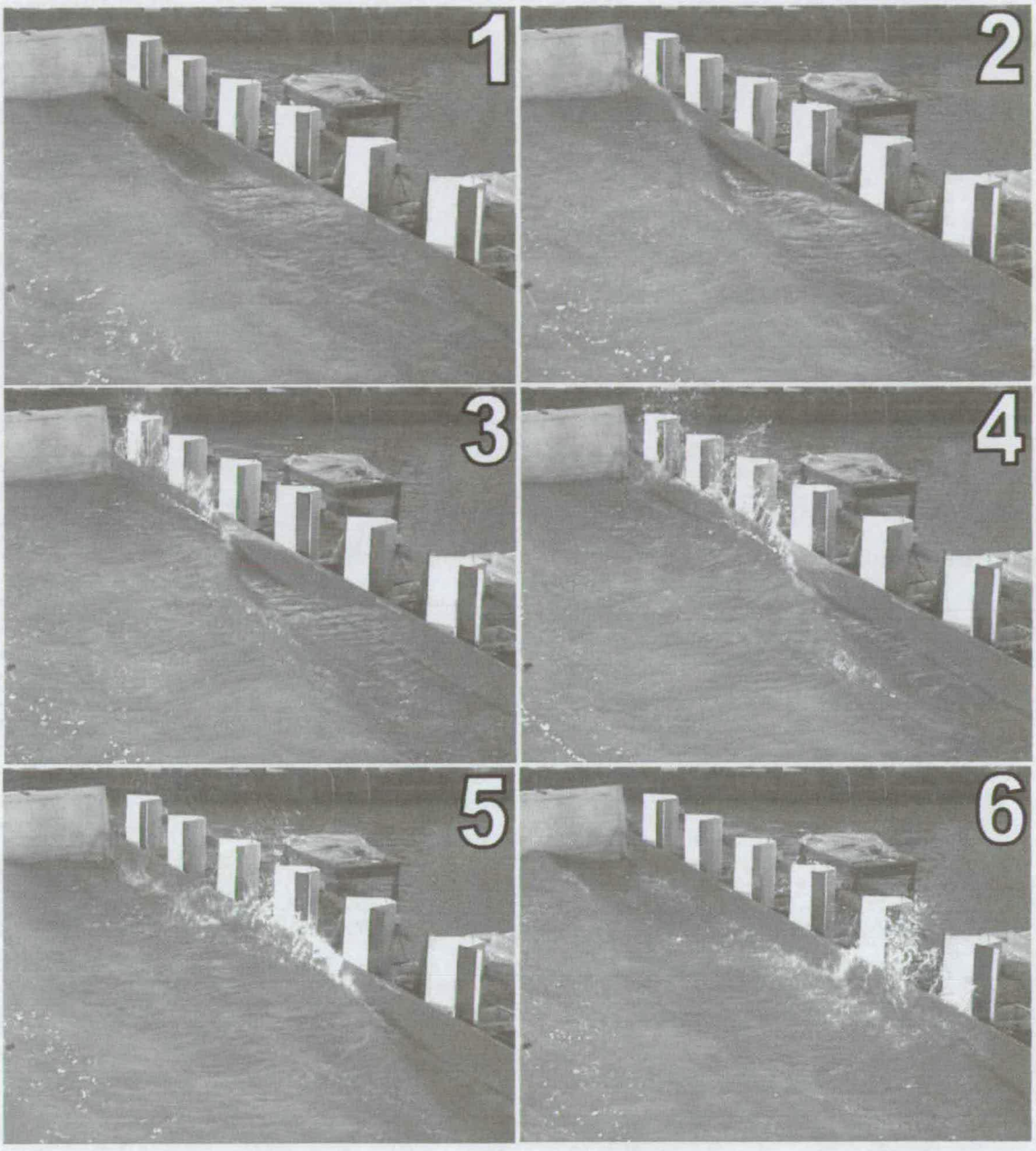

Figure 28: Impacting event at 15° obliquity

Figure 29 gives an example of an "impact-like" event at 15° obliquity. The same physical behaviour can be observed at 30° (see Figure 31). The "impact-like" event in Figure 29 is an example of a small event, whereas the example in Figure 31 is somewhat larger.

In both examples the wave reaches the wall at the far side of the structure (pictures "1" and "2") and at first simply starts reflecting back from the wall. As the wave travels on it builds up in height until the part of the crest, which is just about to reflect from the wall, begins to collapse (break, impact) against the wall covering the little space between wave front and structure (picture "3"). This forms an air pocket which is then compressed. When the forward momentum of the wave is used up the pressure is released suddenly and water is "thrown" upwards.

This phenomenon is called an "impact-like" event because it is only the crest of the wave that is actually breaking (impacting) onto the wall and not the whole wave. It is also important to note that the wave first appears to be in reflecting mode and then the crest (only) collapses. The wave build-up along the wall triggering the "impact-like" event, however, may not be necessary. This depends on the properties of the incoming wave. The "violence" of an "impact-like" event varies from very low, i.e. only a few drops of water are thrown up, to practically impacting in the classical sense (see Figure 28 and Figure 29).

This example of an "impact-like" event also explains to some extend the measured spatial variability for oblique wave attack (see chapters 6 to 8): travelling along the wall the wave first builds up increasing the amount of overtopping water until it swaps from reflecting to "impact-like" behaviour. At this point the overtopping increases even further. When the wave crest starts to break, however, then the wave looses some of its height and eventually tumbles down reducing the overtopping significantly. Once it has stabilised itself it starts building up anew.

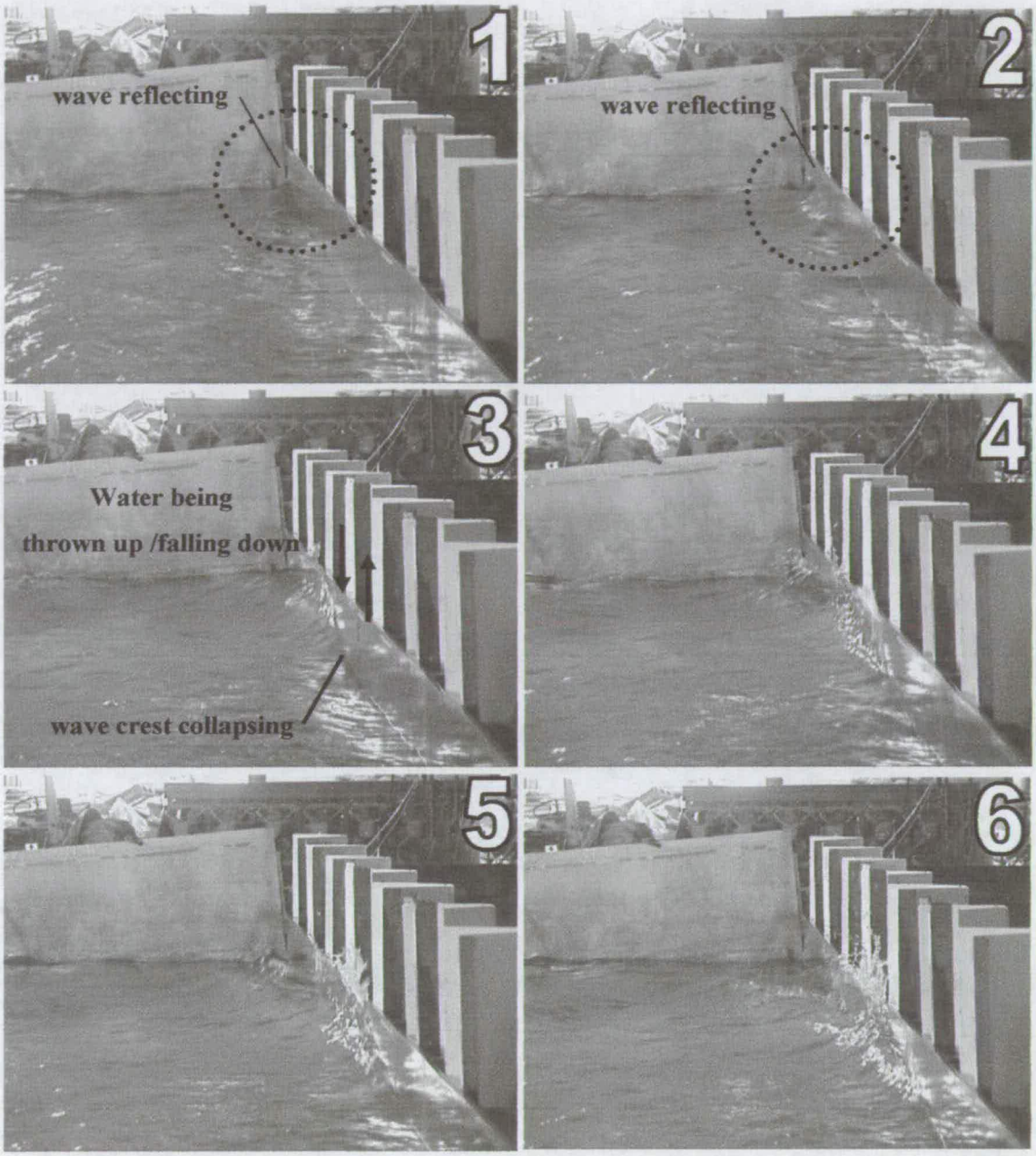

Figure 29: "Impact-like" event at 15° obliquity

4.4 Obliquity 30°

At 30° obliquity the same physical behaviour for wave impacts and "impact-like" events can be observed as in the 15° case. It should be noted, however, that for angles of wave attack as large as 30° an increasing number of waves change from impacting to "impact-like" behaviour. Moreover, the "violence" of all these events is somewhat reduced leading to lower amounts of overtopping (see chapter 6).

Figure 30 and Figure 31 show an impacting event and an "impact-like" event at 30° obliquity, respectively. A description of the physical processes can be found in section 4.3. The incoming wave in Figure 30 breaks completely onto the wall whereas in Figure 31 only the wave crest eventually starts breaking.

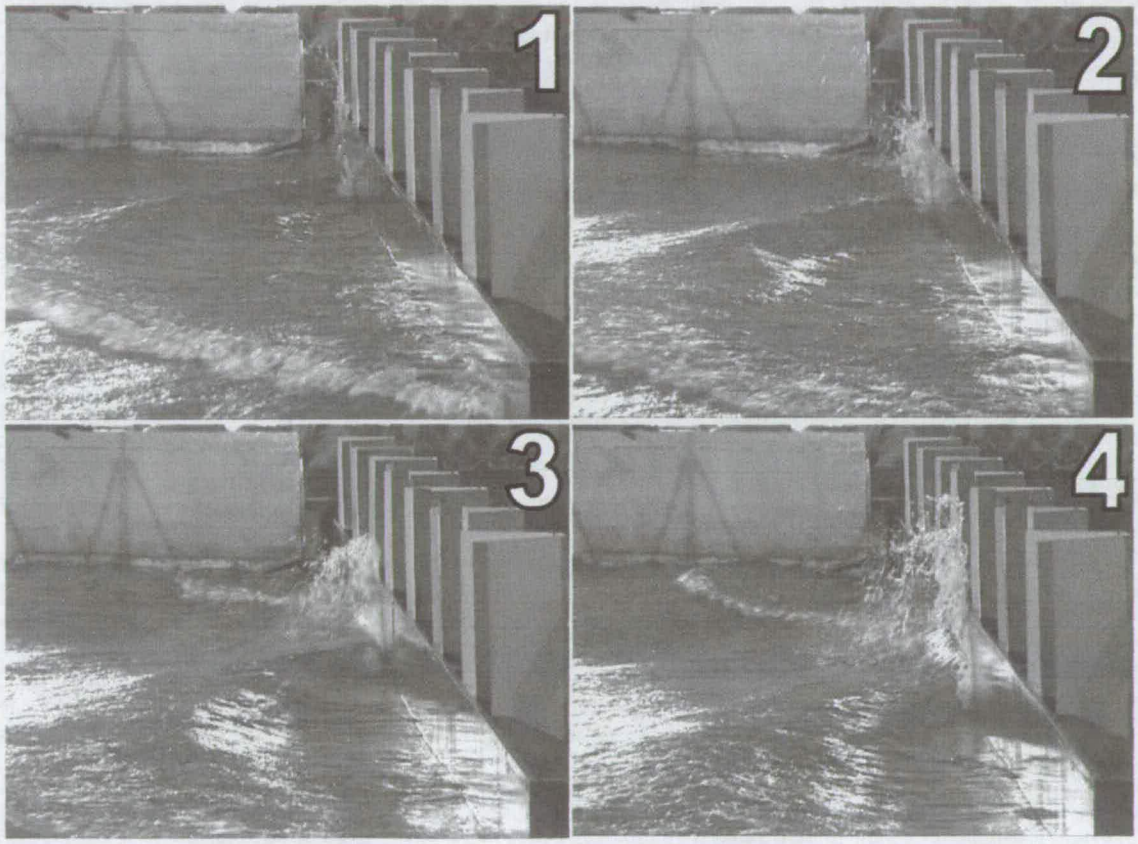

Figure 30: Impacting event at 30° obliquity

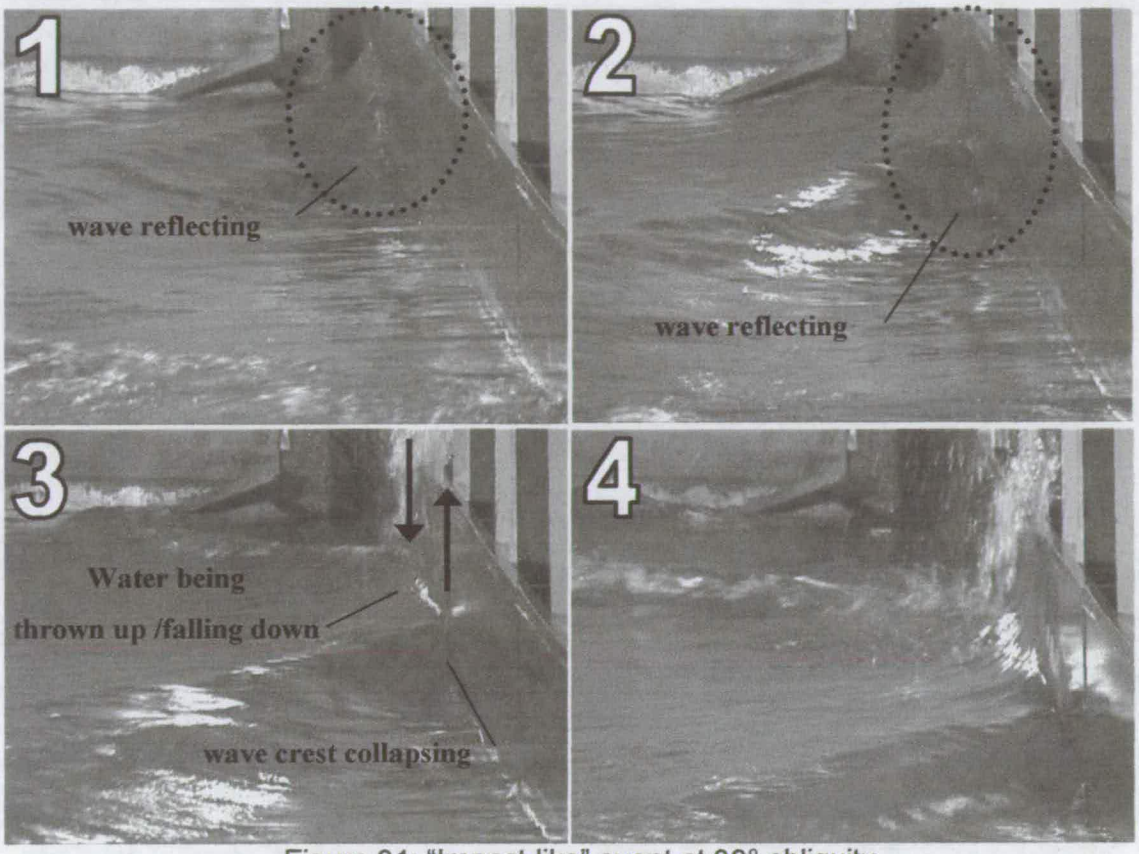

Figure 31: "Impact-like" event at 30° obliquity

4.5 Obliquity 60°

No impacts or "impact-like" events have been recorded at 60° obliquity. Waves broke either clear of the structure or broke along the wall neither entrapping nor compressing pockets of air. Figure 32 shows a standard situation: in picture "1" and "2" the wave reflects from the structure. In picture "3" the wave starts breaking eventually losing height. This loss in height leads to a reduction in overtopping explaining to some extent the spatial variation in overtopping volumes measured along the wall (see chapter 6).

Due to Snell's law at 60° obliquity a reflected wave has no velocity component towards the incoming wave. Thus, a wave is not reflected "backwards", but the direction of propagation is merely "diverted" and the wave is still moving away from the wave maker. This way no air is entrapped and no excessive pressure can build up.

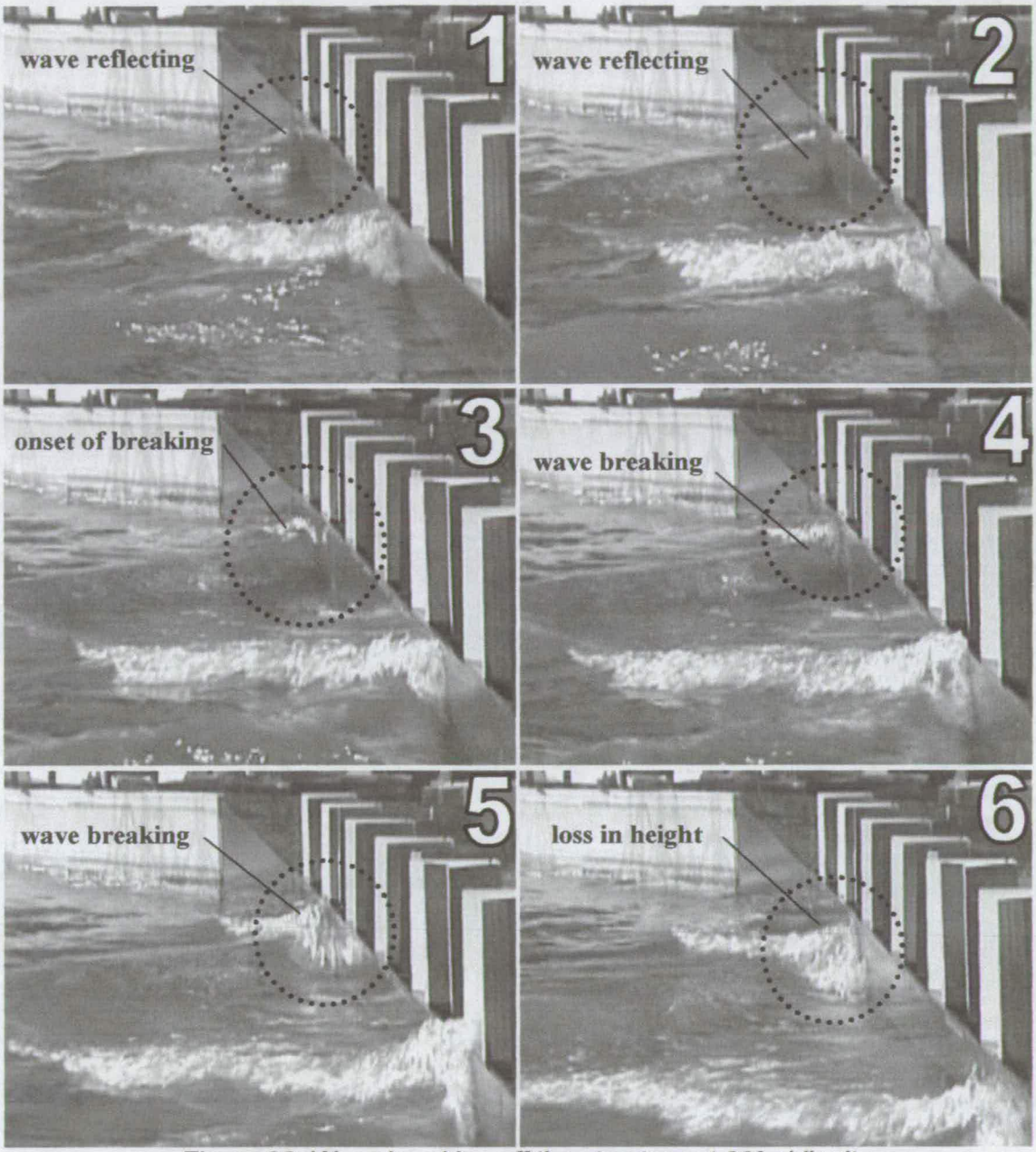

Figure 32: Wave breaking off the structure at 60° obliquity

Figure 33 shows another example of a wave breaking "along" but not "onto" the structure.

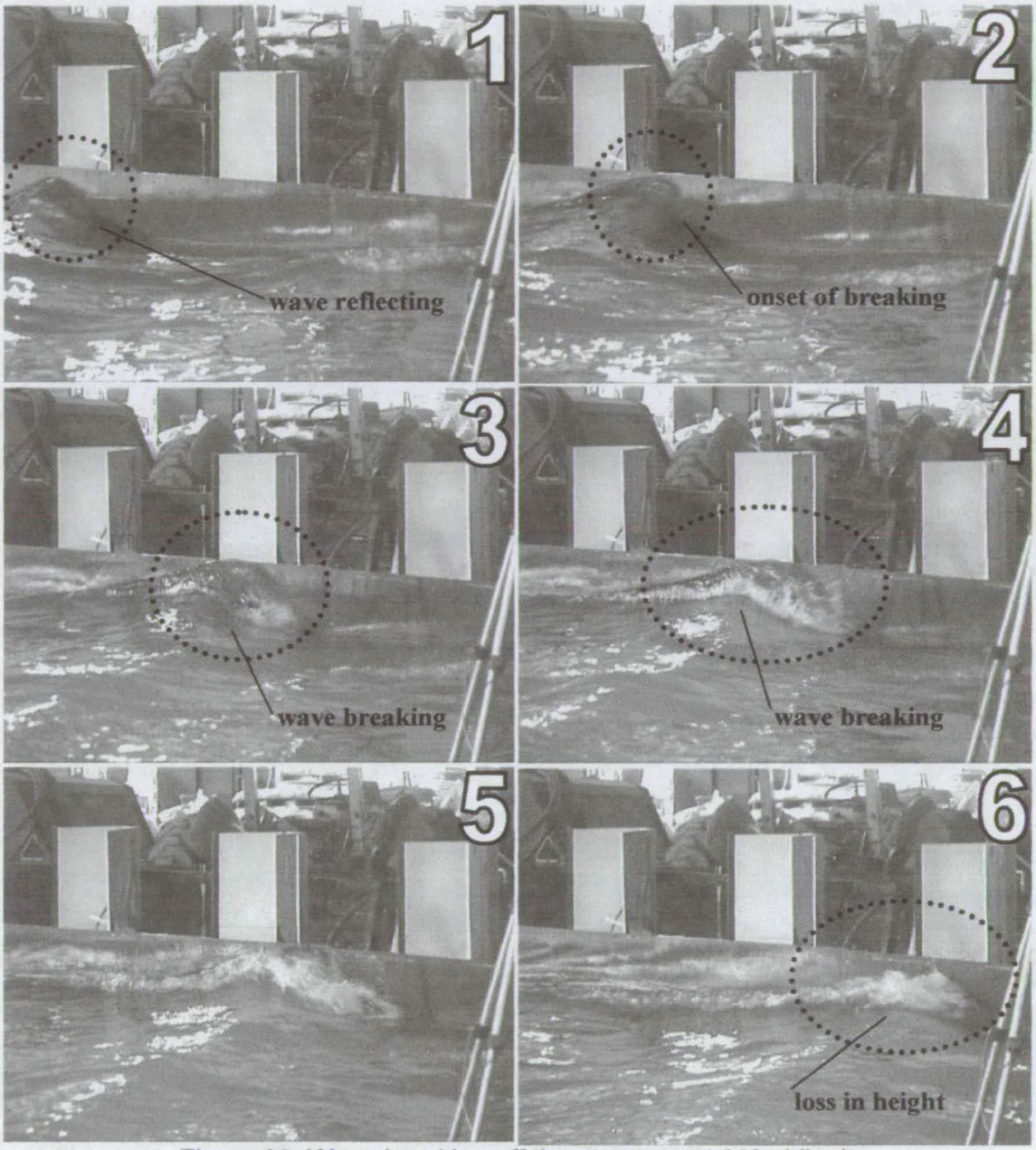

Figure 33: Wave breaking off the structure at 60° obliquity

4.6 Summary and Discussion

In this chapter wave impacts on vertical seawalls and their gradual change towards simple reflections at increasing angles of wave attack have been described and illustrated with series of pictures. An intermediate event has been introduced called "impact-like" event.

At 0° obliquity an approaching wave can interact with a vertical seawall in three basic ways: it can simply reflect from, break onto, or break before the seawall. With no obliquity, only "classical" impacts occur: the wave entraps a pocket of air which is then compressed leading to a subsequent sudden "explosive" release of the pressure. This may result in water being thrown up several times the incident wave height.

When waves approach the structure at angles larger than 0°, the impacting behaviour changes: towards higher angles of wave attack an increasing number of waves which would have broken (impacted) onto the wall at perpendicular wave attack start sliding along the wall "throwing up" water. This behaviour is not an impacting event as defined for the 2D case, but in terms of overtopping it leads to similar results (see chapter 6). In this thesis such an event is called an "impact-like" event.

Thus, waves which would have impacted onto a vertical seawall at perpendicular wave attack now may either impact in the "classical" way or display "impact-like" behaviour. A "classical" impact still breaks in pretty much the same way as at 0° obliquity: the wave front which is closest to the structure starts to break forming an air pocket. Once it hits the wall the air is entrapped and compressed. Subsequently, the pressure is suddenly released and water is thrown up several times the incident wave height. As the wave travels on this happens along the whole front of the seawall.

In the "impact-like" case the wave first simply starts reflecting back from the wall. As the wave travels along the seawall it builds up in height until the part of the crest, which is just about to reflect from the wall, begins to collapse (break, impact) against the wall covering the little space between wave front and structure. This forms an air pocket which is then compressed. The pressure is then released suddenly and water is "thrown" upwards.

This process has been called an "impact-like" event because it is only the crest of the wave that is actually breaking (impacting) onto the wall and not the whole wave. It is also important to note that the wave first appears to be in reflecting mode and then the crest (only) collapses. The wave build-up along the wall triggering the "impact-like" event, however, may not be necessary. This depends on the properties of the incoming wave. The

"violence" of an "impact-like" event varies from very low, i.e. only a few drops of water are thrown up, to practically impacting in the classical sense.

The example of an "impact-like" also explained to some extend the measured spatial variability for oblique wave attack (see chapters 6 and 8): travelling along the wall the wave first builds up increasing the amount of overtopping water until it swaps from reflecting to "impact-like" behaviour. At this point the overtopping increases even further. When the wave crest starts to break, however, then the wave looses some of its height and eventually tumbles down reducing the overtopping significantly. Once it has stabilised itself it starts building up anew.

No wave impacts were observed at 60° obliquity. Due to Snell's law a reflected wave has no velocity component in the opposite direction of the incoming wave. Thus, a wave is not reflected "backwards", but the direction of propagation is merely "diverted" and the wave is still moving away from the wave maker. This way no air is entrapped and no excessive pressure can build up.

5 PERCENTAGE OF IMPACTS

5.1 Introduction

The percentage of impacts has a strong influence on the nature of overtopping. Due to the different underlying physics the overtopping volumes can be up to three orders of magnitude higher if the waves are predominantly in impacting mode rather than in reflecting mode. This shows how important a robust predictor for the mode of the waves is.

The same waves which break onto the structure at perpendicular wave attack eventually switch to reflecting mode at higher obliquities. As has been discussed in chapter 4 when waves come in at increasing angles fewer waves impact onto the wall, but display "impact-like" behaviour. This is a gradual change and with further increasing angles all waves eventually switch to reflecting mode.

As the distinction between reflecting and impacting waves is important, an attempt has been made in this chapter to quantify the percentage of impacting waves as a function of wave conditions and water depth on the one hand side and the angle of wave attack on the other.

The percentage of impacts onto the wall was estimated in a video analysis. Each individual test was video recorded for 2 – 3 minutes, which is about 10 – 15% of the total duration of a test. The number of impacts was determined visually on the video for each test and measurement point, and the percentage of impacts for the entire test was then estimated. A definition of impacting and "impact-like" events at various angles of wave attack is given in chapter 4.

It should be noted that an "impact-like" event is a very comprehensive term. It can mean anything from "nearly" impacting to "nearly" reflecting. In this analysis tests, which displayed "impact-like" behaviour, were counted as impacting. "Impact-like" events only occurred under oblique wave attack and at 60° obliquity all waves were either in reflecting mode or broke clear of the structure.

5.2 Reference Configuration

Figure 34 shows a generic sketch of the basin set-up for the reference configuration (VO00). A more detailed sketch drawn to scale can be found in the Appendix. The measurement points are marked 3 – 6 for technical reasons. The tests were originally designed for 8 measurement points, but only the 4 in the middle were actually deployed.

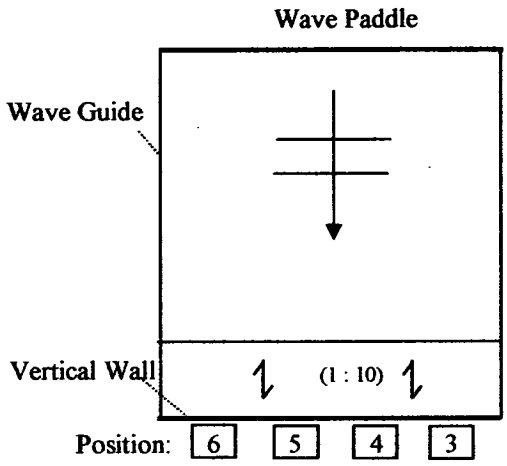

Figure 34: Structure configuration (VO00, reference test, $\beta = 0°$)

Figure 35 shows the percentage of impacts P_i for the reference test (β = 0°) plotted against the h* parameter. After the EA manual (1999) the h* parameter is a measure for the "impulsiveness" (section 4.1) of a sea-state (sections 2.2 and 2.3.3) and should show a clear trend with an increasing percentage of impacts towards lower values of h*. As can be seen in Figure 35 the measurements generally support that expectation. At h* values of about 0.22 the first tests show a few impacts and towards lower h* values the percentage of impacts increases significantly to values of up to over 40%.

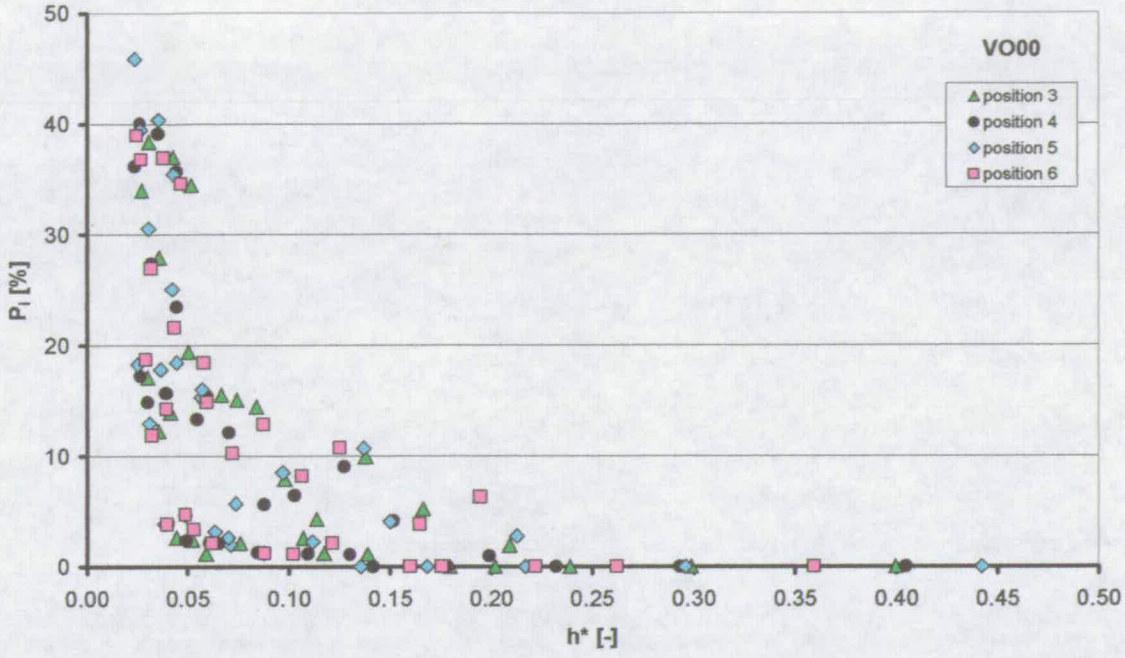

Figure 35: Percentage of impacts P_i ($\beta = 0°$) against h*

There are, however, three things to note. First, there is quite a significant cloud of points at h* values between 0.05 and 0.20. Some tests, for example, with h* = 0.20 showed the same percentage of impacts as other tests with h* = 0.05, in spite of a difference in h* of a factor of 4. Second, in the range of $0.03 < h^* < 0.06$ tests displayed any percentage of impacts from one percent up to over 40 percent. In that region there seems to be no actual dependency on h*. Third, even for h* values down to about 0.14 some tests showed no impacts at all and were practically in reflecting mode, while at the same h* value other tests actually had over 10% of the waves impacting onto the structure. h* is defined (see section 2.2):

$$h^* = \frac{h}{H_s}\frac{2\pi h}{g T_m^2} \tag{63}$$

Thus, the mean wave period T_m has a strong influence on the h* parameter. An increase in the wave period reduces h* which should lead to a more impulsive sea-state. A closer analysis of the percentage of impacts P_i, however, revealed that there was effectively no correlation between the wave period T_m and P_i for the matrix of test conditions in this study. This may be the case because the range of tested mean wave periods from about 1.1s to 1.6s was too small to reveal any such correlation.

It should be noted that the test matrix was designed to study the effect of obliquity on violent wave overtopping and not to reinvestigate 2d prediction tools. It might, however, be of interest for future work to extend the test matrix towards longer periods (leaving all other parameters constant) and to investigate the effect this has on the wave breaking behaviour.

As will be shown in section 6.2 tests in impacting and reflecting mode can be separated successfully based on their overtopping behaviour by plotting ratios of overtopping against relative wave heights H_{si}/h_i (see Figure 49). In Figure 36 this has been done for the percentage of impacts P_i ($\beta = 0°$) as well.

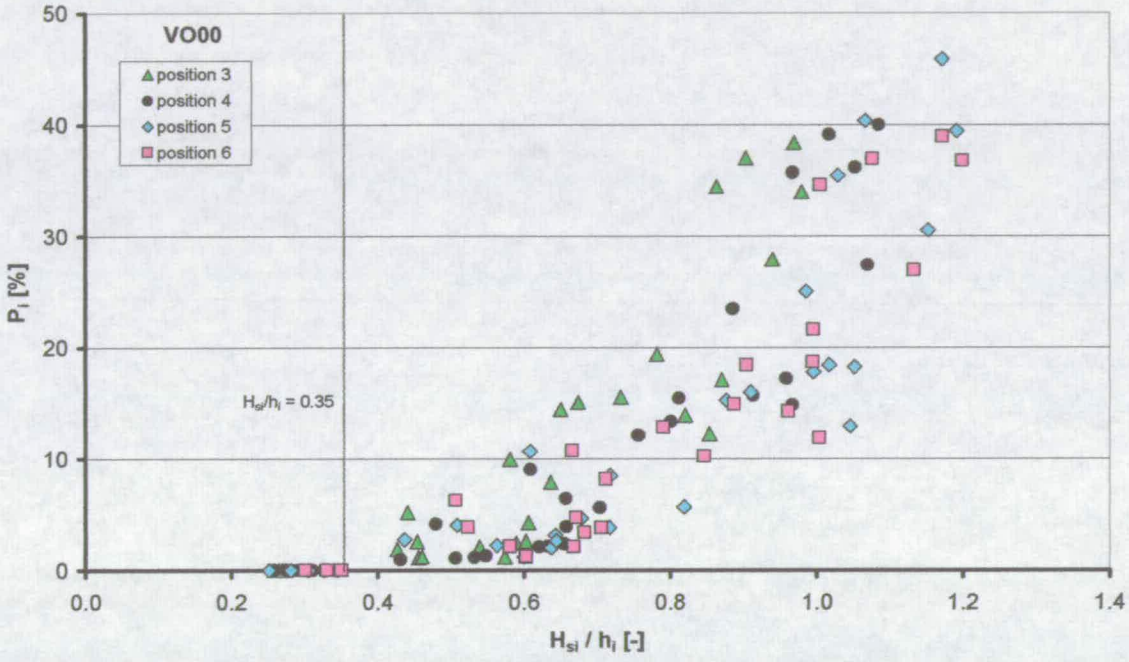

Figure 36: Percentage of impacts ($\beta = 0°$) against H_{si} / h_i

Although the scatter is still quite large (P_i varies between ±5% and ±15% for any given H_{si}/h_i) the overall trend appears to be clearer than in Figure 35. Consistent with the "PROVERBS parameter map" (Oumeraci et al., 2001; see section 2.2) all tests below H_{si}/h_i = 0.35 show no wave impacts onto the wall at all. Towards higher relative wave heights the percentage of wave impacts increases from "zero" to up to about 40% at $1.1 < H_{si}/h_i < 1.2$.

Allsop and Calabrese (1999) determined the percentage of impacts based on pressure measurements but came to very similar results (Figure 37, green triangles, note: axes scaled differently from Figure 36): below relative wave heights of H_{si}/h_i = 0.35 all tests were in

reflecting mode and above, between $H_{si}/h_i = 0.35$ and 0.6, P_i increases to values between still 3% and 13%, which is broadly in line with Figure 36.

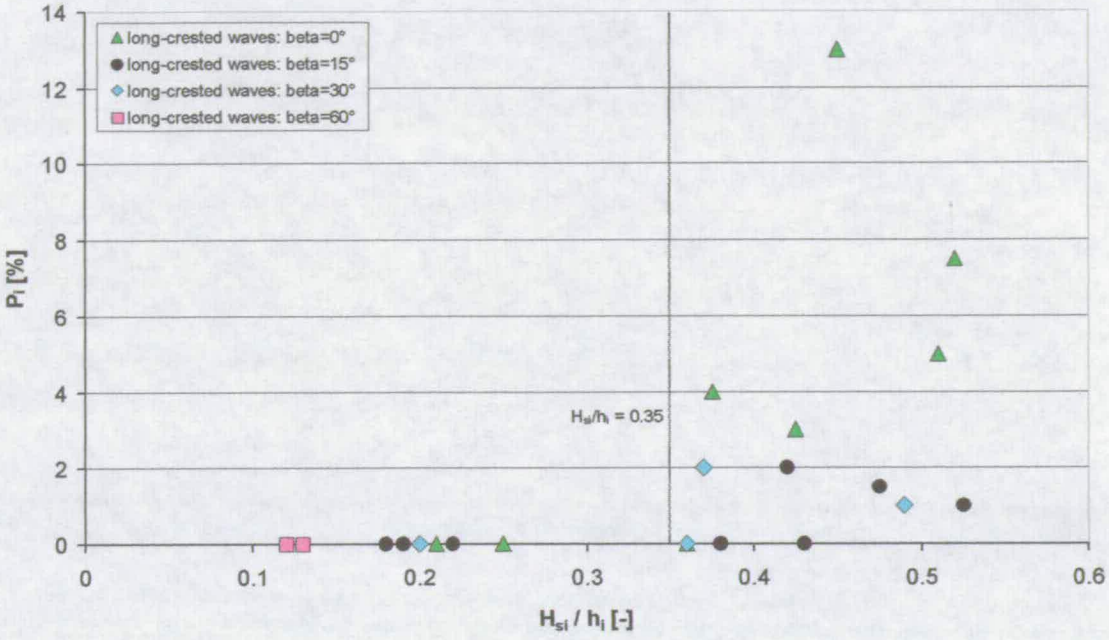

Figure 37: Percentage of impacts after Allsop / Calabrese (1999)

The PROVERBS workshop (Oumeraci et al., 2001) has developed a simple procedure to give estimates of the percentage of waves P_b breaking onto or in front of a vertical wall (section 2.2). This method can be considered an upper bound for the percentage of wave impacts (P_i) as the prediction includes broken waves as well. Figure 38 shows the prediction of breaking waves P_b for the reference test ($\beta = 0°$):

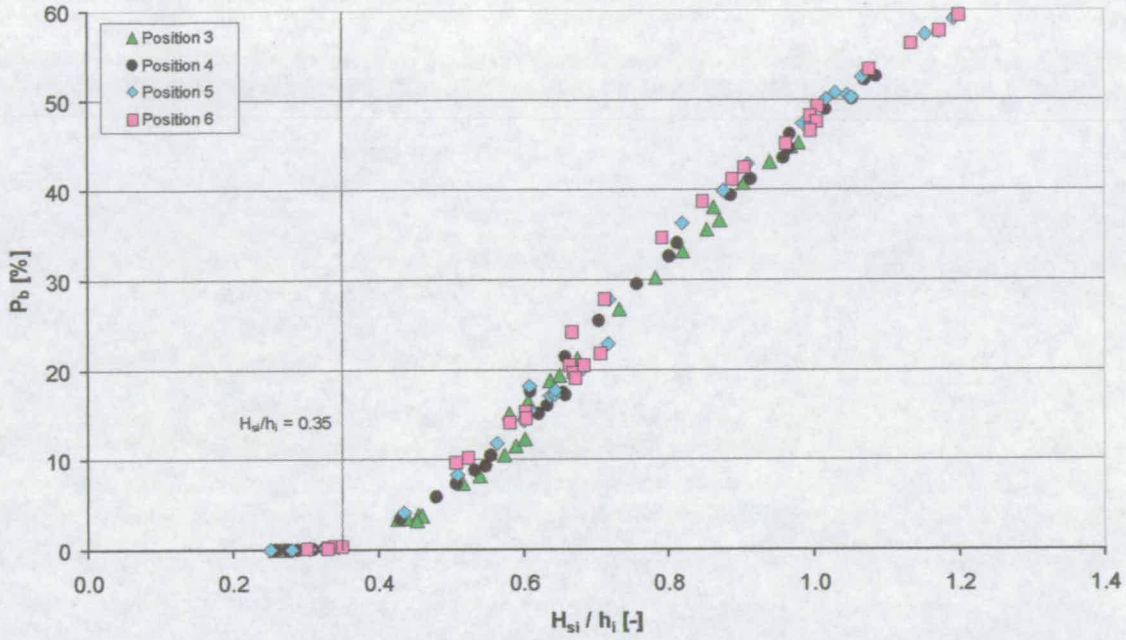

Figure 38: Prediction of upper bound for P_i (Oumeraci et al., 2001) for $\beta = 0°$

As expected for relative wave heights $H_{si}/h_i < 0.35$ (see Figure 38) the prediction of the percentage of waves breaking in front of the vertical wall is very low, i.e. less than 0.5%. From then on P_i increases along with the relative wave height to values of up to 60% at $H_{si}/h_i \approx 1.20$. In Figure 39 the estimated percentage of impacts P_i for the reference test ($\beta = 0°$) has been plotted again against the relative wave height H_{si}/h_i. This time the predicted percentage of waves breaking in front of the structure has been added. As has been expected the prediction for P_b works very well as an upper bound for the percentage of impacts P_i measured in this study.

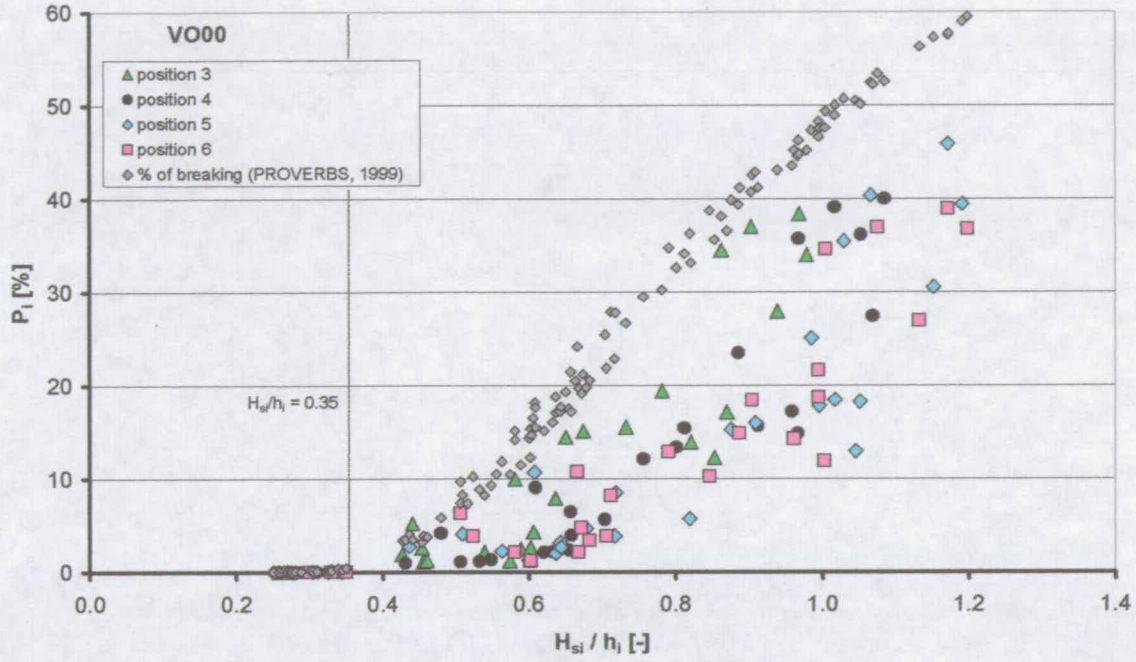

Figure 39: Estimated P_i and predicted P_b (upper bound) against H_{si} / h_i ($\beta = 0°$)

The PROVERBS workshop has also developed a simple procedure to estimate the percentage of waves breaking before but not onto the structure. The result can then be subtracted from the percentage of breaking waves yielding an estimate of the percentage of waves actually breaking straight onto the structure. Figure 40 shows the prediction of P_i after Oumeraci et al., 2001 plotted together with the measurements for the reference tests against the relative wave height H_{si}/h_i.

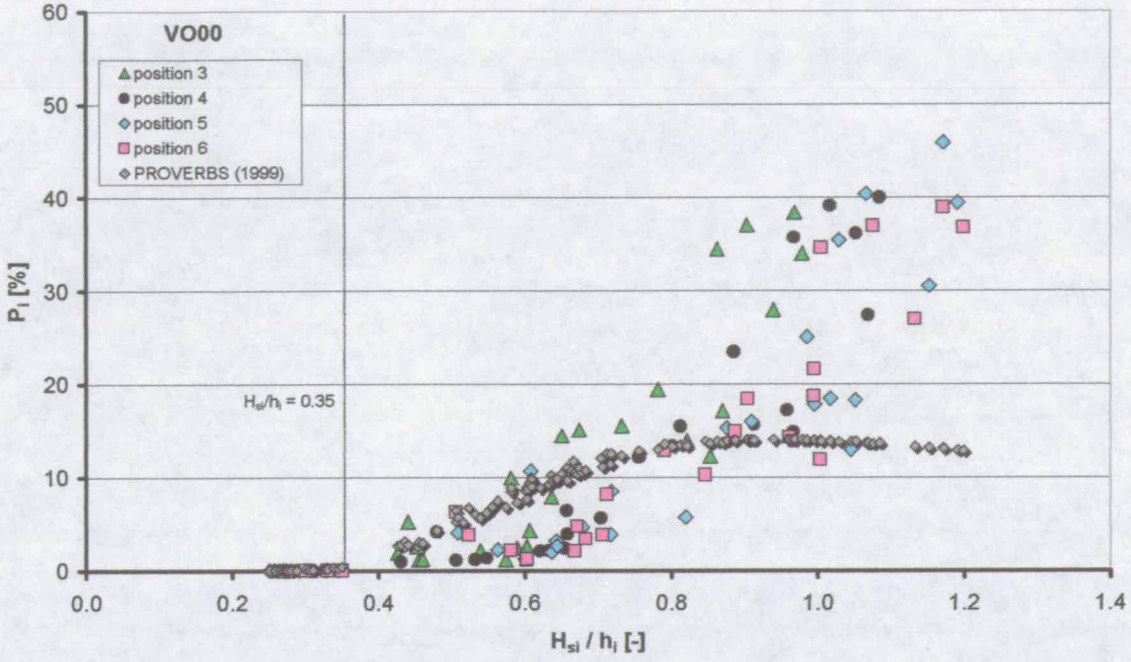

Figure 40: Estimated and predicted P_i against H_{si} / h_i ($\beta = 0°$)

Generally, as can be seen in Figure 40, the measurements follow a different trend than the prediction. This is most apparent for relative wave heights H_{si}/h_i above 0.8, where the prediction is nearly flat and from about $H_{si}/h_i \approx 1.0$ even down curving, while the measured values are still increasing almost linearly.

More specifically, the prediction works very well for reflecting conditions ($H_{si}/h_i < 0.35$) and up to $H_{si}/h_i \approx 0.50$. From then on up to $H_{si}/h_i \approx 0.7$ it actually over predicts many of the measurements by about 50%. For $H_{si}/h_i > 0.80$ it then starts to significantly under predict the percentage of breaking waves onto the structure. The actual measured values of P_i were up to 3 times larger than the prediction. It should be noted, however, that the scatter in the measured data is fairly large and that the prediction lies well within this scatter in most cases. Only at high relative wave heights H_{si}/h_i above 1.05 the measurements are under predicted at all times.

Apparently the percentage of waves breaking before and not onto the structure is over predicted, especially for high relative wave heights ($H_{si}/h_i > 0.8$). It should be noted, however, that the length of the approach bathymetry used in this study is only 1.3 – 2.6 times the peak wave length and also fairly steep with a slope of 1:10. Thus, due to the limited space between onset of breaking and structure many waves, which probably would break

well before the structure on longer, shallower bathymetries, have actually broken onto the structure. This leads to the conclusion that a method to predict wave impacts should take account of the slope angle of the approach beach. This, however, is not the case for the method suggested by the PROVERBS workshop (see also chapter 2.2).

5.3 Oblique Configurations

Wave-structure interactions change when waves approach the structure at angles larger than 0°. Especially the process of wave impacts looks quite different at larger angles. Towards higher angles of wave attack an increasing number of waves which would have broken (impacted) onto the wall at perpendicular wave attack start sliding along the wall with only part of the wave actually collapsing (breaking / impacting) onto the seawall. This behaviour is not an impacting event as defined for the 2D case, but in terms of overtopping it leads to similar results. In this thesis such an event is called an "impact-like" event as discussed more thoroughly in chapter 4.

These "impact-like" events are clearly not simply reflecting waves and they appear to contribute substantially to the amount of overtopping water. Thus, in the video analysis of oblique wave attack – the wave impacts were evaluated visually – these "impact-like" events were included to P_i. It should be noted that for 30° obliquity more than 50% of impacts were strictly speaking "impact-like" events.

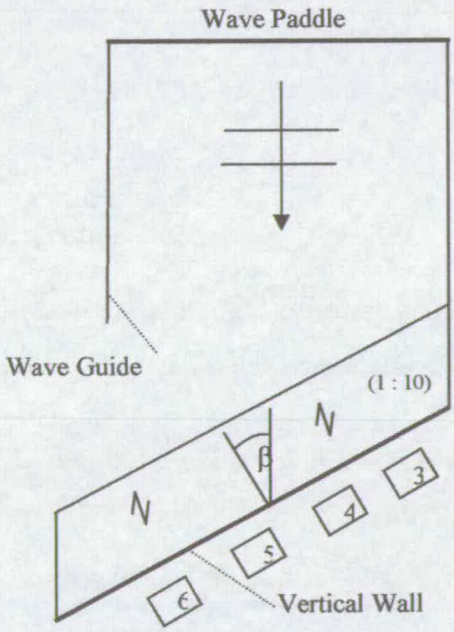

Figure 41: generic sketch of oblique tests

Figure 41 gives a generic sketch of the structure configuration of oblique tests. A more detailed sketch can be reviewed in the Appendix.

Figure 42 shows the percentage of impacts P_i for 15° obliquity plotted against the relative wave height (H_{si}/h_i). Although "impact-like" events have been included the overall percentage of wave impacts P_i is lower than for the reference case ($\beta = 0°$). It can be shown

that the reduction in P_i is more pronounced for relative wave heights of $0.35 < H_{si}/h_i < 0.60$ than for ones above 0.60 (see Figure 44). The reduction is about 50% for lower values and about 20% for higher values indicating that in terms of impulsiveness higher relative wave heights are less affected by the increase in the angle of wave attack to 15° than lower ones.

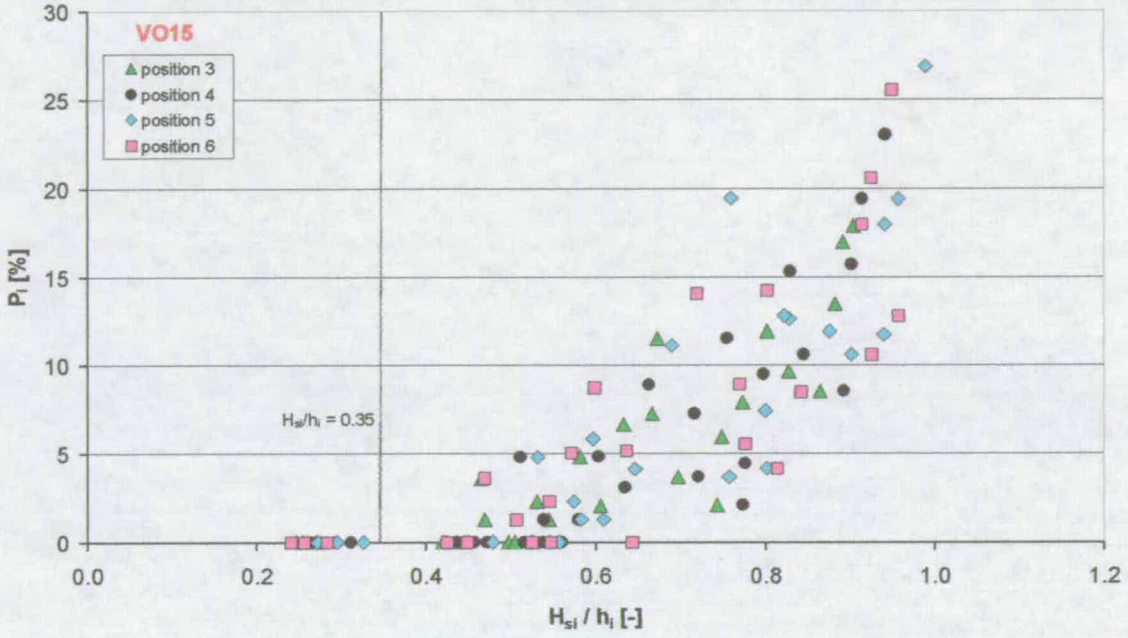

Figure 42: Percentage of impacts P_i ($\beta = 15°$)

Figure 43 shows the percentage of impacts P_i for 30° obliquity plotted again against the relative wave height H_{si}/h_i. The threshold at which impacts occur appears to have moved from $H_{si}/h_i \approx 0.35$ (at $\beta = 0°$) to $H_{si}/h_i \approx 0.45 - 0.50$. It should be noted, however, that at 30° obliquity and in this range of H_{si}/h_i it is very difficult to draw the line between reflecting and "impact-like" events. In terms of overtopping it can be shown that tests in this range of H_{si}/h_i still fit better to a modified trend line for impacting conditions after the EA manual (1999) than to the reflecting formula (see section 0).

Although it is difficult to distinguish visually between reflecting and "impact-like" events it could be shown that – like in the 15° obliquity case – the percentage of impacts between $0.35 < H_{si}/h_i < 0.60$ is more affected by 30° obliquity. In this range P_i was reduced by about 90% as compared to the reference test whereas for $H_{si}/h_i > 0.60$ P_i was reduced by about 25% only (Figure 44).

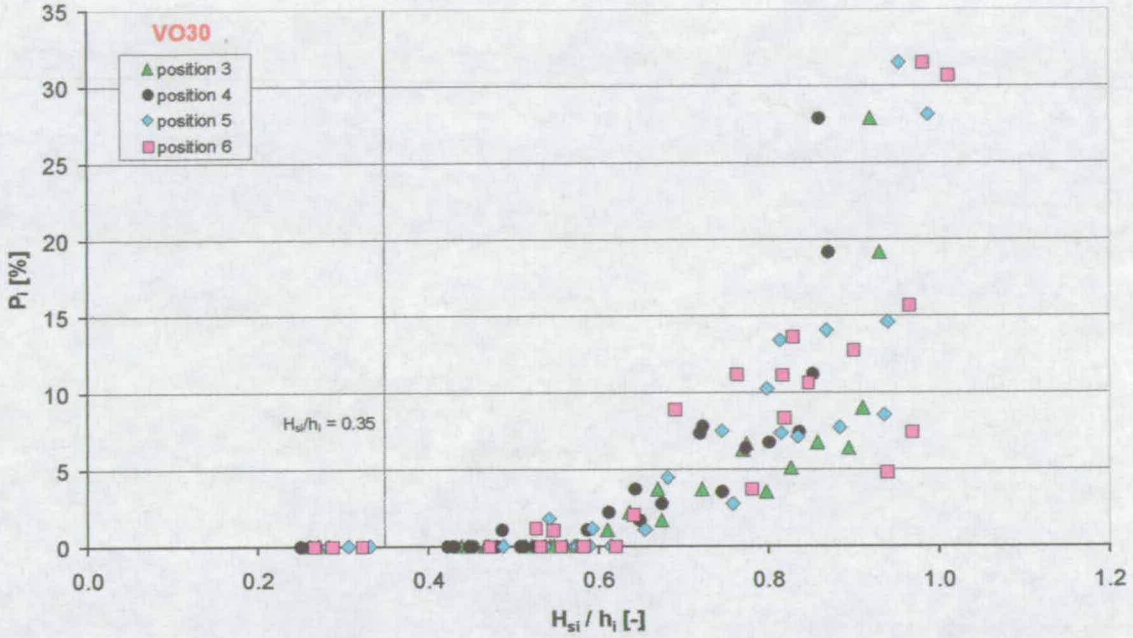

Figure 43: Percentage of impacts P_i ($\beta = 30°$)

The tests of 60° obliquity showed no impacts or "impact-like" events at all. Figure 44 summarises the influence of the angle of wave attack β on the percentage of impacts P_i. It shows the ratio of P_i at β to P_i at $\beta = 0°$ plotted against β. The ratio has been determined for two ranges of relative wave heights H_{si}/h_i. The first range ($0.35 < H_{si}/h_i < 0.60$) represents low relative wave heights and the second range ($0.60 < H_{si}/h_i < 1.00$) high relative wave heights. $H_{si}/h_i = 0.35$ is the threshold between impacting and reflecting conditions after the PROVERBS workshop (Oumeraci et al., 2001) which could be confirmed in this study as shown in section 5.2 and 6.2. Below $H_{si}/h_i = 0.35$ all tests were in reflecting mode.

A value of $H_{si}/h_i = 0.60$ has been chosen to separate low and high relative wave heights because of its effect on the mean overtopping discharge. Mean overtopping appears to be less effected by an increase in the angle of wave attack of up to 30° at relative wave heights above 0.60 (see Figure 54 and Figure 58). Figure 44 now shows that this is also the case for the percentage of impacts: for angles of wave attack of up to 30° P_i reduces much faster at low relative wave heights than at large ones.

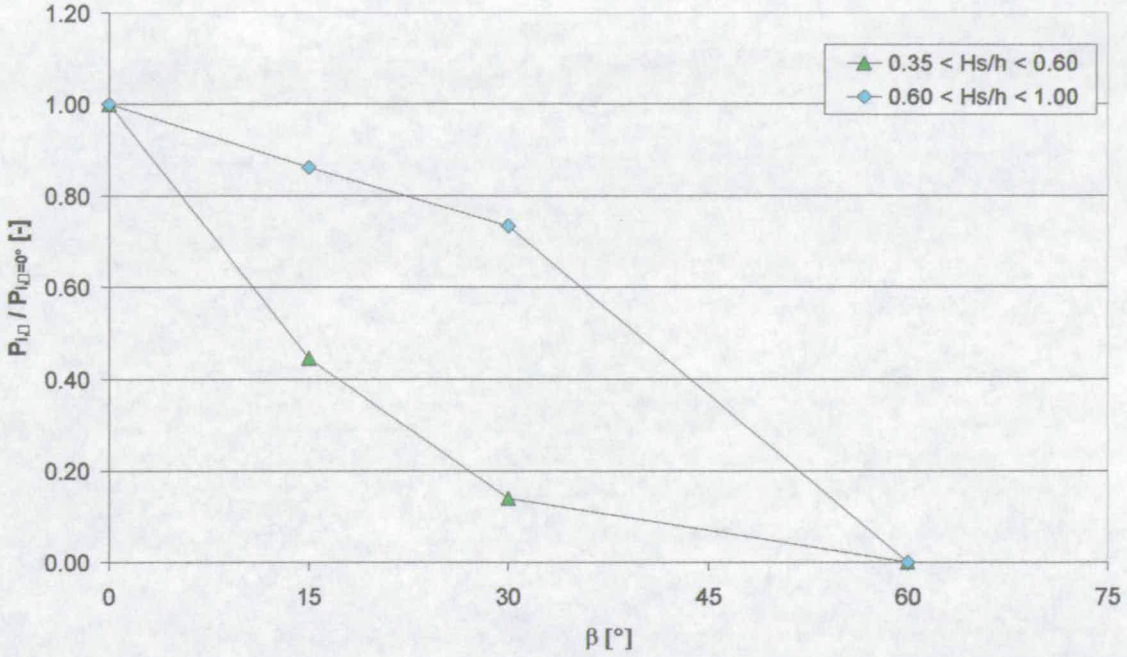

Figure 44: Ratio of the percentage of impacts P_i at β to P_i at β = 0° against β

Finally, the results for the percentage of impacts P_i is summarised in Figure 45 for 0°, 15°, 30° and 60° obliquity. Each obliquity contains the results for all measurement positions. As can be seen P_i reduces with an increasing angle of wave attack and for 60° obliquity no impacts occurred at all. It should be noted that oblique tests include "impact-like" events as defined in chapter 4.

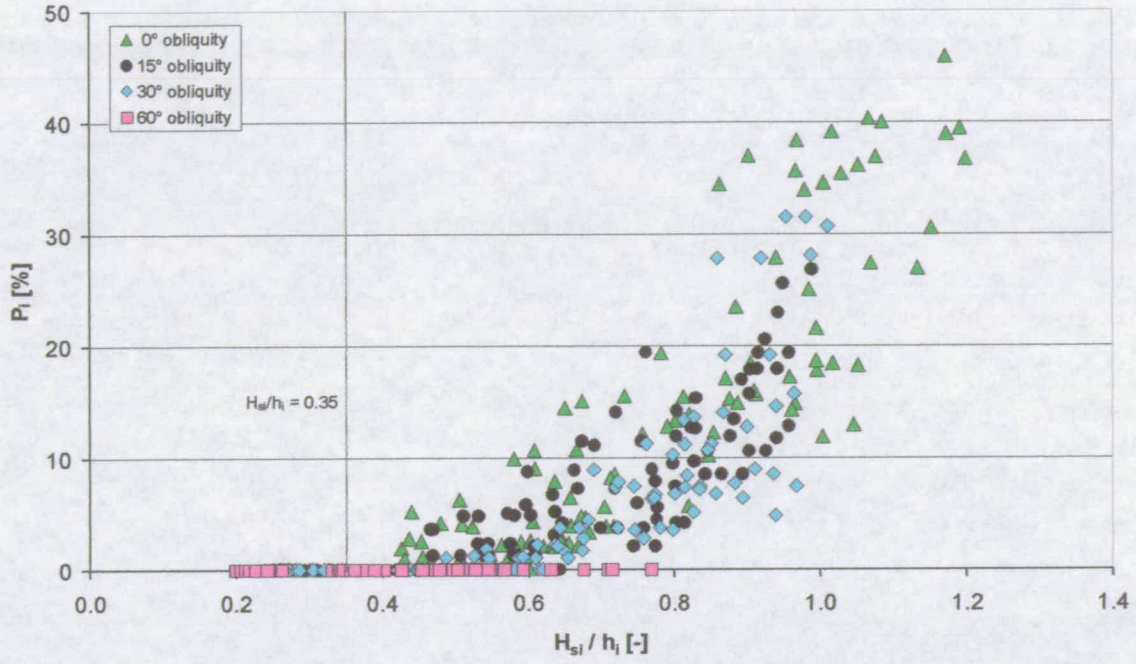

Figure 45: Percentage of impacts P_i as a function of β (all positions included)

5.4 Summary and Discussion

The percentage of impacts has a great influence on wave overtopping volumes. In this chapter an attempt has been made to quantify the percentage of impacting waves as a function of wave conditions and water depth on the one hand side and the angle of wave attack on the other. This has been accomplished by a video analysis. Although the scatter in the results was too large to derive any prediction tools, the findings for perpendicular wave attack were broadly in line with work done by Allsop and Calabrese (1999) and guidelines offered by the PROVERBS workshop (Oumeraci et al., 2001).

The EA manual (1999) suggests the h* parameter as a measure for the impulsiveness in a framework of overtopping prediction tools. Generally, decreasing values of h* gave an increasing percentage of impacts. However, this approach showed some significant scatter and could not clearly separate tests in reflecting mode from tests in impacting mode. Tests were considered to be in reflecting mode if no wave impacts could be observed.

A second approach used the relative wave height H_{si}/h_i to plot up the percentage of impacts. This clearly separated tests in reflecting mode from tests in impacting mode with a threshold of $H_{si}/h_i = 0.35$. The results were consistent with the work by Allsop and Calabrese

(1999) and by the guidance offered by the PROVERBS workshop (Oumeraci et al., 2001). The relative wave height H_{si}/h_i gave better results than the h^* parameter not only for perpendicular wave attack but also for oblique wave attack.

The PROVERBS guidelines first determine the percentage of breaking waves and then subtract the percentage of broken waves which then gives the percentage of impacting waves P_i. The first step provided a clear upper bound for P_i. The percentage of broken waves, however, was strongly over predicted leading to a prediction of P_i which was on average too low by a factor of about two. This could be explained by the short and steep approach bathymetry used in this study, which was only about 1.3 – 2.6 times the peak wave length long. Many waves, which would have broken clear of the structure, still impacted. It should also be noted that the prediction was still within the scatter of the "counted" percentage of impacts, though at the lower end.

When the percentage of impacts was established for the oblique cases, "impact-like" tests were included. Thus, the values of P_i did not reduce as fast as they would have if only "classical" impacts had been accounted for.

The results showed that there was a transition from impacting to reflecting conditions, i.e. the percentage of impacts reduced with an increasing angle of wave attack. At 60° obliquity no wave impacts or "impact-like" events were observed. It was also noted that all tests with low relative wave heights of $H_{si}/h_i < 0.35$ were in reflecting mode at all angles. Medium relative wave heights of $0.35 < H_{si}/h_i < 0.60$ were more effected by the increasing angle of wave attack than high ones ($H_{si}/h_i > 0.60$), i.e. the reduction in P_i was more pronounced. This also has an effect on the mean overtopping discharges which also reduces stronger at $0.35 < H_{si}/h_i < 0.60$ (see section 6.3 and 0).

6 MEAN OVERTOPPING DISCHARGE

6.1 Introduction

One of the main objectives of this thesis is the validation of prediction tools for mean overtopping discharge under perpendicular wave attack (reference case) and their modification and extension to angled wave attack (see chapters 1 and 2).

This topic is addressed in this chapter. As a first step, the prediction tools for the reference case are validated. The test matrix consists mostly of tests in (predominantly) impulsive mode for the reference configuration. The few tests in reflecting mode are validated separately.

As has been discussed in chapters 4 and 5, when waves come in at increasing angles, fewer waves impact onto the wall and display "impact-like" behaviour. This is a gradual change and eventually all waves are in reflecting mode. It could be shown that at 15° and 30° obliquity a large number of tests is still either in impacting or in "impact-like" mode. At 60° obliquity all tests are in reflecting mode.

In the course of this chapter the applicability of the 2D method for impulsive wave attack and its modifications necessary are discussed for 15°, 30°, and 60° obliquity. It will also be shown that the prediction of the regime of the waves (i.e. either impacting or reflecting) has an important influence on the predicted overtopping discharges, an influence that can reach three orders of magnitude.

A final issue to be addressed is the existence of spatial variability and its implications on the design of vertical sea-walls under oblique wave attack.

6.2 Obliquity 0° (Reference Configuration)

The reference configuration (VO00, $\beta = 0°$) was regarded a flume-like 2d case (see chapter 3) and, hence, provided an important benchmark for all other configurations. Its prediction formulae for mean overtopping had been validated several times in 2d wave flume tests at small and large scale (EA manual, 1999; Bruce, 2001; Pearson, 2002). Thus, in terms of mean overtopping it is considered a "known" condition. This section now shows that the measured data is broadly in line with the prediction tools and, hence, that there were no major basin- or model-effects.

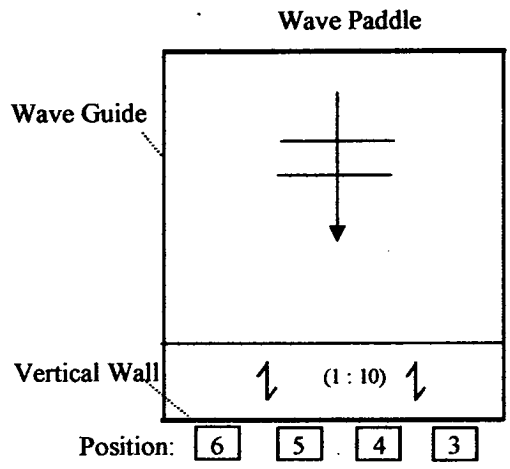

Figure 46: Sketch of basin set-up for reference test ($\beta = 0°$)

Figure 46 gives a rough overview of the basin set-up. A more detailed sketch drawn to scale can be reviewed in the Appendix. Four measurement points along the wall have been used marked position 3 – 6.

Figure 47 shows the results of the overtopping measurements for the mean discharge plotted for impacting conditions after the EA manual (1999). The dimensionless discharge Q_h is presented against the dimensionless freeboard R_h.

$$Q_h = \frac{Q}{\sqrt{gh^3}} \frac{1}{h^{*2}} \tag{64}$$

$$R_h = \frac{R_c}{H_s} h^* \tag{65}$$

More details on this method can be found in sub-section 2.3.3. It should be noted that due to the nature of h^* the dimensionless freeboard R_h is strongly influenced by H_s, T_m, and h_s ($1/H_s^3$, $1/T_m^2$, and h_s^2). Thus, while raising the water depth will decrease R_c it will also increase h_s, which may lead to an overall increase of R_h.

The solid black line in Figure 47 represents the prediction line for impacting conditions after the EA manual (1999) plotted fully over its valid range, whereas the solid red line is the trend-line fitted through the measured data. Only tests with predominantly impacting waves were taken into account ignoring the encircled cluster of points, which could be shown to be in reflecting mode (i.e. no impacts could be observed, see chapter 5). The red trend-line represents the combined trend of all 4 measurement points. As has been expected, no significant spatial variation along the wall can be seen and the overall trend is very much in line with the EA manual's prediction.

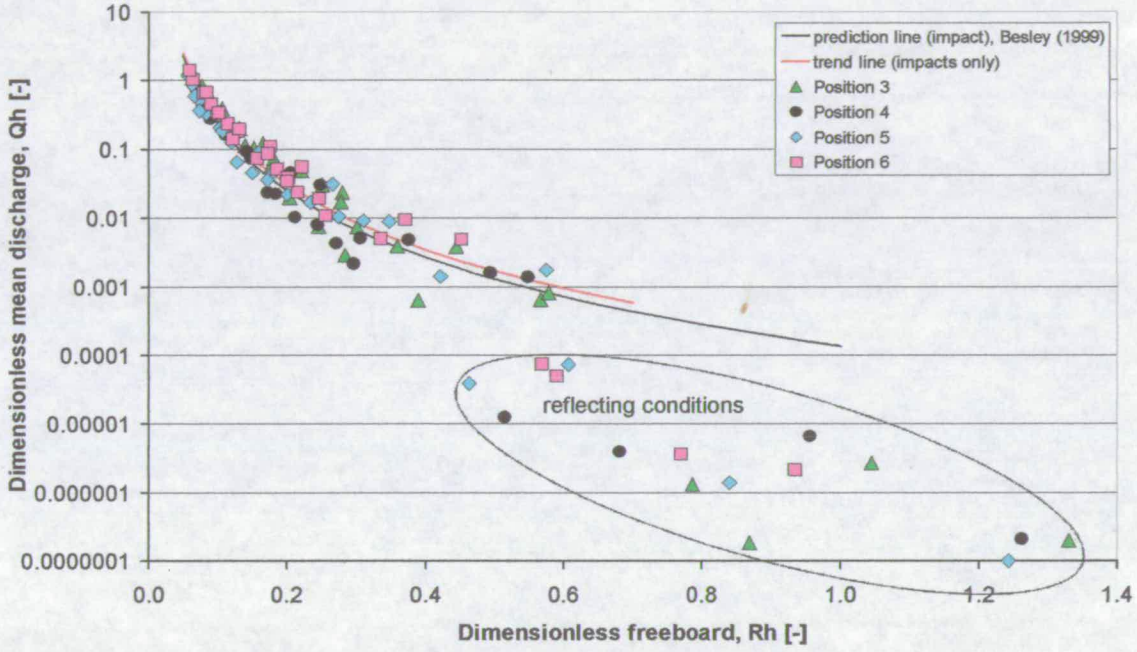

Figure 47: Mean discharge ($\beta = 0°$) plotted for impacting conditions after the EA manual (1999)

The EA manual (1999) suggests the h* parameter to predict whether the waves of a particular sea-state are predominantly impacting or reflecting. He draws the line at $h^* = 0.3$: all sea-states with $h^* \leq 0.3$ are predominantly impacting; those with $h^* > 0.3$ reflecting. The cluster of points in Figure 47, however, were identified to be in reflecting mode (see chapter 5), yet giving h* values of 0.14 – 0.30. Other tests, on the other hand, with h* parameters in a similar range were in impacting mode, as shown in Figure 48.

In Figure 48 the ratio of measured to predicted mean discharge for the reference test ($\beta = 0°$) has been plotted against the h* parameter. The prediction assumed impacting conditions

for all sea-states and was determined again after the EA manual (1999). All impacting tests are within a factor of "3" of the ideal value ("1.0"), except for one test which is off by a factor of about "5". The reflecting tests are over predicted by one to three orders of magnitude underlining the importance of a robust predictor of the regime which the waves are in.

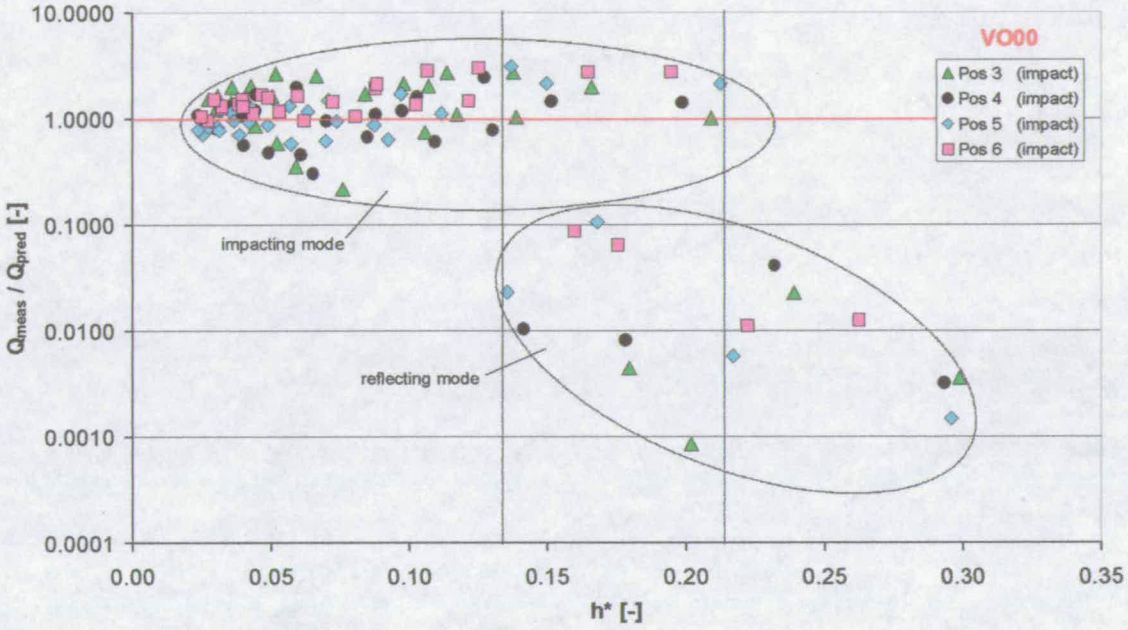

Figure 48: Ratio of measured to predicted mean discharge ($\beta = 0°$) against h*, prediction for impacting conditions after the EA manual (1999)

Figure 48 shows up limitations of h* as the only predictor for the impulsiveness: within the range of $0.14 \leq h^* \leq 0.21$ impulsive and reflecting tests apparently coexist (between vertical lines drawn on Figure 48). Given the definition (see section 2.2 for details):

$$h^* \equiv \left(\frac{h_s}{H_{si}}\right)\left(\frac{2\pi h_s}{gT_{mi}^2}\right) \tag{66}$$

h* states that in terms of impulsiveness an increase in wave period can compensate for a reduction in wave height. This, however, could not be confirmed in this study. In fact, no influence of the wave period on the percentage of impacting waves could be found at all, as was shown in section 5.2. The range of sea-states tested, however, should have been sufficient to show up the influence of the period. The mean wave period T_m varied from 1.1s to 1.6s yielding a range of wave steepness of 0.014 – 0.052.

The test matrix in this study was designed to investigate the effect of obliquity on violent wave overtopping and not to validate 2d prediction tools. Thus, the number of sea-states tested for the 2d reference case was too limited to re-evaluate the h* parameter.

It might, however, be of interest for future work to extend the test matrix towards even longer wave periods (leaving all other parameters constant) and to investigate the effect this has on the wave breaking behaviour.

The PROVERBS parameter map (Oumeraci et al., 2001) also provides an indicator for the occurrence of wave impacts at plain vertical walls (section 2.2). It distinguishes between "small" and "large" waves with waves being small if the ratio of inshore significant wave height to water depth at the toe of the wall is $H_{si}/h_i < 0.35$ and large if $H_{si}/h_i > 0.35$. "Small" waves are predicted to be in reflecting mode and "large" waves in impacting. Figure 49 shows again the ratio of measured to predicted mean discharge for the reference test ($\beta = 0°$) this time plotted against H_{si}/h_i. As in Figure 48, the prediction assumed impacting conditions for all sea-states and was determined after the EA manual (1999).

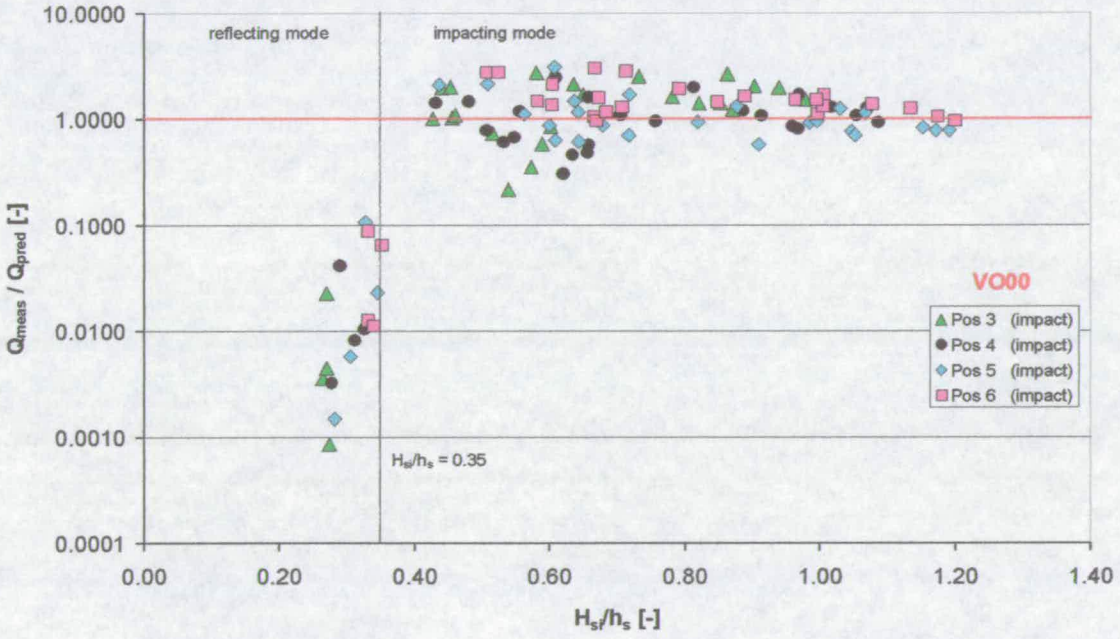

Figure 49: Ratio of measured to predicted mean discharge ($\beta = 0°$) against H_{si}/h_i, prediction for impacting conditions after the EA manual (1999)

The result is unambiguous: all reflecting tests lie to the left of the threshold ($H_{si}/h_i = 0.35$) and all impacting tests to the right. Thus, the PROVERBS parameter map seems to give a

robust indication whether waves are in impacting mode or not. The wave period does not appear to have an influence for the wave conditions tested in this study. This has been discussed further in chapter 5, which took a closer look at the percentage of impacts.

In Figure 50 the same tests (reference test, $\beta = 0°$) have been plotted now for reflecting conditions after the EA manual (1999) and Franco and Franco (1999). The dimensionless freeboard, R_c / H_s, is given on the x-axis and the dimensionless mean discharge Q# on the y-axis (for further details see sub-section 2.3.3). All four measurement points (3 – 6) have been plotted. This time the solid black line represents the prediction line for reflecting conditions after the EA manual (1999) also plotted over its stated range. The dotted brown line shows the prediction line after Franco et al. (1994). As can clearly be seen the tests in impacting mode are under predicted and do not follow this prediction line. Low dimensionless freeboards ($1.0 < R_c/H_s < 2.5$) are closer to the prediction, though under predicted in each case. Towards higher dimensionless freeboards the points move further away from the prediction line into the unsafe zone.

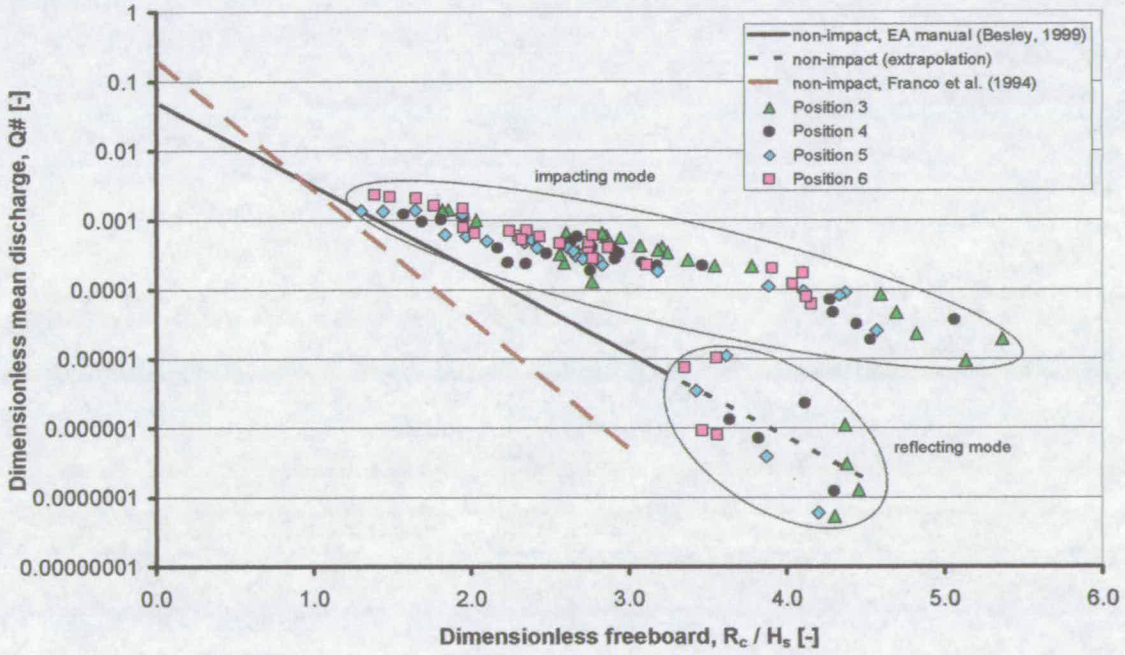

Figure 50: Mean discharge ($\beta = 0°$) plotted for reflecting conditions after the EA manual (1999)

The tests in reflecting mode are just outside the valid range of the EA manual prediction line towards higher dimensionless freeboards. The dotted extrapolation of the prediction line

appears to go right through this cluster of points. The extrapolation of Franco's et al. (1994) prediction line, however, seems to under predict the tests in reflecting mode.

Figure 47 and Figure 50 show that there is good agreement between the measurements and the prediction tools offered by the EA manual (1999) indicating that there were no major basin-effects. The only other prediction method found in literature, which covers mean discharge over vertical seawalls under impulsive conditions is the one offered by Goda (2000). However, the wave steepness and relative freeboard covered by Goda are too low and, thus, his method is not applicable to the test conditions of this study (see sub-section 2.3.3).

6.3 Obliquity 15°

A generic overview of the basin set-up for obliquities is given in Figure 51 (for further details on the 15° case see the Appendix). Four measurement points along the wall have been analysed marked positions 3 – 6.

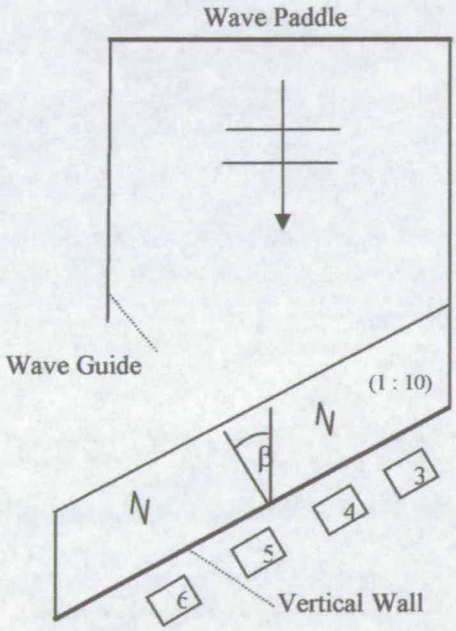

Figure 51: generic sketch of oblique tests

In Figure 52 the dimensionless mean discharge (β = 15°) has been plotted against the dimensionless freeboard after the EA manual (1999) for impacting conditions. The solid black line represents the prediction line for perpendicular (2D) wave attack after the EA manual. Three trend lines have been added. The solid red line shows the overall trend for all measurement points. The dotted black line gives the trend for position 4 only and the dotted pink one for position 6. These two positions gave consistently the lowest and highest overtopping, respectively. All trend lines were derived with the results for predominantly impacting test conditions only. At 15° obliquity this includes "impact-like" behaviour, in which only the crest of the wave breaks straight onto the wall (see chapter 4). In terms of overtopping this behaviour shows similar characteristics as "full" impacts. The encircled cluster of tests could be shown to be in simple reflecting mode (see chapter 5) and, hence, were ignored.

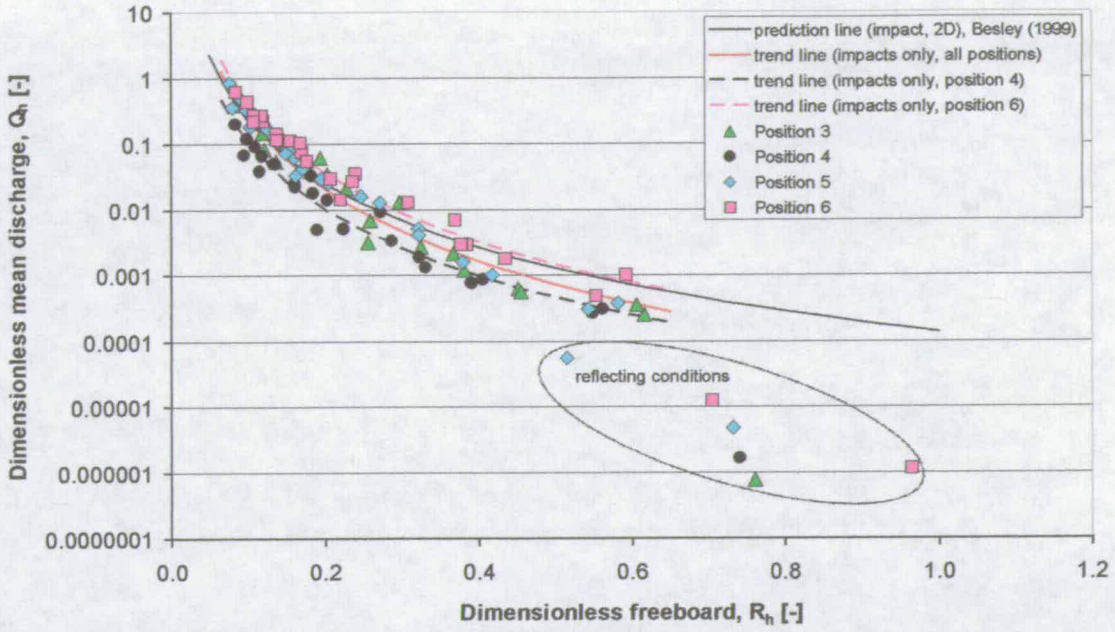

Figure 52: Mean discharge ($\beta = 15°$) plotted for impacting conditions after the EA manual (1999)

The overall trend for all measurement points (solid red line) has a similar shape (i.e. a power law relationship) as the 2D prediction line. For low dimensionless freeboards R_c between 0.06 and 0.25 it is within ±25% of the 2D prediction and then with increasing R_h it reduces to values of about 50% lower than the 2D prediction.

There is a noticeable difference between individual positions: the highest dimensionless overtopping could be measured at position 6, the lowest at position 4. The difference between the two positions is about a factor of three. Their trend lines lie almost equally spaced on either side of the red overall trend, i.e. a factor of about $\sqrt{3}$ above and below, respectively. Positions 3 and 5 gave volumes in the mid-range with a trend line, which is – for all practical applications – identical to the "red" trend line.

This spatial variation was very consistent for all tested wave conditions and could also be confirmed qualitatively for 30° obliquity (see next section 0). The location of reduced overtopping might vary with the actual length of the seawall and, hence, cannot be predicted with certainty based on this set of studies. Thus, for a conservative design the use of the trend line for position 6 – which is practically identical to the 2D prediction line – should be

recommended. If, however, the flood risk is more important for the design of the seawall, then the average trend line of all positions can be used (for recommendations see chapter 9).

Figure 53 shows the ratio of measured to predicted overtopping (Q_{meas}/Q_{pred}) against the h* parameter. The prediction is based again on the EA manual's (1999) method for impacting conditions and perpendicular (2D) wave attack. The spatial variability of overtopping volumes can be seen even more clearly in this Figure: Overtopping at position 6 appears to be on average slightly higher than the 2D prediction, whereas position 4 lies noticeably lower. Position 3 and 5 both gave very similar results in the mid-range slightly lower than the 2D prediction.

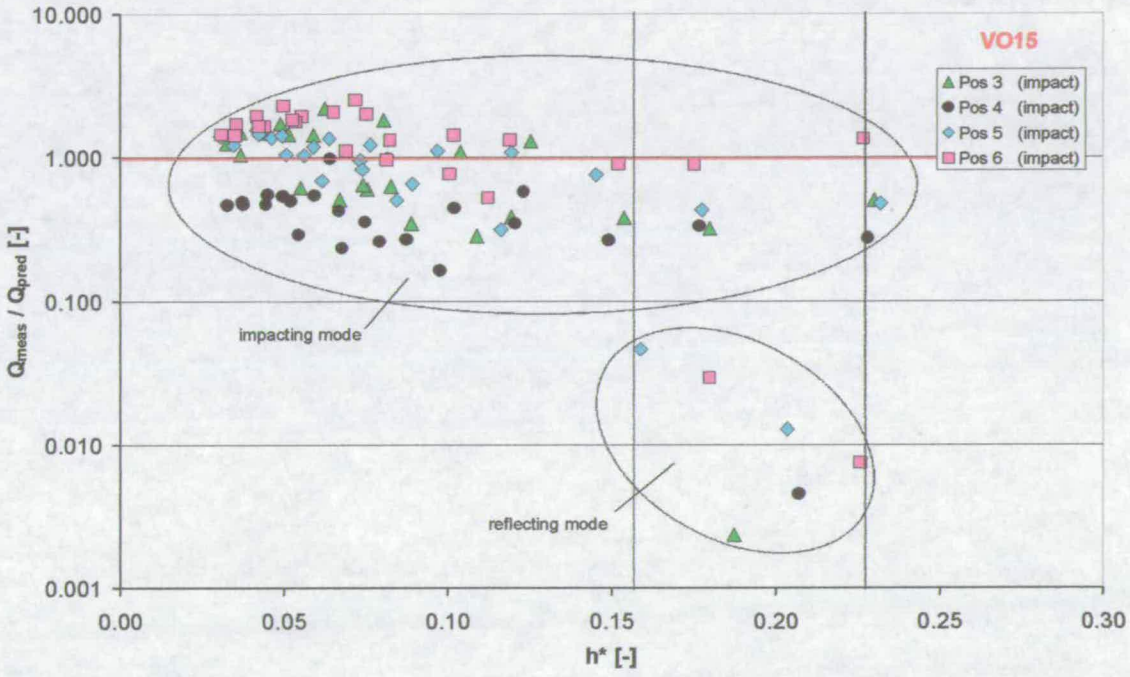

Figure 53: Ratio of measured ($\beta = 15°$) to predicted mean discharge ($\beta = 0°$) against h*, prediction for impacting conditions after the EA manual (1999)

Whether a sea-state was in impacting or reflecting mode was determined by a video analysis (see chapter 5). As can be seen in Figure 53 the h* parameter does not properly separate impacting from reflecting seas, which has also been noticed for the reference test (see Figure 48).

Plotting the same ratio of Q_{meas}/Q_{pred} against the ratio of significant wave height to local water depth (H_{si}/h_i) appears to give better results (Figure 54). All tests with $H_{si}/h_i < 0.35$

were in reflecting and all tests with $H_{si}/h_i > 0.35$ were in impacting mode (see also Figure 49, which shows the 2D case).

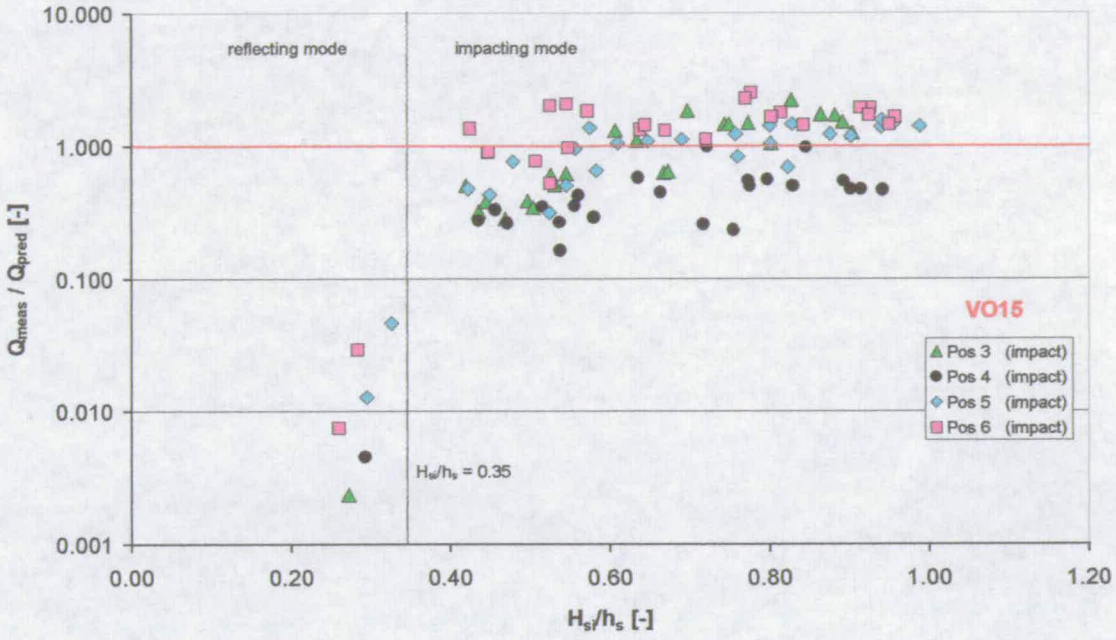

Figure 54: Ratio of measured ($\beta = 15°$) to predicted mean discharge ($\beta = 0°$) against H_{si}/h_i, prediction for impacting conditions after the EA manual (1999)

The ratio of Q_{meas}/Q_{pred} for impacting tests with $H_{si}/h_i > 0.60$ (Figure 54) appears to be fairly constant for each individual measurement point. Comparing Q_{meas}/Q_{pred} ($\beta = 15°$) in this range to the reference test ($\beta = 0°$), no significant reduction in overtopping could be detected as a result of the change of angle of wave attack (see Figure 49). The only exception is position 4 which is due to the spatial effect mentioned above.

In contrast to the reference test ($\beta = 0°$), the ratio of Q_{meas}/Q_{pred} at 15° obliquity reduces slightly for values of $0.35 < H_{si}/h_i < 0.60$. Thus, those tests seem to be more influenced by the change in the angle of wave attack to 15° than the more impulsive ones with higher relative wave heights. This greater influence on low relative wave heights can also be seen at the reduction in the percentage of impacting waves, where the percentage of impacts reduces faster for low relative wave heights of $0.35 < H_{si}/h_i < 0.60$ (see chapter 5). Most tests in this range were in "impact-like" mode which gave similar results in terms of overtopping. Thus, $0.35 < H_{si}/h_i < 0.60$ appears to be a transition zone. This is much more pronounced at 30°

obliquity showing that tests with low relative wave heights then start to transform to reflecting conditions.

Figure 55 shows the results for mean overtopping discharge presented with the reflecting method (EA manual, 1999). The solid black line represents the prediction line for an angle of wave attack of 15°, whereas the dotted black line indicates the prediction line for the 2D case. As for the reference test (β = 0°) a prediction of overtopping volumes of impacting tests with the reflecting method leads to an unsafe design. Tests in reflecting mode, however, appear to scatter around the extrapolation of the prediction line.

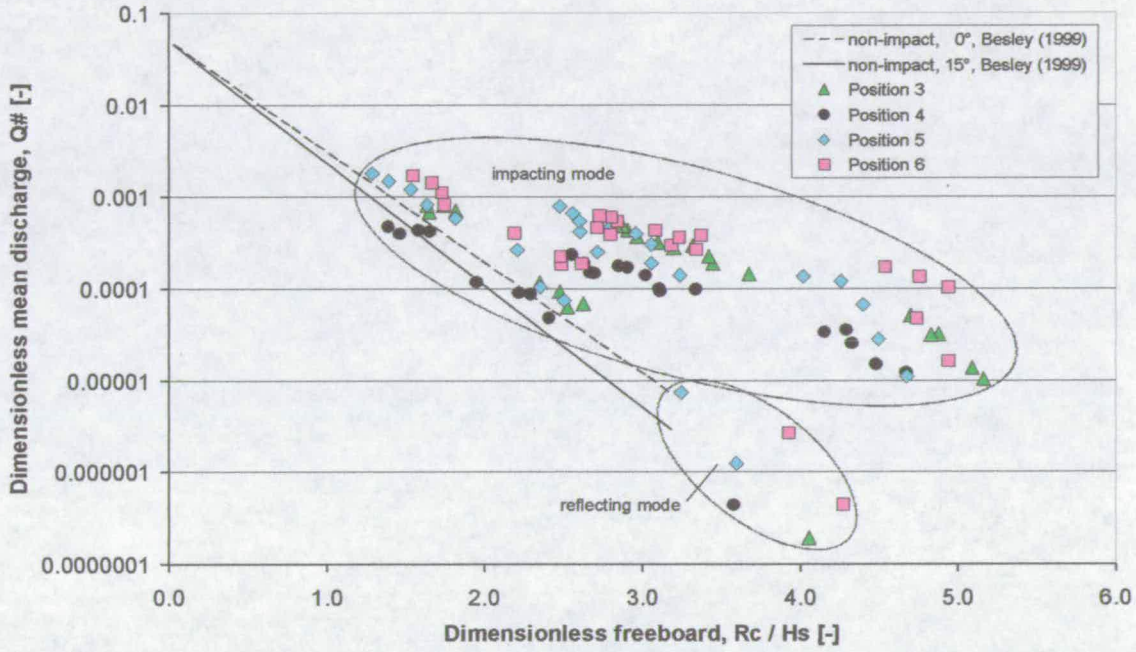

Figure 55: Mean discharge (β = 15°) plotted for reflecting conditions after the EA manual (1999)

6.4 Obliquity 30°

Figure 56 gives a generic overview of the basin set-up for oblique structure configurations (see also the Appendix). As for the tests of 0° and 15° obliquity four measurement points along the wall have been analysed marked positions 3 – 6.

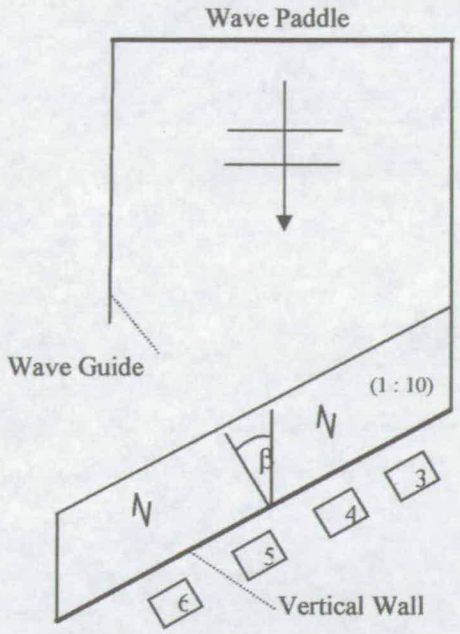

Figure 56: generic sketch of oblique tests

As for the other plan geometries the dimensionless mean discharge ($\beta = 30°$) has been plotted against the dimensionless freeboard after the EA manual (1999) for impacting conditions (Figure 57). Again, the solid black line represents the prediction line for perpendicular (2D) wave attack after the EA manual. Three trend lines have been added. The solid red line shows the overall trend for all measurement points. The dotted black line gives the trend for position 4 only and the dotted pink one for position 6. All trend lines were derived with the results for predominantly impacting test conditions only. The definition of "impacting tests" at an angle of 30° obliquity includes tests which display "impact-like" behaviour. This is a condition in which only the crest of the wave breaks straight onto the wall (see chapter 4). For this configuration no overtopping could be measured for tests in simple reflecting mode.

The overall trend for all measurement points (solid red line) has again a similar shape as the 2D prediction line (i.e. a power law relationship). This time for low R_h of about 0.075 the trend lies within ±25% of the 2D prediction and reduces towards higher R_h of up to 0.650 down to about 10% of the 2D prediction.

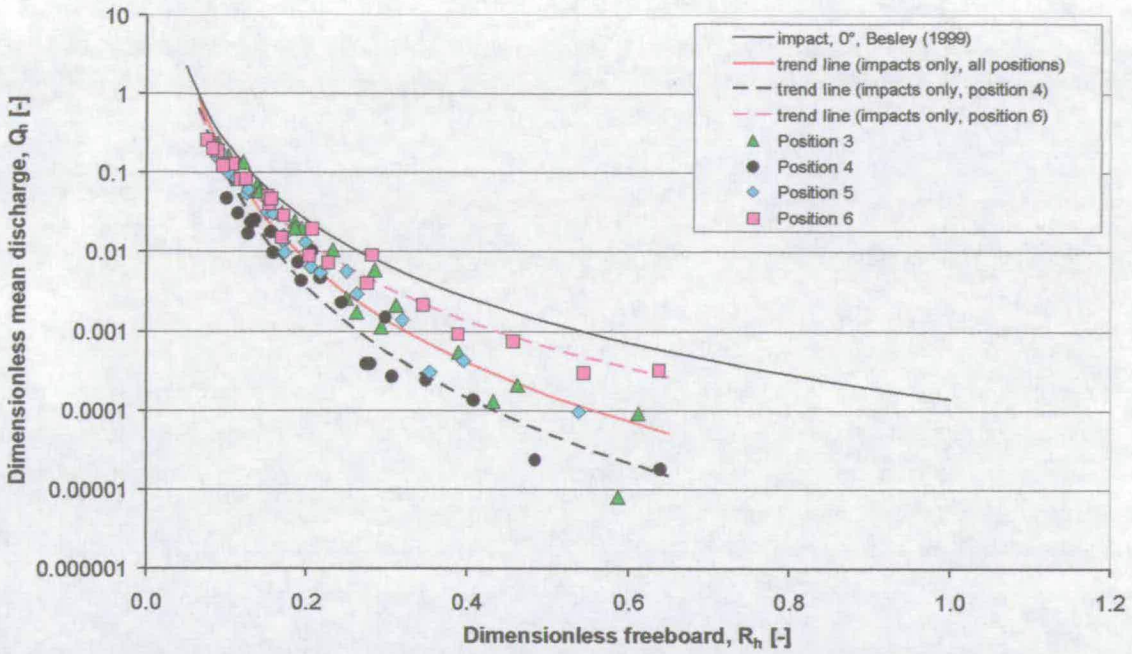

Figure 57: Mean discharge ($\beta = 30°$) plotted for impacting conditions after the EA manual (1999)

As for 15° obliquity there is a noticeable difference between individual positions: the highest dimensionless overtopping could be measured at position 6 again, the lowest at position 4. For low R_h (≈ 0.075) all trend lines give similar dimensionless mean discharges Q_h which vary by less than 30%. Towards higher R_h of up to 0.650 the difference then increases: at position 6 Q_h lies up to five times higher than the overall trend, and at position 4 down to 3 times lower. Positions 3 and 5 gave volumes in the mid-range, which were – as for the 15° case – practically identical to the overall trend.

The location of reduced overtopping might vary with the actual length of the seawall and, hence, cannot be predicted with certainty based upon theses studies. Recommendations for design are given in chapter 9.

In Figure 58 the ratio of measured to predicted overtopping (Q_{meas}/Q_{pred}) has been plotted against the relative wave height H_{si}/h_i. The prediction is based again on the EA manual's (1999) method for impacting conditions and perpendicular (2D) wave attack. The spatial variability of overtopping volumes can be seen even more clearly in this Figure: Overtopping at position 6 lies on average slightly lower than the 2D prediction, whereas position 4 lies

noticeably lower. Position 3 and 5 both gave very similar results in the mid-range between positions 4 and 6.

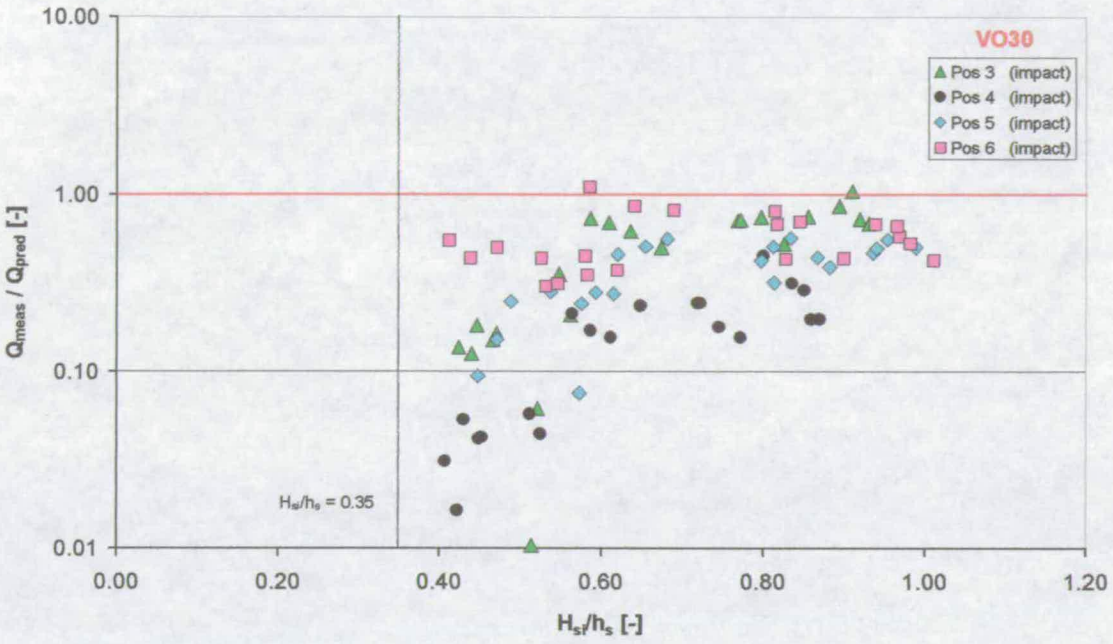

Figure 58: Ratio of measured ($\beta = 30°$) to predicted mean discharge ($\beta = 0°$) against H_{si}/h_i, prediction for impacting conditions after the EA manual (1999)

Despite of different absolute values all positions display fairly constant ratios of Q_{meas}/Q_{pred} for relative wave heights $H_{si}/h_i > 0.60$. Towards lower relative wave heights ($H_{si}/h_i < 0.60$) the ratio of Q_{meas}/Q_{pred} reduces significantly down to about 20% of the constant value for $H_{si}/h_i > 0.60$. The only exception is position 6 which reduces only slightly. The sharp reduction for positions 3 – 5 ($0.35 < H_{si}/h_i < 0.60$) is due to the transition from impacting to reflecting conditions with increasing angle of wave attack. Relative wave heights $H_{si}/h_i < 0.35$ have been shown to be in reflecting mode independent of the angle of wave attack (see section 6.2).

This reduction in overtopping is consistent with the reduction in the percentage of impacts which is more pronounced at smaller relative wave heights $H_{si}/h_i < 0.60$ (see chapter 5). As can be seen in Figure 44 at 30° obliquity the percentage of impacts between $0.35 < H_{si}/h_i < 0.60$ has reduced to about 14% of the reference case ($\beta = 0°$) whereas the percentage of impacts between $0.60 < H_{si}/h_i < 1.00$ has only reduced to about 73%.

Figure 59 shows the results for mean overtopping discharge for 30° presented with the reflecting method (EA manual, 1999). The solid black line represents the prediction line for an angle of wave attack of 30°, whereas the dotted black line indicates the prediction line for the 2D case.

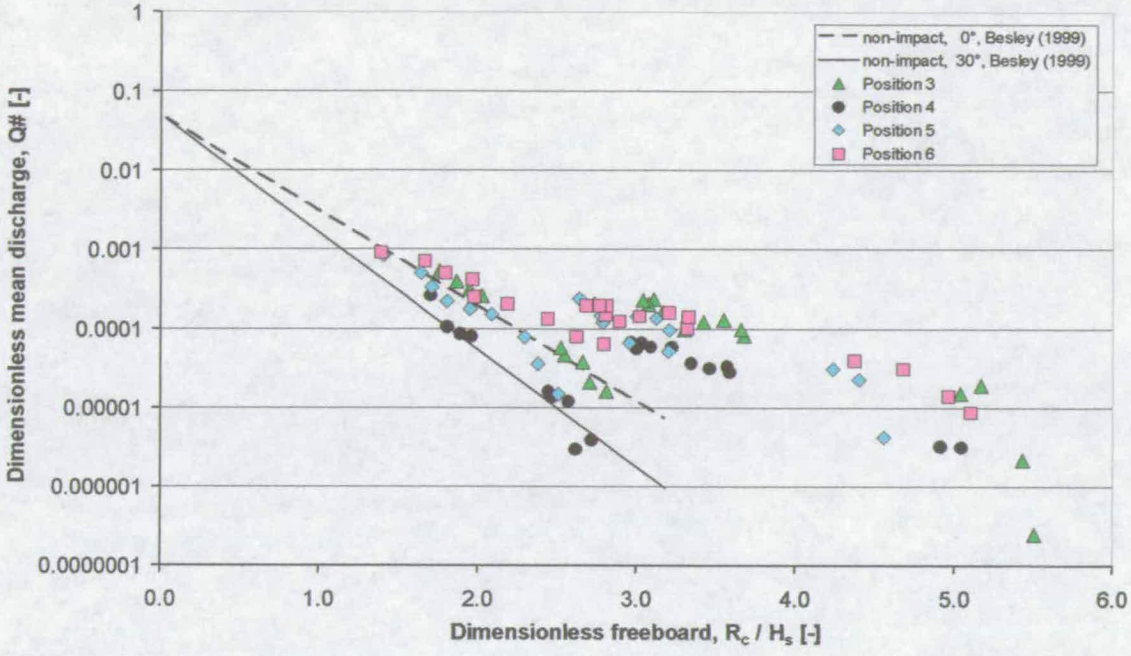

Figure 59: Mean discharge ($\beta = 30°$) plotted for reflecting conditions after the EA manual (1999)

A prediction of overtopping volumes of impacting tests with the reflecting method leads to an unsafe design in most of the cases. Those tests which scatter around the 2D prediction line are difficult to predict and, hence, a modified impacting formula is recommended (chapter 9).

6.5 Obliquity 60°

Figure 60 gives a generic overview of the basin set-up for the 60° obliquity test (see also the Appendix). As for the other configurations four measurement points along the wall have been analysed marked positions 3 – 6.

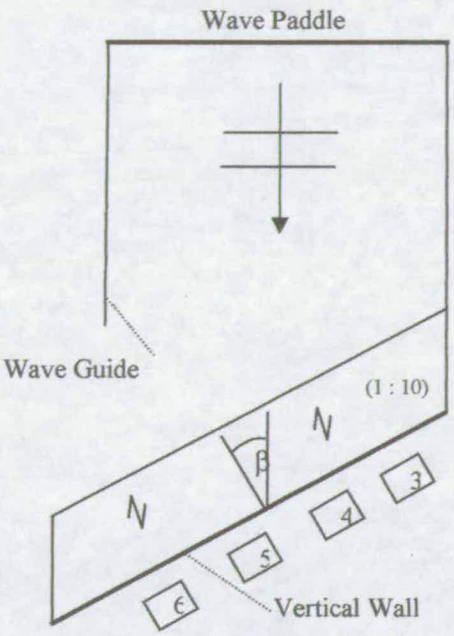

Figure 60: generic sketch of oblique tests

Figure 61 shows the dimensionless mean discharge (β = 60°) against the dimensionless freeboard after the EA manual (1999) for impacting conditions. Again, the solid black line represents the prediction line for perpendicular (2D) wave attack. At 60° obliquity no wave impacts could be detected at all. Thus, the prediction method for impacting conditions does not apply and no trend line has been added to the measured data.

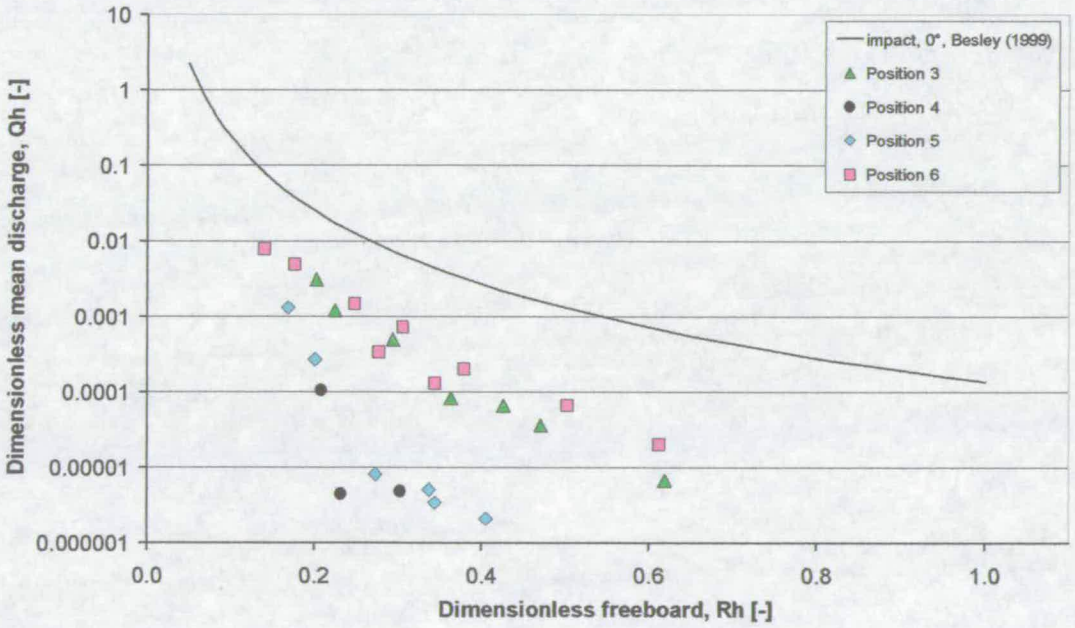

Figure 61: Mean discharge (β = 60°) plotted for impacting conditions (EA manual, 1999)

A certain degree of spatial variability can be seen between the positions: positions 3 and 6 give very similar overtopping volumes, whereas positions 4 and 5 give much less.

Figure 62 shows the results for mean overtopping discharge for 60° presented with the reflecting method (EA manual, 1999). The solid black line represents the prediction line for an angle of wave attack of 60°, whereas the dotted black line indicates the prediction line for the 2D case.

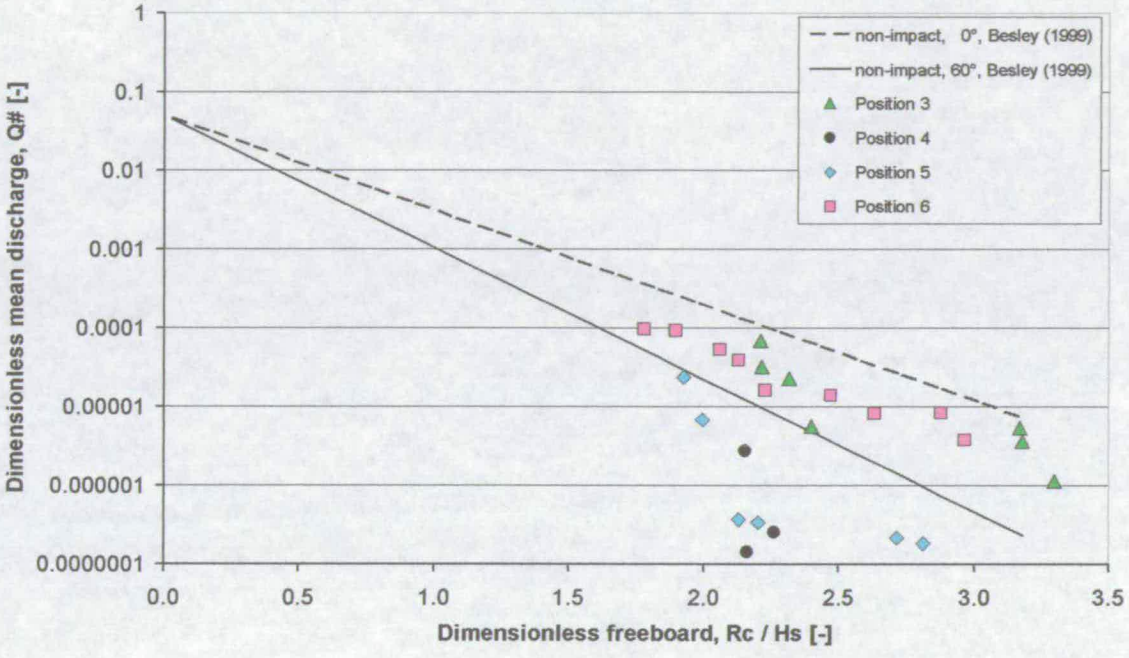

Figure 62: Mean discharge ($\beta = 60°$) plotted for reflecting conditions after the EA manual (1999)

Positions 4 and 5 give noticeably less overtopping than predicted by the EA manual (1999). This is due to the spatial effect mentioned above. Positions 3 and 6, however, appear to lie between the prediction for 60° and the one for perpendicular wave attack ($\beta = 0°$). It should be noted that the measured volumes here are extremely small and, thus, the scatter that must be expected is larger.

6.6 Summary and Discussion

In this chapter the prediction tools for mean overtopping discharge under perpendicular wave attack (reference case) have been validated and their extension to angled wave attack

(15°, 30°, and 60°) has been investigated. The discussion of the actual design guidance has been deferred to chapter 9.

The EA manual's (1999) method for mean overtopping discharges first distinguishes between waves predominantly in impacting or reflecting mode using the h* parameter. While this worked well in most cases there was a grey zone with h* values between 0.14 and 0.21, where waves in impacting and reflecting mode coexisted. The threshold suggested by the PROVERBS parameter map (Oumeraci et al., 2001), however, managed to separate both regimes clearly. All tests with H_{si}/h_i below 0.35 were in reflecting mode and all others above 0.35 were in impacting mode (see also section 5.2). This could also be confirmed for 15° and 30° obliquity.

Once tests in predominantly impacting mode had been separated from tests in reflecting mode the 2D method by the EA manual (1999) worked well for both regimes. Measurements for tests in impacting mode lay within a factor of three of the prediction and tests in reflecting mode were scattered around the extrapolation of the EA manual's (1999) prediction line for reflecting conditions. As the reference 2D case was considered a benchmark or a "known" case, the good fit of the results showed that no major basin effects were present and the measurement techniques and equipment worked well.

At 15° and 30° obliquity, tests with no impacts could be separated by the relative wave height ($H_{si}/h_i < 0.35$) in the same way as at 0° obliquity. Although an increasing number of waves showed "impact-like" rather than impacting behaviour for large relative wave heights ($H_{si}/h_i > 0.35$) tests at 15° and 30° obliquity still followed a slightly modified power law relationship after the EA manual (1999). The reduction in the percentage of impacts has been particularly strong for medium relative wave heights of $0.35 < H_{si}/h_i < 0.60$ (see section 5.3). In this region the reduction in overtopping has also been more pronounced, particularly at 30° obliquity (see Figure 54 and Figure 58). Similar to the reference case, tests in reflecting mode ($H_{si}/h_i < 0.35$) were well predicted by the extrapolation of the EA manual's (1999) prediction line for reflecting conditions and 15° obliquity. No overtopping has been measured for tests in reflecting conditions at 30° obliquity.

For 15° and 30° obliquity, spatial variability could be observed and measured. The largest difference between measurement positions was on average slightly larger than a factor of three. As only one basin set-up per structure configuration has been tested no tools could be derived to predict the exact location of low and high discharges. Thus, care must be taken in order to ensure a conservative design (see chapter 9).

The last structure configuration tested was 60° obliquity. The discharges measured were very low with many tests giving no measurable volumes at all. All tests were in reflecting mode (see also section 5.3). The formula for reflecting conditions and 60° obliquity after the EA manual (1999) gave good mean values for the mean overtopping discharge with most measured values within an order of magnitude of the prediction, whereas the 0° obliquity formula gave a good upper bound.

No general increase in mean overtopping at small angles of wave attack (e.g. 15°) could be measured, although, due to spatial variability, this might be the case at some (local) point along the seawall between measurement positions.

7 PROPORTION OF OVERTOPPING WAVES

7.1 Introduction

In the previous chapter prediction tools for the mean overtopping discharge have been derived. They can be used to evaluate flood risk and work as input parameters for some hazard models. Hazard models, however, can also be linked to peak individual overtopping volumes and not to mean discharges (section 2.5). In this chapter a prerequisite parameter for the prediction of individual volumes – the proportion of overtopping waves – is discussed for the 2D case and then extended to oblique wave attack.

As a first step (section 7.2) the measured proportion of overtopping waves for the reference configuration (0° obliquity) is compared to results by the EA manual (1999). The minimum overtopping volume to mark an "event" is determined by the sensitivity of the overtopping event detector as described in chapter 3. This thesis is essentially interested in violent overtopping, thus, only tests in impacting mode are considered. Additionally, a new approach to predict the proportion of overtopping waves is suggested, which seems to reduce the overall scatter.

Subsequently in section 7.3, both approaches are extended to 15° and 30° obliquity. No impacts have been observed at 60° obliquity and, thus, both approaches give no useful results at this angle of wave attack. Instead the EA manual's (1999) approach for reflecting conditions has been applied.

7.2 Reference Configuration

The EA manual (1999) presents a method to predict the proportion of overtopping waves for vertical seawalls under impacting conditions and perpendicular wave attack (see section 2.3 for details). He defines a dimensionless freeboard R_h:

$$R_h = \frac{R_c}{H_s} \quad h^* = \frac{R_c}{H_s} \frac{h}{H_s} \frac{2\pi h}{g T_m^2} \tag{67}$$

The proportion of overtopping waves is then given by:

$$\frac{N_{ow}}{N_w} = 0.031 R_h^{-0.99} \tag{68}$$

Figure 63 shows the proportion of overtopping waves N_{ow}/N_w measured for the reference configuration (perpendicular wave attack) plotted against R_h. Only tests in impacting mode have been considered. The dotted black line gives the prediction by the EA manual (1999) and the solid black line the overall trend for all measurement points.

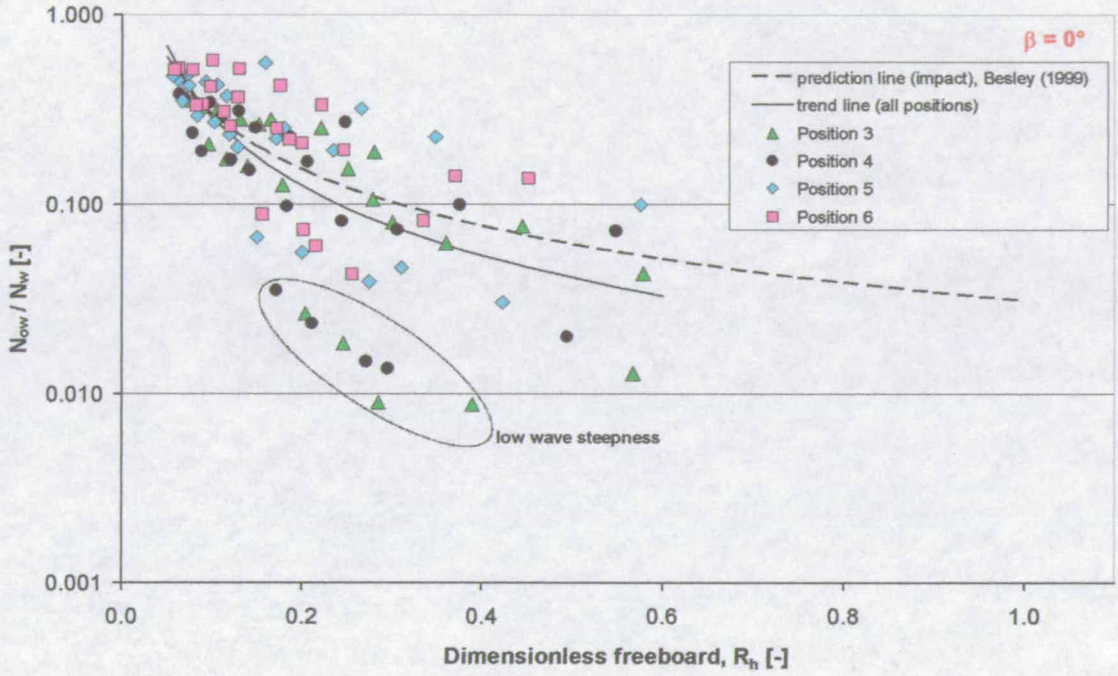

Figure 63: Proportion of overtopping waves against R_h, prediction line after the EA manual (1999)

Although the scatter in Figure 63 appears to be quite large ($R^2 \approx 0.49$) the overall trend line for all measurement points seems to follow the prediction line after the EA manual (1999) reasonably well. However, waves with a low steepness have N_{ow}/N_w particularly over predicted by this approach (see Figure 63). It should be noted that these tests displayed very low overtopping discharges and, as can be seen, only low proportions of overtopping events (i.e. less than 4%) were measured. Hence, their N_{ow} is subject to a somewhat higher level of uncertainty. If these tests are removed the overall trend falls onto the prediction line with all measurements within a factor of three above and below the predictions.

Given the scatter seen in Figure 63 an attempt is made to derive a better predictor for the proportion of overtopping waves. Chapter 5 has shown that the wave period has little or no influence on the proportion of impacts for the test conditions in this study. Removing the term containing the wave period from R_h (equation 67) gives:

$$R_{h,new} = \frac{R_c}{H_s} \frac{h}{H_s} \tag{69}$$

The proportion of overtopping waves plotted against $R_{h,new}$ yields Figure 64. The solid black line represents the trend line for all measurement positions. The scatter around the trend line is lower than for the approach after the EA manual (1999) with $R^2 \approx 0.92$.

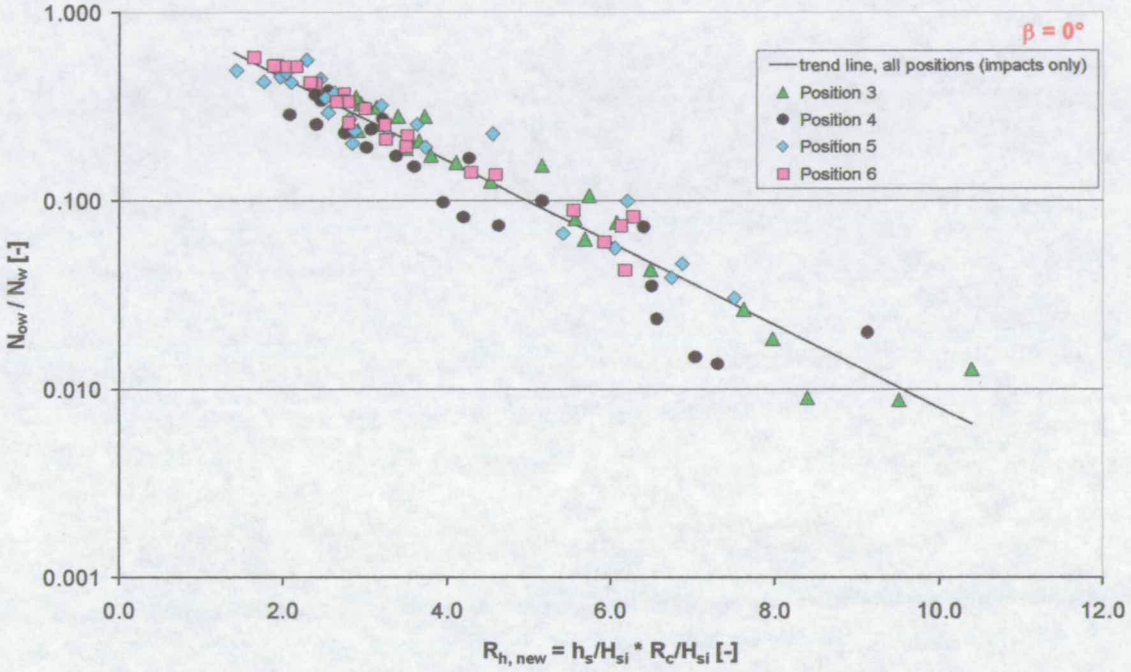

Figure 64: Proportion of overtopping waves against new dimensionless freeboard $R_{h,new}$

The next two figures compare the quality of both prediction methods. Figure 65 shows the ratio of measured to predicted proportion of overtopping against the relative wave height H_{si}/h_i and Figure 66 shows the same ratio against h*. The triangles represent the predictions after the EA manual (1999) and the diamonds the new approach. Both methods give good predictions with the new approach giving less scatter.

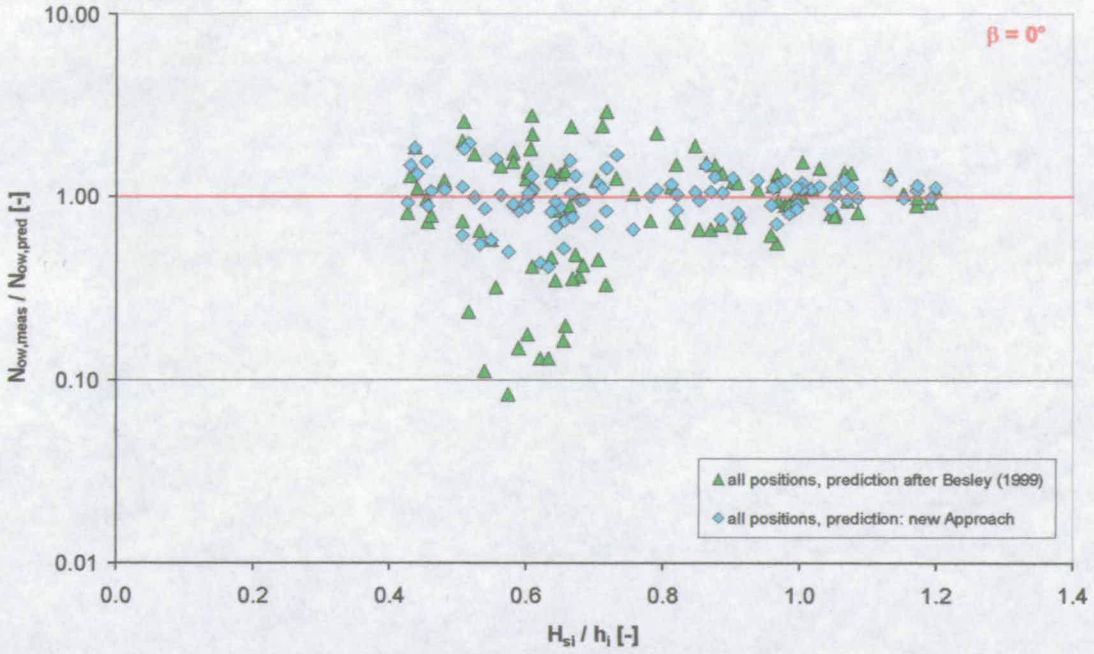

Figure 65: Comparison: EA manual's (1999) vs. new approach, plotted against H_{si}/h_i

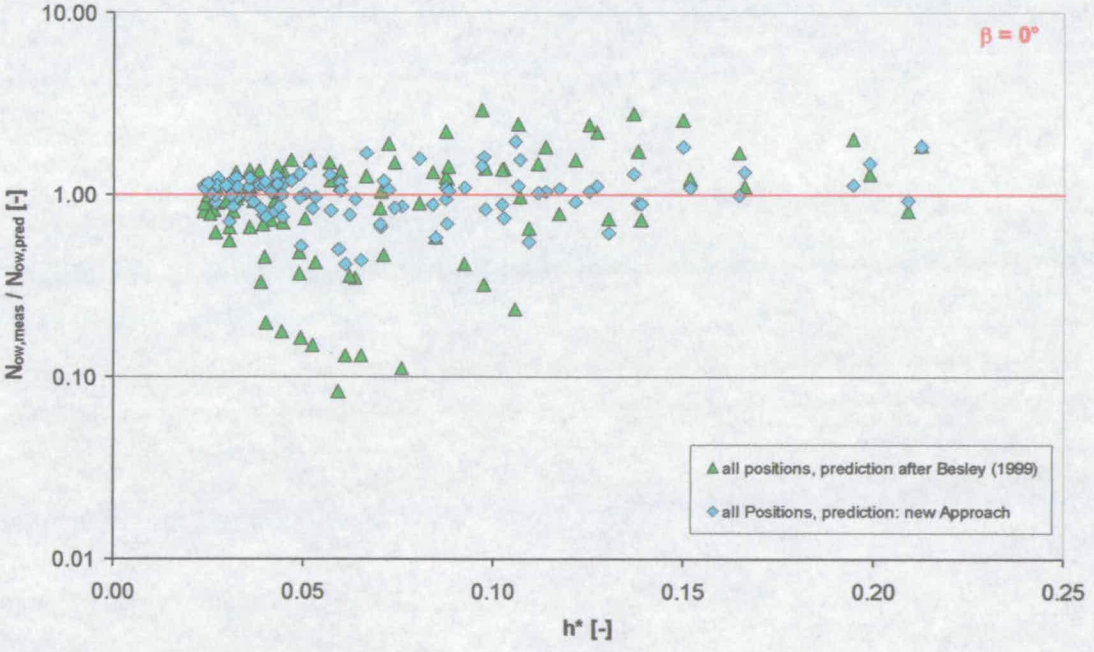

Figure 66: Comparison: EA manual's (1999) vs. new approach, plotted against h*

As mentioned earlier the number of overtopping events N_{ow} is needed to predict extreme overtopping events. It will be shown later that both prediction methods for N_{ow} yield input values which lead to good predictions of individual extreme events. Thus, although the new approach for N_{ow} appears to give somewhat less scatter in this study the old approach after the EA manual (1999) will be recommended as it gives overall results of similar quality and has been derived from and tested upon a much larger range of tests. Moreover, it should be noted that analysis on yet unpublished "VOWS 2d" data showed better results for the old approach by the EA manual (1999).

7.3 Oblique Configurations

In this section the prediction methods for the proportion of overtopping waves are extended to oblique wave attack. As the previous section has shown, both the prediction method after the EA manual (1999) and the new approach, work well for impacting conditions and perpendicular wave attack. For mean overtopping a modified approach for 2D wave impacts could be used up to angles of wave attack of 30° (see chapter 6). Only at 60° no wave impacts could be observed. Thus, the two approaches for the prediction of the proportion of overtopping waves should be applicable in a modified way to 15° and 30° as well.

In Figure 67 N_{ow}/N_w for 15° obliquity has been plotted against the dimensionless freeboard R_h (equation 67) as defined after the EA manual (1999). The solid black line represents the trend line for all measurement positions. The trend line seems to be a good representative of the individual tests. The scatter is noticeably lower than for the 0° case ($R^2 \approx 0.74$).

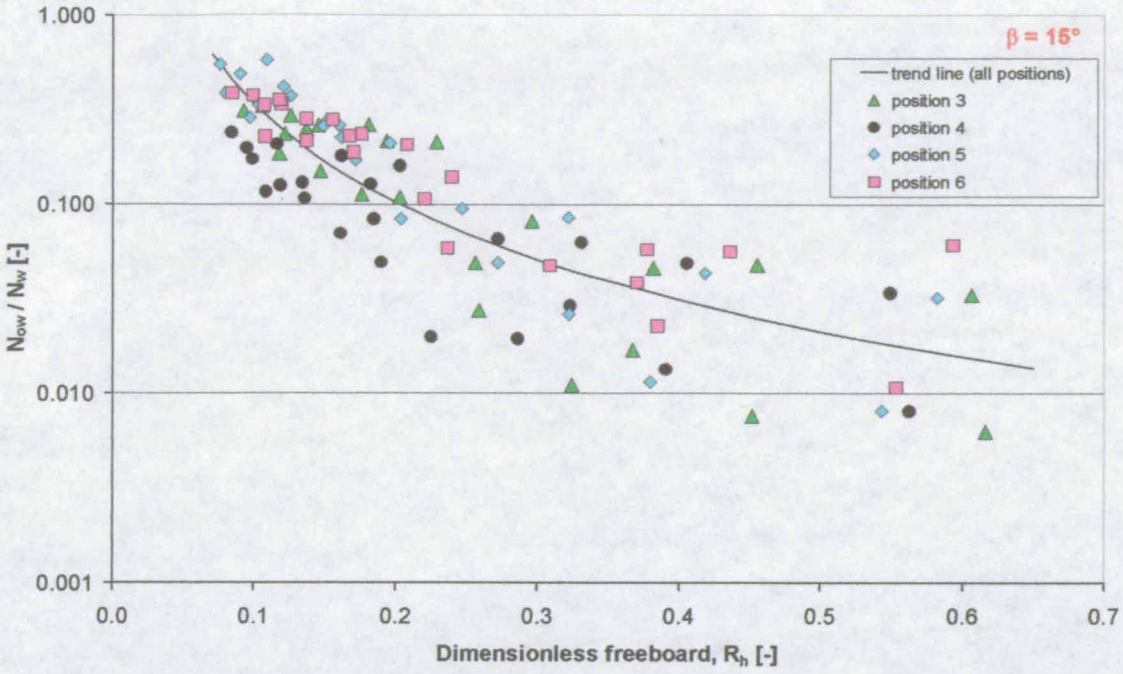

Figure 67: Proportion of overtopping waves against R_h (15° obliquity)

The same ratio N_{ow}/N_w for 15° has been plotted against the new dimensionless freeboard $R_{h,new}$ (equation 69) as defined in the previous section (Figure 68). The solid black line again represents the trend line for all measurement positions. The degree of scatter around the trend line ($R^2 \approx 0.83$) is similar to the approach with R_h as defined by the EA manual (1999) (Figure 67) and, hence, both approaches appear to be equally suitable.

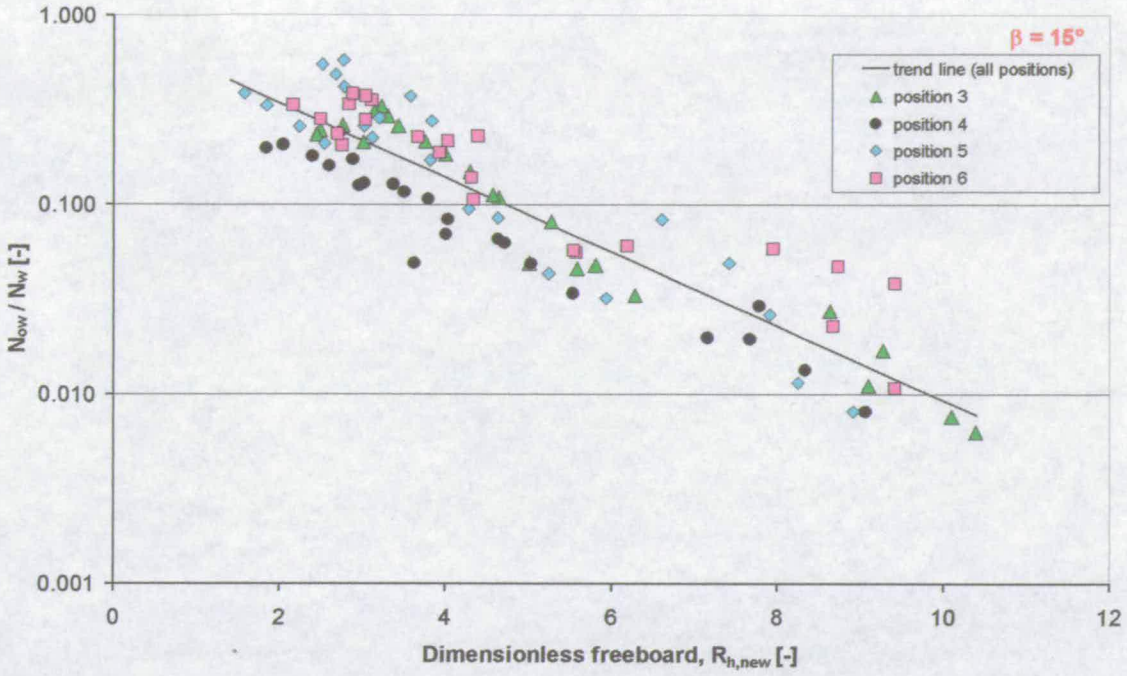

Figure 68: Proportion of overtopping waves against $R_{h,new}$ (15° obliquity)

The results for 30° obliquity are very similar to 15°. Figure 69 shows the ratio N_{ow}/N_w for 30° plotted against the dimensionless freeboard R_h as defined by the EA manual (1999). The solid black line gives the trend line for all measurement positions. The degree of scatter is about the same as for 15° ($R^2 \approx 0.74$).

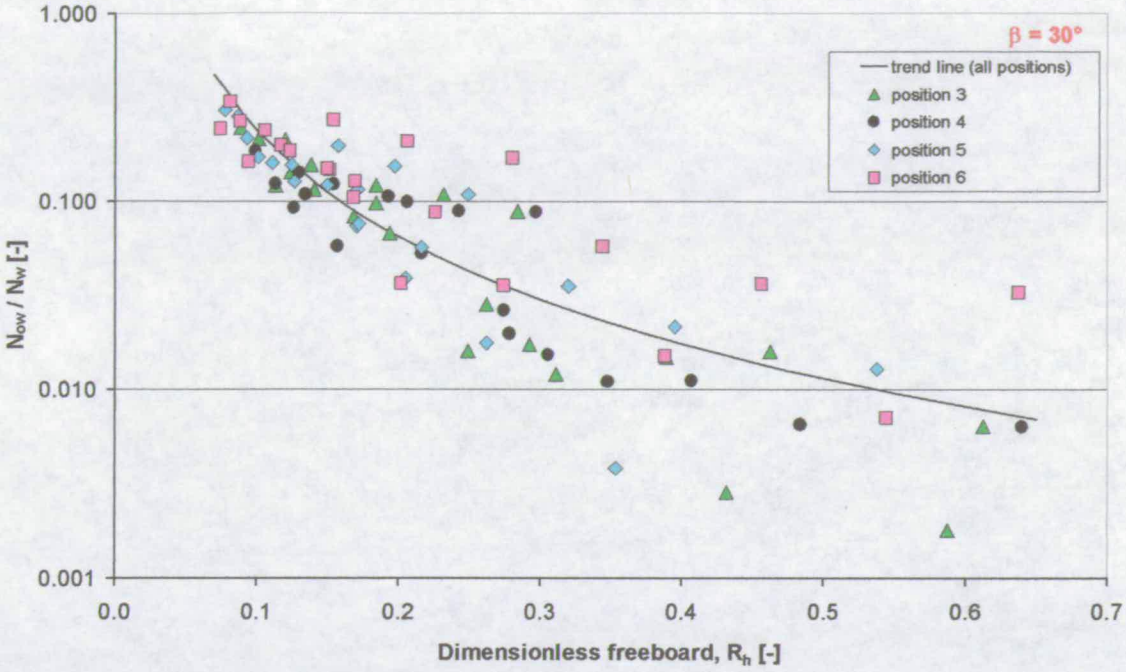

Figure 69: Proportion of overtopping waves against R_h (30° obliquity)

As for the 15° case, the same ratio N_{ow}/N_w for 30° has been plotted against the new dimensionless freeboard $R_{h,new}$ as defined in the previous section (Figure 70). The solid black line again represents the trend line for all measurement positions. The degree of scatter around the trend line ($R^2 \approx 0.79$) is very similar to the approach with R_h as defined by the EA manual (1999) (Figure 69) and, hence, both approaches appear to be equally suitable as has been noted for the 15° case as well.

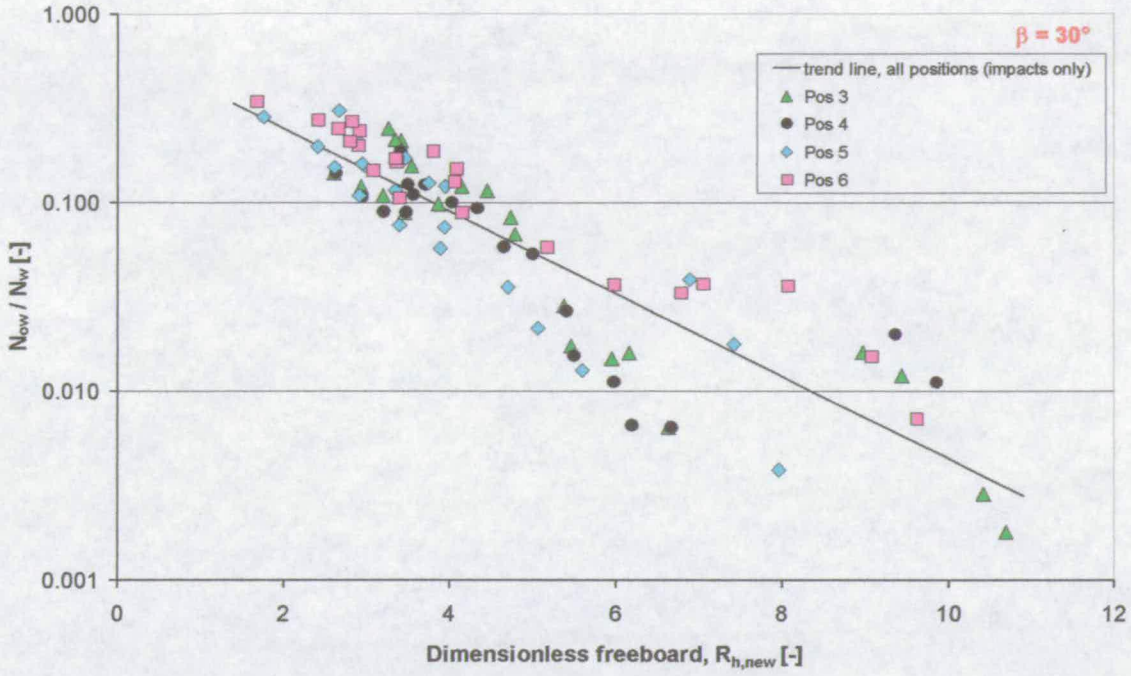

Figure 70: Proportion of overtopping waves against $R_{h,new}$ (30° obliquity)

At 60° obliquity no wave impacts have been observed. Thus, both approaches for impacting conditions are no longer applicable. Instead, the prediction formula for reflecting conditions and angled wave attack after the EA manual (1999) is presented in Figure 71.

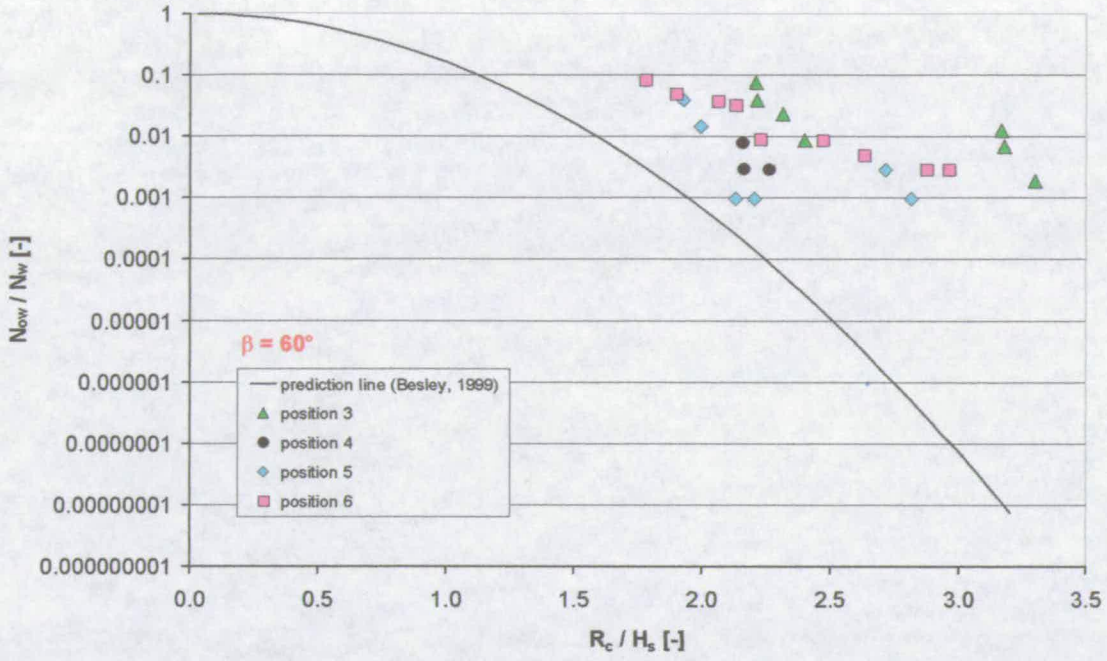

Figure 71: Proportion of overtopping waves, 60°, refl. cond. (EA manual, 1999)

Unfortunately, the proportion of overtopping waves is under predicted by up to several orders of magnitude. It should be mentioned, however, that the proportion of overtopping waves is very small. In this chart only tests with at least one overtopping event are presented. With about 1000 waves per test this gives a minimum proportion of about 0.001. Test conditions with no recorded overtopping waves might have given some events – and thus proportions larger than zero and smaller than 0.001 – if they had been run for (far) more than 1000 waves. For wave conditions with such low overtopping reliable measurements are difficult and results depend strongly on the definition of individual events.

7.4 Summary and Discussion

In this chapter an existing and a new tool to predict the proportion of overtopping waves (impacting conditions) have been validated against the data from the reference condition (0° obliquity) and extended to angled wave attack (15° and 30° obliquity). The recommended formulae will be summarised in chapter 9.The proportion of overtopping waves is needed for the prediction of individual overtopping volumes. The minimum overtopping volume to mark an "event" has been given by the sensitivity of the overtopping event detector as described in section 3.4.

The existing prediction tool for perpendicular wave attack by the EA manual (1999) gave good results although the level of scatter was high. In order to reduce the scatter a new approach has been introduced, which does not take account of the wave period. This seemed to help reduce the amount of scatter.

The extension of both methods to angles of wave attack of 15° and 30°, however, showed that both approaches gave a similar and acceptable amount of scatter and were both equally suitable. At 60° obliquity, both methods failed and the EA manual's (1999) approach for reflecting waves was presented. Unfortunately, the proportion of overtopping waves was under predicted by up to several orders of magnitude. The actual number of overtopping events, both predicted and measured, for most wave conditions in this study at 60° obliquity, however, were either "one" or "zero" and thus too low to be plotted on a chart.

8 INDIVIDUAL OVERTOPPING DISCHARGE

8.1 Introduction

One of the main objectives of this thesis is the validation of prediction tools for maximum individual overtopping discharge under perpendicular wave attack (reference case) and their modification and extension to angled wave attack. It has been suggested in literature that hazards due to wave overtopping at seawalls are closely linked to individual overtopping discharges (section 2.5). The prediction of the mean overtopping discharge as discussed in chapter 6, however, gives no information on the individual discharges per wave, which differ substantially from the mean.

This chapter now discusses and validates the available prediction tool for individual and maximum discharges for perpendicular and violent wave attack by the EA manual (1999) and extends it to angled wave attack. The presentation and discussion of actual design tools is deferred to chapter 9.

In the first section (8.2) the reference case (0° obliquity) is discussed. As a first step the method to predict individual and maximum discharges after the EA manual (1999) is discussed and validated against measured data. In the subsequent sub-sections the influence of individual input parameters on this model are discussed (sub-sections 8.2.2 – 8.2.4). Finally, in sub-section 8.2.5, other measures for individual overtopping discharges are presented and discussed.

In the last section (8.3) the EA manual's (1999) method is extended to angled wave attack, i.e. 15° and 30° obliquity. At 60° obliquity waves are no longer in impacting mode and recommendations on the use of the EA manual's (1999) formulae for reflecting conditions are given.

8.2 Reference Configuration

8.2.1 Prediction of V_{max} after the EA manual (1999)

The EA manual (1999) presents a method to predict the maximum expected overtopping volume for a vertical seawall under perpendicular wave attack (see section 2.4). This requires the total number of overtopping events during the duration of a storm surge and the mean discharge rate. He found that individual overtopping volumes follow a two parameter Weibull probability distribution:

$$P(V_i < V) = 1 - \exp(-(V/a)^b) \tag{70}$$

where $P(V_i < V)$ is the probability of an overtopping event V_i being smaller than a given Volume V, a is the scale parameter, which can be calculated from Q and N_{ow}, and b is the shape parameter.

Re-arranging equation (70) leads to an expression giving the volume V for a certain exceedance probability $(1 - P_v)$:

$$V = a\,[-\ln(1 - P_v)]^{1/b} \tag{71}$$

where $(1 - P_v)$ is the probability of an overtopping event V_i being larger than or equal to a Volume V. Figure 72 shows an example plot for a test run (VO0030a). The a and b parameters were set to $a = 0.92\ V_{bar}$ and $b = 0.85$, respectively (see chapter 2).

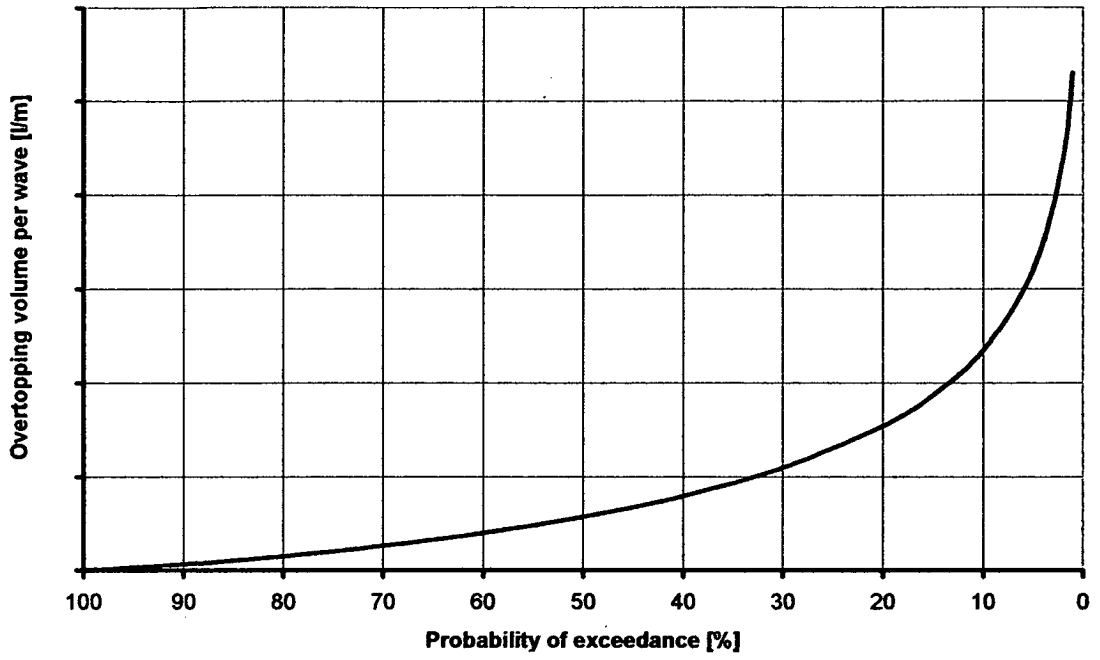

Figure 72: Example of a probability distribution function for overtopping volumes per wave (VO0030a, position 3)

The maximum expected overtopping volume in a sequence of N_{ow} overtopping waves can then be determined by:

$$V_{\max} = a(\ln(N_{ow}))^{1/b} \tag{72}$$

For waves in impacting mode the EA manual (1999) defines a and b:

$$a = 0.92\ V_{bar} \quad \text{and} \quad b = 0.85 \tag{73}$$

where V_{bar} can be determined from:

$$V_{bar} = QT_m N_w / N_{ow} \tag{74}$$

where Q is the mean overtopping rate, T_m is the mean wave period, and N_w is the number of waves and N_{ow} the number of overtopping waves during a storm.

Figure 73 shows the result of this prediction method for the measurements taken for the reference configuration (perpendicular wave attack). The ratio of measured to predicted maximum overtopping events has been plotted against the relative wave height H_{si}/h_i separating reflecting from impacting conditions (see chapters 5 and 6). As can be seen the

prediction gives good results for impacting conditions with all tests within a factor of less than 3 above and below the "1.00-line". For impulsive tests towards lower relative wave heights ($0.45 < H_{si}/h_i < 0.65$) the results tend to be under predicted by a factor of about 1.5 – 2.5. Tests in reflecting mode have generally been over predicted by factors between 5 and 50.

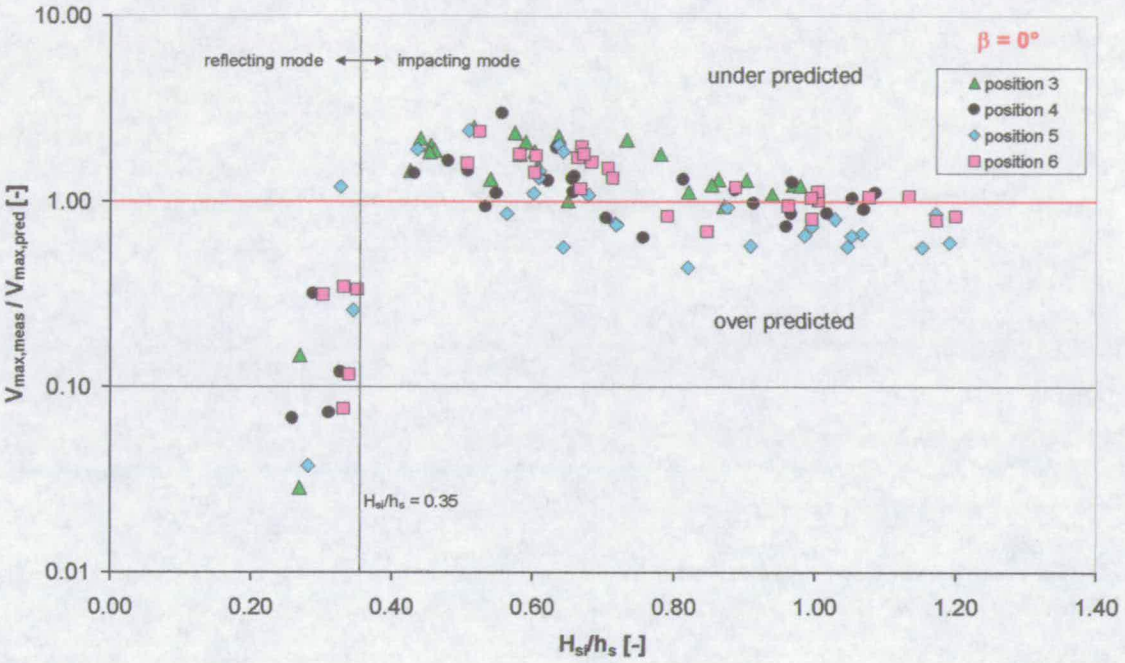

Figure 73: V_{max} measured vs. predicted (EA manual, 1999) against the relative wave height H_{si}/h_i

It is important to note that the scatter in Figure 73 is of about the same magnitude as the scatter in Figure 49 (see section 6.2), where the results for mean discharge (Q_{meas} / Q_{pred}) are presented. As can be seen from equations (72) to (74) the maximum individual overtopping event V_{max} is proportional to the mean discharge rate Q. Thus, for V_{max} a lower amount of scatter as for Q cannot be expected.

Figure 74 shows the same ratio of measured to predicted V_{max} this time against the h* parameter. As can be seen h* is not as successful in separating reflecting from impacting waves as H_{si}/h_i (see chapters 5 and 6).

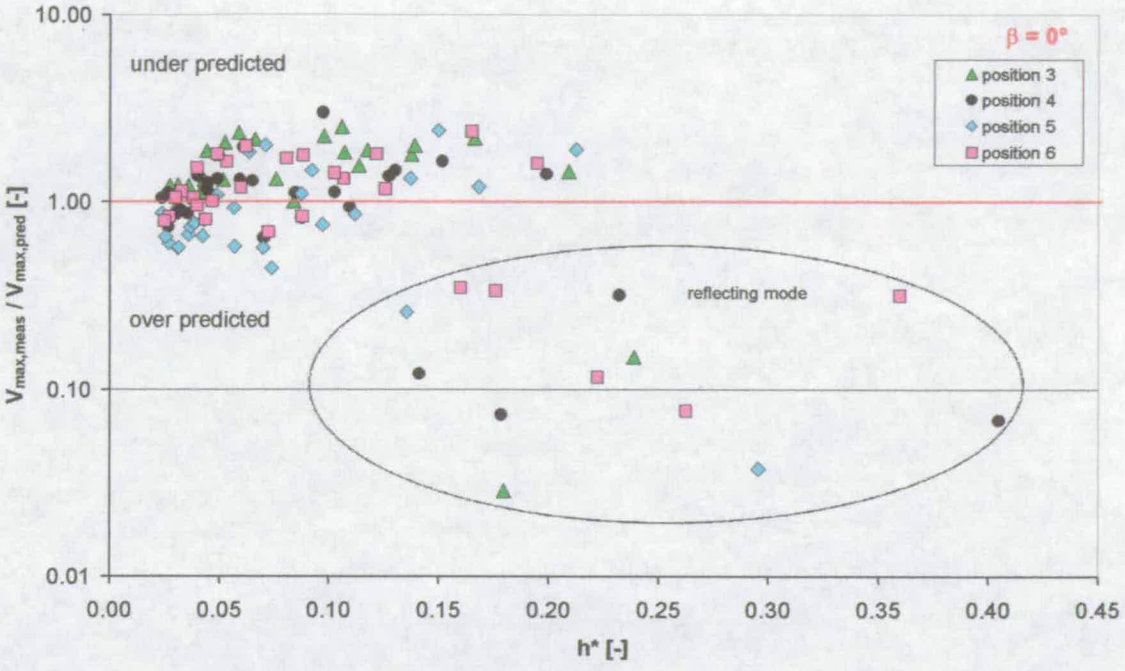

Figure 74: V_{max} measured vs. predicted (EA manual, 1999) against h*

The design guidance after the EA manual (1999) gives a robust prediction for maximum individual overtopping events and the scatter involved is not significantly larger than for the prediction of the mean discharge Q.

8.2.2 Variation of Weibull "a" and "b" parameters

Although a lower scatter in V_{max} seems unlikely to be achieved (the scatter of V_{max} is similar to the scatter in Q, see sub-section 8.2.1) a closer look at the derivation of the formula for V_{max} and the underlying Weibull distribution will be taken. Figure 75 shows a typical example of individual overtopping events V_i on a Weibull plot. On the y-axis the term "ln(-ln(1-P(V_i<V)))" represents the probability of an individual event where P(V_i<V) is the actual probability that V_i is lower than a given volume V. The x-axis gives a measure of the relative individual overtopping volume ln(V_i/V_{bar}). V_{bar} is the mean individual overtopping volume. The upper part of the Weibull distribution is nearly a straight line and a relationship between individual overtopping volumes and their probability of occurrence can be established.

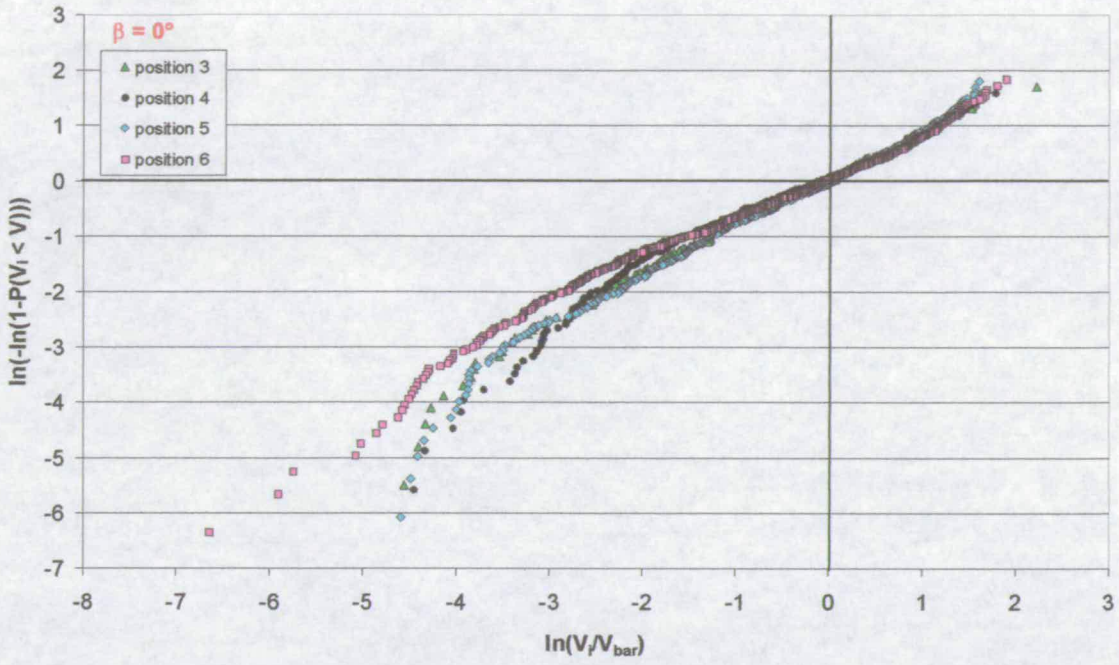

Figure 75: Weibull distribution of individual overtopping events (test: VO0030a)

Figure 76 shows a section of the same plot as Figure 75. This time only positive x- and y-values are displayed. As can be seen all 4 measurement stations follow the same trend line. The trend line can be represented by slope "m" and offset "n". It can be shown that the "a" and "b" parameters in equation (72) can be determined straight from this plot (Figure 76):

$$a = V_{bar} \exp(-\frac{n}{m}) \quad \text{and} \quad b = m \tag{75}$$

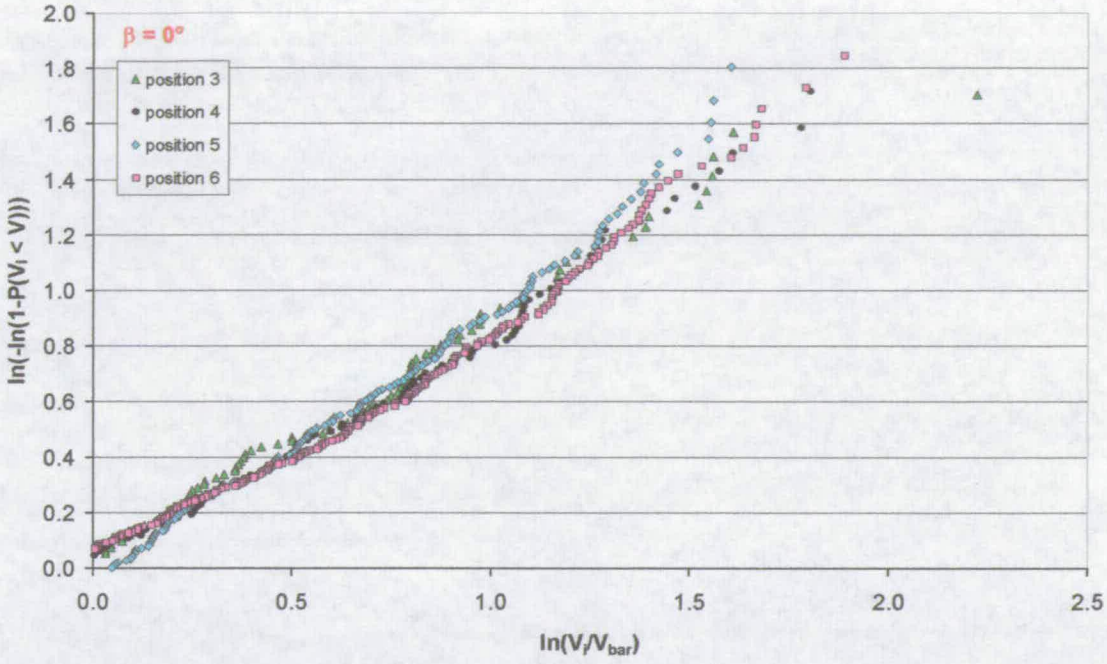

Figure 76: Upper part of Weibull distribution of individual overtopping events (test: VO0030a)

Figure 77 and Figure 78 present the results of the Weibull analysis of the reference configuration. In Figure 77 "a/V_{bar}" has been plotted against the h* parameter. The "a" parameter has been divided by V_{bar} in order to remove the influence of the mean individual overtopping volume. "a/V_{bar}" seems to be slightly dependent on h* and a linear trend has been added. While the linear trend is certainly questionable, it is still an improvement as compared to a simple mean value. It will be shown later that this improvement is rather insignificant and a mean value leads to a similar quality of prediction. The actual mean value of $a/V_{bar} = 1.0$ lies very close to the EA manual's (1999) recommendation of $a/V_{bar} = 0.92$.

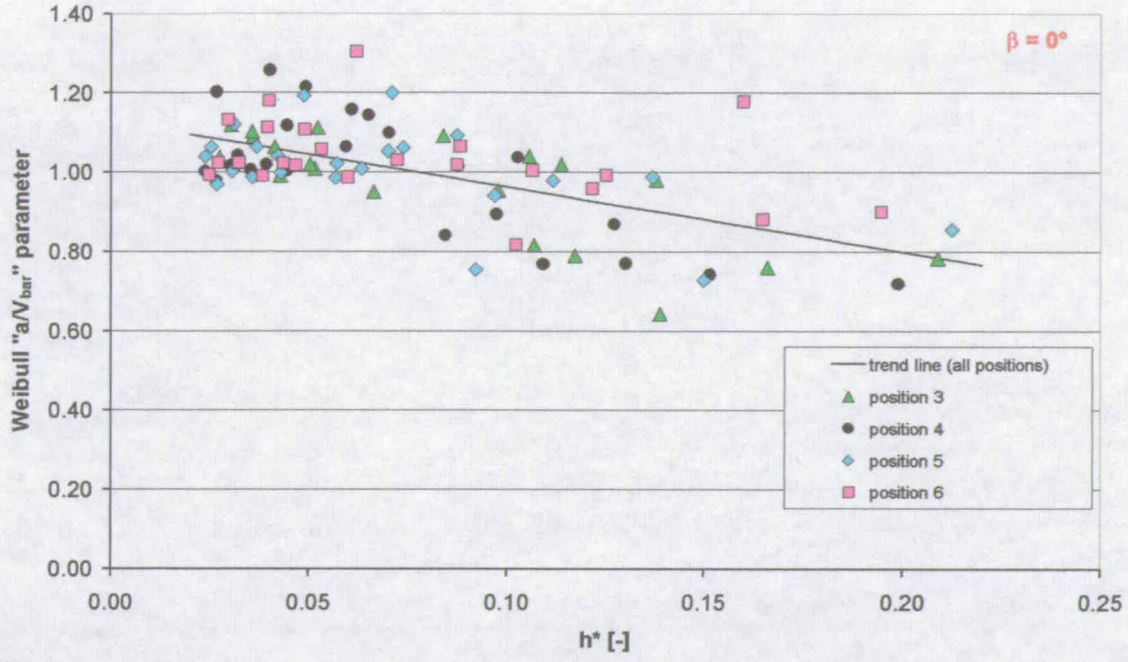

Figure 77: Weibull "a/V_{bar}" parameter

The "b" parameter also shows a dependency on h* which is slightly stronger (Figure 78). This time a power law trend has been added. As for "a/V_{bar}" the actual mean value of the "b" parameter with b = 0.96 lies very close to the EA manual's (1999) recommendation of b = 0.85.

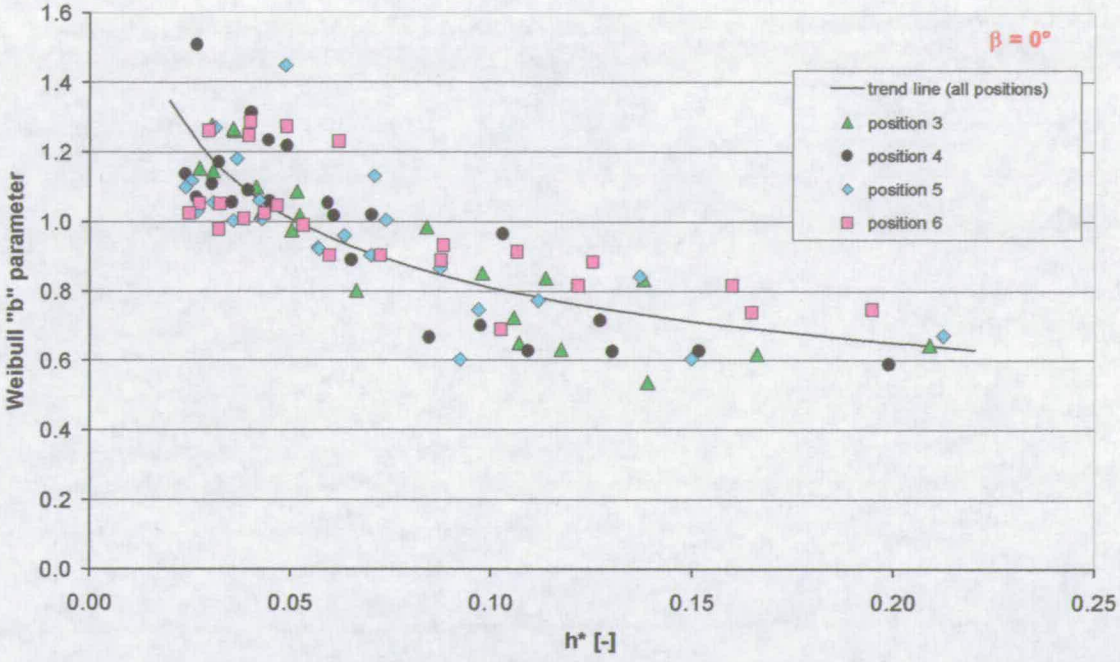

Figure 78: Weibull "b" parameter

A prediction of V_{max} based on the newly derived "a" and "b" parameters is presented in Figure 79. It shows again the ratio of measured to predicted V_{max}. Apart form the "a" and "b" parameters all other input parameters such as Q and N_{ow} are still predicted after the EA manual (1999).

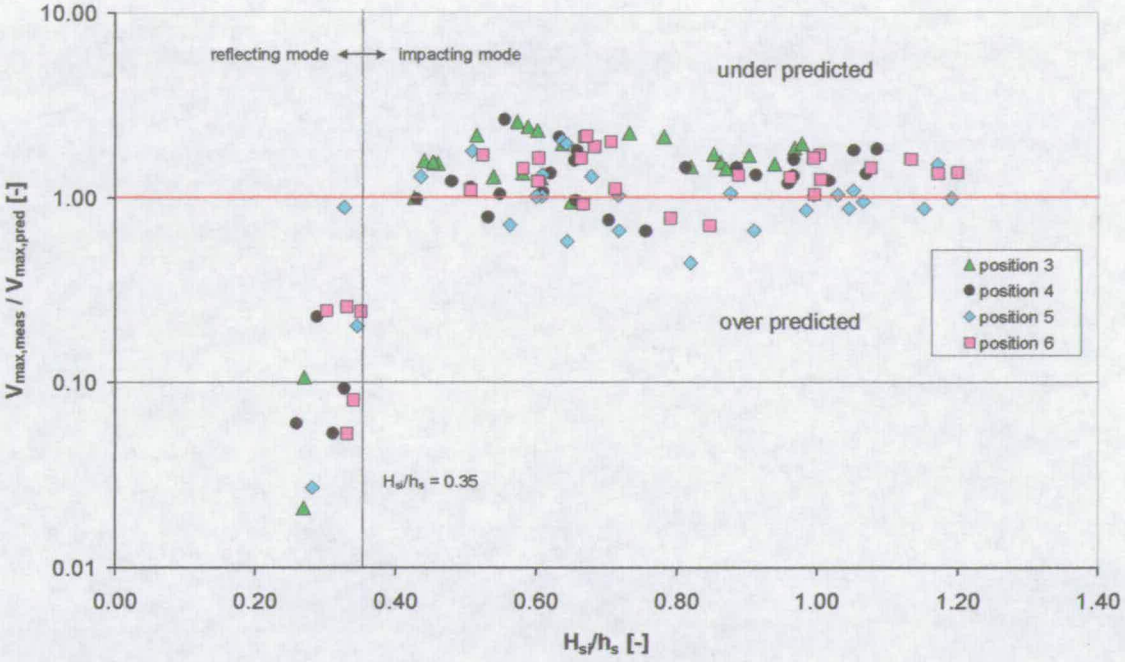

Figure 79: V_{max} measured vs. predicted after the EA manual (1999) with "a" and "b" derived from measurements

Although the "a" and "b" parameters are now more accurate the scatter of V_{max} has not been reduced significantly. This is due to the inherent scatter in Q which is at about the same level. The mean value of $V_{max,meas}/V_{max,pred}$ with about 1.25 is slightly higher than the ideal "1.0-line". All tests lie within a factor of 2.5 above and below the "1.0-line". For future design the use of the "a" and "b" parameters after the EA manual's (1999) guidelines are recommended (see chapter 9), because the quality of the predictions are similar and they have been derived as best fit values over a large dataset.

8.2.3 Influence of Choice of Predictor for N_{ow} upon prediction of V_{max}

The prediction of V_{max} after equation (72) requires the mean discharge Q, the number of overtopping waves N_{ow}, and the "a" and "b" parameters. The prediction of Q has been discussed in chapter 6 and the influence of the "a" and "b" parameters in the previous sub-section. In chapter 7 an alternative method to predict the number of overtopping waves has been presented. In this sub-section the influence of this new method on the prediction of V_{max} will be discussed briefly.

Figure 80 shows the prediction of V_{max} based on equation (72), but N_{ow} has now been established after the new method as discussed in chapter 7. The "a" and "b" parameters have been predicted after the slightly more accurate method as described in the previous sub-section, i.e. they have been established as functions of h*. The result, however, is very similar to the methods presented above which use the EA manual's (1999) predictor for N_{ow}: the mean value of $V_{max,meas}/V_{max,pred}$ is again about 1.25 and thus slightly higher than the ideal "1.0-line". The scatter, too, is still within a factor of 2.5 above and below the "1.0-line".

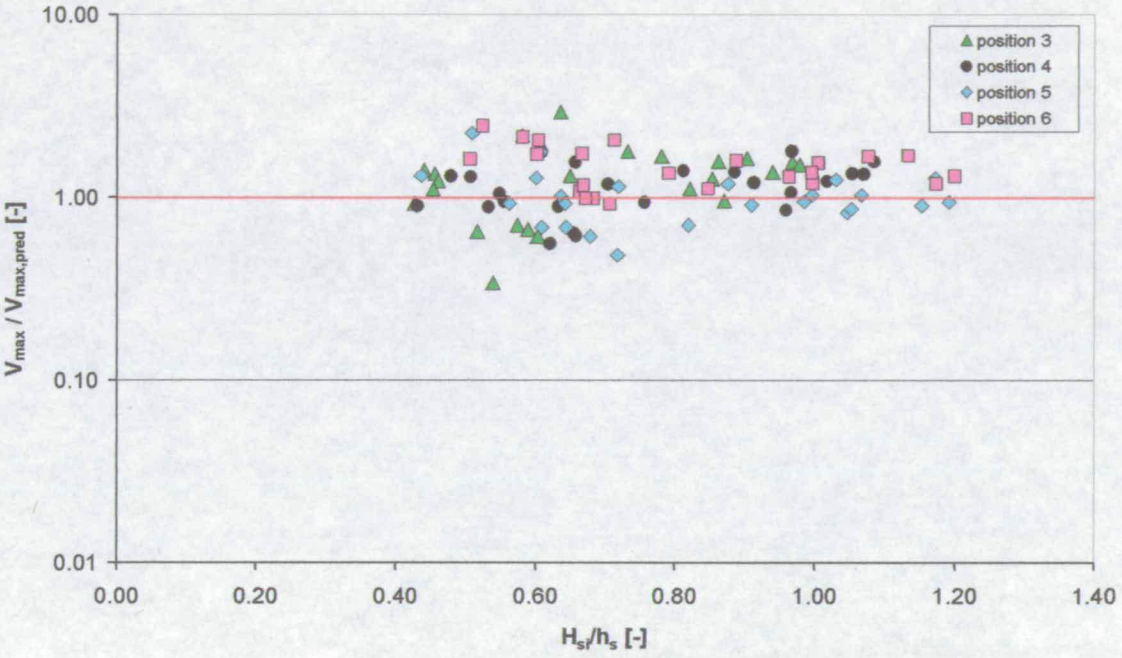

Figure 80: V_{max} measured vs. predicted with "a", "b", and N_{ow} derived from measurements

This shows that the new predictor for N_{ow} as described in chapter 7 does not yield better results for V_{max} and, hence, its use is not recommended.

8.2.4 Influence of the number of waves on predicted V_{max}

Equation (72) states that V_{max} increases with the number of overtopping waves N_{ow}, which for a given proportion of overtopping waves is a function of the duration of the storm surge or the number of incoming waves N_w. The previous sub-sections have only looked at predictions and measurements of 1000 waves. Real storm surges along the coast line of the

North Sea, however, – though limited by the tidal cycle – may give up to 2000 or 3000 waves. Thus, extrapolation may become necessary.

This raises two questions: how do the different variations of the prediction method for V_{max} as discussed in the previous sub-sections compare when extrapolating and what is the general uncertainty and influence of the "a" and "b" parameters, which were derived at 1000 waves. In this sub-section example calculations are presented in order to explore the uncertainties which are to be expected when extrapolating to up to 3000 waves.

Given the nature of equation (72) V_{max} depends on the mean discharge Q, the proportion of overtopping waves N_{ow}/N_w and the "a" and "b" parameters. In the previous sub-sections different approaches to predict N_{ow}/N_w and the "a" and "b" parameters have been discussed, while the mean discharge Q has been accepted as discussed in chapter 6.

Figure 81 shows an example calculation for a typical test run comparing the results for the three variations presented above as a function of the number of waves: (1) the prediction based completely on the EA manual (1999), (2) the "a" and "b" parameters as functions of the h* parameter, but N_{ow} still predicted after the EA manual (1999), and (3) the "a" and "b" parameters as functions of the h* parameter and the new approach for N_{ow}.

Figure 81 presents the result of one example test, which is meant to show the typical differences between the individual methods. The results of the calculations for the three different approaches have been divided by the results after the EA manual (1999). Thus, the EA manual's (1999) results are "1.0" for all numbers of incoming waves N_w.

Figure 81 cannot show which methods works best. Depending on the actual sea state the different approaches may give higher or lower predictions than the others. For example, for a different sea state the EA manual's (1999) approach may give the worst and not the best result. As has been said before the overall good fit of the variations and their scatter is very similar (see Figure 73, Figure 79, and Figure 80). Figure 81 is only meant to quantify typical differences between these variations and how they extrapolate towards higher numbers of waves.

Generally, it has been found that the highest and lowest results of the three approaches at 3000 waves differ by less than a factor of two. Typically the difference lies between a factor of about 1.3 – 1.5. Thus, there is no one best approach and the easiest and most universal one is recommended, which is the one presented by the EA manual (1999).

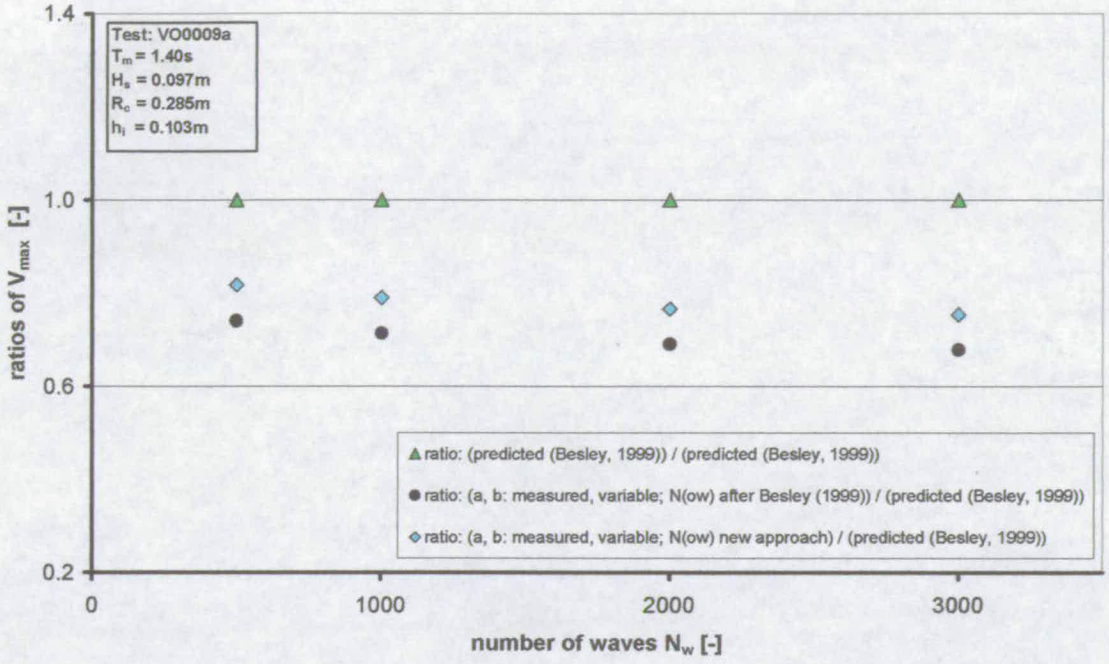

Figure 81: Example calculation for all three different approaches for V_{max}

The second of the two issues mentioned above is the uncertainty or variability of the "a" and "b" parameters which were derived at 1000 waves. It must be expected that sampling 2000 – 3000 waves will result in slightly different parameters. In order to explore the variability of these parameters as a function of the number of waves each test has been broken down into subsections of 2×500, 4×250, and 8×125 waves.

The underlying assumption is that the scatter obtained by breaking 1000 waves down into these subsections is similar to the scatter obtained by breaking down samples of e.g. 2000 waves into subsections of 2×1000, 4×500 and 8×250 waves. This should then give an indication of the variability of these parameters when extrapolating towards higher number of waves.

In this analysis only tests with at least 10 overtopping waves per subsection have been considered. This leaves a minimum of about 5 data points for the actual Weibull analysis. At lower numbers the scatter increases dramatically and the result becomes meaningless. Figure 82 and Figure 83 show the results for a typical test run.

In Figure 82 the "a" parameter of a typical test run has been presented as a normalised Weibull parameter (a_x/a_{1000}) by dividing "a" as derived for a subsection of x waves by the

result for the full test run of 1000 waves. As can be seen for subsections of down to 250 waves the scatter remains small, i.e. within ± 10%.

Figure 82: Normalised Weibull parameter "a" as function of number of waves

The same has been done for the "b" parameter, which has been normalised by dividing "b" as derived for a subsection of x waves by the result for the full test run of 1000 waves (Figure 83). Here, too, the scatter remains small, i.e. within ± 10%, for subsections of down to 250 waves.

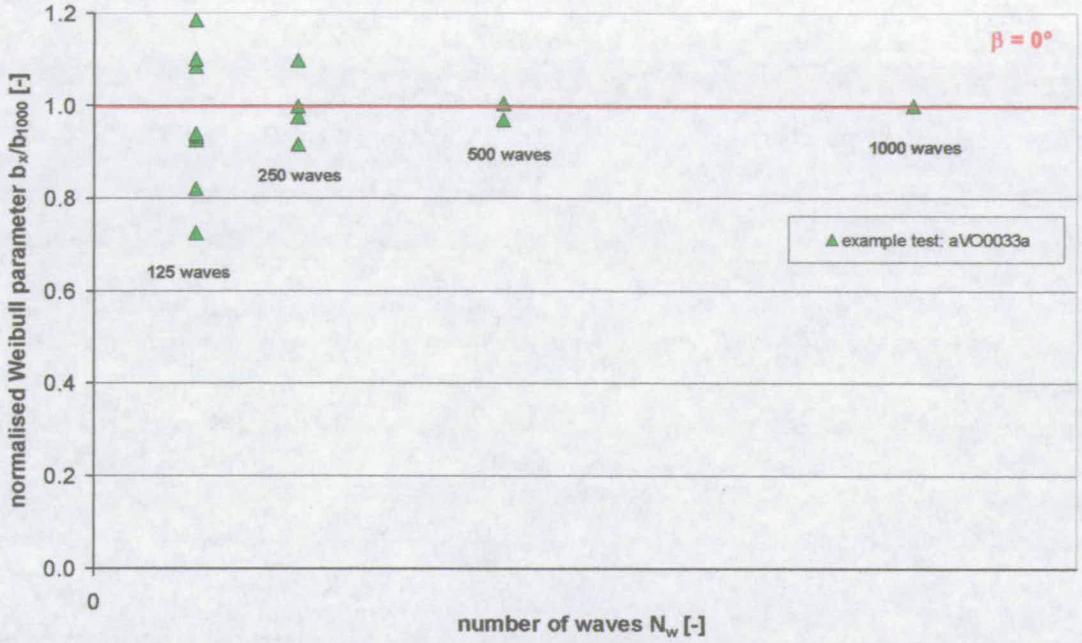

Figure 83: Normalised Weibull parameter "b" as function of number of waves

All pairs of "a" and "b" parameters as presented in Figure 82 and Figure 83 have been used to predict maximum overtopping discharges $V_{max,i}$, where the index "i" indicates the number of waves in the particular subsection in which the parameters have been derived (i.e. 125, 250, 500, or 1000). In order to make the volumes comparable among each other all predictions have been based on 1000 waves. For the example case in Figure 84 these values for $V_{max,i}$ have been normalised by dividing them by $V_{max,1000}$, which is the maximum predicted volume with "a" and "b" parameters derived at the full test run of 1000 waves.

Typically, the predictions with parameters derived in subsections of 500 and 250 waves remain close to the 1000-wave-case, i.e. about a factor of 1.2 above and below the "1.0-line". At subsections with 125 waves the scatter increases slightly to factors of up to 1.6.

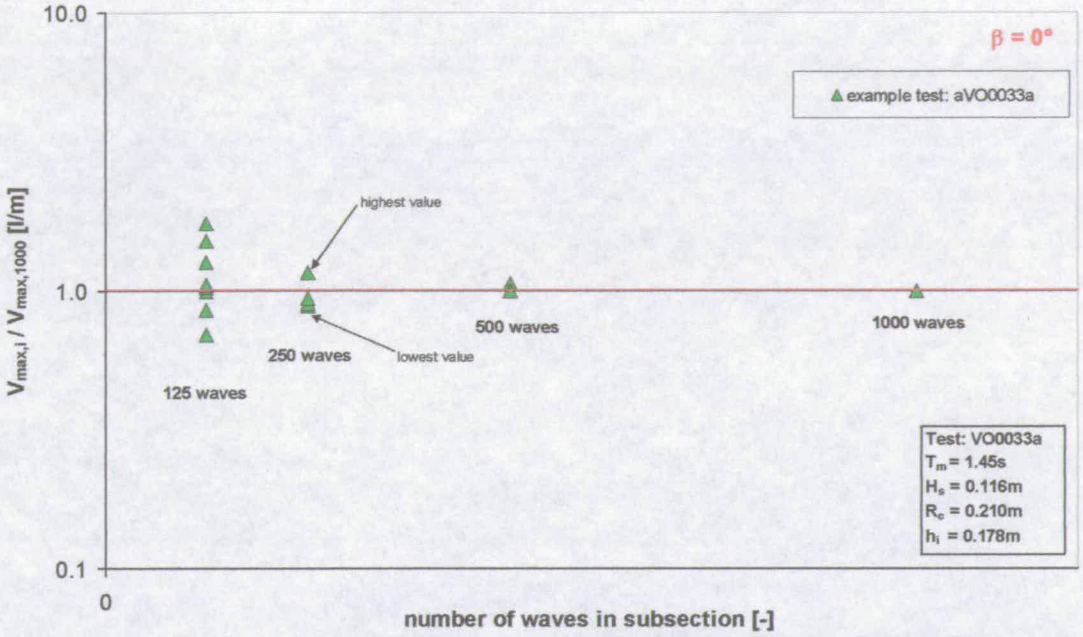

Figure 84: ratios of predicted $V_{max,i}$ / $V_{max,1000}$ at 1000 waves with "a" and "b" Weibull parameters derived at different samples

As mentioned above "a" and "b" derived at 1000 waves are not "exact" values but also subject to some variability. However, as breaking down 1000 waves into 2×500 and 4×250 waves only yields a small amount of scatter, it will be assumed that the values at 2000 and 3000 waves are very similar to the values at 1000 waves.

In order to get an indication of this variability and its effect on extrapolating towards higher numbers of waves a "worst case" analysis has been performed. On the basis of 250 waves the pair of "a" and "b" parameters has been chosen which give the highest and lowest predictions at 1000 waves. These cases have been highlighted in Figure 84. The corresponding "a" and "b" values have then been used to predict V_{max} at 500, 1000, 2000, and 3000 waves. Figure 85 and Figure 86 compare these results for the example test run to predictions made based on "a" and "b" derived at 1000 waves.

250 waves have been chosen as a basis for this comparison, because the duration of real storm surges is limited by the tidal cycle and extrapolations will only be made to 2000 perhaps 3000 waves. Thus, breaking down 1000 waves by a factor of four should be sufficient when extrapolations are only made to factors of up to 2-3. Additionally, the scatter for subsections of 125 waves or less becomes unreasonably large because the number of

overtopping events gets too low for many tests leaving too few data points for the Weibull analysis.

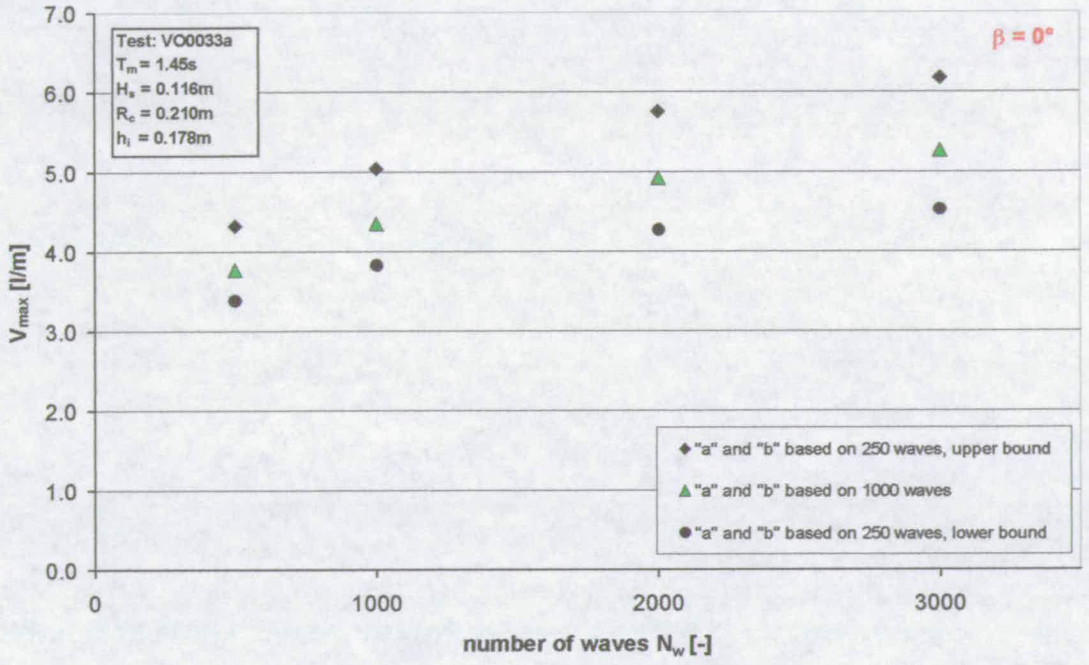

Figure 85: Example for scatter introduced by "a" and "b" parameters (absolute values)

As can be seen for the example test run in Figure 85 and Figure 86 the scatter remains fairly low. Even for extrapolations to 3000 waves the difference is typically less than 20%. In Figure 86 the indices "x" and "1000" as in $V_{max,x}/V_{max,1000}$ refer to how the "a" and "b" parameters were derived, i.e. at 250 and 1000 waves, respectively.

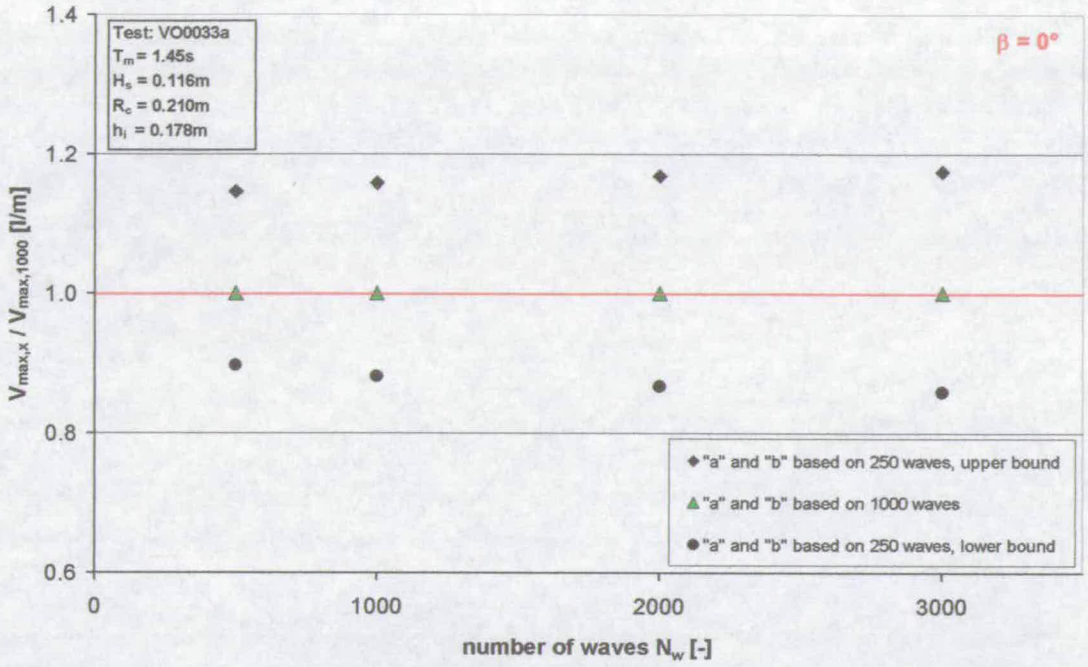

Figure 86: Example for scatter introduced by "a" and "b" parameters (relative values)

8.2.5 Other measures for individual overtopping discharges

The previous sub-sections focused on the prediction of the maximum discharge V_{max} as a representative for individual overtopping discharges. While this appears to be a very useful quantity when it comes to assessing hazards (see section 2.5) the term "V_{max}" might be misleading as it implies that no higher individual volumes must be expected. This, however, is not the case. "V_{max}" can be considered as the "most probable" highest volume, which can be exceeded during design conditions. Moreover, it is only one extreme value, which might be subject to an increased level of scatter. In this sub-section two other measures for individual overtopping discharges, $V_{x\%}$ and $V_{1/m}$, are discussed and validated against the measured data.

These two quantities, $V_{x\%}$ and $V_{1/m}$, can be determined directly from the two parameter Weibull probability distribution (see sections 2.4 and 8.2.1). $V_{x\%}$ is defined as the individual overtopping volume, which is exceeded by x% of all overtopping events; whereas $V_{1/m}$ is the mean volume of the highest 1/m overtopping events.

Re-arranging equation (43) leads to an expression for $V_{x\%}$:

$$V_{x\%} = a(-\ln(1 - P(V_{x\%})))^{1/b} \tag{76}$$

where $V_{x\%}$ is the individual overtopping volume, which is exceeded by x% of all overtopping events, a and b are the Weibull parameters and $P(V_{x\%})$ is the probability that any other overtopping volume is lower than $V_{x\%}$, and is in fact $P(V_{x\%}) = 1\text{-}x\%$, leading to:

$$V_{x\%} = a(-\ln(1 - x\%))^{1/b} \tag{77}$$

and thus, $V_{x\%}$ is completely independent of the duration of the storm.

Similarly, $V_{1/m}$ can be determined from equations (78) – (80):

$$V_i = a(\ln(N_{ow}) - \ln(i))^{1/b} \tag{78}$$

where V_i is the volume of the i^{th} highest overtopping event, a and b are again the Weibull parameters, N_{ow} is the number of overtopping events and i the position number of the i^{th} highest overtopping event.

Equation (78) can then be used to determine $V_{1/m}$:

$$V_{1/m} = \frac{1}{n}\sum_{i=1}^{n} V_i \tag{79}$$

where $V_{1/m}$ is the mean volume of the highest 1/m overtopping events and n is the actual number of the 1/m overtopping events, which is given by:

$$n = \frac{1}{m} N_{ow} \tag{80}$$

In order to verify both approaches against the measured data example calculations have been done for $V_{1\%}$, $V_{4\%}$, and $V_{10\%}$ and also for $V_{1/100}$, $V_{1/25}$, and $V_{1/10}$. As the quality of the results is very similar for the different percentages (i.e. 1%, 4%, and 10% on the one hand side and 1/100, 1/25, and 1/10 on the other) only $V_{1\%}$ and $V_{1/100}$ are presented here.

Figure 87 shows the result for $V_{1\%}$, where the ratio of measured to predicted $V_{1\%}$ is plotted against the relative wave height H_{si}/h_s. Only tests with at least 100 overtopping events could be used, thus the number of data points is reduced to about 70% as compared to the result of V_{max} in Figure 73. The scatter, however, is rather similar with all values being between a

factor of 2.3 up and down the "1.0" line. Very similar results were found for $V_{4\%}$, and $V_{10\%}$ with similar levels of scatter.

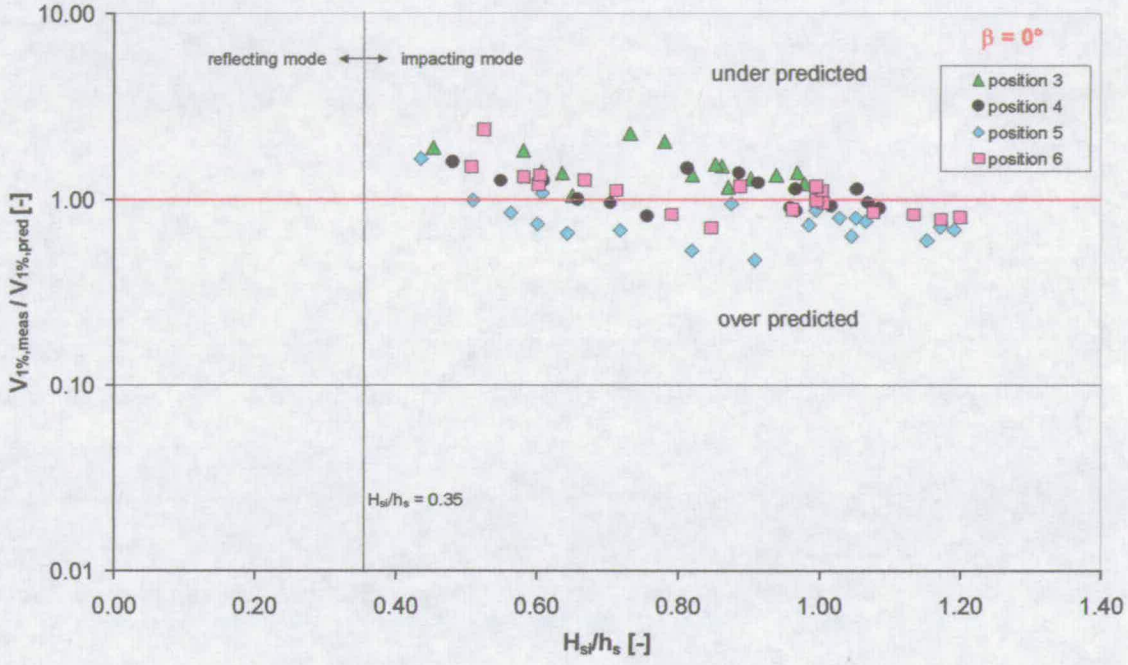

Figure 87: Ratio of measured to predicted $V_{1\%}$

In Figure 88 the ratio of measured to predicted $V_{1/100}$ has been plotted against the relative wave height H_{si}/h_s. Here, too, the number of data points is about 30% lower than for the V_{max} case, as only tests with 100 and more overtopping events could be used. The scatter is very similar to the cases of V_{max} and $V_{1\%}$ with extreme values of about a factor of 2.2 above and below the "1.0" line. The results for $V_{1/25}$ and $V_{1/10}$ were also very similar and are not presented here.

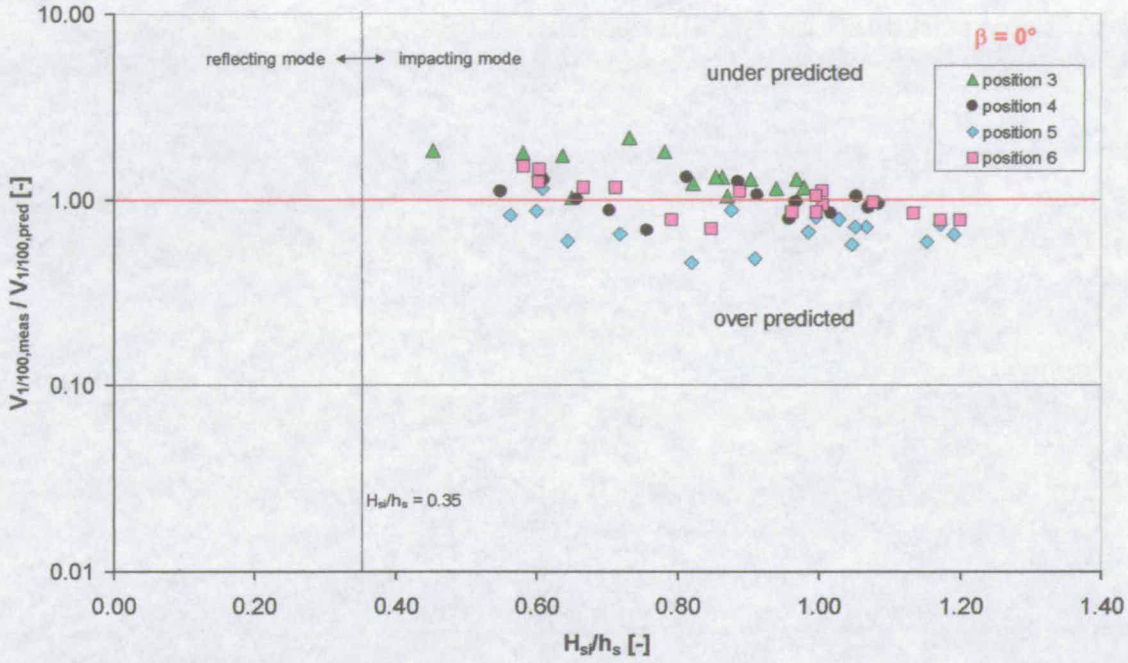

Figure 88: Ratio of measured to predicted $V_{1/100}$

In order to compare the sensitivity of each measure of individual discharges to the duration of the design conditions, i.e. the number of waves N_w, an example calculation is presented. In Figure 89 the absolute values for V_{max}, $V_{1/100}$, and $V_{1\%}$ ("V_y") have been determined for 500, 1000, 2000, and 3000 waves. As expected, V_{max} is the largest value and $V_{1\%}$ the lowest ($V_{max} > V_{1/100} > V_{1\%}$). Only at 500 waves V_{max} equals $V_{1/100}$, because the number of overtopping waves dropped to about 100. V_{max} is clearly the most sensitive measure to the duration of the design conditions, whereas $V_{x\%}$ is completely independent of the number of waves (see equation (77)).

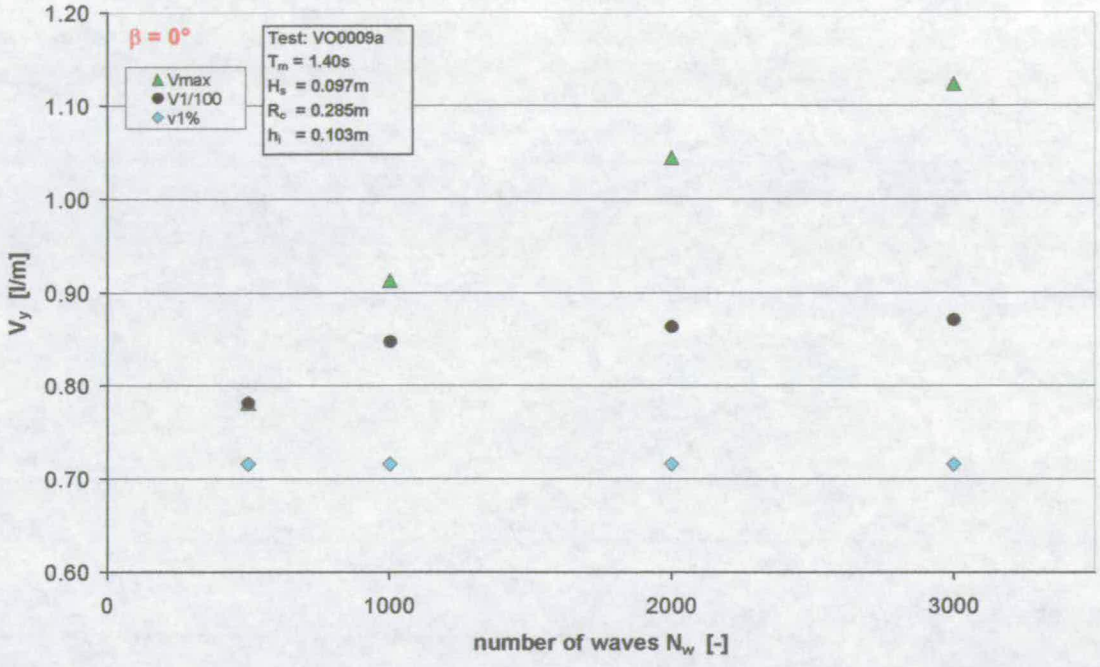

Figure 89: Example calculation for individual discharges (absolute values)

Figure 90 shows the same example, but with each value divided by the result at 1000 waves. While V_{max} increases by over 20% at 3000 waves, $V_{1/100}$ only goes up by less than 3%. $V_{1\%}$ does not change at all.

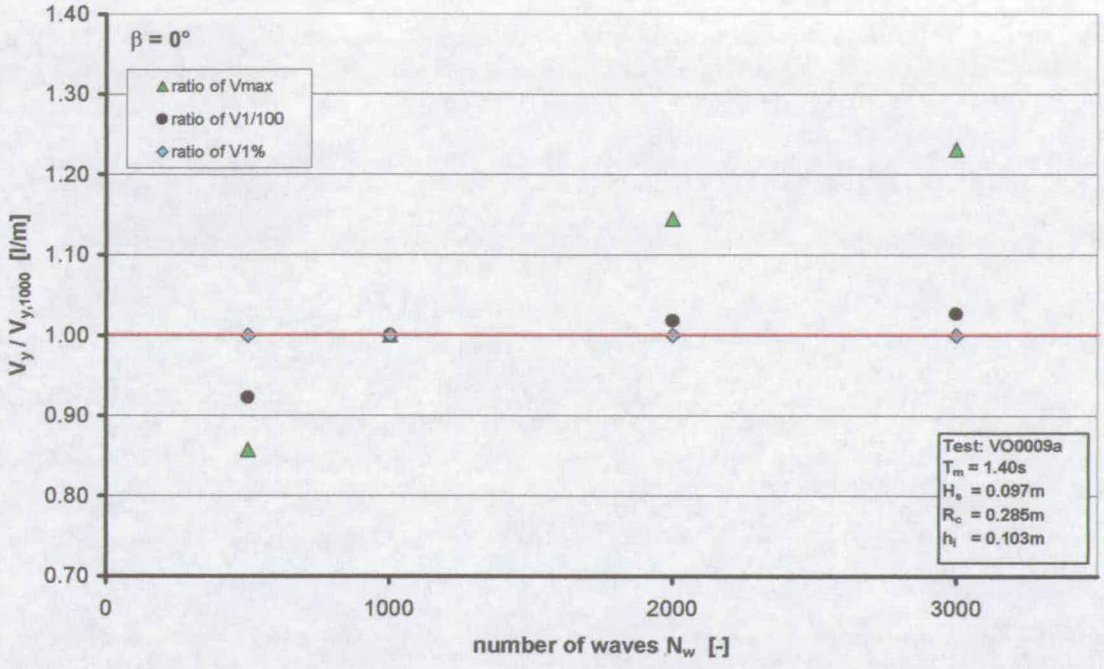

Figure 90: Example calculation for individual discharges (relative values)

In this sub-section two more measures for individual overtopping discharges, $V_{x\%}$ and $V_{1/m}$, have been presented. They were both derived from the Weibull distribution and could be validated against measured data, but showed no significant reduction in scatter. $V_{1/m}$ is much less sensitive towards the duration of the design conditions (i.e. the number of incoming waves) than V_{max}, and $V_{x\%}$ is completely independent (see equation (77)).

Assuming that hazards in wave overtopping are mostly linked to few extreme events, the higher sensitivity of V_{max} relative to the other measures appears to be an advantage. Furthermore V_{max} can be determined easily, whereas $V_{1/m}$ needs to be determined numerically (see equations (72) and (79)).

8.3 Oblique Configurations

8.3.1 Obliquity 15°

The analysis shows that individual overtopping discharges measured at 15° obliquity follow a Weibull distribution as well. The "a/V_{bar}" and "b" parameters appear to be slightly dependent on the structural and hydraulic parameters in a similar way as the reference case (see Figure 77 and Figure 78). The influence on the overall predictions of V_{max}, however,

could be shown to be very low (see also section 8.2). Thus, simple mean values for the "a/V_{bar}" and "b" parameters have been determined which do not significantly decrease the quality of the predictions. Only tests in impacting mode have been considered (chapter 5).

In order to obtain an impression of the quality a simple prediction of V_{max} at 15° obliquity using equation (72) is presented in Figure 91. The mean result for the mean overtopping discharge Q (chapter 6), hence ignoring any spatial effects, and the result for the proportion of overtopping waves (chapter 7) – both derived at 15° obliquity and based on the EA manual's (1999) approach – have been taken as input parameters.

Figure 91 shows the results plotted as the ratio of measured to predicted V_{max} against the relative freeboard H_{si}/h_s. The scatter for tests in impacting mode is slightly larger than for the reference case (Figure 73) with the worst values about a factor of 2.6 above and below the "1.0" line. There is, however, a certain degree of spatial variability with position 4 being on average over predicted and the other positions mostly under predicted. This is consistent with the findings for the mean discharge where position 4 gave noticeably less overtopping (section 6.3), and hence using the mean results for Q as input for V_{max} leads to over predictions at position 4.

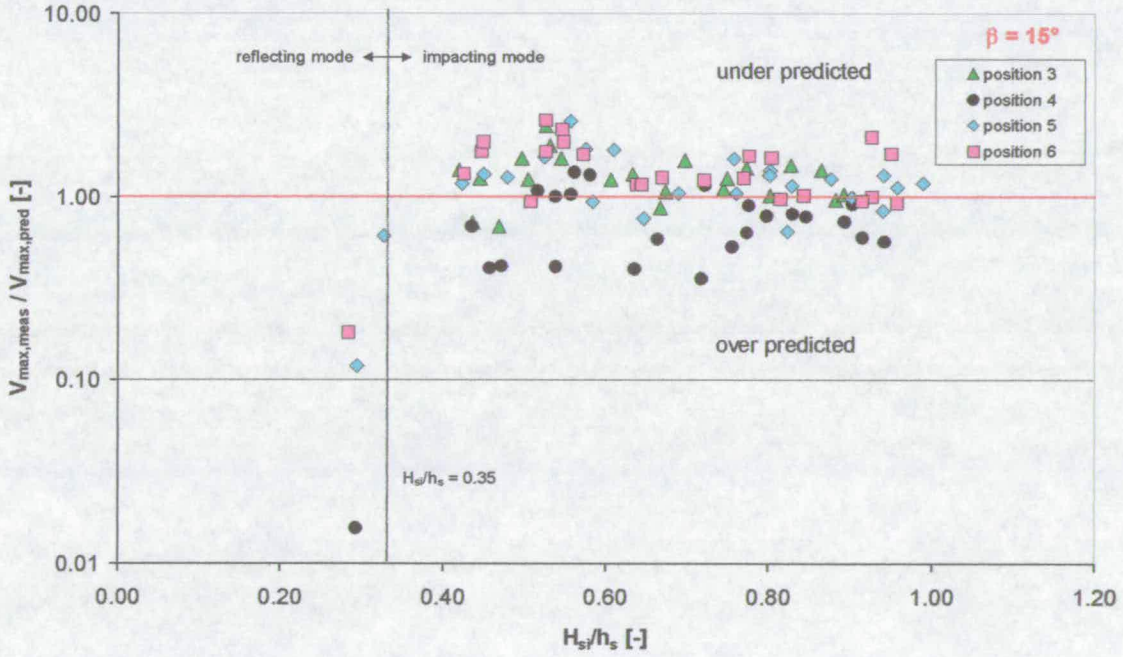

Figure 91: Prediction V_{max}; input derived at 15°, no consideration of spatial effects

Taking account of the spatial variability a new prediction of V_{max} has been made using the results of the mean discharge Q and the proportion of overtopping waves N_{ow}/N_w measured at individual positions for 15°. The Weibull parameters remain the same, i.e. the mean values for "a/V_{bar}" and "b" derived at 15° obliquity.

Figure 92 shows the results. Tests in impacting mode are now better predicted than in Figure 91 with the mean of all positions less than a factor of 1.2 above and below the "1.0" line. No significant spatial variations remain, thus the overall reduction in the scatter.

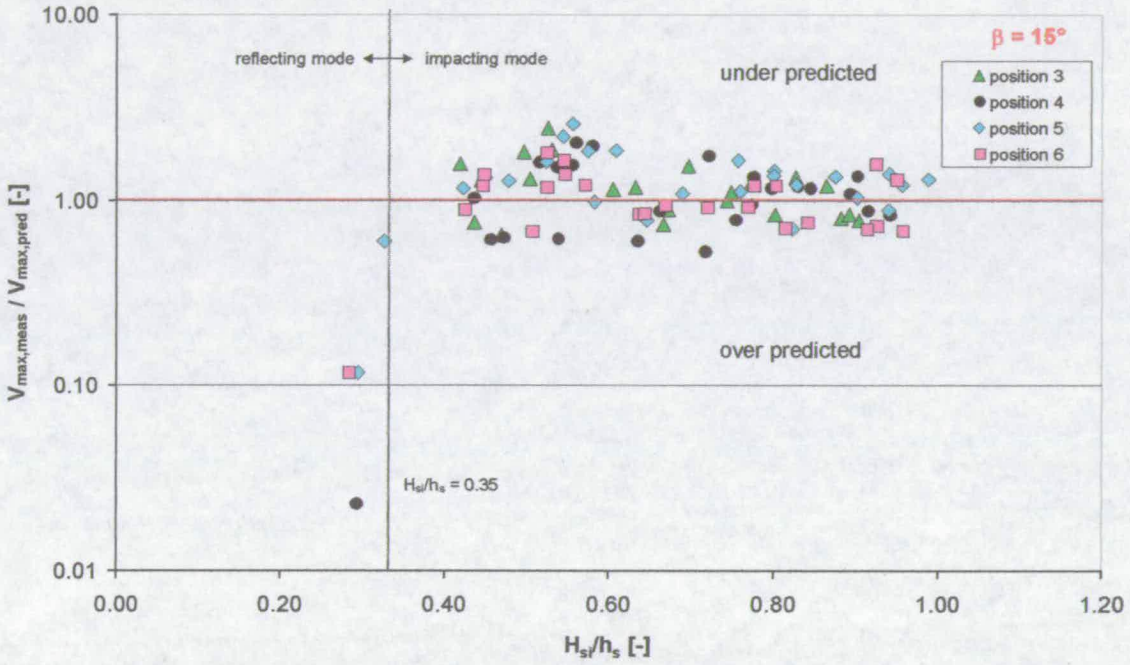

Figure 92: Prediction of V_{max}; N_{ow} and Q spatially distributed; a, b derived mean values from test

In practical applications, however, there are no tools available to determine the exact positions of spatial variations along the seawall. Thus, either the spatial variability must be neglected accepting the higher level of scatter as in Figure 91 or a worst case analysis can be done. Although the "worst case" analysis will result in a similar level of scatter it is mostly on the "safe side". This can be useful if the assessment of overtopping hazards is linked to the few highest expected individual events.

The highest individual overtopping discharges have been measured at position 6. This went along with the highest measurements in the mean discharge Q and proportion of

overtopping waves N_{ow}/N_w. Applying the derived trends for both quantities at position 6 to all other positions leads to a conservative design. Figure 93 shows the results. At position 6 the ratios of measured to predicted V_{max} have not changed with a mean value almost exactly on the "1.0" line. Positions 3 and 5 have now moved down slightly so that their mean is about a factor of 1.1 below the "1.0" line, i.e. in the safe zone. Only position 4, where the lowest discharges have been measured, is out by a factor of 2 down towards the safe zone.

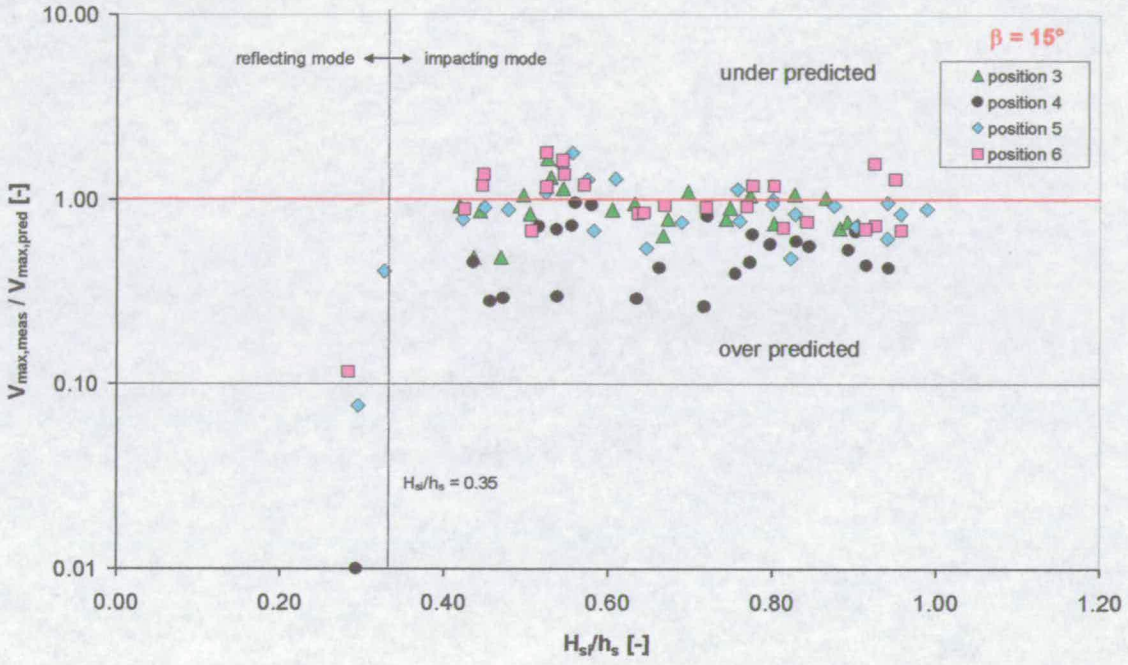

Figure 93: Prediction of V_{max}; N_{ow} and Q derived at position 6 (worst case)

In summary of this short sub-section the existing prediction tool for maximum individual overtopping events at vertical seawalls and impulsive wave attack for the 2D case has been extended to angled wave attack of 15°. It has been found that spatial variability has an effect on maximum discharges. While neglecting spatial effects gives good "mean" predictions of V_{max} along the seawall it leads to local under predictions with measured discharges up to 2.6 times higher than predicted ones. Thus, a conservative "worst case" approach is recommended using the highest measured discharges Q and proportion of overtopping events (for details see chapter 9). This reduces the worst ratio of measured to predicted discharges to about 1.8.

8.3.2 Obliquity 30°

The 30° obliquity case can be treated in the same way as the 15° case. Individual overtopping discharges of tests in impacting mode follow a Weibull distribution in a similar way as the 0° and 15° cases. The Weibull parameters "a/V_{bar}" and "b" seem to be weakly dependent on the structural and hydraulic parameters, but the effect on the prediction of V_{max} could be shown to be low (see also section 8.2). Thus, simple mean values have again been derived.

The 15° case has shown that spatial variability has an influence on the individual overtopping volumes. The same can be seen at 30° in Figure 94, where the ratio of measured to predicted V_{max} is plotted against the relative wave height H_{si}/h_s. The prediction used equation (72) and mean values for the mean overtopping Q (chapter 6) and for the proportion of overtopping waves N_{ow}/N_w (chapter 7) as input parameters. No overtopping has been measured for the small number of tests in reflecting mode.

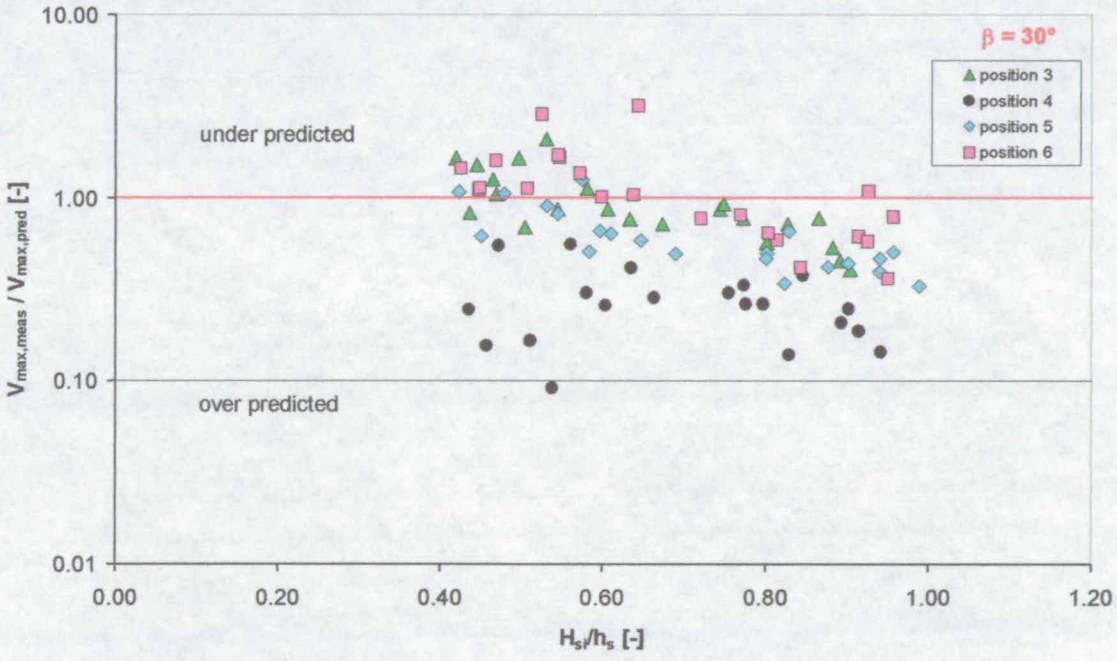

Figure 94: Prediction V_{max}; input derived at 30°, no consideration of spatial effects

The spatial effects can be seen clearly. Position 4, where the lowest mean and individual discharges have been measured (see also chapter 6), is over predicted by an average factor of

over 2.3. The other positions are better predicted but the overall scatter as well as the scatter for individual positions is larger than for the 15° case.

Another prediction has been made taking spatial variability into account. The mean discharge Q and the proportion of overtopping waves now reflect the spatial variability measured at 30° obliquity. The Weibull parameters "a/V_{bar}" and "b" remain the same.

Figure 95 presents the results as usual as the ratio of measured to predicted V_{max}. Although the scatter for each individual container has not been reduced, the mean of the predictions for each container is now within a factor of about 1.2 from the measurements.

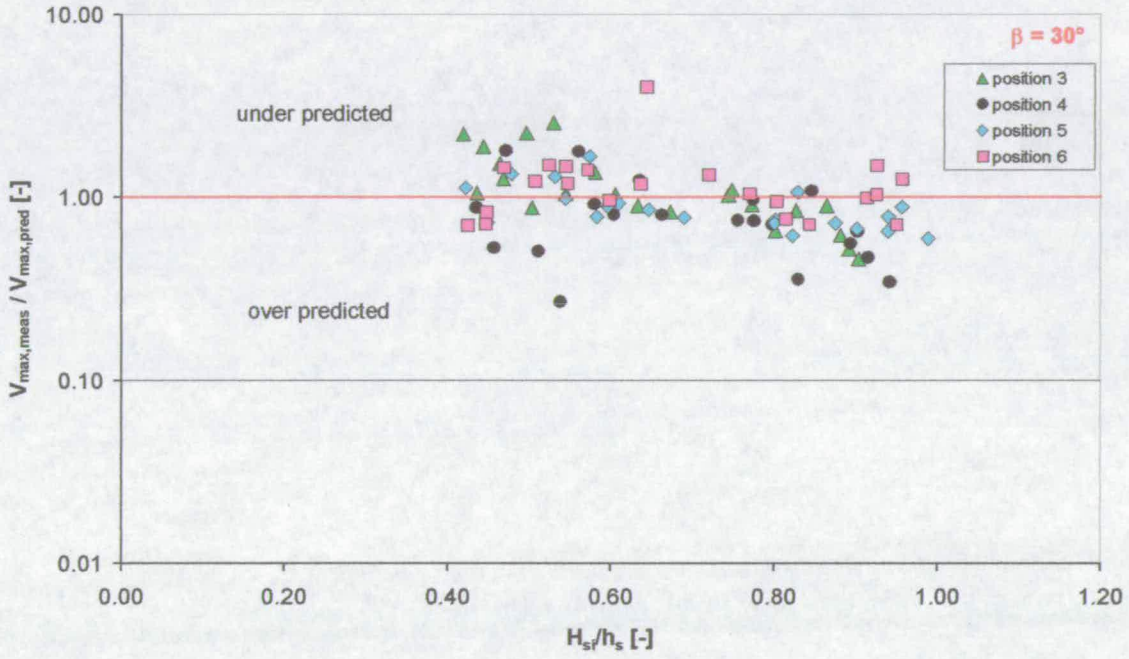

Figure 95: Prediction of V_{max}; N_{ow} and Q spatially distributed; a, b derived mean values from test

For practical applications, however, the spatial distribution of overtopping events is not known. Thus, as for the 15° case the spatial variability must either be neglected accepting the higher level of scatter as in Figure 94 or a "worst case" analysis can be performed. Although the "worst case" analysis will result in a similar level of scatter it is mostly on the "safe side".

The highest individual overtopping discharges have again been measured at position 6. This went along with the highest measurements in the mean discharge Q and proportion of

overtopping waves N_{ow}/N_w. Applying the derived trends for both quantities at position 6 to all other positions leads to a conservative design. Figure 96 shows the results. At position 6 the ratios of measured to predicted V_{max} have not changed with a mean value very close to the "1.0" line. Positions 3 and 5 have now moved down slightly so that their mean is about a factor of 1.1 below the "1.0" line, i.e. in the safe zone. Only position 4, where the lowest discharges have been measured, is out by a factor of 5 towards the safe zone.

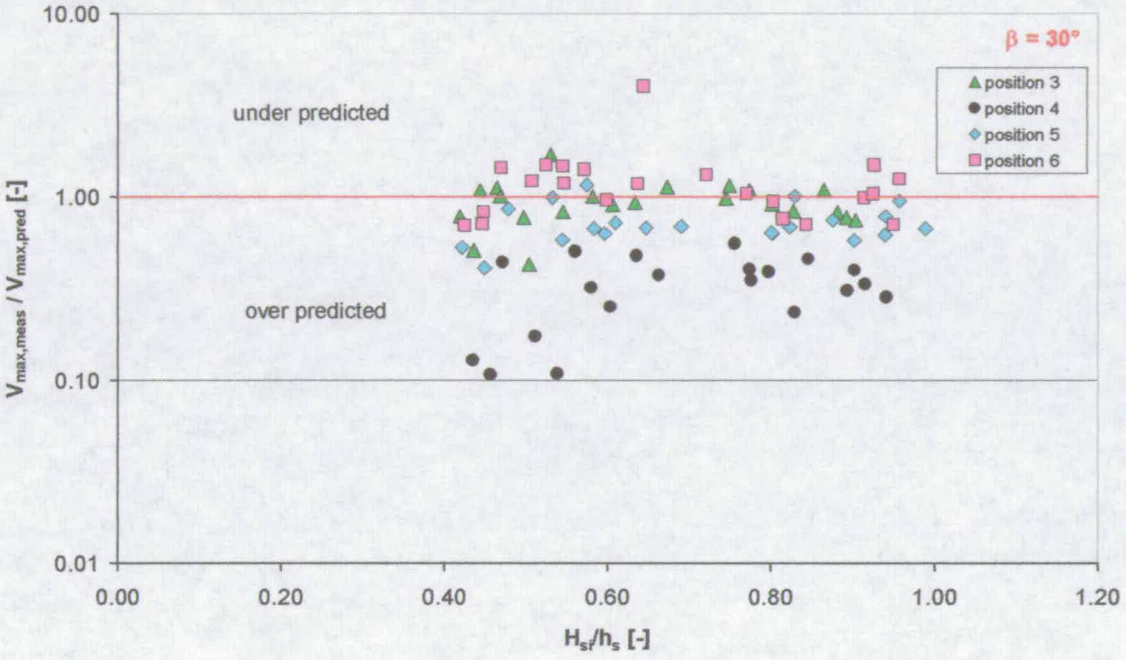

Figure 96: Prediction of V_{max}; N_{ow} and Q derived at position 6 (worst case)

In summary this short sub-section extended the existing prediction tool for maximum individual overtopping events at vertical sea-walls and perpendicular, impulsive wave attack to the 30° case. The findings are very similar to the 15° case and spatial variations along the seawall influence the maximum discharges. Neglecting these spatial effects gives still reasonably good "mean" predictions of V_{max} along the seawall but may lead to local under predictions with measured discharges up to 3 times higher than predicted ones. A conservative "worst case" approach is recommended using the highest measured discharges Q and proportion of overtopping events (for details see chapter 9).

8.3.3 Obliquity 60°

At 60° obliquity all tests were in reflecting mode and no wave impacts could be observed (see chapter 5). The EA manual (1999) offers prediction tools for both the proportion of overtopping waves and V_{max} for angled wave attack and reflecting waves (see chapter 2). The prediction of the proportion of overtopping waves, however, under estimates the measurements significantly, leading to actual number of overtopping waves of less than one. The calculation of individual overtopping volumes after the EA manual (1999), see equations (72) and (74), requires values of at least one or more.

In order to assure a conservative design the number of overtopping waves can be set to "one", which implies that the average individual overtopping volume equals the maximum individual volume ($V_{bar} = V_{max}$), thus all overtopping took place in one single event. This should lead to a conservative design as the mean overtopping discharge Q is reasonably well predicted (see chapter 6). Alternatively, the sea-wall can be designed for an angle of wave attack of 30°, which will give higher, and hence conservative, values.

8.4 Summary and Discussion

In this chapter the available prediction tool for individual and maximum overtopping discharges (V_i and V_{max}) for perpendicular wave attack (EA manual, 1999) has been validated and its input parameters have been discussed (section 8.2). Additionally, a discussion of the influence of the number of waves on maximum individual events was given and other measures of peak discharges were presented. Finally, the prediction method of maximum events was extended to angled wave attack (section 8.3).

As a first step the prediction tool for V_{max} (EA manual, 1999) could be validated (8.2.1). The scatter in the prediction of V_{max} was not significantly larger than for the prediction of the mean discharge Q – an input parameter, which feeds linearly into the formula for V_{max}. Additionally, as expected, no spatial variation could be observed at 0° obliquity.

The next three sub-sections (8.2.2 – 8.2.4) looked at the input parameters for V_{max}, which are the mean discharge Q, the Weibull "a" and "b" parameters, the proportion of overtopping waves, and the number of incoming waves (i.e. the storm duration). All other input parameters can be derived from these five. The mean discharge Q had already been discussed at length in chapter 6, thus, this sub-section focused on the other four.

Sub-section 8.2.2 took a closer look at the derivation of the formula for V_{max} and the underlying Weibull distribution. Simple prediction formulae for the "a" and "b" Weibull parameters were derived improving their accuracy to some extend. Yet, the scatter of V_{max} could not be reduced significantly. This is due to the inherent scatter in the other input parameters, e.g. in Q which is at about the same level. The mean value of $V_{max,meas}/V_{max,pred}$ (about 1.25) was slightly higher than the ideal "1.0-line". All tests lay within a factor of 2.5 above and below the "1.0-line". For future design the use of the "a" and "b" parameters after the EA manual's (1999) guidelines are recommended as the scatter involved is not significantly higher and thus the scope for improvement is very low. Additionally, they have been derived as best fit values on a large number of other data.

The next sub-section (8.2.3) dealt with the influence of the predictor for the proportion of overtopping waves on V_{max}. In section 7.2 a new predictor had been introduced. The new predictor and the old one (EA manual, 1999) were both used to predict V_{max} and the resulting level of scatter was compared. It could be shown that the new predictor yielded no better results and hence its use is not recommended. It should be mentioned that the proportion of overtopping waves goes into the formula for V_{max} twice (see equations (72) and (74)) both increasing and reducing V_{max}. Thus, its influence is somewhat reduced (a lower prediction of the proportion of overtopping waves will – counter intuitively – increase the prediction of V_{max}).

The last of the three input parameters of V_{max} discussed in this sub-section is the number of waves or the storm duration. This has been done in sub-section 8.2.4. It could be shown that for extrapolations from 1000 to 3000 incoming waves the different approaches of the input parameters for V_{max} gave predictions typically within factors of 1.3 – 1.5 of each other. This is important as it shows that no unreasonable errors are introduced when choosing one method or another. Thus, the easiest or most common method can be accepted, which is the one by the EA manual (1999).

The second issue addressed in this sub-section (8.2.4) is the uncertainty of the Weibull "a" and "b" parameters, which were derived at 1000 waves. A "worst case" analysis has been performed, in which the 1000 waves were broken down into subgroups of 500, 250, and 125 waves and the "a" and "b" parameters for each subgroup were determined. The underlying assumption was that the resulting scatter would be similar to the one obtained from breaking down storms of 2000 – 3000 waves into smaller subgroups. The pair of "a" and "b" parameters derived at 250 waves which gave the highest and lowest results for V_{max} were

chosen and it could be shown that for extrapolations to up to 3000 waves the uncertainty remained within less than 20% of the results for the "a" and "b" parameters derived at 1000 waves. Thus, the inherent uncertainties of the "a" and "b" parameters as a function of the duration of the storm are small as compared to the overall scatter.

In sub-section 8.2.5 two other measures for individual overtopping discharges, $V_{x\%}$ and $V_{1/m}$, have been presented. $V_{x\%}$ was defined as the individual overtopping volume, which is exceeded by x% of all overtopping events; whereas $V_{1/m}$ is the mean volume of the highest 1/m overtopping events. They were both derived from the Weibull distribution and could be validated against measured data, but showed no significant reduction in scatter. $V_{1/m}$ is much less sensitive to the duration of the design conditions (i.e. the number of incoming waves) than V_{max}. $V_{x\%}$ is completely independent of N_w. Assuming that hazards in wave overtopping are mostly linked to few extreme events, the higher sensitivity of V_{max} relative to the other measures appears to be an advantage. Furthermore V_{max} can be determined easily, whereas $V_{1/m}$ needs to be determined numerically (see equations (78) to (80)).

In the final part of this chapter the EA manual's (1999) prediction method for V_{max} has been extended to oblique wave attack (8.3). It could be confirmed that the Weibull approach is valid at 15° and 30° obliquity as well. It has been found that spatial variability has an effect on maximum discharges. While neglecting spatial effects gives good "mean" predictions of V_{max} along the sea-wall it leads to local under predictions with measured discharges up to three times higher than predicted ones. Thus, a conservative "worst case" approach is recommended using the results at the location of the highest measured discharges Q and proportion of overtopping events. This reduces the number of under predicted tests and the worst ratio of measured to (under) predicted discharges goes down to about 1.8.

At 60° obliquity (8.3.3) no wave impacts have been observed and all tests were in reflecting mode. Thus, the appropriate approach after the EA manual (1999) was pursued. The proportion of overtopping waves, however, was under predicted by about one to five orders of magnitude giving less than one overtopping event in many instances. Yet, the overtopping discharge was larger than zero. In order to assure a conservative design it has been suggested to set the number of overtopping waves in those cases to "one", which implies that all overtopping happened in one single event. As the mean overtopping discharge Q has been reasonably well predicted (see chapter 6) this will lead to an upper

bound of V_{max}. Alternatively, it was suggested to design the sea-wall for an angle of wave attack of 30°, which will give higher, and hence conservative, values.

9 DISCUSSION AND IMPLICATIONS FOR DESIGN

9.1 Introduction

In the previous chapters (4 to 8) the overtopping behaviour over vertical seawalls under violent (impulsive) perpendicular and oblique wave attack has been discussed. In this chapter the derived prediction tools for mean and individual discharges are summarised and design guidance is offered. The recommendations are essentially extensions to the existing tools for wave overtopping presented in the environmental agency (EA) manual (1999).

The first step in a design of a plain vertical seawall is to establish whether the waves at the toe of the structure are predominantly in reflecting or impacting mode. At this point the angle of wave attack has no influence, unless it is 60° or larger (see below). The EA manual (1999) suggests here the h* parameter:

$$h^* \equiv \left(\frac{h}{H_s}\right)\left(\frac{2\pi h}{gT_m^2}\right) \tag{81}$$

The notations and symbols are used in the usual way and can be reviewed in the Appendix (Table 1).

where g the acceleration due to gravity (m/s^2), h the water depth at the toe of the structure (m), T_m the mean wave period at the toe of the structure (s), and H_s the significant wave height at the toe of the structure (m).

If $h^* > 0.3$ then reflecting waves predominate, otherwise if $h^* \leq 0.3$ then impacting waves predominate. While this could generally be confirmed there has been a transition zone of $0.14 \leq h^* \leq 0.21$ where impulsive and reflecting tests apparently coexisted (see sections 5.2 and 6.2). Another criterion to distinguish between both modes offered by the PROVERBS workshop (Oumeraci et al., 2001) is the relative wave height H_{si}/h_i where reflecting waves predominate if $H_{si}/h_i < 0.35$, otherwise it is impacting waves. In this study this criterion led to a clear distinction between both modes.

It should be noted that both criteria are guidelines only and it is recommended to test wave conditions against both. In order to ensure a conservative design it is suggested to assume impacting conditions if either criterion indicates that such conditions could exist.

The h^* parameter and the PROVERBS parameter map to distinguish between reflecting and impacting wave conditions were strictly speaking derived for perpendicular wave attack. With increasing angles of wave attack an increasing number of waves, which would have impacted onto the seawall at 0° obliquity switches to "impact-like" behaviour and eventually to reflecting conditions (chapter 4). It could be shown that "impact-like" events occur up to angles of wave attack of 30° and – in terms of overtopping discharge prediction – can be treated as impacting events (chapters 6 and 8). Thus, once waves are established to be in impacting mode for perpendicular wave attack, they must be treated as impacting up to 30° obliquity.

If waves are in reflecting condition then the appropriate formulae presented in the EA manual (1999) are recommended. Guidelines for impulsive conditions are given below. In the case of perpendicular wave attack they are identical to the EA manual (1999).

9.2 Mean overtopping discharge

As has been mentioned above the design guidance for mean overtopping discharge at perpendicular wave attack as offered in the EA manual (1999) could be validated in this study. This was very consistent for all measurement positions along the vertical seawall. Thus, the same formulae will be offered for this case in this section.

Tests with oblique wave attack showed some spatial variability of overtopping volumes. At certain positions higher volumes were measured, which could not be explained by simple local variations in wave conditions and structural parameters (sections 6.3 and 0). In spite of the spatial variations, no general increase in mean overtopping at small angles of wave attack (e.g. 15°) could be measured.

In order to account for the spatial effects two approaches are presented here. In the first one no spatial variations have been considered and the best fit formulae for all measurement positions are given. In practical designs this can be useful if the evaluation of flood risk is the driving force. In the second approach the spatial variations have been considered as a worst case. As the position of maximum overtopping cannot be predicted the formulae for the second approach have been derived from the measurement point with the highest

overtopping. This can be useful for a conservative design or for the evaluation of overtopping hazards if the methods are based on mean rather than individual peak discharges.

In the case of perpendicular wave attack no spatial variability has been measured. The results of this work lie so close to the formula of the EA manual (1999) that no amendment is recommended (see sections 2.3.3 and 6.2):

$$Q_h = 0.000137\, R_h^{-3.24} \tag{82}$$

where Q_h is the dimensionless discharge, given by:

$$Q_h = \frac{Q}{(gh^3)^{0.5}\ h^{*2}} \tag{83}$$

and R_h is the dimensionless freeboard, given by:

$$R_h = \frac{R_c}{H_s}\ h^* \tag{84}$$

h^* is given in equation (57). The valid range of equation (82) is $0.05 < R_h < 1.00$.

With increasing obliquity (i.e. 15° and 30°) an increasing number of waves – which would have impacted onto the wall at perpendicular wave attack – start to display "impact-like" behaviour (see chapter 4). In terms of wave overtopping this behaviour can still be considered as impacting, although the discharges are lower (see chapter 6). Thus, the mean discharges can be described with some modifications to equation (82).

15° obliquity yields (mean values for all measurement positions, section 6.3):

$$Q_h = 0.000058\, R_h^{-3.66} \tag{85}$$

30° obliquity yields (mean values for all measurement positions, section 0):

$$Q_h = 0.000008\, R_h^{-4.22} \tag{86}$$

The valid range in both cases is $0.07 < R_h < 0.65$.

All impacts ceased at 60° obliquity and all tests were in reflecting mode (section 6.5). The approach for reflecting conditions and 60° obliquity by the EA manual (1999) gave good

mean values for all measurement positions ignoring any spatial effects. The formula for 0° obliquity can be used as an upper bound.

Taking spatial variability into account as a worst case scenario (second approach), i.e. only the measurement position with the highest overtopping is considered, leads to lower reductions in the mean overtopping due to oblique wave attack. At perpendicular wave attack no spatial variability could be measured and, hence, the use of equation (82) is still recommended. The highest measurements at 15° obliquity showed no reductions to the perpendicular case and equation (82) is again recommended. At 30° the highest measurements gave the same reductions as the 15° case with the mean of all measurement points and hence equation (85) is recommended. At 60° the EA manual's (1999) formula for reflecting conditions and perpendicular wave attack gave an upper bound to all measurements. A summary is given in Table 4.

Table 4: Summary of prediction formulae for mean discharge

	0°	15°	30°	60°
1st approach (mean)	$Q_h = 0.000137\ R_h^{-3.24}$	$Q_h = 0.000058\ R_h^{-3.66}$	$Q_h = 0.000008\ R_h^{-4.22}$	EA manual(1999) refl. cond. 60°
2nd approach (worst case)	as per 1st approach and 0° obliquity	as per 1st approach and 0° obliquity	as per 1st approach and 15° obliquity	EA manual(1999) refl. cond. 0°

Valid ranges:

perpendicular wave attack: $0.05 < R_h < 1.00$

all oblique cases: $0.07 < R_h < 0.65$

9.3 Individual Overtopping Discharge

The spatial variability of overtopping volumes mentioned in the previous section also affects the peak individual overtopping discharges (see chapter 8). There are no tools available to determine the exact location of peak discharges and, in order to ensure a

conservative prediction of maximum discharges, the worst case approach is recommended. Thus, the tools presented in this section are based on the highest measurements along the seawall.

As a first step prediction tools for the proportion of overtopping waves (N_{ow}/N_w) are presented. They will later on be needed as input parameters for the formulae of the maximum events. It should be noted that the formulae given for N_{ow}/N_w are associated with the highest measured peak discharges. This is important as a higher proportion of overtopping waves (N_{ow}/N_w) has been measured at this position, as well. Thus, a "mean" peak discharge along the wall neglecting spatial variability cannot be predicted by applying the formulae for N_{ow}/N_w given here combined with the appropriate formulae for a "mean" Q (i.e. neglecting spatial variability). This would lead to an unsafe design as – counter intuitively – a higher predicted N_{ow}/N_w leads to a lower prediction in V_{max}.

0° obliquity (same as EA manual (1999), see sections 2.4 and 7.2):

$$\frac{N_{ow}}{N_w} = 0.031\, R_h^{-0.99} \tag{87}$$

where N_{ow} is the number of overtopping events during design conditions (-), N_w is the total number of incoming waves during design conditions (-), and R_h is the relative freeboard as defined in equation (84).The valid range is $0.05 < R_h < 1.00$.

15° obliquity (see section 7.3):

$$\frac{N_{ow}}{N_w} = 0.010\, R_h^{-1.58} \tag{88}$$

valid range: $0.07 < R_h < 0.65$

30° obliquity (see section 7.3):

$$\frac{N_{ow}}{N_w} = 0.010\, R_h^{-1.40} \tag{89}$$

valid range: $0.07 < R_h < 0.65$

As all waves were in reflecting mode at 60° obliquity the approach after the EA manual (1999) for reflecting conditions at 60° obliquity is recommended. If the actual number of overtopping events turns out to be less than one ($N_{ow} < 1$) then a conservative approach

would be to set N_{ow} to one (N_{ow} = 1) implying that all overtopping happened in one single event.

The general formula for maximum overtopping discharges has been derived from a Weibull probability distribution and is given as:

$$V_{max} = a\left(\ln(N_{ow})\right)^{1/b} \quad (90)$$

where a and b are the Weibull parameters and N_{ow} is the number of overtopping waves. N_{ow} can be derived from the proportion of overtopping waves N_{ow}/N_w and the number of incoming waves N_w during design conditions. The input parameters are summarised in the table below:

Table 5: Summary of input parameters for V_{max}

	0°	15°	30°	60°
Q	$Q_h = 0.000137\ R_h^{-3.24}$	$Q_h = 0.000137\ R_h^{-3.24}$	$Q_h = 0.000058\ R_h^{-3.66}$	EA manual(1999)
$\frac{N_{ow}}{N_w}$	$\frac{N_{ow}}{N_w} = 0.031\ R_h^{-0.99}$	$\frac{N_{ow}}{N_w} = 0.010\ R_h^{-1.58}$	$\frac{N_{ow}}{N_w} = 0.010\ R_h^{-1.40}$	EA manual(1999)
a, b:	$a=0.92V_{bar}$ $b=0.85$	$a=1.06V_{bar}$ $b=1.18$	$a=1.04V_{bar}$ $b=1.27$	EA manual(1999)
valid range:	$0.05 < R_h < 1.00$	$0.07 < R_h < 0.65$	$0.07 < R_h < 0.65$	EA manual(1999)

with: $$V_{bar} = Q\ T_m\ N_w / N_{ow} \quad (91)$$

where V_{bar} is the mean individual overtopping discharge (m^3).

The formulae for the mean discharge Q represent the worst case approach as discussed in the previous section (9.2). The formulae for the proportion of overtopping waves are associated with the highest peak discharges. It should be noted that – counter intuitively – a higher prediction of N_{ow}/N_w actually leads to lower predicted peak discharges and, thus, to a less safe design. This is due to the structure of the formula for V_{max} where N_{ow}/N_w goes in

twice, simultaneously increasing and decreasing V_{max}, whereby the decreasing component prevails.

This is important because the "mean" maximum discharges over all containers (hence ignoring spatial variability) cannot be obtained by simply choosing the "mean" mean discharge Q and leaving all other parameters constant. This would not lead to a safe design.

At 60° obliquity all waves were in reflecting mode and the approach after the EA manual (1999) is recommended. V_{max} can be seen as the most probable peak value. As the actual value during design conditions is probabilistically distributed it can be exceeded.

9.4 Summary and Conclusions

In this chapter the derived prediction tools for mean and individual overtopping discharges over plain vertical seawalls subject to violent (i.e. impulsive) wave attack have been summarised and design guidance has been offered. The recommendations are essentially extensions to the existing tools for wave overtopping presented in the EA manual (1999), and cover guidance for 0°, 15°, 30°, and 60° obliquity.

In the case of mean overtopping discharges two sets of design formulae have been offered. In the first set no spatial variations have been considered and the best fit formulae for all measurement positions were given. In practical designs this can be useful if the evaluation of flood risk is the driving force. For the second set of formulae the spatial variations have been considered as a worst case. As the position of maximum overtopping could not be predicted the formulae for the second set have been derived from the measurement point with the highest overtopping. This can be useful for a conservative design or for the evaluation of overtopping hazards if the methods are based on mean rather than individual peak discharges.

The spatial variability of overtopping volumes also affected the peak individual overtopping discharges (see chapter 8). No tools could be derived to predict the exact location of peak discharges and, in order to ensure a conservative prediction, a set of formulae to predict the highest individual peak discharges measured along the seawall has been presented. It has been pointed out that V_{max} is the most probable peak value. It can be exceeded as the actual volumes during design conditions are probabilistically distributed.

For 60° obliquity all tests were in reflecting conditions and the appropriate formulae for mean and individual peak discharges by the EA manual (1999) were recommended.

10 CONCLUSIONS AND FUTURE WORK

This PhD thesis investigated the overtopping response of a plain vertical seawall subject to impulsive and oblique wave attack. The main conclusions are as follows:

10.1 Conclusions Relating to Overtopping Processes

- Due to the different underlying physics overtopping volumes can be up to three orders of magnitude higher if the waves are predominantly in impacting mode rather than in reflecting mode.
- The analysis in this thesis has shown that the h* parameter as suggested by Allsop et al. (1995) and the EA manual (1999) can distinguish reflecting from impacting wave conditions, although there is a grey zone, where waves in both modes coexist. The PROVERBS parameter map can separate all tests of this study correctly into reflecting and impacting conditions. As waves in impacting mode can lead to much higher overtopping discharges, a conservative approach is recommended. Waves should be considered in impacting mode if either method flags this up.
- This thesis confirmed the h* parameter as an indicator for the impulsiveness of a sea-state, although better results were achieved with the relative wave height H_{si}/h_i.
- The analysis has shown that mean overtopping discharges for vertical seawalls under impulsive conditions reduce with increasing angle of wave attack. There is no evidence of the small increase in overtopping at small obliquities as reported in some earlier studies.
- The research has shown that the occurrence of "classical" wave impacts diminishes with increasing obliquity. An increasing number of waves swap to "impact-like" behaviour between 15° and 30° obliquity and eventually, at 60° obliquity, all tests are in reflecting mode.
- The existence of spatial variability in mean and maximum overtopping volumes under oblique wave attack was shown. The largest difference between measurement positions in this study was on average slightly larger than a factor of three. As only

one basin set-up per structure configuration has been tested no tools could be derived to predict the exact location of low and high discharges. Thus, care must be taken in order to ensure a conservative design.

- Low relative wave heights (i.e. $0.35 < H_{si}/h_i < 0.60$) appeared to be more affected by increasing obliquities than high relative wave heights ($H_{si}/h_i > 0.60$). Relative wave heights in this study of $H_{si}/h_i < 0.35$ were all in reflecting mode (PROVERBS parameter map criterion).
- As has been shown individual overtopping discharges still follow a Weibull probability distribution when waves attack at angles of 15° and 30°.

10.2 Conclusions Relating to Engineering Design Guidance

- The method by Allsop and Calabrese (1999) for the prediction of the percentage of breaking waves, which includes broken and impacting waves, gives very good upper bound for the percentage of impacting waves.
- The methods offered by the Environment Agency manual (EA manual, 1999) give good results for the prediction of mean and maximum overtopping discharges when the waves attack perpendicularly.
- In terms of wave overtopping, "impact-like" events have similar characteristics as impulsive events. Thus, wave conditions, which are in impacting mode at perpendicular wave attack, must be treated as impacting up to angles of wave attack of 30°.
- Design guidance is given in this thesis for mean and maximum overtopping discharges over plain vertical seawalls subject to violent and oblique wave attack. In the case of mean overtopping discharges two sets of design formulae are offered. In the first set no spatial variations are considered and the best fit formulae for all measurement positions are given. In practical designs this can be useful if the evaluation of flood risk is the driving force. For the second set of formulae the spatial variations are considered as a worst case. As the position of maximum overtopping could not be predicted the formulae for the second set are derived from the measurement point with the highest overtopping. This can be useful for a conservative design or for the evaluation of overtopping hazards if the methods are based on mean rather than individual peak discharges.

- The spatial variability of overtopping volumes also affects the peak individual overtopping discharges. No tools could be derived to predict the exact location of peak discharges and, in order to ensure a conservative prediction, a set of formulae to predict the highest individual peak discharges measured along the seawall is presented. It has been pointed out that V_{max} is the most probable peak value. It can be exceeded as the actual volumes during design conditions are probabilistically distributed.
- Waves are in reflecting mode when attacking at 60° obliquity and the guidance offered by the EA manual (1999) for simple reflecting conditions works well.

10.3 Recommendations for Future Research

- Two prediction methods showing whether waves are predominantly in impacting or reflecting conditions, the h* parameter and the PROVERBS parameter map, have been discussed in this thesis. Contrary to the PROVERBS parameter map the h* parameter is a function of the wave period and h* states that in terms of impulsiveness an increase in wave period can compensate for a reduction in wave height. This, however, could not be confirmed in this study. In fact, no influence of the wave period on the percentage of impacting waves could be found at all and better results were achieved with the parameter map criterion. This might be the case, because the range of sea-states tested was too limited to show up the influence of the period. The test matrix in this study was designed to study the effect of obliquity on violent wave overtopping and not to reinvestigate 2d prediction tools. It might, however, be of interest for future work to extend the test matrix towards longer periods (leaving all other parameters constant) and to investigate the effect this has on the wave breaking behaviour.
- The transition from "impact-like" to reflecting waves occurs between 30° and 60° degrees. At 30° there is still a velocity component of the reflected waves facing the incoming waves, which is not the case at 60°. A closer look at this transition especially at 45° obliquity would give more insight into the physical processes.
- Spatial variability could be observed and measured for 15° and 30° obliquity. The largest difference between measurement positions was on average slightly higher than a factor of three. Although this is a significant difference the actual length of the seawall has not been long enough to show whether this is the largest amount which has to be expected due to spatial variability. This can be explored in tests with a

seawall long enough to allow for several build-ups of waves along the wall leading to more than one location of minimum and peak overtopping and hence showing the total extent of spatial variability. This may be important for the evaluation of hazards which are mostly caused by few and extreme overtopping events.

- Another important issue is the comparison of these results to numerical models. It should be assured that numerical simulations, are able to reflect the physical behaviour of the wave – seawall interaction, including the distinction between impulsive and reflecting conditions at perpendicular wave attack, and the additional effects such as "impact-like" behaviour and spatial variability which occur under oblique wave attack.
- A final recommendation for future work is the examination of overtopping responses of other common types of vertical seawalls including one with recurves and parapets under oblique wave attack. All seawall types should also be tested under different plan geometries such as corners and elbows.

11 REFERENCES

Allsop N.W.H., Besley P. & Madurini L.(1995): "Overtopping performance of vertical and composite breakwaters, seawalls and low reflection alternatives" Paper 4.7 in MCS Final Report, publn University of Hannover.

Allsop N.W.H., McKenna J.E., Vicinanza D. & Whittaker T.J.T. (1996a) "New design formulae for wave loadings on vertical breakwaters and seawalls" 25th International Conference on Coastal Engineering, September 1996, Orlando, publn. ASCE, New York.

Allsop NWH, Vicinanza D, & McKenna JE (1996b) "Wave forces on vertical and composite breakwaters" Strategic Research Report SR 443, pp 1-94, HR Wallingford, March 1996, Wallingford.

Allsop, N.W.H. & Calabrese, M. (1998): "Impact loadings on vertical walls in directional seas", Proc. 26th Int. Conf. on Coastal Eng., pp 2056 - 2068, June 1998, Copenhagen, ISBN 0-7844-0411-9, ASCE.

Allsop, N.W.H. & Calabrese, M. (1999): "Forces on vertical breakwaters: effects of oblique or short-crested waves", Research Report SR465, HR Wallingford.

Allsop N.W.H. & Durand N.(1999b): "Influence of steep seabed slopes on breaking waves for structure design" MAST III / PROVERBS, Final Report, Volume IIa, Hydrodynamic Aspects, Chapter 2.1, April 1999.

Allsop N.W.H., Bruce T., Pearson J. Alderson J.S. & Pullen T. (2003) *Violent wave overtopping at the coast, when are we safe?* Int. Conf. on Coastal Management 2003, pp 54-69, ISBN 0 7277 3255 2, publn. Thomas Telford, London.

Ahrens J.P. & Heimbaugh M.S. (1988): "Seawall Overtopping Model" Proc. 21st Int. Conf. on Coastal Eng., Malaga, pp.795-806.

Banyard L. & Herbert D.M.(1995): "The effect of wave angle on the overtopping of sea walls" HR Wallingford, Report SR 396, December 1995.

Bruce, T., Allsop, N.W.H. & Pearson, J. (2001): "Violent overtopping of seawalls – extended prediction methods", Proc. Int. Conf. on "Breakwaters, coastal structures and coastlines '01" ICE, publn Thomas Telford, London.

Bruce T., Pearson J. & Allsop W. (2002): "Hazards at Coast and Harbour Seawalls – Velocities and Trajectories of Violent Overtopping Jets" Proc. 28th Int. Conf. Coastal Eng., 2002, Cardiff, UK, pp 2216-2226, ASCE.

Calabrese, M. (1998): "Onset of breaking in front of vertical and composite breakwaters" Proc. 8th Int. Conf. ISOPE. Montreal, pp 590 – 595, ISBN 1-880653-34-6, publn ISOPE, San Francisco.

Calabrese, M. (1999): "Occurrence of breaking on vertical breakwaters" Proc. 9th Int. Conf. ISOPE. Brest, pp 429 - 433, ISBN 1-880653-43-5, publn ISOPE, San Francisco.

CEM (2002): Coastal Engineering Manual, http://www.coastal.ufl.edu/~sheppard/eoc6430/ Coastal_Engineering_Manual.htm

CLASH (2002) CLASH EVK3-CT-2001-00058, General MethodologyReport

Daemrich, K. F. & Mathias, H. J. (1999): "Overtopping at vertical walls with oblique wave approach", Proc. Conf. COPEDEC V, Cape Town, pp 1294-1301, publn. COPEDEC, Sri Lanka.

Dodd, N. (1998): "A numerical model of wave run-up, overtopping and regeneration", Proc ASCE, Jo. Waterway, Port, Coast & Ocean Eng., Vol 124, No 2, pp 73-81, ASCE.

Douglas S.L.(1984): "Irregular wave overtopping rates" Proc. 19th ICCE, 1984, Houston, pp316-327, publn. ASCE, New York.

Dean, R.G. & Dalrymple R.A. (1991): "Water wave mechanics for engineers and scientists", Advanced Series on Ocean Engineering – Volume2, World Scientific, ISBN 9810204205.

de Waal J.P. & van der Meer J.W. (1992): "Wave Runup and Overtopping on Coastal Structures" Proc.23rd ICCE, Venice, pp 1758-1771, ASCE.

de Waal J.P., Toenjes P. & Van der Meer J.W.(1996): "Wave Overtopping of Vertical Structures including Wind Effect" Proc. 25th Int. Conf. Coastal Eng., 1996, Orlando, pp 2216-2229, publn. ASCE, New York.

EA manual (1999): "Overtopping of seawalls – design and assessment manual", R & D Technical Report W 178, ISBN 1 85705 069 X, Environment Agency, Bristol.

de Rouck J., Troch P., van de Walle B., van Gent M., van Damme L., de Ronde J., Frigaard P. & Murphy J. (2001): "Wave run-up on sloping coastal structures: prototype measurements versus scale model tests" Proc. Int. Conf. on "Breakwaters, coastal structures and coastlines '01" ICE, publn Thomas Telford, London.

de Rouck J., van der Meer J.W., Allsop N.W.H., Franco L. & Verhaeghe H. (2002): "Wave Overtopping at Coastal Structures: Development of a Database towards up-graded Prediction Methods", Proc. 28th Int. Conf. Coastal Eng., 2002, Cardiff, UK, pp 2140-2152, ASCE.

De Rouck J., van der Meer J.W., Allsop N.W.H., Franco L. & Verhaeghe H (2003): "Wave overtopping at coastal structures – a database towards up-graded prediction methods" Proc. 28th Int. Conf. Coastal Engineering (ASCE), Cardiff, July 2002, pp 2140-2152, ISBN 981 238 238 0, publn. World Scientific Publishing, Singapore.

Franco L., de Gerloni M. & van der Meer J.W. (1994): "Wave overtopping on vertical and composite breakwaters" Proceedings 24th ICCE, Kobe, pp 1030-1045, ASCE, New York.

Franco, C., Franco, L., Restano, C. & van der Meer, J.W. (1995): "The effect of wave obliquity and short-crestedness on the overtopping rate and volume distribution on caisson breakwaters", MAST II-MCS Project Final Proceedings, University of Hannover.

Franco C. (1996): "Wave overtopping and loads on caisson breakwater under three-dimensional sea-states" LIP-MAST-TAW Full Final Rep., DIIAR, Politecnico di Milano, Milan, Italy.

Franco C. & Franco L.(1999): "Overtopping Formulas For Caisson Breakwaters with Nonbreaking 3D Waves" Jo. Waterway, Port, Coastal & Ocean Engineering, Vol. 125, No 2, March / April 1999, ASCE, New York, pp 98-107.

Fukuda N., Uno T. & Irie I. (1974): "Field observations of wave overtopping of wave absorbing revetment" Coastal Engineering in Japan, Vol. 17, pp. 117-128.

Galland J.C.(1994): "Rubble mound breakwaters stability under oblique waves: and experimental study" Proc. 24th Int. Conf. Coastal Eng., 1994, Kobe, Japan, publn. ASCE, New York.

Goda Y. (1971): "Expected rate of irregular wave overtopping of seawalls" Coastal Engineering in Japan, Vol 14, pp 45-51, JSCE, Tokyo.

Goda Y., Kishira Y. & Kamiyama Y (1975): "Laboratory investigation on the overtopping rates of seawalls by irregular waves" Ports and Harbour Research Institute, Vol 14, No. 4, pp3-44,PHRI, Yokosuka.

Goda Y. (2000): "Random seas and maritime structures, 2nd edition" ISBN 981-02-3256-X, World Scientific Publishing, Singapore.

Gronbech J., Hald T, Frigaard P. & Burcharth H.F. (1997): "Wave loading and overtopping on caisson breakwaters in multidirectional breaking waves" IAHR seminar on "Multidirectional Waves and their Interaction with Structures", San Francisco, USA.

Hedges T.S. & Reis M.T.(1998): "Random wave overtopping of simple sea walls: a new regression model" Proc. ICE, Water, Maritime and Energy, Vol. 130, March 1998, publn. Thomas Telford, London.

Hedges, T.S. & Reis, M.T. (1999): "Risk assessment of coastal defences", Proc. 34th MAFF Conference of River & Coastal Engineers, Keele, 30 June - 2 July 1999, pp 4.2.1 - 4.2.13, publn. MAFF, Eastbury House, London.

Hibberd, S. & Peregrine, D.H. (1979): "Surf and run-up on a beach: a uniform bore" J. Fluid Mech., Cambridge, U.K., 95, 323-345.

Hiraishi T. & Maruyama H.: (1998)"Directional Wave Overtopping Estimation Model and Experimental Verification" Proc. 26th Int. Conf. Coastal Eng., 1998, Copenhagen, pp 2249-2261, publn. ASCE, New York.

Hu K., Mingham CG. & Causon DM (2000): "Numerical simulation of wave overtopping of coastal structures using the nonlinear shallow water equations" Coastal Engineering, 41:433-465.

Ingram D.M., Causon D.M., Mingham C.G. & Zhou, J.G. (2002): "Numerical Simulation of Violent Wave Overtopping" Proc. 28th Int. Conf. Coastal Eng., 2002, Cardiff, UK, pp 2286-2298, ASCE.

Isobe M., Takahashi S., Yu SP, Sakakiyama T., Fujiina K., Kawasaki K., Jiang Q., Akiyama M. & Oyama H. (1999): "Interim report on the development of numerical wave flume for maritime structure design" JSCE Proceedings of Civil Engineering in the Ocean, 15:321-326.

Isobe M., Hanahara Y., Yu X. & Takahashi S. (2002): "Numerical Simulation of Waves Overtopping a Breakwater" Proc. Int. Conf. on Coastal Eng. 2002, pp. 2273-2285, Cardiff, July 2002, ASCE.

Juhl J. & Sloth P.(1994): "Wave Overtopping of Breakwaters under Oblique Waves" Proc. 24th Int. Conf. Coastal Eng., 1994, Kobe, Japan, pp 1182-1196, publn. ASCE, New York.

Kobayashi N., Otta A.K. & Roy I. (1987): "Wave reflection and run-up on rough slopes" J. Waterways, Port, Coast, and Oc. Engrg., 113(3), 282-298.

Kobayashi N. & Watson K.D. (1987): "Wave reflection and run-up on smooth slopes" Proc. Coast. Hydrodynamics, ASCE, New York, pp. 548-563.

Kobayashi N. & Wurjanto A. (1989): "Wave overtopping on coastal structures" J. Waterways, Port, Coast, and Oc. Engrg.,115(2), 235-251.

Kobayashi N. & Raichle A. (1994): "Irregular wave overtopping revetments in surf zones" J. Waterways, Port, Coast, and Oc. Engrg., ASCE, 120(1), 56-73.

Medina J.R. (1999): "Neural Network modelling of run-up and overtopping" Proc. Conf. Coastal Structures'99, Vol. 1, pp.421-429, AA-Balkema.

Medina J.R., Gonzalez-Escriva J.A., Garrido J., & de Rouck J. (2002): "Overtopping using Neural Networks" Proc. 28th Int. Conf. Coastal Eng., 2002, Cardiff, UK, pp 2153-2164, publ. World Scientific.

Mingham, C.G., Causon, D.M., Ingram, D.M. & Richardson, S.R. (2002): "Numerical simulation of wave-seawall interaction", Proc. Int. Conf. on Coastal Eng. 2002, pp. 2264-2271, Cardiff, July 2002, ASCE.

Mizuguchi M.(1993): "Wave overtopping rate over a vertical wall and reflection coefficient" Coastal Eng. in Japan, Vol. 36, No.1, pp.37-47.

Moriya Y. & Mizuguchi M.(1996): "Wave Overtopping Rate and Reflection Coefficient for Obliquely Incident Waves" Proc. 25th Int. Conf. Coastal Eng., 1996, Orlando, pp 2598-2611, publn. ASCE, New York.

Ohle N., Möller J., Schüttrumpf H., Daemrich K.-F., Oumeraci H., & Zimmermann C. (2002): "The Influence of Refrection and Shoaling on Wave Run-Up under Oblique Waves" Proc. 28th Int. Conf. Coastal Eng., 2002, Cardiff, UK, pp 885-894, ASCE.

Oumeraci H. (2003): "Role of Large-Scale Model Testing in Coastal Engineering – selected Example Studies Performed in GWK Hannover" Towards a Balanced Methodology in European Hydraulic Research, Budapest, 22-23 May 2003, ISBN 9635111320.

Owen, M.W. (1980): "Design of sea walls allowing for wave overtopping", Report EX 924, HR Wallingford.

Pearson, J., Bruce, T., Allsop N.W.H. & Gironella, X. (2002): "Violent wave overtopping – measurements at large and small scale", Proc. Int. Conf. on Coastal Eng. 2002, Cardiff, July 2002, pp. 2227-2238, ASCE.

Oumeraci H., Kortenhaus A., Allsop W., de Groot M., Crouch R., Vrijling H. & Voortman H. (2001): "Probabilistic design tools for vertical breakwaters" Proverbs workshop, ISBN 90 5809 249 6.

Richardson SR., Ingram DM., Mingham CG. & Causon DM. (2002): "On the Validity of the Shallow Water Equations for Violent Wave Overtopping" In BL Edge, editor, Ocean Wave Measurement and Analysis, pp. 1112-1125, ASCE, Reston, Virginia.

Sakakiyama T. & Kajima R.(1996): "Wave overtopping and stability of armor units under multidirectional waves" Proc. 25th Int. Conf. Coastal Eng., 1996, Orlando, pp 1862-1875, publn. ASCE, New York.

Schäffer, H.A. & Klopman, G. (1997): "Review of Multidirectional Active Wave Absorption Methods" IAHR Seminar on Multidirectional Waves and their Interaction with Structures", XXVII IAHR Congress, San Francisco.

Schuettrumpf H., Kortenhaus A. & Oumeraci H.(1998): "Appllication of Overtopping Models to Vertical Walls against Sturm Surges" Proc. 26th Int. Conf. Coastal Eng., 1998, Copenhagen, pp 1553-1566, publn. ASCE, New York.

Schuettrumpf H., Oumeraci H. & Moeller J.(1999): "Wave overtopping on a high mound composite type breakwater" Proc. of the Int. Conf. Coastal Structures'99, Santander, Spain, pp 397 -404, ISBN 90 5809 092 2, Coastal Structures '99, A.A.Balkema / Rotterdam / 2000.

Shiach J.B., Mingham C.G., Ingram D.M. & Bruce T. (2004): "The applicability of the shallow water equations for modelling violent wave overtopping" Coastal Engineering CENG-01090.

Tautenhain E., Kohlhase S. & Partenscky H.W.(1982): "Wave runup at sea dikes under oblique wave approach" Proc. 18th ICCE, ASCE, Cape Town, South Africa, no. 18, Volume I, pp. 804-810, publn. ASCE, New York.

Titov V. & Synolakis C. (1995): "Modelling of breaking and non-breaking long-wave evolution and run-up using VTCS-2" J. Waterways, Port, Coast, and Oc. Engrg., 121(6), 308-316.

Troch P. (1997): "VOFbreak², a numerical model for simulation of wave interaction with rubble mound breakwaters" In Proc. of the 27th IAHR Congress, San Francisco, USA, pp 1366-1371.

Tsuruta S. & Goda Y.(1968): "Expected Discharge of Irregular Wave Overtopping" Proc. Int. Conf. Coastal Eng., 1968, pp 833-852, publn. ASCE, New York.

van der Meer J.W (2002): "Technical Report – Wave Run-up and Overtopping at Dikes" Technical Advisory Committee for Water Retaining Structures, Delft May, 2002.

ACKNOWLEDGEMENTS

Special thanks are given to Dr Jonathan Pearson, Dr Tim Pullen and Ibrahim Bay for their help with and advice on the physical model testing. I am particularly grateful to Dr Jonathan Pearson for his quick and extremely helpful advice and feedback during all stages of my thesis including the physical model testing, the data analysis, and the write-up of my thesis. Without his aid my work would have been much more difficult.

I would also like to thank my two supervisors Tom Bruce and Prof William Allsop for their help. Their support and guidance at all stages of my work are very much appreciated. I am also very grateful for them giving me such a highly relevant and interesting topic and for their faith in letting me present my work at three major international conferences.

The work described in this thesis has been supported by the UK EPSRC (GR/M42312, GR/R42306), and supported by the VOWS Management Committee including members from Manchester Metropolitan University (Derek Causon, David Ingram, Clive Mingham), HR Wallingford (Philip Besley), Posford-Haskoning (Dick Thomas), Bullen & Co, whose support is gratefully acknowledged. The VOWS project is particularly pleased to acknowledge guidance and helpful supervision to their collaborative work from the EPSRC CEWE Project Manager, Michael Owen.

The physical modelling was also substantially assisted by sharing test facilities, test structures, measurement devices and related recourses funded by the DEFRA / EA research projects FD 2410 & FD2412 Coastal Flooding Hazard by Wave Overtopping (SHADOW Phase I & II).

Außerdem möchte ich meinen Eltern und meinem Bruder danken, die meine Arbeit hier erst ermöglicht haben und immer für mich da waren.

APPENDIX

Table 1: Notation and Symbols (Part I)

Parameter	Dimension	Description
a	[-]	Weibull "scale" parameter
b	[-]	Weibull "shape" parameter
g	[m/s²]	Acceleration due to gravity
H_{m0}	[m]	Significant wave height from spectral analysis, defined $4.0m_0^{0.5}$
H_s	[m]	Significant wave height, average of highest one third of wave heights
H_o'	[m]	Equivalent deepwater wave height, which is defined as H_{so} adjusted for refraction and diffraction effects
H_{si}	[m]	Significant inshore wave height, average of highest one third of wave heights
H_{so}	[m]	Significant offshore wave height, average of highest one third of wave heights, unaffected by shallow water
h	[m]	Local water depth at the toe of the structure
$L_{...}$	[m]	Wave length, in the direction of wave propagation
L_o	[m]	Deep water wave length, $gT^2/2\pi$
L_p	[m]	Wave length related to peak period (T_p)
L_{pi}	[m]	Local inshore wave length related to peak period at structure
m_0		0^{th} moment of the wave energy density spectrum
N_{ow}	[-]	Number of overtopping waves
N_w	[-]	Number of waves
P	[-]	Encounter probability
Q	[m³/s/m]	Mean overtopping discharge per unit length of structure
Q^*	[-]	Dimensionless overtopping discharge
R_c	[m]	Crest freeboard, level of crest less static water level
$R_{u2\%}$	[m]	Run-up level exceeded by 2% of run-up crests
R^*	[-]	Dimensionless freeboard
s_{op}	[-]	Deep water wave steepness related to the offshore peak wave period

Table 1: Notation and Symbols (Part II)

Parameter	Dimension	Description
V	[m³]	Overtopping volume
V_{bar}	[m³]	Mean of individual overtopping volumes
V_i	[m³]	Individual overtopping volume
V_{max}	[m³]	Maximum expected individual overtopping volume
α	[°]	Structure front slope angle to horizontal
β	[°]	Direction of wave propagation relative to normal to structure alignment
$\gamma_{...}$	[-]	influence factors
γ_b	[-]	influence factor for berm
γ_f	[-]	influence factor for roughness of slope
γ_h	[-]	influence factor for shallow water
γ_β	[-]	influence factor for oblique wave attack
γ_v	[-]	influence factor for vertical wall
ξ_{op}	[-]	Iribarren number or surf similarity parameter based on the offshore peak wave steepness s_{op}

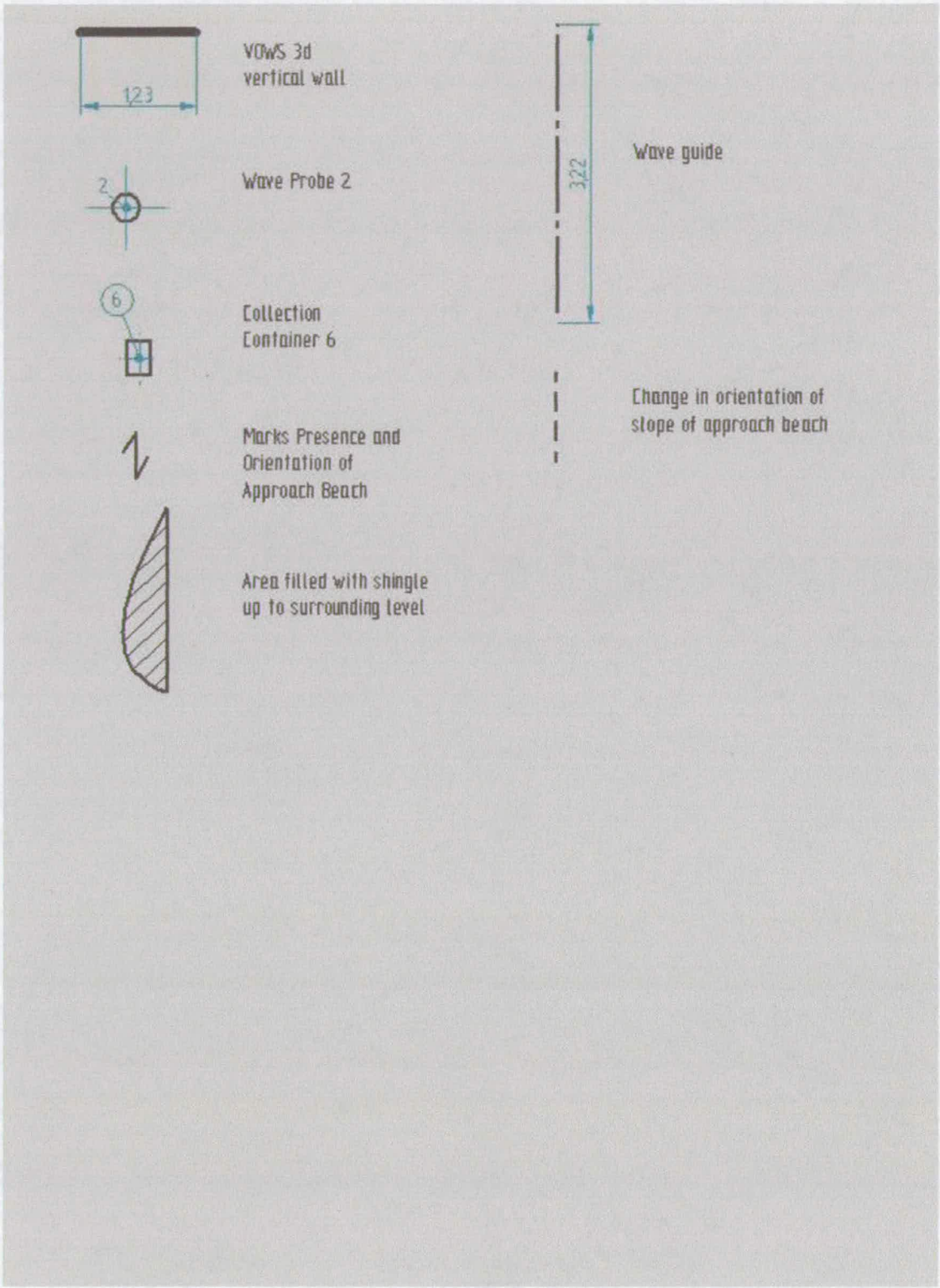

Figure 1: Legend to basin sketches

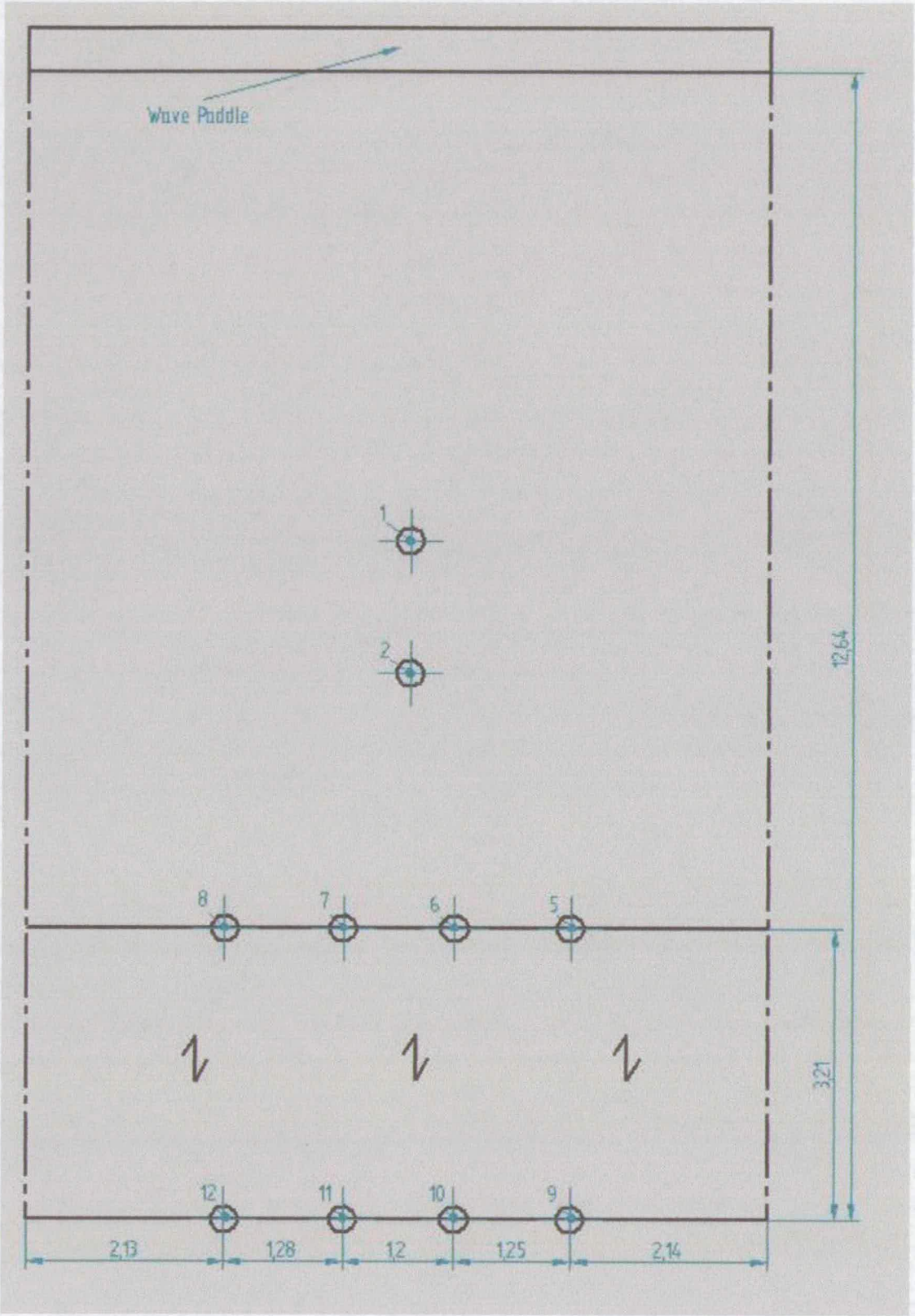

Figure 2: Basin set-up for calibration test cVO00 ($\beta = 0°$)

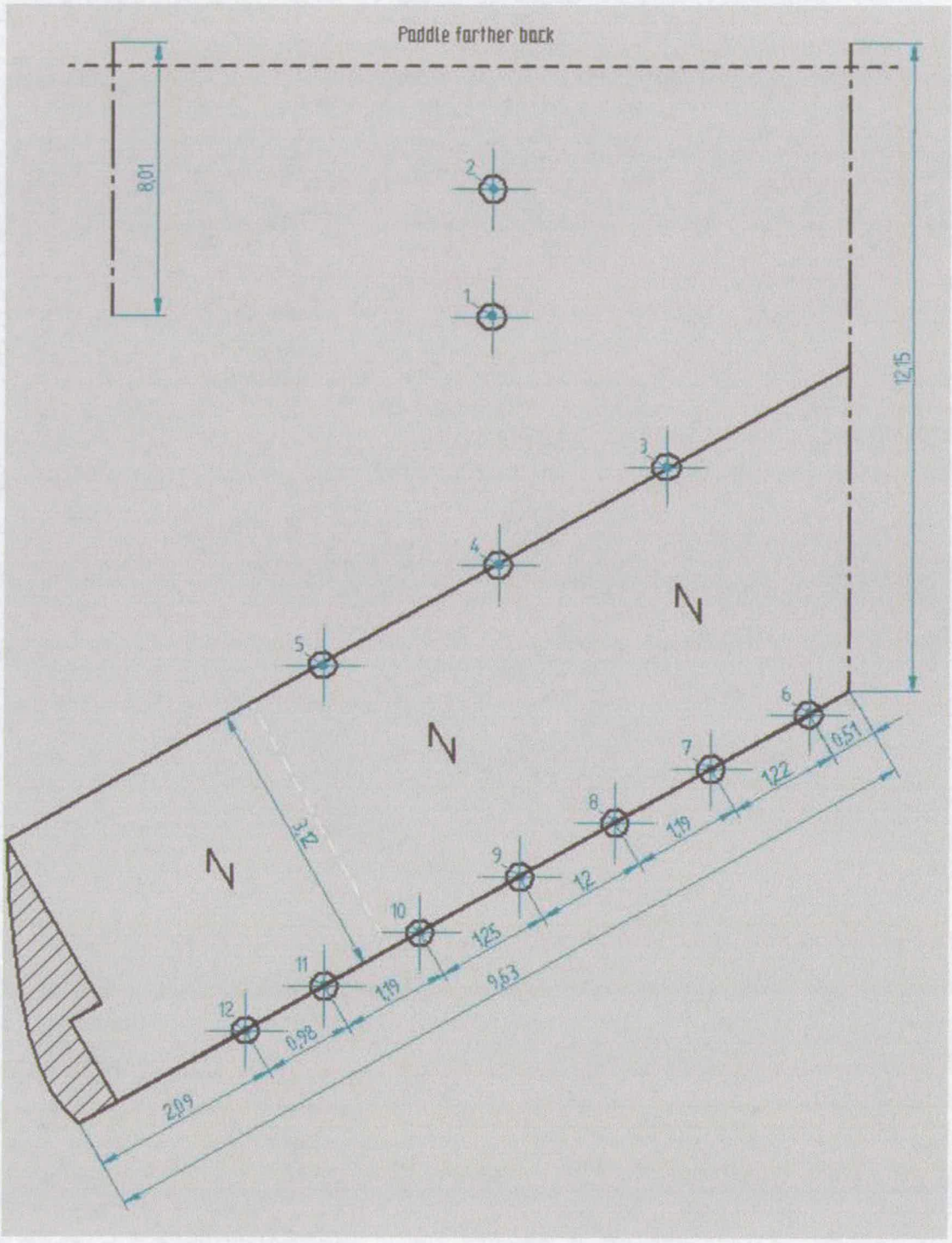

Figure 3: Basin set-up for calibration test cVO30 ($\beta = 30°$)

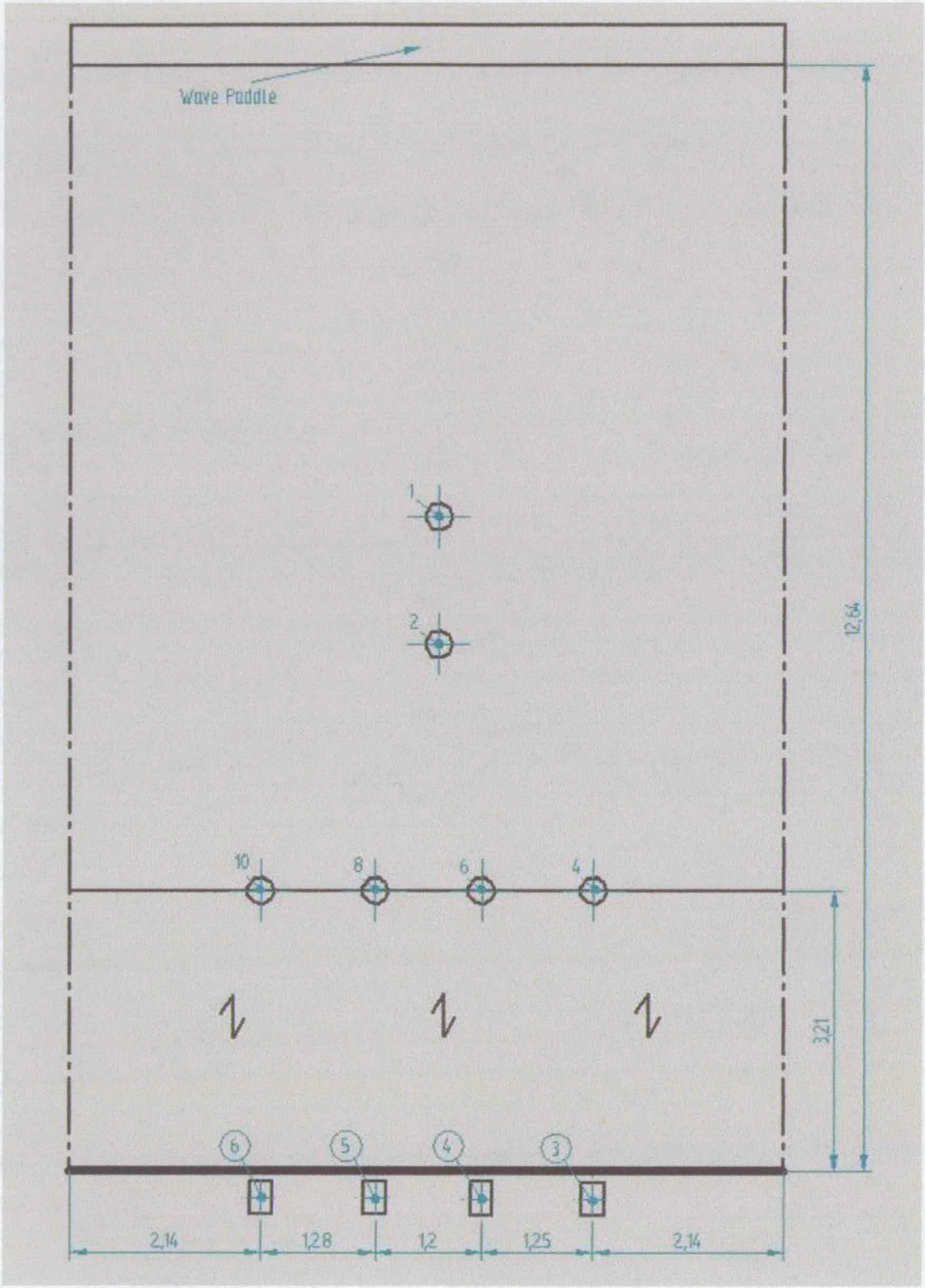

Figure 4: Basin set-up for test VO00 ($\beta = 0°$)

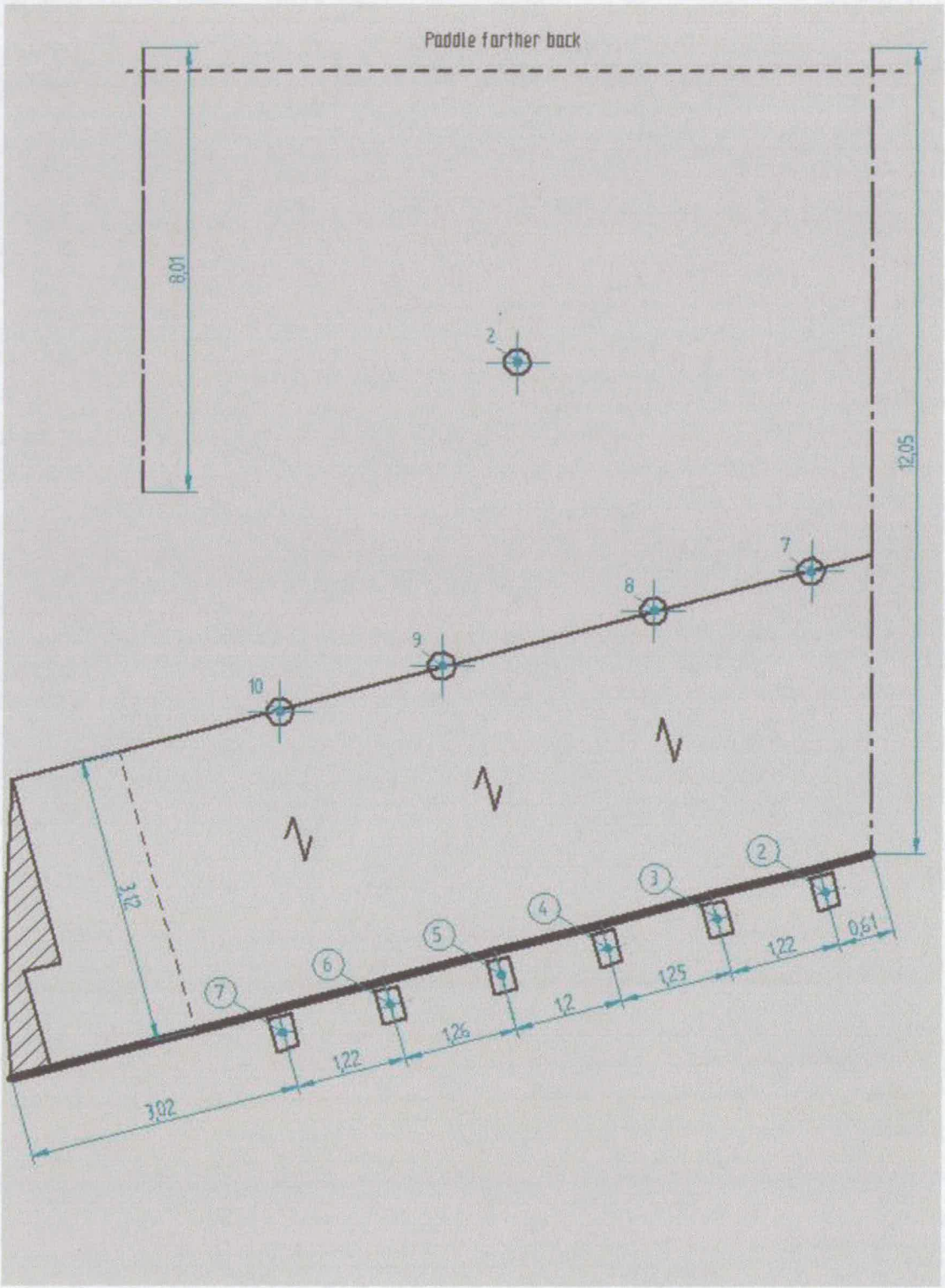

Figure 5: Basin set-up for test VO15 (β = 15°)

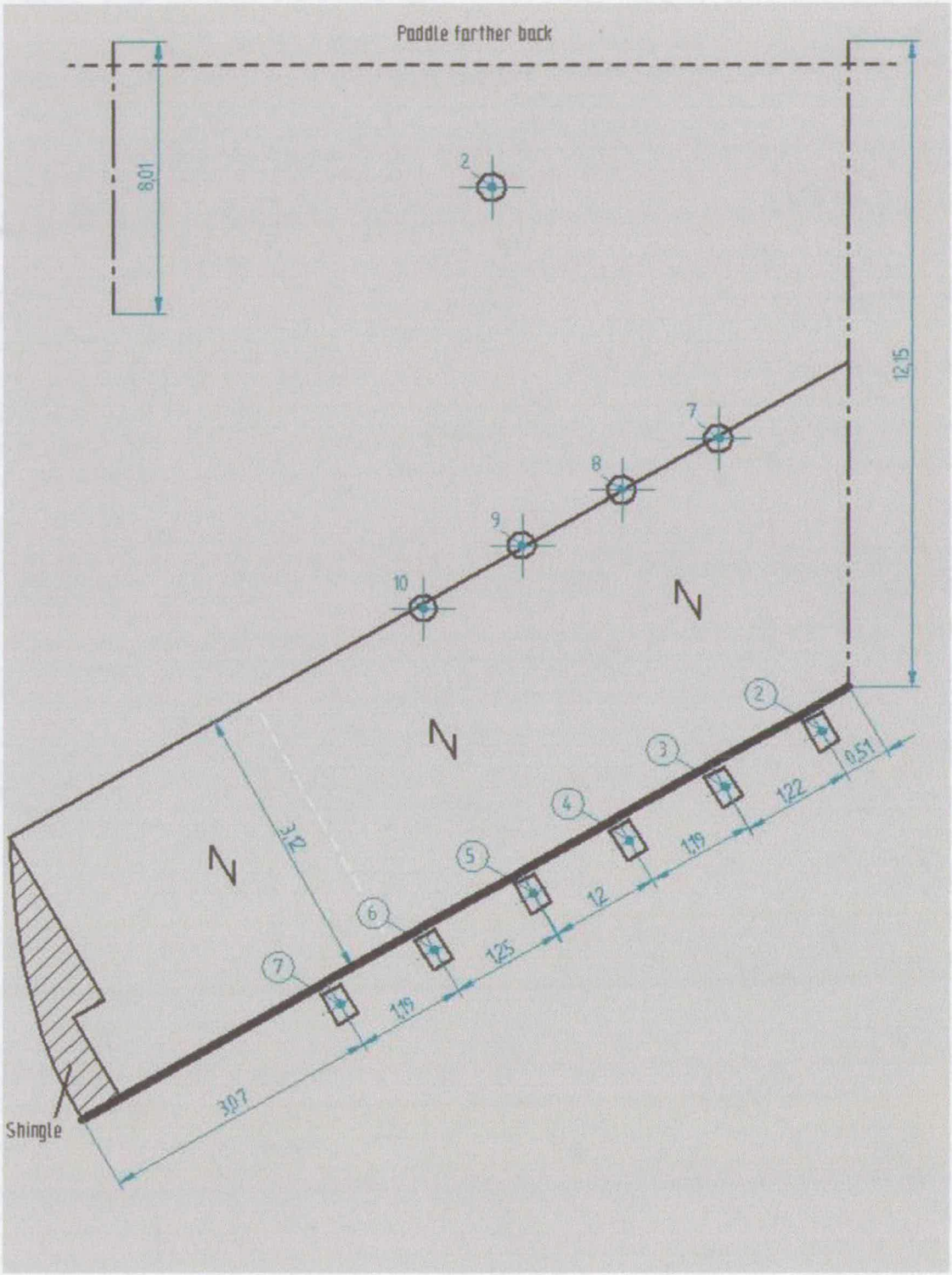

Figure 6: Basin set-up for test VO30 (β = 30°)

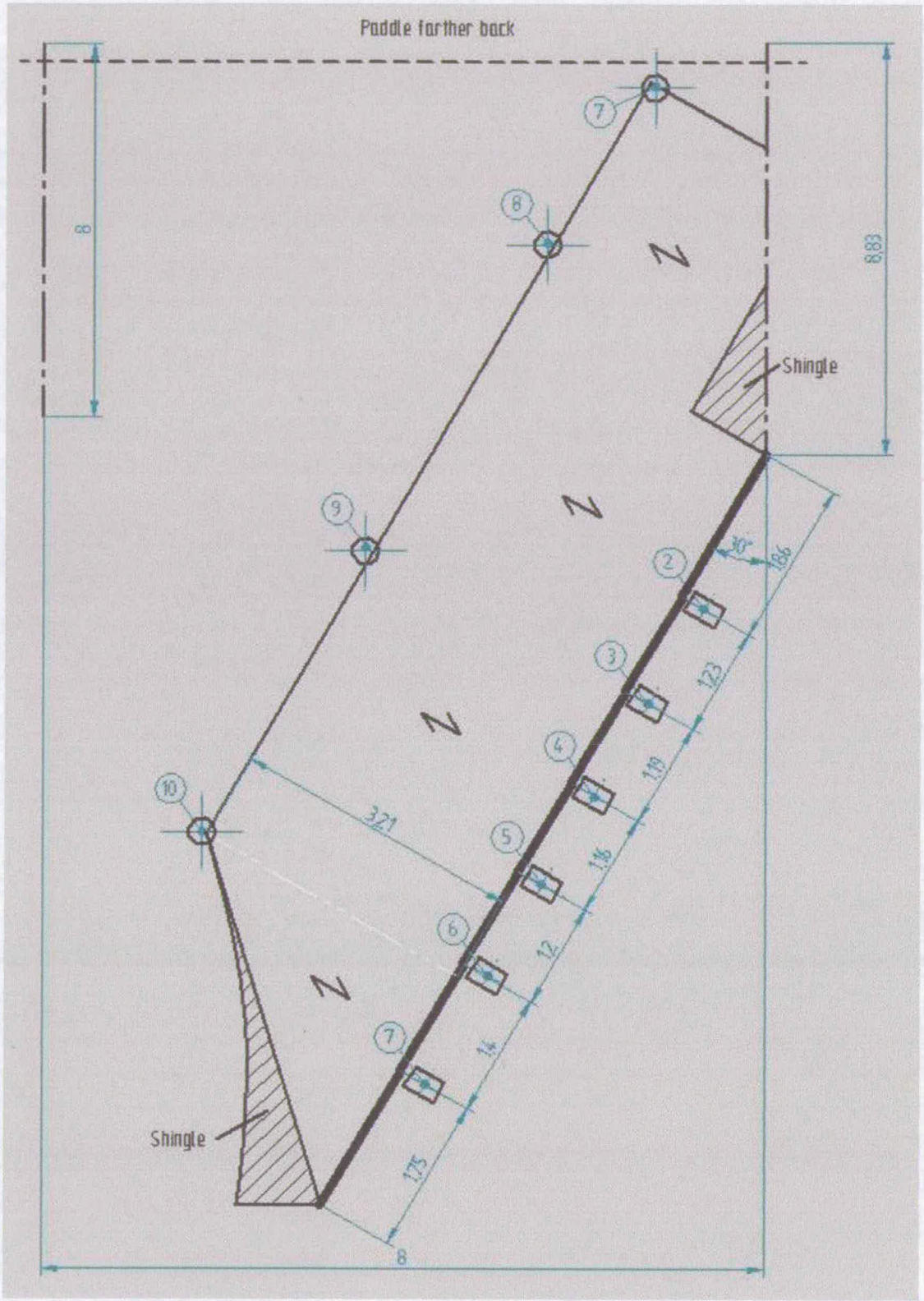

Figure 7: Basin set-up for test VO60 (β = 60°)

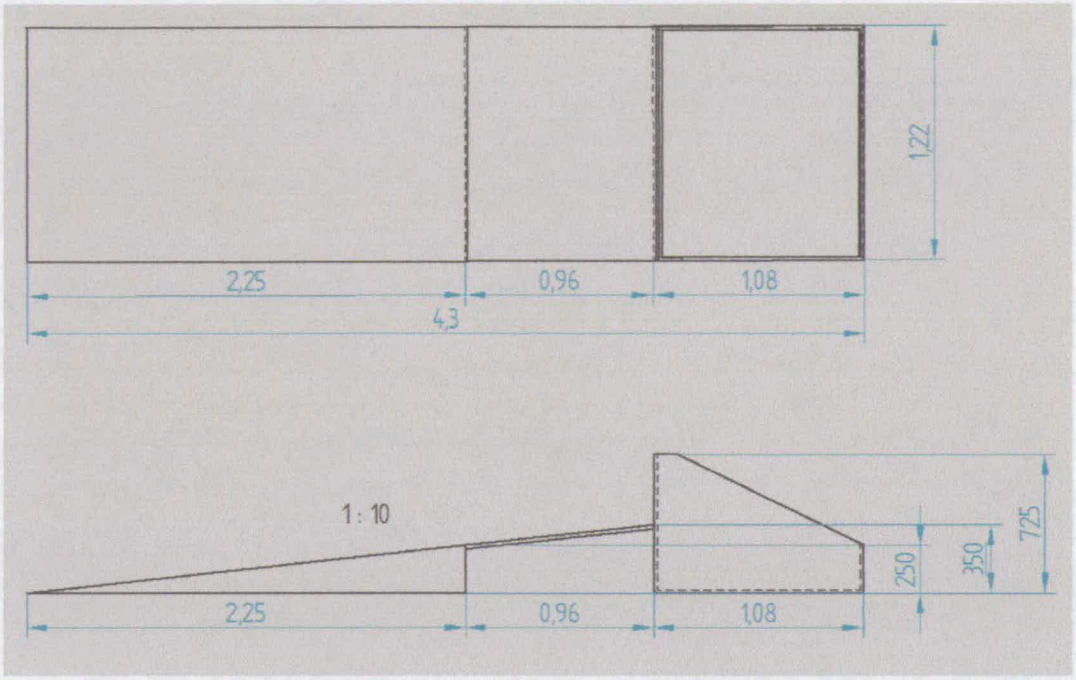

Figure 8: Test structure (2d sketch)

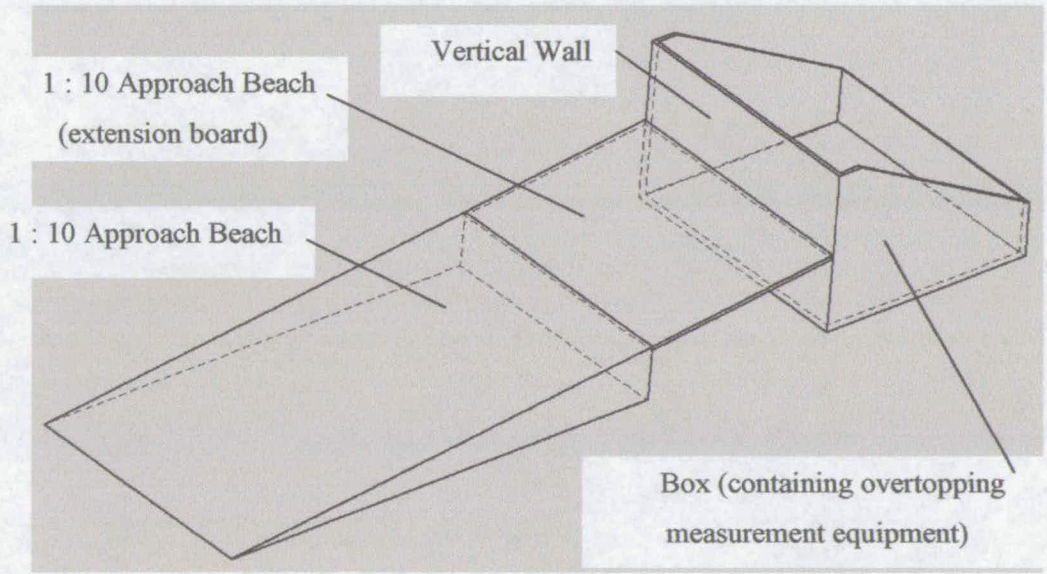

Figure 9: Test structure (3d sketch)

Table 2: Structural parameters β = 0° (VO00)

VO00	Nominal wave conditions			Structural Parameters											
				Pos: 3			Pos: 4			Pos: 5			Pos: 6		
Test Condition	d [m]	$T_{m,req}$ [m]	$H_{s,req}$ [m]	h_3 [m]	$R_{c,3}$ [m]	B_3 [m]	h_4 [m]	$R_{c,4}$ [m]	B_4 [m]	h_5 [m]	$R_{c,5}$ [m]	B_5 [m]	h_6 [m]	$R_{c,6}$ [m]	B_6 [m]
01	0.450	1.20	0.060	0.103	0.285	0.373	0.101	0.284	0.373	0.102	0.284	0.373	0.103	0.284	0.371
02	0.450	1.20	0.090	0.103	0.285	0.373	0.101	0.284	0.373	0.102	0.284	0.373	0.103	0.284	0.371
03	0.450	1.20	0.120	0.103	0.285	0.373	0.101	0.284	0.373	0.102	0.284	0.373	0.103	0.284	0.371
04	0.450	1.30	0.060	0.103	0.285	0.373	0.101	0.284	0.373	0.102	0.284	0.373	0.103	0.284	0.371
05	0.450	1.30	0.090	0.103	0.285	0.373	0.101	0.284	0.373	0.102	0.284	0.373	0.103	0.284	0.371
06	0.450	1.30	0.120	0.103	0.285	0.373	0.101	0.284	0.373	0.102	0.284	0.373	0.103	0.284	0.371
07	0.450	1.40	0.060	0.103	0.285	0.373	0.101	0.284	0.373	0.102	0.284	0.373	0.103	0.284	0.371
08	0.450	1.40	0.090	0.103	0.285	0.373	0.101	0.284	0.373	0.102	0.284	0.373	0.103	0.284	0.371
09	0.450	1.40	0.120	0.103	0.285	0.373	0.101	0.284	0.373	0.102	0.284	0.373	0.103	0.284	0.371
10	0.450	1.50	0.060	0.103	0.285	0.373	0.101	0.284	0.373	0.102	0.284	0.373	0.103	0.284	0.371
11	0.450	1.50	0.090	0.103	0.285	0.373	0.101	0.284	0.373	0.102	0.284	0.373	0.103	0.284	0.371
12	0.450	1.50	0.120	0.103	0.285	0.373	0.101	0.284	0.373	0.102	0.284	0.373	0.103	0.284	0.371
13	0.450	1.60	0.060	0.103	0.285	0.373	0.101	0.284	0.373	0.102	0.284	0.373	0.103	0.284	0.371
14	0.450	1.60	0.090	0.103	0.285	0.373	0.101	0.284	0.373	0.102	0.284	0.373	0.103	0.284	0.371
15	0.450	1.60	0.120	0.103	0.285	0.373	0.101	0.284	0.373	0.102	0.284	0.373	0.103	0.284	0.371
22	0.525	1.20	0.060	0.178	0.210	0.373	0.176	0.209	0.373	0.177	0.209	0.373	0.178	0.209	0.371
23	0.525	1.20	0.100	0.178	0.210	0.373	0.176	0.209	0.373	0.177	0.209	0.373	0.178	0.209	0.371
24	0.525	1.20	0.140	0.178	0.210	0.373	0.176	0.209	0.373	0.177	0.209	0.373	0.178	0.209	0.371
25	0.525	1.30	0.060	0.178	0.210	0.373	0.176	0.209	0.373	0.177	0.209	0.373	0.178	0.209	0.371
26	0.525	1.30	0.100	0.178	0.210	0.373	0.176	0.209	0.373	0.177	0.209	0.373	0.178	0.209	0.371
27	0.525	1.30	0.140	0.178	0.210	0.373	0.176	0.209	0.373	0.177	0.209	0.373	0.178	0.209	0.371
28	0.525	1.40	0.060	0.178	0.210	0.373	0.176	0.209	0.373	0.177	0.209	0.373	0.178	0.209	0.371
29	0.525	1.40	0.100	0.178	0.210	0.373	0.176	0.209	0.373	0.177	0.209	0.373	0.178	0.209	0.371
30	0.525	1.40	0.140	0.178	0.210	0.373	0.176	0.209	0.373	0.177	0.209	0.373	0.178	0.209	0.371
31	0.525	1.50	0.060	0.178	0.210	0.373	0.176	0.209	0.373	0.177	0.209	0.373	0.178	0.209	0.371
32	0.525	1.50	0.100	0.178	0.210	0.373	0.176	0.209	0.373	0.177	0.209	0.373	0.178	0.209	0.371
33	0.525	1.50	0.140	0.178	0.210	0.373	0.176	0.209	0.373	0.177	0.209	0.373	0.178	0.209	0.371
34	0.525	1.60	0.060	0.178	0.210	0.373	0.176	0.209	0.373	0.177	0.209	0.373	0.178	0.209	0.371
35	0.525	1.60	0.100	0.178	0.210	0.373	0.176	0.209	0.373	0.177	0.209	0.373	0.178	0.209	0.371
36	0.525	1.60	0.140												

Table 3: Structural parameters β = 15° (VO15)

VO15	Nominal wave conditions			Structural Parameters											
				Pos: 3			Pos: 4			Pos: 5			Pos: 6		
Test	d	$T_{m,req}$	$H_{s,req}$	h_3	$R_{c,3}$	B_3	h_4	$R_{c,4}$	B_4	h_5	$R_{c,5}$	B_5	h_6	$R_{c,6}$	B_6
Condition	[m]	[m]	[m]	[m]	[m]	[m]	[m]	[m]	[m]	[m]	[m]	[m]	[m]	[m]	[m]
01	0.450	1.20	0.060	0.108	0.277	0.372	0.113	0.272	0.372	0.111	0.272	0.371	0.107	0.277	0.370
02	0.450	1.20	0.090	0.108	0.277	0.372	0.113	0.272	0.372	0.111	0.272	0.371	0.107	0.277	0.370
03	0.450	1.20	0.120	0.108	0.277	0.372	0.113	0.272	0.372	0.111	0.272	0.371	0.107	0.277	0.370
04	0.450	1.30	0.060	0.108	0.277	0.372	0.113	0.272	0.372	0.111	0.272	0.371	0.107	0.277	0.370
05	0.450	1.30	0.090	0.108	0.277	0.372	0.113	0.272	0.372	0.111	0.272	0.371	0.107	0.277	0.370
06	0.450	1.30	0.120	0.108	0.277	0.372	0.113	0.272	0.372	0.111	0.272	0.371	0.107	0.277	0.370
07	0.450	1.40	0.060	0.108	0.277	0.372	0.113	0.272	0.372	0.111	0.272	0.371	0.107	0.277	0.370
08	0.450	1.40	0.090	0.108	0.277	0.372	0.113	0.272	0.372	0.111	0.272	0.371	0.107	0.277	0.370
09	0.450	1.40	0.120	0.108	0.277	0.372	0.113	0.272	0.372	0.111	0.272	0.371	0.107	0.277	0.370
10	0.450	1.50	0.060	0.108	0.277	0.372	0.113	0.272	0.372	0.111	0.272	0.371	0.107	0.277	0.370
11	0.450	1.50	0.090	0.108	0.277	0.372	0.113	0.272	0.372	0.111	0.272	0.371	0.107	0.277	0.370
12	0.450	1.50	0.120	0.108	0.277	0.372	0.113	0.272	0.372	0.111	0.272	0.371	0.107	0.277	0.370
13	0.450	1.60	0.060	0.108	0.277	0.372	0.113	0.272	0.372	0.111	0.272	0.371	0.107	0.277	0.370
14	0.450	1.60	0.090	0.108	0.277	0.372	0.113	0.272	0.372	0.111	0.272	0.371	0.107	0.277	0.370
15	0.450	1.60	0.120	0.108	0.277	0.372	0.113	0.272	0.372	0.111	0.272	0.371	0.107	0.277	0.370
22	0.525	1.20	0.060	0.183	0.202	0.372	0.188	0.197	0.372	0.186	0.197	0.371	0.182	0.202	0.370
23	0.525	1.20	0.100	0.183	0.202	0.372	0.188	0.197	0.372	0.186	0.197	0.371	0.182	0.202	0.370
24	0.525	1.20	0.140	0.183	0.202	0.372	0.188	0.197	0.372	0.186	0.197	0.371	0.182	0.202	0.370
25	0.525	1.30	0.060	0.183	0.202	0.372	0.188	0.197	0.372	0.186	0.197	0.371	0.182	0.202	0.370
26	0.525	1.30	0.100	0.183	0.202	0.372	0.188	0.197	0.372	0.186	0.197	0.371	0.182	0.202	0.370
27	0.525	1.30	0.140	0.183	0.202	0.372	0.188	0.197	0.372	0.186	0.197	0.371	0.182	0.202	0.370
28	0.525	1.40	0.060	0.183	0.202	0.372	0.188	0.197	0.372	0.186	0.197	0.371	0.182	0.202	0.370
29	0.525	1.40	0.100	0.183	0.202	0.372	0.188	0.197	0.372	0.186	0.197	0.371	0.182	0.202	0.370
30	0.525	1.40	0.140	0.183	0.202	0.372	0.188	0.197	0.372	0.186	0.197	0.371	0.182	0.202	0.370
31	0.525	1.50	0.060	0.183	0.202	0.372	0.188	0.197	0.372	0.186	0.197	0.371	0.182	0.202	0.370
32	0.525	1.50	0.100	0.183	0.202	0.372	0.188	0.197	0.372	0.186	0.197	0.371	0.182	0.202	0.370
33	0.525	1.50	0.140	0.183	0.202	0.372	0.188	0.197	0.372	0.186	0.197	0.371	0.182	0.202	0.370
34	0.525	1.60	0.060	0.183	0.202	0.372	0.188	0.197	0.372	0.186	0.197	0.371	0.182	0.202	0.370
35	0.525	1.60	0.100	0.183	0.202	0.372	0.188	0.197	0.372	0.186	0.197	0.371	0.182	0.202	0.370
36	0.525	1.60	0.140	0.183	0.202	0.372	0.188	0.197	0.372	0.186	0.197	0.371	0.182	0.202	0.370

Table 4: Structural parameters $\beta = 30°$ (VO30)

VO30	Nominal wave conditions			Structural Parameters											
				Pos: 3			Pos: 4			Pos: 5			Pos: 6		
Test	d	$T_{m,req}$	$H_{s,req}$	h_3	$R_{c,3}$	B_3	h_4	$R_{c,4}$	B_4	h_5	$R_{c,5}$	B_5	h_6	$R_{c,6}$	B_6
Condition	[m]	[m]	[m]	[m]	[m]	[m]	[m]	[m]	[m]	[m]	[m]	[m]	[m]	[m]	[m]
01	0.450	1.20	0.060	0.100	0.283	0.371	0.107	0.276	0.372	0.107	0.279	0.372	0.103	0.279	0.370
02	0.450	1.20	0.090	0.100	0.283	0.371	0.107	0.276	0.372	0.107	0.279	0.372	0.103	0.279	0.370
03	0.450	1.20	0.120	0.100	0.283	0.371	0.107	0.276	0.372	0.107	0.279	0.372	0.103	0.279	0.370
04	0.450	1.30	0.060	0.100	0.283	0.371	0.107	0.276	0.372	0.107	0.279	0.372	0.103	0.279	0.370
05	0.450	1.30	0.090	0.100	0.283	0.371	0.107	0.276	0.372	0.107	0.279	0.372	0.103	0.279	0.370
06	0.450	1.30	0.120	0.100	0.283	0.371	0.107	0.276	0.372	0.107	0.279	0.372	0.103	0.279	0.370
07	0.450	1.40	0.060	0.100	0.283	0.371	0.107	0.276	0.372	0.107	0.279	0.372	0.103	0.279	0.370
08	0.450	1.40	0.090	0.100	0.283	0.371	0.107	0.276	0.372	0.107	0.279	0.372	0.103	0.279	0.370
09	0.450	1.40	0.120	0.100	0.283	0.371	0.107	0.276	0.372	0.107	0.279	0.372	0.103	0.279	0.370
10	0.450	1.50	0.060	0.100	0.283	0.371	0.107	0.276	0.372	0.107	0.279	0.372	0.103	0.279	0.370
11	0.450	1.50	0.090	0.100	0.283	0.371	0.107	0.276	0.372	0.107	0.279	0.372	0.103	0.279	0.370
12	0.450	1.50	0.120	0.100	0.283	0.371	0.107	0.276	0.372	0.107	0.279	0.372	0.103	0.279	0.370
13	0.450	1.60	0.060	0.100	0.283	0.371	0.107	0.276	0.372	0.107	0.279	0.372	0.103	0.279	0.370
14	0.450	1.60	0.090	0.100	0.283	0.371	0.107	0.276	0.372	0.107	0.279	0.372	0.103	0.279	0.370
15	0.450	1.60	0.120	0.100	0.283	0.371	0.107	0.276	0.372	0.107	0.279	0.372	0.103	0.279	0.370
22	0.525	1.20	0.060	0.175	0.208	0.371	0.182	0.201	0.372	0.182	0.204	0.372	0.178	0.204	0.370
23	0.525	1.20	0.100	0.175	0.208	0.371	0.182	0.201	0.372	0.182	0.204	0.372	0.178	0.204	0.370
24	0.525	1.20	0.140	0.175	0.208	0.371	0.182	0.201	0.372	0.182	0.204	0.372	0.178	0.204	0.370
25	0.525	1.30	0.060	0.175	0.208	0.371	0.182	0.201	0.372	0.182	0.204	0.372	0.178	0.204	0.370
26	0.525	1.30	0.100	0.175	0.208	0.371	0.182	0.201	0.372	0.182	0.204	0.372	0.178	0.204	0.370
27	0.525	1.30	0.140	0.175	0.208	0.371	0.182	0.201	0.372	0.182	0.204	0.372	0.178	0.204	0.370
28	0.525	1.40	0.060	0.175	0.208	0.371	0.182	0.201	0.372	0.182	0.204	0.372	0.178	0.204	0.370
29	0.525	1.40	0.100	0.175	0.208	0.371	0.182	0.201	0.372	0.182	0.204	0.372	0.178	0.204	0.370
30	0.525	1.40	0.140	0.175	0.208	0.371	0.182	0.201	0.372	0.182	0.204	0.372	0.178	0.204	0.370
31	0.525	1.50	0.060	0.175	0.208	0.371	0.182	0.201	0.372	0.182	0.204	0.372	0.178	0.204	0.370
32	0.525	1.50	0.100	0.175	0.208	0.371	0.182	0.201	0.372	0.182	0.204	0.372	0.178	0.204	0.370
33	0.525	1.50	0.140	0.175	0.208	0.371	0.182	0.201	0.372	0.182	0.204	0.372	0.178	0.204	0.370
34	0.525	1.60	0.060	0.175	0.208	0.371	0.182	0.201	0.372	0.182	0.204	0.372	0.178	0.204	0.370
35	0.525	1.60	0.100	0.175	0.208	0.371	0.182	0.201	0.372	0.182	0.204	0.372	0.178	0.204	0.370
36	0.525	1.60	0.140	0.175	0.208	0.371	0.182	0.201	0.372	0.182	0.204	0.372	0.178	0.204	0.370

Table 5: Structural parameters $\beta = 60°$ (VO60)

VO60	Nominal wave conditions			Structural Parameters											
				Pos: 3			Pos: 4			Pos: 5			Pos: 6		
Test	d	$T_{m,req}$	$H_{s,req}$	h_3	$R_{c,3}$	B_3	h_4	$R_{c,4}$	B_4	h_5	$R_{c,5}$	B_5	h_6	$R_{c,6}$	B_6
Condition	[m]	[m]	[m]	[m]	[m]	[m]	[m]	[m]	[m]	[m]	[m]	[m]	[m]	[m]	[m]
01	0.450	1.20	0.060	0.102	0.281	0.371	0.107	0.276	0.372	0.108	0.275	0.371	0.107	0.279	0.370
02	0.450	1.20	0.090	0.102	0.281	0.371	0.107	0.276	0.372	0.108	0.275	0.371	0.107	0.279	0.370
03	0.450	1.20	0.120	0.102	0.281	0.371	0.107	0.276	0.372	0.108	0.275	0.371	0.107	0.279	0.370
04	0.450	1.30	0.060	0.102	0.281	0.371	0.107	0.276	0.372	0.108	0.275	0.371	0.107	0.279	0.370
05	0.450	1.30	0.090	0.102	0.281	0.371	0.107	0.276	0.372	0.108	0.275	0.371	0.107	0.279	0.370
06	0.450	1.30	0.120	0.102	0.281	0.371	0.107	0.276	0.372	0.108	0.275	0.371	0.107	0.279	0.370
07	0.450	1.40	0.060	0.102	0.281	0.371	0.107	0.276	0.372	0.108	0.275	0.371	0.107	0.279	0.370
08	0.450	1.40	0.090	0.102	0.281	0.371	0.107	0.276	0.372	0.108	0.275	0.371	0.107	0.279	0.370
09	0.450	1.40	0.120	0.102	0.281	0.371	0.107	0.276	0.372	0.108	0.275	0.371	0.107	0.279	0.370
10	0.450	1.50	0.060	0.102	0.281	0.371	0.107	0.276	0.372	0.108	0.275	0.371	0.107	0.279	0.370
11	0.450	1.50	0.090	0.102	0.281	0.371	0.107	0.276	0.372	0.108	0.275	0.371	0.107	0.279	0.370
12	0.450	1.50	0.120	0.102	0.281	0.371	0.107	0.276	0.372	0.108	0.275	0.371	0.107	0.279	0.370
13	0.450	1.60	0.060	0.102	0.281	0.371	0.107	0.276	0.372	0.108	0.275	0.371	0.107	0.279	0.370
14	0.450	1.60	0.090	0.102	0.281	0.371	0.107	0.276	0.372	0.108	0.275	0.371	0.107	0.279	0.370
15	0.450	1.60	0.120	0.102	0.281	0.371	0.107	0.276	0.372	0.108	0.275	0.371	0.107	0.279	0.370
22	0.525	1.20	0.060	0.177	0.206	0.371	0.182	0.201	0.372	0.183	0.200	0.371	0.182	0.204	0.370
23	0.525	1.20	0.100	0.177	0.206	0.371	0.182	0.201	0.372	0.183	0.200	0.371	0.182	0.204	0.370
24	0.525	1.20	0.140	0.177	0.206	0.371	0.182	0.201	0.372	0.183	0.200	0.371	0.182	0.204	0.370
25	0.525	1.30	0.060	0.177	0.206	0.371	0.182	0.201	0.372	0.183	0.200	0.371	0.182	0.204	0.370
26	0.525	1.30	0.100	0.177	0.206	0.371	0.182	0.201	0.372	0.183	0.200	0.371	0.182	0.204	0.370
27	0.525	1.30	0.140	0.177	0.206	0.371	0.182	0.201	0.372	0.183	0.200	0.371	0.182	0.204	0.370
28	0.525	1.40	0.060	0.177	0.206	0.371	0.182	0.201	0.372	0.183	0.200	0.371	0.182	0.204	0.370
29	0.525	1.40	0.100	0.177	0.206	0.371	0.182	0.201	0.372	0.183	0.200	0.371	0.182	0.204	0.370
30	0.525	1.40	0.140	0.177	0.206	0.371	0.182	0.201	0.372	0.183	0.200	0.371	0.182	0.204	0.370
31	0.525	1.50	0.060	0.177	0.206	0.371	0.182	0.201	0.372	0.183	0.200	0.371	0.182	0.204	0.370
32	0.525	1.50	0.100	0.177	0.206	0.371	0.182	0.201	0.372	0.183	0.200	0.371	0.182	0.204	0.370
33	0.525	1.50	0.140	0.177	0.206	0.371	0.182	0.201	0.372	0.183	0.200	0.371	0.182	0.204	0.370
34	0.525	1.60	0.060	0.177	0.206	0.371	0.182	0.201	0.372	0.183	0.200	0.371	0.182	0.204	0.370
35	0.525	1.60	0.100	0.177	0.206	0.371	0.182	0.201	0.372	0.183	0.200	0.371	0.182	0.204	0.370
36	0.525	1.60	0.140	0.177	0.206	0.371	0.182	0.201	0.372	0.183	0.200	0.371	0.182	0.204	0.370

Table 6: Results of wave calibrations $\beta = 0°$ (VO00)

cVO00 Measured wave conditions

Test Condition	Probe: 2		Probe: 5		Probe: 6		Probe: 7		Probe: 8		Probe: 9		Probe: 10		Probe: 11		Probe: 12	
	$T_{m,2}$ [m]	$H_{s,2}$ [m]	$T_{m,5}$ [m]	$H_{s,5}$ [m]	$T_{m,6}$ [m]	$H_{s,6}$ [m]	$T_{m,7}$ [m]	$H_{s,7}$ [m]	$T_{m,8}$ [m]	$H_{s,8}$ [m]	$T_{m,9}$ [m]	$H_{s,9}$ [m]	$T_{m,10}$ [m]	$H_{s,10}$ [m]	$T_{m,11}$ [m]	$H_{s,11}$ [m]	$T_{m,12}$ [m]	$H_{s,12}$ [m]
01	1.070	0.048	0.956	0.045	1.074	0.048	1.050	0.052	1.028	0.053	1.100	0.053	1.093	0.056	1.078	0.062	1.112	0.068
02	1.119	0.072	1.029	0.066	1.113	0.072	1.070	0.076	1.045	0.072	1.164	0.075	1.158	0.082	1.146	0.089	1.116	0.091
03	1.182	0.095	1.078	0.086	1.164	0.096	1.128	0.099	1.096	0.096	1.216	0.089	1.224	0.098	1.215	0.105	1.186	0.103
04	1.251	0.050	1.065	0.045	1.212	0.048	1.172	0.052	1.180	0.050	1.270	0.056	1.264	0.063	1.202	0.065	1.262	0.069
05	1.275	0.073	1.089	0.068	1.232	0.073	1.210	0.080	1.150	0.078	1.294	0.080	1.280	0.089	1.253	0.100	1.234	0.102
06	1.302	0.097	1.132	0.086	1.249	0.095	1.252	0.100	1.174	0.100	1.306	0.093	1.341	0.103	1.309	0.109	1.266	0.111
07	1.341	0.052	1.185	0.044	1.292	0.046	1.230	0.051	1.279	0.051	1.395	0.059	1.295	0.064	1.266	0.066	1.349	0.070
08	1.366	0.076	1.184	0.066	1.310	0.072	1.286	0.078	1.235	0.076	1.392	0.085	1.343	0.092	1.336	0.102	1.316	0.099
09	1.373	0.099	1.195	0.088	1.340	0.099	1.321	0.105	1.248	0.103	1.396	0.097	1.370	0.108	1.357	0.118	1.347	0.117
10	1.442	0.052	1.319	0.045	1.409	0.047	1.360	0.051	1.341	0.052	1.463	0.061	1.416	0.066	1.404	0.069	1.416	0.069
11	1.438	0.078	1.358	0.068	1.398	0.075	1.390	0.081	1.331	0.079	1.470	0.088	1.484	0.098	1.412	0.107	1.424	0.103
12	1.482	0.103	1.332	0.092	1.443	0.100	1.425	0.108	1.332	0.111	1.485	0.100	1.500	0.110	1.434	0.122	1.423	0.123
13	1.534	0.053	1.472	0.048	1.522	0.048	1.491	0.053	1.493	0.056	1.570	0.062	1.564	0.066	1.535	0.073	1.531	0.073
14	1.534	0.078	1.487	0.071	1.480	0.075	1.512	0.080	1.469	0.081	1.579	0.090	1.588	0.097	1.565	0.107	1.496	0.102
15	1.550	0.104	1.495	0.093	1.499	0.097	1.516	0.108	1.456	0.113	1.568	0.101	1.607	0.106	1.529	0.120	1.507	0.121
22	1.019	0.047	0.937	0.043	1.028	0.043	1.006	0.046	0.970	0.047	1.051	0.046	1.037	0.046	1.010	0.044	1.026	0.054
23	1.098	0.077	1.051	0.069	1.081	0.070	1.081	0.077	1.020	0.080	1.131	0.076	1.147	0.076	1.106	0.077	1.076	0.090
24	1.162	0.106	1.108	0.094	1.143	0.098	1.144	0.106	1.087	0.108	1.193	0.103	1.206	0.107	1.167	0.108	1.169	0.119
25	1.235	0.047	1.096	0.043	1.173	0.043	1.140	0.048	1.153	0.050	1.201	0.047	1.180	0.049	1.168	0.050	1.147	0.059
26	1.257	0.077	1.119	0.072	1.188	0.075	1.163	0.083	1.164	0.080	1.248	0.078	1.245	0.084	1.219	0.090	1.150	0.093
27	1.274	0.106	1.167	0.097	1.225	0.101	1.209	0.113	1.173	0.114	1.286	0.108	1.292	0.116	1.276	0.127	1.227	0.127
28	1.305	0.048	1.232	0.044	1.279	0.044	1.221	0.049	1.240	0.052	1.329	0.048	1.297	0.051	1.308	0.054	1.231	0.060
29	1.327	0.078	1.218	0.075	1.283	0.076	1.290	0.085	1.219	0.088	1.342	0.081	1.307	0.089	1.343	0.100	1.271	0.103
30	1.345	0.108	1.256	0.105	1.313	0.108	1.286	0.121	1.236	0.126	1.353	0.113	1.351	0.124	1.369	0.145	1.284	0.141
31	1.430	0.048	1.368	0.047	1.382	0.046	1.367	0.050	1.367	0.054	1.436	0.049	1.426	0.055	1.437	0.058	1.362	0.062
32	1.428	0.079	1.357	0.077	1.386	0.076	1.394	0.085	1.339	0.093	1.452	0.082	1.392	0.094	1.470	0.106	1.361	0.107
33	1.458	0.108	1.342	0.108	1.409	0.109	1.396	0.126	1.340	0.134	1.445	0.116	1.457	0.133	1.477	0.161	1.365	0.151
34	1.491	0.048	1.467	0.047	1.499	0.047	1.462	0.051	1.478	0.053	1.536	0.048	1.562	0.057	1.557	0.061	1.469	0.059
35	1.521	0.077	1.465	0.077	1.489	0.077	1.514	0.087	1.457	0.092	1.533	0.081	1.559	0.096	1.586	0.114	1.465	0.107
36	1.553	0.108	1.449		1.506		1.499		1.437		1.509		1.601		1.581		1.473	

Table 7: Results of wave calibrations β = 15° (VO15)

VO15	Offshore waves, measured at Probe 2, cVO30		Predicted wave conditions							
			Pos: 3		Pos: 4		Pos: 5		Pos: 6	
Test Condition	$T_{m,2}$ [m]	$H_{s,2}$ [m]	$T_{m,pos3,pred}$ [m]	$H_{s,pos3,pred}$ [m]	$T_{m,pos4,pred}$ [m]	$H_{s,pos4,pred}$ [m]	$T_{m,pos5,pred}$ [m]	$H_{s,pos5,pred}$ [m]	$T_{m,pos6,pred}$ [m]	$H_{s,pos6,pred}$ [m]
01	1.080	0.049	1.080	0.054	1.080	0.058	1.080	0.058	1.080	0.056
02	1.110	0.073	1.110	0.075	1.110	0.081	1.110	0.084	1.110	0.083
03	1.157	0.096	1.157	0.089	1.157	0.095	1.157	0.100	1.157	0.099
04	1.243	0.049	1.243	0.054	1.243	0.061	1.243	0.060	1.243	0.058
05	1.257	0.074	1.257	0.080	1.257	0.087	1.257	0.089	1.257	0.087
06	1.279	0.098	1.279	0.093	1.279	0.101	1.279	0.104	1.279	0.102
07	1.321	0.050	1.321	0.057	1.321	0.063	1.321	0.062	1.321	0.056
08	1.341	0.074	1.341	0.081	1.341	0.088	1.341	0.089	1.341	0.082
09	1.347	0.099	1.347	0.095	1.347	0.102	1.347	0.104	1.347	0.098
10	1.393	0.050	1.393	0.057	1.393	0.063	1.393	0.064	1.393	0.058
11	1.423	0.075	1.423	0.084	1.423	0.090	1.423	0.092	1.423	0.086
12	1.454	0.100	1.454	0.096	1.454	0.103	1.454	0.106	1.454	0.099
13	1.518	0.051	1.518	0.059	1.518	0.066	1.518	0.068	1.518	0.061
14	1.531	0.077	1.531	0.087	1.531	0.094	1.531	0.097	1.531	0.090
15	1.534	0.102	1.534	0.098	1.534	0.106	1.534	0.110	1.534	0.102
22	1.028	0.048	1.028	0.046	1.028	0.050	1.028	0.046	1.028	0.044
23	1.102	0.079	1.102	0.077	1.102	0.082	1.102	0.079	1.102	0.077
24	1.167	0.110	1.167	0.106	1.167	0.113	1.167	0.111	1.167	0.109
25	1.208	0.047	1.208	0.047	1.208	0.050	1.208	0.047	1.208	0.046
26	1.222	0.079	1.222	0.080	1.222	0.086	1.222	0.084	1.222	0.081
27	1.242	0.110	1.242	0.111	1.242	0.119	1.242	0.120	1.242	0.116
28	1.269	0.048	1.269	0.047	1.269	0.051	1.269	0.051	1.269	0.047
29	1.309	0.079	1.309	0.081	1.309	0.089	1.309	0.089	1.309	0.081
30	1.335	0.112	1.335	0.116	1.335	0.125	1.335	0.128	1.335	0.117
31	1.409	0.049	1.409	0.049	1.409	0.055	1.409	0.055	1.409	0.047
32	1.447	0.083	1.447	0.085	1.447	0.096	1.447	0.099	1.447	0.085
33	1.458	0.115	1.458	0.122	1.458	0.135	1.458	0.141	1.458	0.122
34	1.516	0.050	1.516	0.050	1.516	0.058	1.516	0.061	1.516	0.051
35	1.515	0.083	1.515	0.086	1.515	0.101	1.515	0.108	1.515	0.092
36	1.534	0.116	1.534	0.123	1.534	0.142	1.534	0.153	1.534	0.131

Table 8: Results of wave calibrations β = 30° (VO30)

VO30	Offshore waves, measured at Probe 2, cVO30		Predicted wave conditions							
			Pos: 3		Pos: 4		Pos: 5		Pos: 6	
Test Condition	$T_{m,2}$ [m]	$H_{s,2}$ [m]	$T_{m,pos3,pred}$ [m]	$H_{s,pos3,pred}$ [m]	$T_{m,pos4,pred}$ [m]	$H_{s,pos4,pred}$ [m]	$T_{m,pos5,pred}$ [m]	$H_{s,pos5,pred}$ [m]	$T_{m,pos6,pred}$ [m]	$H_{s,pos6,pred}$ [m]
01	1.080	0.049	1.080	0.051	1.080	0.051	1.080	0.058	1.080	0.055
02	1.110	0.073	1.110	0.072	1.110	0.072	1.110	0.081	1.110	0.080
03	1.157	0.096	1.157	0.086	1.157	0.086	1.157	0.094	1.157	0.097
04	1.243	0.049	1.243	0.052	1.243	0.052	1.243	0.061	1.243	0.056
05	1.257	0.074	1.257	0.077	1.257	0.077	1.257	0.087	1.257	0.084
06	1.279	0.098	1.279	0.089	1.279	0.089	1.279	0.100	1.279	0.100
07	1.321	0.050	1.321	0.054	1.321	0.054	1.321	0.063	1.321	0.057
08	1.341	0.074	1.341	0.077	1.341	0.077	1.341	0.087	1.341	0.084
09	1.347	0.099	1.347	0.091	1.347	0.091	1.347	0.101	1.347	0.099
10	1.393	0.050	1.393	0.055	1.393	0.055	1.393	0.063	1.393	0.060
11	1.423	0.075	1.423	0.080	1.423	0.080	1.423	0.089	1.423	0.087
12	1.454	0.100	1.454	0.092	1.454	0.092	1.454	0.102	1.454	0.101
13	1.518	0.051	1.518	0.056	1.518	0.056	1.518	0.066	1.518	0.064
14	1.531	0.077	1.531	0.083	1.531	0.083	1.531	0.093	1.531	0.093
15	1.534	0.102	1.534	0.093	1.534	0.093	1.534	0.106	1.534	0.104
22	1.028	0.048	1.028	0.045	1.028	0.045	1.028	0.049	1.028	0.042
23	1.102	0.079	1.102	0.074	1.102	0.074	1.102	0.081	1.102	0.073
24	1.167	0.110	1.167	0.103	1.167	0.103	1.167	0.113	1.167	0.104
25	1.208	0.047	1.208	0.045	1.208	0.045	1.208	0.049	1.208	0.044
26	1.222	0.079	1.222	0.077	1.222	0.077	1.222	0.086	1.222	0.078
27	1.242	0.110	1.242	0.107	1.242	0.107	1.242	0.119	1.242	0.114
28	1.269	0.048	1.269	0.046	1.269	0.046	1.269	0.051	1.269	0.047
29	1.309	0.079	1.309	0.078	1.309	0.078	1.309	0.089	1.309	0.084
30	1.335	0.112	1.335	0.111	1.335	0.111	1.335	0.124	1.335	0.123
31	1.409	0.049	1.409	0.047	1.409	0.047	1.409	0.056	1.409	0.051
32	1.447	0.083	1.447	0.082	1.447	0.082	1.447	0.098	1.447	0.094
33	1.458	0.115	1.458	0.117	1.458	0.117	1.458	0.136	1.458	0.136
34	1.516	0.050	1.516	0.048	1.516	0.048	1.516	0.060	1.516	0.057
35	1.515	0.083	1.515	0.082	1.515	0.082	1.515	0.105	1.515	0.104
36	1.534	0.116	1.534	0.118	1.534	0.118	1.534	0.145	1.534	0.147

Table 9: Results of wave calibrations $\beta = 60°$ (VO60)

cVO60	Offshore waves, measured at Probe 2, cVO30		Predicted wave conditions							
			Pos: 3		Pos: 4		Pos: 5		Pos: 6	
Test Condition	$T_{m,2}$ [m]	$H_{s,2}$ [m]	$T_{m,pos3,pred}$ [m]	$H_{s,pos3,pred}$ [m]	$T_{m,pos4,pred}$ [m]	$H_{s,pos4,pred}$ [m]	$T_{m,pos5,pred}$ [m]	$H_{s,pos5,pred}$ [m]	$T_{m,pos6,pred}$ [m]	$H_{s,pos6,pred}$ [m]
01	1.080	0.049	1.080	0.041	1.080	0.041	1.080	0.043	1.080	0.046
02	1.110	0.073	1.110	0.057	1.110	0.057	1.110	0.061	1.110	0.064
03	1.157	0.096	1.157	0.068	1.157	0.068	1.157	0.071	1.157	0.075
04	1.243	0.049	1.243	0.041	1.243	0.041	1.243	0.045	1.243	0.048
05	1.257	0.074	1.257	0.060	1.257	0.060	1.257	0.064	1.257	0.068
06	1.279	0.098	1.279	0.070	1.279	0.070	1.279	0.075	1.279	0.079
07	1.321	0.050	1.321	0.042	1.321	0.042	1.321	0.046	1.321	0.049
08	1.341	0.074	1.341	0.060	1.341	0.060	1.341	0.064	1.341	0.068
09	1.347	0.099	1.347	0.071	1.347	0.071	1.347	0.075	1.347	0.079
10	1.393	0.050	1.393	0.043	1.393	0.043	1.393	0.046	1.393	0.049
11	1.423	0.075	1.423	0.062	1.423	0.062	1.423	0.066	1.423	0.069
12	1.454	0.100	1.454	0.072	1.454	0.072	1.454	0.076	1.454	0.079
13	1.518	0.051	1.518	0.044	1.518	0.044	1.518	0.047	1.518	0.051
14	1.531	0.077	1.531	0.064	1.531	0.064	1.531	0.068	1.531	0.072
15	1.534	0.102	1.534	0.072	1.534	0.072	1.534	0.077	1.534	0.082
22	1.028	0.048	1.028	0.036	1.028	0.036	1.028	0.038	1.028	0.040
23	1.102	0.079	1.102	0.060	1.102	0.060	1.102	0.063	1.102	0.066
24	1.167	0.110	1.167	0.083	1.167	0.083	1.167	0.088	1.167	0.092
25	1.208	0.047	1.208	0.036	1.208	0.036	1.208	0.038	1.208	0.040
26	1.222	0.079	1.222	0.062	1.222	0.062	1.222	0.065	1.222	0.069
27	1.242	0.110	1.242	0.086	1.242	0.086	1.242	0.091	1.242	0.096
28	1.269	0.048	1.269	0.036	1.269	0.036	1.269	0.039	1.269	0.041
29	1.309	0.079	1.309	0.062	1.309	0.062	1.309	0.067	1.309	0.071
30	1.335	0.112	1.335	0.089	1.335	0.089	1.335	0.094	1.335	0.099
31	1.409	0.049	1.409	0.038	1.409	0.038	1.409	0.041	1.409	0.044
32	1.447	0.083	1.447	0.065	1.447	0.065	1.447	0.071	1.447	0.078
33	1.458	0.115	1.458	0.093	1.458	0.093	1.458	0.100	1.458	0.108
34	1.516	0.050	1.516	0.038	1.516	0.038	1.516	0.043	1.516	0.048
35	1.515	0.083	1.515	0.065	1.515	0.065	1.515	0.074	1.515	0.083
36	1.534	0.116	1.534	0.093	1.534	0.093	1.534	0.104	1.534	0.115

Table 10: Final number of overtopping events and volumes $\beta = 0°$ (VO00)

VO00	Pos: 3		Pos: 4		Pos: 5		Pos: 6	
Test	N_{ow}	V_{total}	N_{ow}	V_{total}	N_{ow}	V_{total}	N_{ow}	V_{total}
01	14	0.331	22	0.682	34	0.554	89	1.517
02	159	6.211	174	7.245	265	6.849	238	8.692
03	278	15.226	305	15.574	369	15.511	373	18.312
04	9	0.184	14	0.449	50	2.258	44	2.131
05	127	7.589	154	8.962	243	11.003	274	13.766
06	280	18.568	334	20.307	439	21.610	431	25.833
07	9	0.537	16	0.840	43	2.259	63	3.605
08	160	10.642	180	11.258	285	14.866	327	20.323
09a	314	27.260	348	28.548	436	26.218	537	37.425
09b	315	28.642	359	30.213	444	28.668	515	39.453
09c	311	28.656	356	29.439	431	28.178	462	37.631
09d	316	29.405	355	28.150	429	27.923	428	36.253
09e	322	28.273	354	26.923	430	28.691	472	37.574
10	19	1.208	25	1.391	60	2.969	78	5.467
11	177	15.464	193	14.801	312	18.605	358	27.857
12	331	32.613	362	29.544	473	35.190	552	44.996
13	27	2.456	36	2.281	70	4.109	93	7.293
14	210	18.530	240	19.117	360	23.740	361	37.034
15	361	38.926	382	37.603	499	40.765	547	54.835
22	0	0.000	1	0.003	0	0.000	3	0.041
23	46	3.751	76	5.566	108	8.229	154	19.776
24	191	46.688	271	51.666	328	60.755	346	92.175
25	0	0.002	0	0.002	1	0.001	2	0.017
26	80	11.829	104	12.465	242	22.897	160	29.713
27	256	71.868	229	61.138	569	95.570	450	142.380
28	1	0.019	1	0.043	0	0.008	1	0.022
29	65	9.218	79	10.324	200	25.506	213	34.700
30	244	87.687	263	68.453	437	121.265	570	186.619
31	1	0.001	1	0.016	1	0.268	4	0.201
32	83	13.355	88	12.306	227	35.608	233	47.584
33	275	95.989	294	105.040	498	154.400	632	238.192
34	1	0.006	2	0.034	2	0.098	11	0.271
35	111	27.790	100	22.326	202	44.378	277	96.084
36								

Table 11: Final number of overtopping events and volumes $\beta = 15°$ (VO15)

VO15 Test	Pos: 3		Pos: 4		Pos: 5		Pos: 6	
	N_{ow}	V_{total}	N_{ow}	V_{total}	N_{ow}	V_{total}	N_{ow}	V_{total}
01	7	0.178	9	0.238	9	0.216	12	0.302
02	88	4.152	71	3.215	102	4.716	151	8.900
03	223	11.904	133	7.244	269	11.029	290	16.899
04	8	0.264	14	0.337	12	0.636	24	1.023
05	112	6.476	86	3.630	177	7.517	196	11.494
06	264	15.809	132	7.097	423	21.382	343	23.031
07	18	0.701	31	0.654	28	1.652	41	2.216
08	117	8.511	73	4.224	287	13.063	240	14.497
09	304	20.839	131	7.939	599	29.666	369	26.930
10	12	0.752	21	0.992	53	3.330	51	3.312
11	157	12.418	113	6.597	391	19.362	229	15.735
12	340	25.137	177	11.002	499	39.623	386	32.662
13	29	1.358	21	1.046	88	4.402	62	4.799
14	192	13.200	122	8.994	299	26.640	238	21.555
15	325	27.267	248	15.074	569	52.971	400	37.469
22								
23	36	2.038	37	1.555	35	2.264	66	5.642
24								
25								
26	51	2.147	52	3.284	46	3.781	60	6.486
27	224	39.596	167	25.844	219	50.938	215	49.397
28								
29	49	3.556	67	3.853	91	11.300	62	8.522
30	274	52.360	188	31.037	271	88.887	248	72.045
31	0	0.000	1	0.010	2	0.028	0	0.008
32								
33	254	50.781	212	34.279	343	137.311	292	105.232
34	0	0.004	0	0.000	2	0.204	2	0.058
35	52	5.523	52	7.079	236	38.689	113	20.832
36	245	65.547	206	47.352	402	198.638	350	150.140

Table 12: Final number of overtopping events and volumes $\beta = 30°$ (VO30)

VO30 Test	Pos: 3		Pos: 4		Pos: 5		Pos: 6	
	N_{ow}	V_{total}	N_{ow}	V_{total}	N_{ow}	V_{total}	N_{ow}	V_{total}
01	2	0.004	0	0.000	0	0.000	8	0.156
02								
03	102	3.368	103	2.054	120	2.662	153	5.318
04	3	0.039	0	0.000	4	0.096	16	0.282
05	70	2.630	55	0.917	76	2.016	134	3.822
06	158	6.509	126	2.413	158	5.758	203	7.257
07								
08	87	3.425	-1	1.183	127	4.018	157	5.661
09	220	10.515	114	2.936	167	7.689	249	10.063
10	13	0.426	12	0.070	19	0.634	39	0.804
11	122	5.071	61	1.238	134	6.232	197	7.215
12	222	9.831	129	2.738	223	11.827	277	11.165
13	17	0.371	21	0.080	41	0.972	39	1.194
14	127	5.353	97	1.618	179	7.492	172	7.599
15	256	12.031	194	3.531	317	15.365	256	12.475
22								
23	7	0.444	7	0.110	14	0.482	36	1.774
24	91	11.894	91	3.704	112	11.695	177	19.871
25								
26	17	0.677	7	0.095	23	1.352	39	2.633
27	114	16.877	93	4.492	160	20.717	220	29.643
28								
29	16	1.353	12	0.427	38	3.368	62	5.310
30	127	23.544	112	6.356	206	35.458	285	50.227
31								
32	18	1.867	16	0.555	59	8.002	92	10.417
33								
34	0	0.000	0	0.000	0	0.000	0	0.000
35	30	2.511	28	0.699	80	11.175	112	15.767
36	149	40.049	149	20.088	295	87.409	357	97.596

Table 13: Final number of overtopping events and volumes $\beta = 60°$ (VO60)

VO60 Test	Pos: 3		Pos: 4		Pos: 5		Pos: 6	
	N_{ow}	V_{total}	N_{ow}	V_{total}	N_{ow}	V_{total}	N_{ow}	V_{total}
01								
02								
03								
04								
05								
06								
07								
08								
09								
10								
11								
12								
13								
14								
15	0	0.000	0	0.000	0	0.000	0	0.000
22								
23	0	0.000	0	0.000	0	0.000	0	0.000
24	0	0.000	0	0.000	0	0.000	9	0.637
25								
26	0	0.000	0	0.000	0	0.000	3	0.103
27	9	0.214	0	0.000	1	0.014	34	1.755
28								
29	2	0.029	0	0.000	0	0.000	3	0.262
30	24	0.972	3	0.011	1	0.017	38	2.740
31								
32	7	0.104	0	0.000	1	0.006	5	0.309
33	40	1.599	3	0.007	15	0.371	50	5.746
34	0	0.000	0	0.000	0	0.000	0	0.000
35	13	0.166	0	0.000	3	0.008	9	0.621
36	79	3.623	8	0.145	40	1.467	86	7.078